

4174
7087

PRINCIPLES OF AERODYNAMICS

PRINCIPLES OF AERODYNAMICS

BY

JAMES H. DWINNELL

*Assistant Professor of Aeronautical Engineering
University of Washington*

FIRST EDITION

NEW YORK TORONTO LONDON
McGRAW-HILL BOOK COMPANY, INC.
1949

PRINCIPLES OF AERODYNAMICS

Copyright, 1949, by the McGraw-Hill Book Company, Inc. Printed in the United States of America. All rights reserved. This book, or parts thereof, may not be reproduced in any form without permission of the publishers.

PREFACE

Principles of Aerodynamics is an outgrowth of six years' development of a set of printed lecture notes used by the author in undergraduate classes at the University of Washington. The purpose of the book is to present an introduction to some of the more important theoretical and practical aspects of aerodynamics.

In order to provide flexibility in teaching, many chapters have been designed as independent units. Thus, for instance, any of Chaps. 4, 7, 8, 9, 10, 12, and 15 may be omitted without destroying the continuity of the text.

While the assistance of all the scientists and engineers whose work has made this volume possible can scarcely be acknowledged separately, the author takes pleasure in thanking particularly the National Advisory Committee for Aeronautics, the Aeronautical Research Council, and the University of Washington Aeronautical Laboratories for permission to use some of the great wealth of material available in their reports. He wishes also to express his gratitude to his colleagues at the University of Washington and to Prof. F. S. Eastman, Prof. V. M. Ganzer, Prof. A. V. Hall, Dr. Alexander Klemin, and Prof. V. J. Martin for their helpful criticisms during the preparation of the manuscript.

JAMES H. DWINNELL

SEATTLE, WASH.

July, 1949

CONTENTS

PREFACE	v
ABBREVIATIONS	xi
ENGLISH-LETTER NOMENCLATURE	xii
GREEK-LETTER NOMENCLATURE	xvii

CHAPTER 1

INTRODUCTION

1-1 Newton's Laws of Motion	1
1-2 Fluid Mass Density	4
1-3 Fluid Compressibility	6
1-4 Fluid Viscosity	8
1-5 Air Properties	11
1-6 Temperature Variation with Altitude	12
1-7 Pressure and Mass-density Variation with Altitude	13
1-8 Speed-of-sound Variation with Altitude	14
1-9 Viscosity Variation with Altitude	15
1-10 Absolute and Gage Pressure	15
1-11 Manometry	17

CHAPTER 2

FLUID DYNAMICS

2-1 The Perfect Fluid	23
2-2 The Continuity Equation	24
2-3 The Bernoulli Equation	24
2-4 Implications of Continuity and Bernoulli Equations	26
2-5 Fluid Forces	29
2-6 Jets	30
2-7 Body Pressure Distribution for a Perfect Fluid	39
2-8 Body Pressure Distribution for a Real Fluid	42
2-9 The General Force Equation	45
2-10 The General Moment Equation	51
2-11 Principal Aerodynamic Forces and Moments	52

CHAPTER 3

AERONAUTICAL NOMENCLATURE

3-1 Aircraft Types	57
3-2 Airplane Components	58

3-3	Wing	59
3-4	Fuselage	67
3-5	Power Plant	68
3-6	Landing Gear	71
3-7	Empennage	71
3-8	Control Surfaces	71
3-9	Aircraft Instruments	72

CHAPTER 4

EXPERIMENTAL FACILITIES

4-1	Early Testing Techniques	76
4-2	Classification of Wind Tunnels	77
4-3	Visual Flow Aids	94

CHAPTER 5

AIRFOIL CHARACTERISTICS

5-1	Force Representation	98
5-2	Lift	100
5-3	Drag	111
5-4	Lift/Drag Ratio	111
5-5	Pitching Moment	112
5-6	Airfoil Balance and Stability	118

CHAPTER 6

ASPECT RATIO AND PLAN-FORM INFLUENCES

6-1	The Momentum Theory	124
6-2	Plan-form Effects	131
6-3	The Circulation Theory	133
6-4	Section Characteristics	138
6-5	Spanwise Lift Distribution	139
6-6	Modifications to Induced-drag and Angle-of-attack Formulas	143
6-7	Airplane Efficiency Factor	146

CHAPTER 7

VISCOSITY PHENOMENA

7-1	The Boundary Layer	153
7-2	Laminar Boundary Layer	154
7-3	Turbulent Boundary Layer	156
7-4	Transition	158
7-5	Separation	160
7-6	Scale Effect on a Sphere	160
7-7	Scale Effect on a Cylinder	164
7-8	Scale Effect on a Normal Flat Plate	165
7-9	Scale Effect on an Airfoil	166
7-10	Scale Effect on Low-drag Airfoils	169

CHAPTER 8

COMPRESSIBILITY PHENOMENA

8-1	Continuity and Bernoulli Equations	174
-----	--	-----

CONTENTS

ix

8-2	Implications of the Continuity and Bernoulli Equations	175
8-3	Compressible Flow in a Laval Nozzle	177
8-4	Subsonic Airfoil Flow—Two-dimensional	179
8-5	Supersonic Airfoil Flow—Two-dimensional	184
8-6	Transonic Airfoil Flow—Two-dimensional	190
8-7	Three-dimensional Flow	195
8-8	Practical Aspects of High-speed Flight	202

CHAPTER 9

THE OPTIMUM AIRFOIL

9-1	Historical Sketch	206
9-2	Airfoil Geometry	208
9-3	Angle of Zero Lift, α_{l_0}	213
9-4	Lift Curve Slope, $dc_l/d\alpha$	214
9-5	Maximum Lift Coefficient, $c_{l_{max}}$	216
9-6	Minimum Drag Coefficient, $c_{d_{0min}}$	217
9-7	Section Drag-curve Shape	219
9-8	Maximum Ratio of Lift to Drag, $(L/D)_{max}$	220
9-9	Maximum Ratio of $C_L^{3/4}/C_D$, $(C_L^{3/4}/C_D)_{max}$	221
9-10	Maximum Ratio of $C_L^{1/2}/C_D$, $(C_L^{1/2}/C_D)_{max}$	221
9-11	Aerodynamic Center, ac	222
9-12	Pitching Moment Coefficient about the Aerodynamic Center, c_{mac}	222
9-13	Critical Mach Number, M_{cr}	223

CHAPTER 10

AUXILIARY LIFT DEVICES

10-1	Flaps	229
10-2	Slots	235
10-3	Comparison of Flaps and Slots	236
10-4	Boundary-layer Control	237
10-5	Dive Brakes	239

CHAPTER 11

PARASITE-DRAG AND POWER CONSIDERATIONS

11-1	Parasite Drag of Some Common Bodies	242
11-2	Interference	245
11-3	Airplane Parasite Drag	248
11-4	Power Considerations	251
11-5	Power Required	252
11-6	Representative Power Required	254
11-7	Scale and Compressibility Effects	256

CHAPTER 12

AIRCRAFT ENGINES

12-1	Unsupercharged Engines	260
12-2	Gear-driven Supercharger	262

12-3	Turbosupercharger	265
12-4	Fuel Consumption	267
12-5	Jet Propulsion	267

CHAPTER 13

PROPELLERS

13-1	The Ideal Propeller	270
13-2	The Simple Blade-element Theory	273
13-3	Thrust Coefficients	275
13-4	Power Coefficients	276
13-5	Propeller Efficiency	277
13-6	Comparison of Propeller and Airfoil Characteristics	278
13-7	Propeller Geometry	280
13-8	Choice of Propeller Diameter	282
13-9	Power Available	284

CHAPTER 14

AIRPLANE PERFORMANCE

14-1	Maximum Velocity	291
14-2	Minimum Velocity	292
14-3	Climbing Flight	293
14-4	Time to Climb	296
14-5	Gliding Flight	297
14-6	Cruising Conditions	299
14-7	Range	301
14-8	Endurance	303
14-9	Take-off	304
14-10	Landing	311
14-11	Performance with a Turbo-jet	313
14-12	Rapid Performance Methods	318

CHAPTER 15

STABILITY AND CONTROL

15-1	Definitions	325
15-2	Longitudinal Stability	326
15-3	Directional Stability	338
15-4	Lateral Stability	341
15-5	Theoretical Hinged-surface Characteristics	342
15-6	Actual Hinged-surface Characteristics	347
15-7	Practical Aspects of High-speed Flight	354

BIBLIOGRAPHY	357
------------------------	-----

APPENDIX A: Tables	361
------------------------------	-----

APPENDIX B: Charts	367
------------------------------	-----

INDEX	383
-----------------	-----

ABBREVIATIONS

AAL	Ames Aeronautical Laboratory, Moffett Field, Calif.
ACR	Advanced Confidential Report (of the NACA)
ARC	Aeronautical Research Council, England
ASME	American Society of Mechanical Engineers
CAA	Civil Aeronautics Administration, United States
DVL	Deutsche Versuchsanstalt für Luftfahrtforschung (German Institute for Aeronautical Research), Berlin and Göttingen, Germany
FRA	Fuselage reference axis
GALCIT	Guggenheim Aeronautical Laboratory, California Institute of Technology
JAS	Journal of the Aeronautical Sciences, United States
JRAS	Journal of the Royal Aeronautical Society, England
LDT	Two-Dimensional Low-Turbulence Pressure Tunnel (of the NACA)
LMAL	Langley Memorial Aeronautical Laboratory, Langley Field, Va.
LTT	Two-Dimensional Low-Turbulence Tunnel (of the NACA)
MIT	Massachusetts Institute of Technology
NACA	National Advisory Committee for Aeronautics, United States
NPL	National Physical Laboratory, Teddington, England
RAE	Royal Aeronautical Establishment, Farnborough, England
R&M	Reports and Memoranda (of the ARC). See the Bibliography for list of <i>R&M</i> used in this text.
SAE	Society of Automotive Engineers
TM	Technical Memorandum (of the NACA). See the Bibliography for list of <i>TM</i> used in this text.
TN	Technical Note (of the NACA). See the Bibliography for list of <i>TN</i> used in this text.
TR	Technical Report (of the NACA). See the Bibliography for list of <i>TR</i> used in this text.
UWAL	University of Washington Aeronautical Laboratories
VDT	Variable-Density Tunnel (of the NACA)
WR	Wartime Report (of the NACA). See the Bibliography for list of <i>WR</i> used in this text.

ENGLISH-LETTER NOMENCLATURE

- α an area, sq ft or sq in.
 speed of sound, fps or mph
 slope of lift curve, $dC_L/d\alpha$, per deg (see m)
 factor denoting fractional increase in velocity through propeller disk, $b/2$, dimensionless
 equivalent flat-plate area, $D_p/1.28q$, sq ft
 acceleration, fps per sec
 area downswept by wing, $(\pi b^2/4) + bG$, sq ft
- ac aerodynamic center, fraction of chord from leading edge
- A cross-sectional area of stream tube, wind tunnel, jet, etc., sq ft
 propeller disk area, $\pi D^2/4$, sq ft
 aspect ratio, b^2/S , dimensionless
- A_t tail aspect ratio, dimensionless
- AF activity factor, $(100,000/16) \int_{0.5}^{1.0} (r/R)^3 (b/D) d(r/R)$, dimensionless
- b factor denoting fractional increase in velocity behind propeller, $2a$, dimensionless
 wing span, ft or in.
 propeller blade width, ft or in.
- bhp engine brake horsepower
- B number of blades of propeller
- c a constant
 chord, ft or in.
 specific fuel consumption, lb per bhp-hr (see w)
- c_d section drag coefficient, D/qS , positive aft, dimensionless
- c_l section lift coefficient, L/qS , positive up, dimensionless
- c_m section pitching moment coefficient, M/qSc , positive for climbing moment, dimensionless
- c_r wing-root chord, ft or in.
- c_t wing-tip chord, ft or in.
- cp center of pressure, positive aft of leading edge, fraction of chord
- cg center of gravity, frequently expressed as fraction of chord from leading edge
- C a constant
 chordwise force, positive aft, lb
- C degrees centigrade

- C_D drag coefficient of wing or airplane, D/qS , positive aft, dimensionless
 C_{D_i} induced drag coefficient, $C_L^2/\pi A$, dimensionless
 C_{D_0} profile drag coefficient = wing drag coefficient for infinite aspect ratio, $C_D - C_{D_i}$, dimensionless
 C_{D_p} parasite drag coefficient, $C_{D_0} + C_{D_r}$ or $C_D - C_{D_i}$, dimensionless
 $C_{D_{pe}}$ "effective" parasite drag coefficient at $C_L = 0$ for representative parabolic polar curve, dimensionless
 C_{D_r} residual drag coefficient, $C_{D_p} - C_{D_0}$, dimensionless
 $C_{D_{pr}}$ proper drag coefficient, dimensionless
 C_F general force coefficient, F/qA , dimensionless
 C_h rate of climb $(P_a - P_r)/(33,000/W)$, fpm
 C_H hinge moment coefficient, H/qSc , where Sc is based on surface aft of hinge line, positive when an applied aerodynamic torque on the hinge tends to increase the deflection of a positively deflected flap, dimensionless
 C_l rolling moment coefficient, L/qSb , positive clockwise viewed from rear, dimensionless
 C_L lift coefficient, L/qS , positive up, dimensionless
 C_m pitching moment coefficient, M/qSc , positive for climbing moment, dimensionless
 C_n yawing moment coefficient, N/qSb , positive clockwise viewed from above, dimensionless
 C_N normal coefficient, N/qS , positive up, dimensionless
 C_p pressure coefficient, $\Delta P/q$, dimensionless
 C_{p_s} stagnation pressure coefficient, dimensionless
 C_P power coefficient, $p/\rho n^3 D^5$, or $10^{11} P/2\sigma N^3 D^5$, dimensionless
 C_s speed-power coefficient, $\rho v/\sqrt[5]{pn^2}$, or $0.638 V\sigma/\sqrt[5]{PN^2}$, dimensionless
 C_T thrust coefficient, $T/\rho n^2 D^4$, or $10^7 T/6.61\sigma N^2 D^4$, dimensionless
 C_Y side force coefficient, Y/Sq , positive right viewed from rear, dimensionless
 d diameter, ft or in.
 D diameter (propeller, sphere, cylinder, etc.), ft or in.
 drag, $C_D Sq$, lb (see coefficient definitions above for subscript definitions)
 e Oswald's airplane efficiency factor, $\frac{dC_{D_i}/dC_L^2}{dC_D/dC_L^2}$, dimensionless
 Napierian logarithm base
 e_w wing efficiency factor corresponding to e for an airplane, dimensionless
 E modulus of elasticity (solid or fluid), psi or psf
 endurance, hr

- f equivalent parasite area, D_p/q , sq ft (in performance equations, parasite drag is that at zero lift)
 fhp friction horsepower
 F degrees Fahrenheit
 F force, lb
 friction force, lb
 torque force, lb
 F_t tip-speed correction factor for propeller efficiency, dimensionless
 FRA fuselage reference axis
 g acceleration of gravity, 32.2 fps per sec
 G biplane gap, ft
 Froude Number, v^2/lq , dimensionless
 h height, ft or in.
 altitude, ft
 H absolute ceiling, ft
 total pressure, psf
 hinge moment, $C_H q S c$, lb-in. (see definition of C_H)
 H_s service ceiling, ft
 i_w wing incidence angle usually measured from fuselage reference axis, deg
 i_s stabilizer angle usually measured from either fuselage reference axis or wing chord, deg
 ihp indicated horsepower, $bhp + fhp$
 J propeller advance ratio, v/nD or $88V/ND$, dimensionless
 k constant
 K constant
 control-surface effectiveness factor, $(\partial\alpha/\partial\delta)_{C_N}$, dimensionless
 l length, ft or in.
 l_t tail length measured from airplane center of gravity to tail aerodynamic center, ft or in.
 l_w wing loading, W/S , psf
 L length, ft or in.
 lift, $C_L S q$, positive up, lb
 rolling moment, $C_l q S b$, positive clockwise viewed from rear, lb-in.
 m mass, W/g , slug
 slope of lift curve, $dC_L/d\alpha$, per radian (see a)
 M mass flow of fluid, slug per sec
 Mach number, v/a , dimensionless
 pitching moment, $C_m q S c$, positive for climbing moment, lb-in.
 M_{cr} critical Mach number, dimensionless
 n revolutions per sec
 distance from leading edge, positive rearward, fraction of chord
 N revolutions per minute

- N yawing moment, $C_{nq}Sb$, positive clockwise when viewed from above, lb-in.
 normal force C_NqS , positive up, lb
- p power, ft-lb per sec
 static pressure, psf
- p_s stagnation pressure, psf
- P engine bhp
- P_a thrust horsepower available
- P_{t_w} P_a or P_r adjusted for altitude and weight, hp
- P_r airplane horsepower required
- q dynamic pressure, $\frac{1}{2} \rho v^2$, or $V^2 \sigma / 391$, psf
- Q torque, lb-ft
- r radius, ft or in.
- R radius, ft or in.
 rolling moment, $C_{lq}Sb$, positive clockwise viewed from rear, lb-in.
 range, miles
 resultant force, lb
 test Reynolds number; also frequently used for effective Reynolds number R_e , $\rho vl / \mu$, dimensionless (l is arbitrary characteristic length that is chosen as chord for airfoil and diameter for cylinder, sphere, etc.)
 resistance force during take-off, $F + D$, lb
- R_e effective Reynolds number, simulating free air conditions, $(R)(TF)$, dimensionless
- s distance, ft or in.
 distance along the surface of a body, commonly measured either from front stagnation point or from leading edge of chord, ft or in.
- sg specific gravity, dimensionless
- S wing area, sq ft
- S_f wing area defined by flap span, sq ft
- S_r proper area (maximum projected frontal area), sq ft
- t thickness, ft, in., or fraction of chord
 time, sec, min, or hr
 temperature, °F (see T)
- thp thrust horsepower, $Tv/550$ or $TV/375$
- T thrust, $C_{T\rho n^2 D^4}$ or $(6.61 \times 10^{-7}) C_{T\sigma} N^2 D^4$, lb
 time, sec, min, or hr
 minimum time to climb, min
 temperature, $459.4 + t$, °F abs, (see t)
- T_c thrust coefficient, $T/\rho v^2 D^2$, dimensionless
- TF turbulence factor, R_e/R , dimensionless
- u velocity within boundary layer, fps

- U velocity just outside boundary layer, fps
- v velocity, fps
 - true air speed, fps (see V)
- v_i indicated velocity, $v\sqrt{\sigma}$, fps
- v_l landing velocity, fps
- v_o remote velocity, fps
- v_s slip-stream velocity, $v(1 + b)$, fps
 - stalling speed, fps
- v_t take-off velocity, fps
 - tangential velocity, fps
- v_w sinking speed, fps
- v_w wind speed, fps
- V_{t_w} air speed adjusted for weight and altitude, mph
- V velocity, mph (see v for subscript definitions)
 - true air speed, mph (see v)
 - volume, cu ft
 - specific volume, cu ft per lb
- w density, lb per cu ft
 - down-wash velocity, fps
 - velocity introduced by circulation, fps
 - width, ft or in.
 - fuel consumption, lb fuel per hr per lb thrust (see c)
- W weight, lb
 - width, ft or in.
- W_a air flow, lb per sec
- W_f fuel flow, lb per hr
- x distance from aerodynamic center measured parallel to zero-lift chord, positive aft, dimensionless
 - horizontal distance, ft or in.
- y distance perpendicular to surface for boundary-layer measurement, ft or in.
- Y side force, C_{YqS} , positive right when viewed from rear, lb
- z distance perpendicular to zero-lift chord, positive up, dimensionless

GREEK-LETTER NOMENCLATURE

alpha α	angle of attack measured between chord line and remote velocity, positive for trailing edge down, deg or radians
α_i	induced angle of attack, $C_L/\pi A$, radians, or $18.24C_L/A$, deg
α_0	angle of attack for infinite aspect ratio, deg or radians
α_{l_0}	section angle of zero lift, deg or radians
α_{L_0}	angle of zero lift, deg or radians
beta β	propeller-blade between plane of rotation and chord line, deg (usually measured at three-quarter radius)
	deflection angle of streamlines in passing through a shock wave, deg
gamma γ	ratio of specific heats (1.4 for dry air), dimensionless
	angle between airfoil resultant and lift, deg
Gamma Γ	dihedral angle, positive for wing tips up, deg
	circulation, sq ft per sec
delta δ	control-surface deflection, positive deflection causes positive lift or side force, deg (subscript designates surface considered; i.e., δ_e for elevator, δ_a for aileron, etc.)
	induced drag correction factor for taper and aspect ratio, dimensionless
	boundary-layer thickness defined where 99 per cent of local velocity is attained, ft or in.
Delta Δ	prefix meaning "increment;" e.g., ΔP means "pressure increment"
epsilon ϵ	down-wash angle, deg or radians
	exchange coefficient in turbulent flow, slug per ft-sec
eta η	propeller efficiency, dimensionless
η_i	tail efficiency factor, proportional to the ratio of dynamic pressure at tail to the remote dynamic pressure, dimensionless
theta θ	an angle, deg or radians
	angle of pitch, positive for climbing moment, deg
	glide angle, deg
	climb angle, deg
	shock wave angle, deg
lambda λ	wing-taper ratio, tip chord/root chord, dimensionless
Lambda Λ	sweepback angle, deg

mu μ	coefficient of viscosity, dv/dy , slug per ft-sec
	coefficient of friction, dimensionless
	Mach angle, deg
nu ν	kinematic coefficient of viscosity, μ/ρ , sq ft per sec
	frequency, per sec
xi ξ	camber, fraction of chord, dimensionless
pi π	a constant, 3.14
rho ρ	mass density, w/g , slug per cu ft
sigma σ	ratio of any mass density to standard sea-level mass density of air, ρ/ρ_0 , dimensionless
tau τ	shearing stress, subscripts L and T refer to laminar and turbulent, respectively, psf
	induced angle of attack correction for taper and aspect ratio, dimensionless
phi ϕ	propeller helix angle, $\beta - \alpha$, deg
	angle of roll, positive clockwise viewed from rear, deg
psi ψ	angle of yaw, positive clockwise viewed from above, deg

CHAPTER 1

INTRODUCTION

Aerodynamics is a branch of fluid mechanics that deals with the particular fluid, air. The laws that govern fluid mechanics are fundamentally identical to those used in the usual mechanical studies, but they frequently appear in an unfamiliar or extended form, giving the impression of novelty. In this introductory chapter, some of the general laws of fluid mechanics will be discussed, with particular reference to applications in aerodynamics. It is thought advisable to generalize the discussion wherever possible, to prevent creating the impression that the relations are peculiar to aerodynamics.

1.1 Newton's Laws of Motion. From an engineering standpoint, the most important laws governing both solid and fluid mechanics are those encompassed by the laws¹ of Sir Isaac Newton:

1. Every body continues in a state of rest or uniform motion in a straight line unless acted upon by some external force.
2. An acceleration, which is proportional to the force, will be produced in the direction of the force.
3. Action and reaction are equal and opposite.

The meaning of the first and third laws is evident from physical experience. The implications contained in the second law are not apparent without study. According to the statement of the law,

$$F \propto a \quad (1.1)$$

where F is force

a is acceleration

There is no statement as to the size of the acceleration, but only that one will be produced if there is an unbalanced force on the body. In the form of an equality,

$$F = ma \quad (1.2)$$

where m is a constant called *mass*. Mass is a physical character-

¹ The laws are not stated exactly as originally proposed. They are reworded, without reservation, for simplicity of presentation.

istic of the body that may be regarded as a measure of its material content or "how much matter" it has. By this is meant that the mass of a body is constant if no molecules are added to or subtracted from the body, even though it may undergo changes in state. This definition does not describe all the properties of mass, but has an advantage of giving to it a degree of tangibility.

Mass may be considered from another viewpoint. Let a stationary body be suspended in a vacuum from an infinite string. If a horizontal force is applied for a short time and is then removed, the body attains a constant linear velocity in accordance with Newton's first law. If the force is applied continuously, the velocity increases linearly with time; hence the acceleration is constant. Now let the experiment be repeated on half the body (half the mass). With the same force, the resultant acceleration must be double, in accordance with Newton's second law. Therefore, mass may be regarded as a measure of the *inertia*, or "resistance to acceleration," of a body.

The character of mass has been described; its magnitude will next be discussed. One of the most elementary of algebraic processes is that involved in determining a constant of proportionality in an equation such as

$$x = ky \quad (1.3)$$

where x and y are variables and k is a constant. The procedure is to substitute any known value of x and its corresponding value of y . For instance, if $x = 6$ when $y = 3$, substitution shows that $k = 2$. This constant, once determined, is fixed for all values of x and y within the meaning of the equation. Similarly, Eq. (1.2) may be regarded as an equation involving two variables, F and a , and a constant, m . If *any* force and its corresponding acceleration are known for the body, the constant of proportionality, m , may be found in a manner similar to that described above. One such combination may be chosen if the body is allowed to fall freely in a vacuum, where the force is the weight and the acceleration is that due to gravity, thus

$$m = \frac{W}{g} \quad (1.4)$$

The *magnitude* of mass may be obtained from Eq. (1.4) by use of the standard acceleration of gravity, 32.2 fps per sec.

Mass is a scalar quantity, while weight is a vector quantity. The relation between them is seen to arise only from experimental convenience.

If W is the weight in pounds and g is the acceleration in feet per second per second, the dimensions of mass may be obtained from Eq. (1·4):

$$m \approx \frac{\text{lb-sec}^2}{\text{ft}} \quad (1·5)$$

This unwieldy combination of terms is combined to form the engineering unit of mass called a *slug*; hence,

$$1 \text{ lb force} = (1 \text{ slug mass}) (1 \text{ fps per sec acceleration})$$

Equation (1·2) may be written in several forms dependent upon convenience. For instance,

$$\begin{aligned} F &= ma = m \frac{dv}{dt} \\ F dt &= m dv \end{aligned} \quad (1·6)$$

If F is independent of time and m is independent of velocity, integration of Eq. (1·6) gives

$$Ft = m(v_f - v_i) \quad (1·7)$$

$$= m \Delta v \quad (1·8)$$

$$= mv_f - mv_i \quad (1·9)$$

$$F = \frac{m}{t} (v_f - v_i) \quad (1·10)$$

$$F = M \Delta v \quad (1·11)$$

where F is force, lb

m is mass, slug

a is acceleration, fps per sec

v is velocity, with subscript f indicating final and subscript i indicating initial, fps

t is time, sec

Ft is impulse, lb-sec

mv is momentum, slug-ft per sec

M is mass per unit time, slug per sec

Δv is change in velocity, fps

Example 1. A force of 1.5 lb is applied continuously to a 25-lb body for 30 sec. If the original velocity is 20 fps, find the final velocity.

Solution. According to Eq. (1-7),

$$\begin{aligned}\text{Final velocity } v_f &= \frac{Ft}{m} + v_i \\ &= \frac{(1.5)(30)(32.2)}{25} + 20 \\ &= 78.0 \text{ fps}\end{aligned}$$

Example 2. A machine gun fires 0.1-lb bullets at a rate of 850 per min with a muzzle velocity of 3000 fps. Find the average recoil force.

Solution. This problem involves a continuous mass movement, and so may be solved by Eq. (1-11).

$$\text{Mass per sec, } M = \frac{(850)(0.1)}{(60)(32.2)} = 0.0440 \text{ slug per sec}$$

$$\text{Change in velocity, } \Delta v = 3000 \text{ fps}$$

$$\text{Average recoil force } F = M \Delta v = (0.0440)(3000) = 132 \text{ lb}$$

1-2 Fluid Mass Density. The density, or specific weight, of a substance is defined as weight per unit volume, designated by the symbol w . Correspondingly, mass density¹ is defined as mass per unit volume, designated by the symbol ρ . The relation between the two is shown by an equation:

$$\rho = \frac{w}{g} \quad (1-12)$$

where ρ is mass density, slug per cu ft

w is specific weight, lb per cu ft

Mass density is used almost without exception in aerodynamic calculations in preference to specific weight; however, the following statements regarding ρ may also be applied to w , in view of Eq. (1-12).

The mass density of a solid or liquid is essentially constant, but the mass density of a gas depends upon the temperature and pressure according to the *equation of state*,

$$\frac{pV}{T} = R \quad (1-13)$$

where p is pressure, psf

V is specific volume, cu ft per lb

T is temperature, F abs

R is constant which, for dry air, is 53.3 ft per degree Fahrenheit

¹ In aerodynamics, "density" frequently implies "mass density."

Strictly speaking the equation applies only to a "perfect gas," but except under extreme conditions of temperature and pressure, it may be applied without appreciable error in all aerodynamic problems.

As its name implies, the equation of state has to do with the state of a gas and is independent of the thermodynamic process by which the state was established. Thus, for instance, if the temperature and pressure of a particular gas are specified, the specific volume is uniquely defined.

The equation of state involves three variables. The *process* describes the relation between two of these variables. Three processes that are immediately apparent involve holding one of the three variables constant. This leads to the *isobaric* (constant-pressure), *isochoric* (constant-volume), and *isothermal* (constant-temperature) processes. Evidently addition or release of heat is required during each of these processes; therefore none of them is *adiabatic*. In a fourth process, the system is thermodynamically insulated (adiabatic) and contains no dissipative forces. This is called an *isentropic* process.

This text will be concerned mostly with processes that are either isothermal or isentropic. The isothermal process is represented by the equation

$$pV = C \quad (1.14)$$

where C is a constant. [Equation (1.14) is evidently a mathematical statement of *Boyle's law*.] The isentropic process is represented by

$$pV^\gamma = C_1 \quad (1.15)$$

where C_1 is a constant and γ is the ratio of specific heat at constant pressure to the specific heat at constant volume, having a value of 1.4 for dry air.

The equation of state may be written in several forms, of which the following will be particularly useful in subsequent discussions:

$$\left. \begin{aligned} \frac{p_0 V_0}{T_0} &= \frac{p_1 V_1}{T_1} \\ \frac{p_0}{\rho_0 T_0} &= \frac{p_1}{\rho_1 T_1} \\ \rho_1 &= \left(\frac{p_1}{p_0} \right) \left(\frac{T_0}{T_1} \right) \rho_0 \end{aligned} \right\} \quad (1.16)$$

Notice that the isothermal equation is obtained by setting $T_0 = T_1$ in the above equations.

The isentropic equation may also be written in several forms

$$\begin{aligned} p_0 V_0^\gamma &= p_1 V_1^\gamma \\ \frac{p_0}{\rho_0} &= \frac{p_1}{\rho_1} \\ \rho_1 &= \left(\frac{p_1}{p_0} \right)^{1/\gamma} \rho_0 \end{aligned} \quad (1-17)$$

Substitution of these relations in one of the forms of the equation of state gives a relation between p and T , V and T , or ρ and T .

In Eqs. (1-16) and (1-17) the dimensions of the variables are inconsequential, except that the dimensions of *each* variable must be consistent within an equation; *e.g.*, pressure may be expressed as pounds per square foot, pounds per square inch, or inches of mercury, etc., but p_0 and p_1 must have the *same* chosen dimensions.

Example. Find the mass density of air in a variable-density wind tunnel in which the pressure is 14 atm and the temperature is 35 C, knowing that for standard conditions ($t = 15$ C or 59 F, and $p = 1$ atm or 14.7 psi) the mass density $\rho_0 = 0.002378$ slug per cu ft.

Solution. Absolute zero on the centigrade scale is -273 C; hence, by Eq. (1-16),

$$\begin{aligned} \text{Mass density } \rho &= \left(\frac{p_1}{p_0} \right) \left(\frac{T_0}{T_1} \right) \rho_0 = \left(\frac{14}{1} \right) \left(\frac{288}{308} \right) (0.002378) \\ &= 0.0311 \text{ slug per cu ft} \end{aligned}$$

1-3 Fluid Compressibility. A relation that occurs in many branches of mechanics is the following:

$$\text{Stress} \propto \text{unit strain} \quad (1-18)$$

The stress in this relation may be produced by pressure or shear, and the resulting strain may be a change in volume, area, or linear dimension. If the relation is written as an equation, the constant of proportionality may be regarded as a measure of "elasticity" or "resistance to deformation" whose magnitude can be obtained experimentally.

Equation (1-18) may be used for describing the deformation ΔV occurring in a fluid as a result of a change in pressure Δp .

$$\Delta p = E \frac{-\Delta V}{V} \quad (1-19)$$

where Δp is pressure increment, psf

V is specific volume, cu ft per lb

$-\Delta V$ is specific volume decrement, cu ft per lb

E is bulk modulus of elasticity, psf

In the limit, as Δp approaches zero,

$$E = -V \frac{dp}{dV} \quad (1-20)$$

The negative signs in Eqs. (1-19) and (1-20) are inserted because E is conveniently defined as a positive quantity, and a positive dP always produces a negative dV . For isothermal conditions in a gas,

$$pV = C$$

hence

$$\frac{dp}{dV} = -\frac{p}{V}$$

and therefore

$$E = p \quad (1-21)$$

For isentropic conditions

$$pV^\gamma = C_1$$

$$\frac{dp}{dV} = -\frac{\gamma p}{V}$$

and therefore

$$E = \gamma p \quad (1-22)$$

The bulk modulus is seen to be a physical characteristic of a gas that depends only upon the pressure. It is the fundamental criterion of gaseous compressibility. In a great many aerodynamic problems, particularly those associated with high-speed flight, the rate at which a pressure wave travels in air has more physical significance than the bulk modulus, and it may be shown¹ that there is a simple relation between these two variables

$$E = \rho a^2 \quad (1-23)$$

where ρ is mass density, slug per cu ft

a is speed of infinitesimal pressure-wave propagation in air,
equal to speed of sound in air, fps

¹ See, for example, DODGE, R. A., and M. J. THOMPSON, "Fluid Mechanics," McGraw-Hill, New York, 1937.

Equation (1.23) gives rise to the use of the speed of sound, a , as a criterion for air compressibility. If pressure-wave phenomena are assumed isentropic, Eqs. (1.23) and (1.22) may be combined:

$$a = \sqrt{\frac{\gamma p}{\rho}} \quad (1.24)$$

By further combining Eqs. (1.24) and (1.13), speed of sound may be expressed in terms of the absolute temperature as follows:

$$a = 41.4\sqrt{\gamma T}$$

where a is speed of sound in dry air, fps

γ is ratio of specific heats, having a value 1.4 for dry air, dimensionless

T is temperature, F abs

This equation was developed from theoretical considerations, but experiments have shown very close correlation. The accepted equation for speed of sound based upon experimental evidence is

$$a = 1120\sqrt{\frac{T}{518.4}} \quad (1.25)$$

The speed of sound will be shown later to play an important role in judging the importance of air compressibility on the aerodynamic forces of an airplane.

1.4 Fluid Viscosity. All fluids are viscous to some extent, whereas solids are generally assumed to be inviscid. The viscous property of a fluid asserts itself only when the fluid is in motion and is observable as a retarding action of one layer of fluid on a contiguous layer.

In order to develop the equations relating to viscous phenomena, it is necessary to introduce the concepts of *laminar* and *turbulent flow*. Laminar flow implies a periodic fluctuation of the velocity about its mean value, caused entirely by *molecular agitation*. Turbulent flow implies a periodic fluctuation of larger magnitude caused by *fluid-particle agitation*, which is superimposed upon the molecular fluctuations. A simple example will demonstrate the physical characteristics of each regime: a burning cigarette in still air produces a thin ribbon of smoke that rises until the flow becomes unstable and breaks down into a billowing column. The thin ribbon is laminar, while the billowing column is turbulent.

In the following development, which assumes laminar flow, an element of fluid is considered that has a shearing stress produced by a velocity gradient perpendicular to the direction of flow, as shown in Fig. 1-1. According to Newton, the following equation relates the stress and deformation:¹

$$\tau = \mu \frac{dv}{dy} \quad (1-26)$$

where τ is shearing stress, psf

μ is coefficient of viscosity, slug per ft-sec

$\frac{dv}{dy}$ is velocity gradient, per sec

The deformation is continuous during the application of the stress, and remains at a fixed value upon its removal. The constant of proportionality, μ , may be regarded as a measure of "viscosity" or "resistance to continuous deformation." Equation (1-26) may be considered one of the family of expressions given by Eq. (1-18).

The magnitude of the coefficient of viscosity for a perfect gas may

be shown by considering two planes of gas separated by a distance λ , which is the mean transverse distance that the molecules travel between collisions (Fig. 1-2). The lower plane is assumed to move with velocity v , and the upper plane is assumed to move with velocity $v + \Delta v$. Owing to molecular agitation, there is continual transfer of molecules from one plane to the other. The

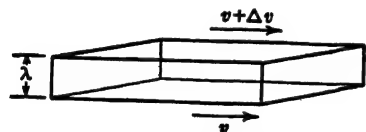


FIG. 1-2. Two planes of fluid separated by a distance λ and having a relative velocity Δv .

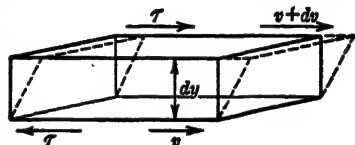


FIG. 1-1. Element of fluid, dy high, subjected to shearing stress τ that produces a continuous deformation dv .

low-speed molecules from the lower plane are speeded up upon reaching the upper plane, but by Newton's second law of motion, this implies there is an inertia force in a direction opposite to the acceleration. Correspondingly, there must be an inertia force in the opposite direction arising from the deceleration of molecules

¹ Strictly speaking, the relation applies only to the so-called "Newtonian fluids," of which air and water are two examples. The text will not be concerned with non-Newtonian fluids.

passing from the upper to lower planes. The resulting shearing force per unit area (shearing stress) depends upon the transverse mean molecular velocity, the density, and the change in velocity, in accordance with Eq. (1.11); hence

$$\tau \propto \rho \bar{v}_m \Delta v \quad (1.27)$$

where ρ is density of gas, slug per cu ft

\bar{v}_m is root-mean-square molecular velocity, fps

Δv is change in velocity, in direction of flow, fps

An equation for shearing stress in terms of the coefficient of viscosity has already been given in Eq. (1.26). The two relations may be equated.

$$\mu \frac{dv}{dy} \propto \rho \bar{v}_m \Delta v \quad (1.28)$$

From the physical conditions of the problem

$$\frac{dv}{dy} = \frac{\Delta v}{\lambda} \quad (1.29)$$

and

$$\rho \propto \frac{1}{\lambda} \quad (1.30)$$

Substituting Eqs. (1.29) and (1.30) in Eq. (1.28) yields

$$\mu \propto \bar{v}_m \quad (1.31)$$

From the *kinetic theory of gases*, the absolute temperature of a gas is directly proportional to the kinetic energy of its molecules, or

$$T \propto \bar{v}_m^2 \quad (1.32)$$

hence from Eqs. (1.32) and (1.31)

$$\mu \propto \sqrt{T} \quad (1.33)$$

Equation (1.33) indicates that the coefficient of viscosity is independent of pressure and varies as the square root of the absolute temperature; however, this analysis has been made for a perfect gas. Actually the coefficient of viscosity of air varies more closely with the three-quarters power of the absolute temperature. Since most aerodynamic calculations are restricted to a limited temperature range, the following linear equation is suggested. It dupli-

cates the data from the International Critical Tables within ± 0.5 per cent for temperatures ranging from -70 to 150 F.

$$\mu = (338.5 + 0.575t)10^{-9} \quad (1-34)$$

where μ is coefficient of viscosity of air, slug per ft-sec
 t is temperature, F (not F abs)

The coefficient of viscosity for gases has been shown to increase with temperature, because of the increased molecular agitation. It decreases for liquids, however, because the intermolecular spacing increases with increasing temperature, and this increased spacing reduces the attraction or "cohesion" between the molecules.

A parameter that will find considerable use in subsequent chapters is the *kinematic coefficient of viscosity*, ν , defined by

$$\nu = \frac{\mu}{\rho} \quad (1-35)$$

1-5 Air Properties. Air close to the earth's surface is a gaseous mixture containing approximately 80 per cent nitrogen and 20 per cent oxygen, by volume. Water vapor is usually present to some extent, but in aerodynamic calculations dry air is generally assumed: the error in density amounts to about 0.5 per cent for average conditions (say 59 F and 50 per cent relative humidity), but may reach 2.5 per cent for extreme conditions (say 100 F and 100 per cent relative humidity).¹ The density of humid air is always less than that of dry air.

Aerodynamic forces arising from relative motion between a body and the surrounding air are dependent not only on the size and shape of the body and the magnitude of the relative velocity but also upon the density, compressibility, and viscosity of the air. As has been shown, air density is dependent upon temperature and pressure, while viscosity and speed of sound are dependent only upon temperature. Even at sea level the natural variations in temperature and pressure are sufficient to cause appreciable changes in aerodynamic forces, and at altitude these conditions are severely aggravated by the natural tendency toward decreasing temperature and pressure with increasing altitude. In order to provide a basis for estimating and comparing airplane performance, a "standard" variation in temperature and pressure with altitude

¹ See Wood, K. D., "Technical Aerodynamics," McGraw-Hill, New York, 1947.

has been assumed. This standard variation is used throughout the United States and is widely accepted elsewhere.

1-6 Temperature Variation with Altitude. Careful scrutiny of the variation of temperature with altitude for various sections of the world has shown an approximately linear decrease in a layer immediately adjacent to the earth's surface, with approximately constant temperature in the contiguous layer. The first layer is called the *troposphere*; the second layer is the *stratosphere*, and the plane separating them is the *tropopause*. Thickness of the layers is primarily a function of latitude and season. For instance, the

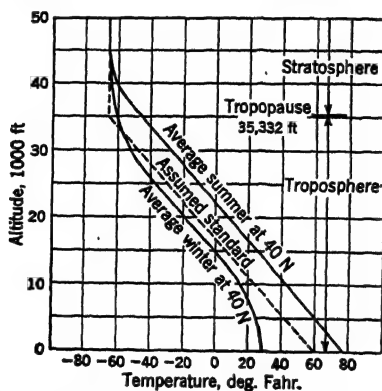


FIG. 1-3. Comparison of average temperature variation at lat 40°N with the assumed standard variation. (From TR 147.)

troposphere is about 25,000 ft thick at the poles and about 55,000 ft thick at the equator. Seasonal variations for a position about lat 40°N in the United States are given in Fig. 1-3.

The approximately linear variation of temperature in the troposphere and stratosphere is represented, for engineering purposes, by an exactly linear variation that has been accepted as standard. This variation is shown in Fig. 1-3. The standard temperature decreases linearly from 59 F at sea level to -67 F at 35,332 ft, then remains constant to 104,987 ft. This covers the altitudes of usual interest in aerodynamics.¹ Below the tropopause the equation for standard temperature is

$$t = 59 - 0.00357h \quad (1-36)$$

where h is altitude, ft

t is temperature corresponding to h , F

¹ Tentative variations for higher altitudes are given in TN 1200.

Equation (1-36) may be written in general form:

$$\left. \begin{aligned} t &= t_0 - 0.00357h \\ T &= T_0 - 0.00357h \end{aligned} \right\} \quad (1-37)$$

where t and t_0 are temperatures at altitude and sea level, respectively, F

T and T_0 are temperatures at altitude and sea level, respectively, F abs

1-7 Pressure and Mass-density Variation with Altitude. Corresponding to the standard sea-level temperature, an atmospheric pressure of 2116.4 psf has been assumed. This requires a standard density of 0.002378 slug per cu ft, according to Eq. (1-13).

The assumed variation in temperature with altitude automatically specifies values of pressure and density at all altitudes. In the following analysis equations will be developed to allow computation of these values.

Let a column of air be 1 ft on a side, as shown in Fig. 1-4. At an altitude h let an element of volume have a height dh . The weight of this element is $w dh$ where w is air density, pounds per cubic foot. Since density is the reciprocal of specific volume, the weight of the element may also be written dh/V , where V is specific volume in cubic feet per pound. Thus the equation relating the forces on the element may be written

$$p + \frac{-dh}{V} \quad p + dp \quad (1-38)$$

$$dp = -\frac{dh}{V} \quad (1-39)$$

where the minus sign in Eq. (1-38) is inserted because a positive dh is in a direction opposite to a positive dp . From Eq. (1-13)

$$V = \frac{53.3T}{p}$$

whence

$$\frac{dp}{p} = -\frac{dh}{53.3T} \quad (1-40)$$

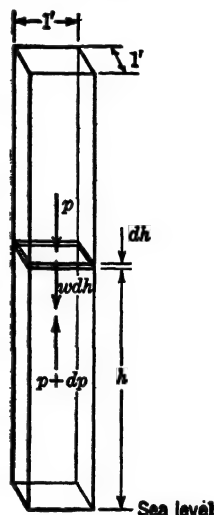


FIG. 1-4. Element of atmosphere, dh high, subjected to pressure and gravitational forces.

Substitution of Eq. (1.37) in Eq. (1.40) gives

$$\frac{dp}{p} = \frac{-dh}{53.3(T_0 - 0.00357h)}$$

$$\int_{p_0}^p \frac{dp}{p} = -5.256 \int_0^h \frac{dh}{(T_0/0.00357) - h} \quad (1.41)$$

By integration, the pressure variation for *standard altitude* is obtained:

$$p = p_0 \left(\frac{T}{T_0} \right)^{5.2} \quad (1.42)$$

From Eq. (1.16),

$$\frac{\rho}{\rho_0} = \left(\frac{p}{p_0} \right) \left(\frac{T_0}{T} \right) \quad (1.43)$$

hence, the density variation for standard altitude is obtained:

$$\rho = \rho_0 \left(\frac{T}{T_0} \right)^{4.2} \quad (1.44)$$

In Eqs. (1.42) and (1.44) the temperature must be in degrees Fahrenheit absolute, not Fahrenheit, because in both equations temperature enters as a ratio, not as a difference. The units of pressure and density are immaterial, provided they are consistent.

The temperature, pressure, and density variations given by Eqs. (1.36), (1.42), and (1.44) are tabulated for various altitudes in Table I, Appendix A. The ratio ρ/ρ_0 , which occurs frequently in aerodynamic calculations, is denoted by the symbol σ . Tabulation of σ , as well as its inverse square root, is also given in Table I, Appendix A.

1.8 Speed-of-sound Variation with Altitude. The speed of sound varies only with temperature. According to Eq. (1.25),

$$a = 1120 \sqrt{\frac{T}{518.4}} \quad (1.45)$$

where T is temperature, degrees Fahrenheit absolute. The speed of sound for standard sea-level conditions is 1120 fps, or 763.6 mph. The variation with altitude is given in Table I, Appendix A.

1-9 Viscosity Variation with Altitude. The coefficient of viscosity for air also varies only with temperature. It is given approximately by Eq. (1-34), repeated below.

$$\mu = (338.5 + 0.575t)10^{-9} \quad (1-46)$$

where μ is coefficient of viscosity, slug per ft-sec

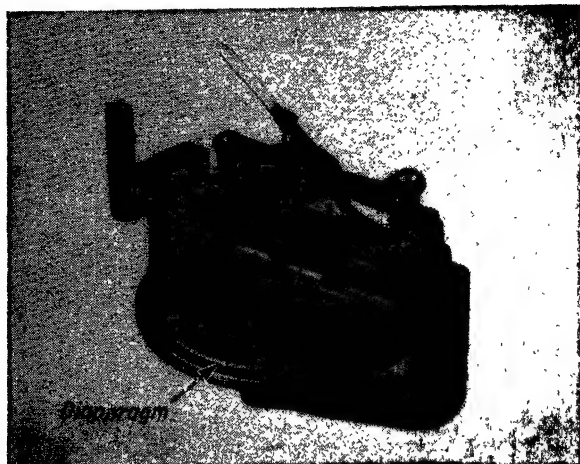
t is temperature, F (not F abs)

The coefficient of viscosity for standard sea-level conditions is 3.73×10^{-7} slug per ft-sec. The variation with altitude is given in Table I, Appendix A.

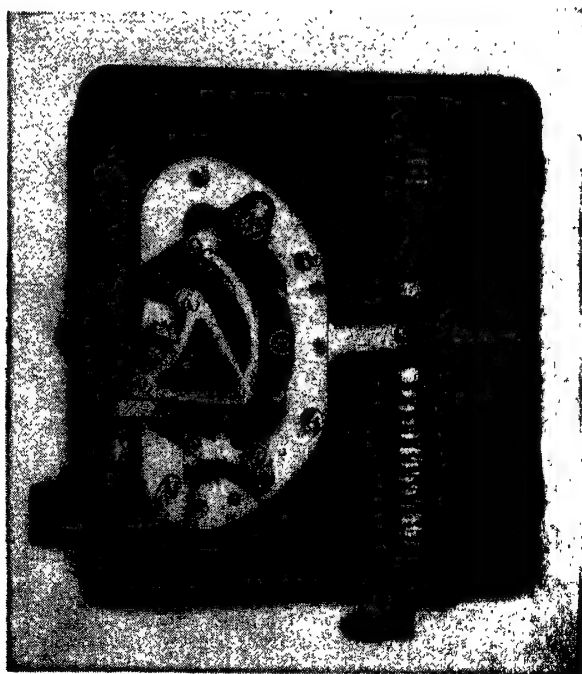
The variation with altitude of the reciprocal of kinematic viscosity, $1/\nu$, is also given in Table I, Appendix A.

1-10 Absolute and Gage Pressure. Two separate but related systems are used to specify pressures. The first uses an *absolute* pressure whose zero corresponds to a complete vacuum, as in a mercury or aneroid barometer. The second uses a *gage* pressure whose zero corresponds to atmospheric pressure, as in a tire pressure gage. Absolute pressure is the sum of the atmospheric and gage pressures. A positive gage pressure means an absolute pressure greater than atmospheric; conversely a negative gage pressure means an absolute pressure less than atmospheric. The two systems are somewhat analogous to the Fahrenheit and Fahrenheit absolute temperature systems. The magnitude of a specified pressure generally makes clear which one is intended, particularly in aerodynamics, where gage pressures are generally small compared with atmospheric pressure. Of course, any instrument may be made to indicate either absolute or gage pressure simply by adjustment of the zero on the scale.

Three mechanical pressure devices form the elements of most aircraft instruments and are frequently used in experimental work. A *diaphragm* consists of a rigid cylindrical shell (Fig. 1-5a) with flexible circular ends. A pressure differential inside the chamber so formed causes deflection of the ends, which may be indicated by a pointer through a suitable linkage system. A *bellows* is similar to the diaphragm except that the cylindrical sides are flexible while the ends are rigid (Fig. 1-5b). A *bourdon tube* consists of a tube that is closed at one end and is bent in the form of a circle (Fig. 1-5c) with the open end held by a support. A pressure differential within the tube causes deflection of the closed



(a)



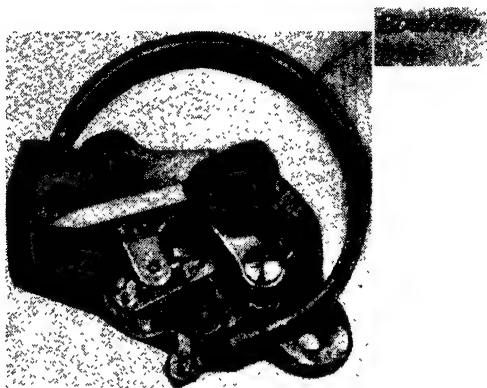
(b)

FIG. 1-5. Mechanical pressure elements: (a) diaphragm, (b) bellows.

end, which again may be suitably connected to a pointer. These three devices are expensive, delicate, and often complicated.

Manometers are used extensively in experimental work because they are relatively cheap, quite rugged, and extremely simple.

1-11 Manometry. A manometer is a hydrostatic device used to indicate differential pressures. The simplest type consists of



(c)
FIG. 1-5. (*continued*) Mechanical pressure elements: (c) bourdon tube.

a glass tube bent in the form of a U, with a common liquid in both legs, as shown in Fig. 1-6a. A difference in pressure in the two legs causes a differential liquid height; whence,

$$\Delta p = wh \quad (1-47)$$

where Δp is pressure differential, psf

w is liquid density, lb per cu ft

h is differential height, ft

For small pressure differentials, the manometer is inclined to facilitate reading. If the angle is too small, however, the meniscus may become difficult to read.

Figure 1-6b shows a modification of the U-tube manometer, consisting of a reservoir attached to one leg. If the horizontal area of the reservoir is large compared with that of the tube, the fluid level in the reservoir may be assumed stationary. Equa-

tion (1.47) can then be applied again, using h as shown. Figure 1.7 illustrates an inclined version of this type of manometer.

Figure 1.8 shows an arrangement of a U-tube manometer in which two reservoirs and two fluids are used. If the areas of the reservoirs are large compared to the area of the tube, so that changes in reservoir liquid level may be neglected, the effective

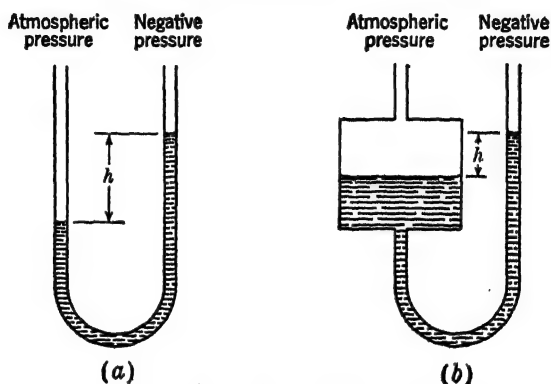


FIG. 1.6. Conventional U-tube manometers.

density may be shown equal to the difference between the densities of the two liquids used (see Prob. 1.8).

There are many kinds of *micromanometers* used to increase the accuracy of readings. Most are based upon the principle of the manometers discussed. For instance, one consists of a conven-

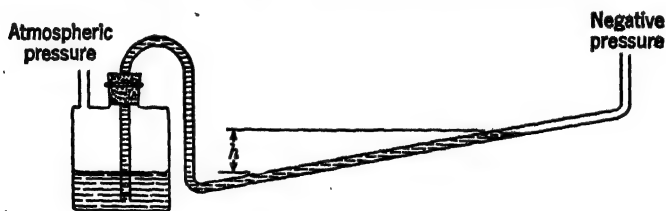


FIG. 1.7. A slant-tube manometer.

tional U-tube manometer, the meniscus of which is observed through a horizontal microscope. Cross hairs in the microscope are made to coincide with the meniscus. The vertical position of the microscope is then indicated on a scale.

Where several pressures are to be indicated simultaneously, a *multiple manometer* is used. A series of glass tubes is connected

to a common reservoir as shown in Fig. 1-9. For recording small pressure differentials, the plane of the tubes may be inclined; however, inaccuracies in the glass tubing generally limit the angle of inclination. Greater precision can be obtained by stretching

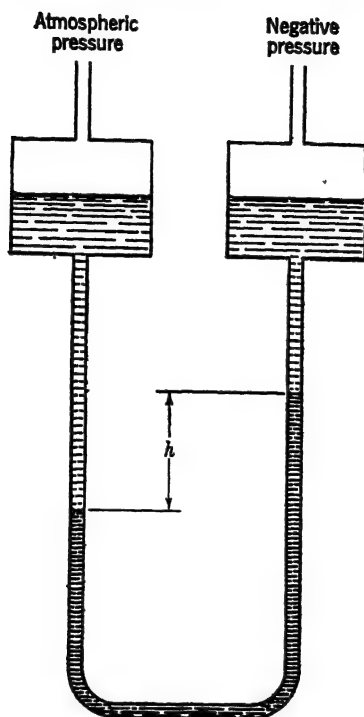


FIG. 1-8. A precision manometer.

transparent plastic tubes between rigid supports, and providing individual eccentrics for each tube or by using bored glass tubes.

In some aerodynamic tests the recorded pressures must be integrated. This may be done hydrostatically by means of an *integrating manometer* consisting of a series of bored glass tubes, all of the same diameter, in combination with a single large bored glass tube which forms the reservoir. Changes in the liquid level of each tube cause proportionate changes in the reservoir level. When the diameters of the tubes and reservoir are known, the change in reservoir level may be related to the sum of the changes in level in all the tubes.

Several different kinds of fluids are used in the various manometers just described. The chosen fluid should have a specific gravity that will give a satisfactory rise in level in the particular manometer selected. A fluid may not be satisfactory because it sticks to the tube in droplets, because it evaporates, because it deteriorates rubber or plastic tubing, because it is combustible,

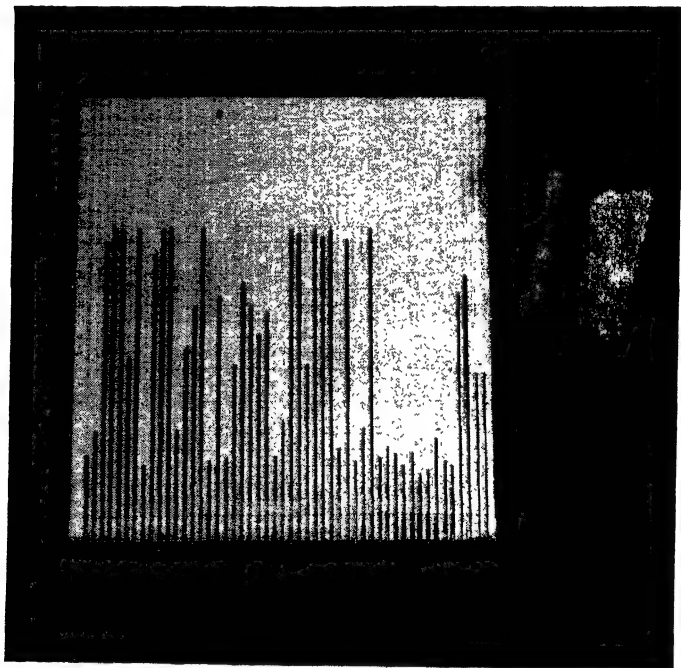


FIG. 1-9. A multiple manometer.

because it cannot be dyed satisfactorily for photographing, or because the meniscus is difficult to read. In Table II, Appendix A, are listed several satisfactory manometer fluids, with some important characteristics of each.

PROBLEMS

1-1. A 7000-lb pursuit plane has four fixed machine guns on its wing leading edge. They each fire eight-hundred .50-caliber bullets per minute with a muzzle velocity of 2800 fps. What will the average deceleration of the airplane be as a result of the simultaneous firing of all four guns? A .50-caliber bullet weighs 1.6 oz.

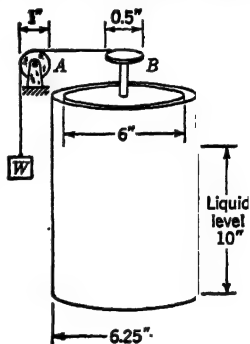
1-2. Two trains travel parallel to each other in the same direction at 20 and 60 mph, respectively. Each train has a cannon pointed at the

other, with the barrel perpendicular to the direction of motion. The low-speed train fires ten 5-lb cannon balls per minute at the other train in a continuous stream with a muzzle velocity of 100 fps. The balls come to rest on the high-speed train, then are returned at the same rate with the same muzzle velocity, so as to come to rest ultimately on the low-speed train. Find the magnitude and direction of the average force on each train resulting from the simultaneous firing of both cannons.

1-3. Air at temperature $t_1 = 0^\circ\text{F}$ and pressure $p_1 = 14.7$ psi is compressed isentropically until $t_2 = 59^\circ\text{F}$. Find p_2 . HINT: Keep all equations in symbolic form until final solution.

1-4. Obtain an equation for speed of sound assuming that the pressure and density changes resulting from the wave propagation are accomplished isothermally. Explain why this assumption gives a lower speed than Eq. (1-25).

1-5. A solid cylinder 6 in. in diameter is enclosed by an open-ended drum 6.25 in. in diameter, so as to be free to turn on a bearing at its base. A weight $W = 1.0$ lb is attached by a pulley A having a diameter of 1.0 in. to a second pulley B having a diameter of 0.5 in. as shown. A liquid having coefficient of viscosity, $\mu = 0.0005$ lb-sec per sq ft, is poured in between the cylinder and drum to a height of 10 in. Ignoring mechanical friction and the viscous force on the bottom of the cylinder, find the steady velocity v (fps) with which the weight W falls. (Assume laminar shearing stress.)



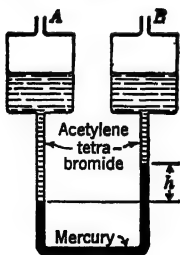
1-6. Find the kinematic coefficient of viscosity, ν , for air if $\rho = 0.00210$ slug per cu ft, and $p = 28$ in. of mercury.

1-7. Check the values of absolute pressure, mass density, coefficient of viscosity, and speed of sound given in Table I, Appendix A, at 50,000 ft.

1-8. A manometer has mercury ($\text{sg} = 13.6$) in its U tube and acetylene tetrabromide ($\text{sg} = 2.97$) in its reservoirs as shown. With no difference in pressure at A and B , the mercury levels are the same in the two legs of the U tube, and the acetylene tetrabromide levels are the same in the reservoirs.

a. Find the effective specific gravity of the manometer; i.e., find the specific gravity of a liquid that would produce the same vertical rise of fluid in a simple U-tube manometer. Ignore the change in level of the liquid in the reservoirs.

b. Find the height h (in.) of mercury rise corresponding to a difference in pressure between A and B of 3 psi.



CHAPTER 2

FLUID DYNAMICS

The flow over an arbitrary body or through a tube of arbitrary shape does not lend itself to precise mathematical description except under very unusual circumstances. It is almost always necessary to introduce simplifying assumptions relating to the geometry of the body or to the physical properties of the fluid itself. These assumptions, of course, limit the use of the mathematical expressions; hence considerable care is required in their interpretation. One of the most fundamental simplifications of this whole text is that steady motion is assumed; *i.e.*, conditions such as temperature, pressure, density, velocity, and acceleration at a point past which a fluid is flowing are assumed to be independent of time. Other assumptions will be introduced periodically throughout the text.

In the following discussions pressures will frequently be referred to. In a fluid, pressures may be either *static* or *dynamic*. The atmospheric pressure at sea level results from the weight of air above. Similarly the hydrostatic pressure on the floor of the ocean results from the weight of water and air above. These pressures are associated with stationary fluid and are properly called static pressures. Static pressure frequently results from gravitational attraction between the fluid and the earth, but it may arise in other ways. For instance, the pressure in an automobile tire is, for practical purposes, independent of gravity. Pascal's law states that static pressure acts equally in all directions; therefore, for instance, atmospheric pressure on the floor of a room is exactly the same as that acting on the walls and ceiling (ignoring the slight difference in altitude of the floor and ceiling). Dynamic pressure is associated with a fluid in motion and is evidenced by an increase in static pressure when the fluid is brought to rest. The relation between these two pressures will be discussed in the following articles.

2-1 The Perfect Fluid. In a real fluid, five¹ important forces act on the fluid and determine its equilibrium:²

1. Gravitational forces
2. Fluid pressure (static) forces
3. Compressive forces
4. Shearing (viscous) forces
5. Inertia forces

Only the first three are associated with fluids at rest, but all are present for fluids in motion. The first force is often ignored in gases, and the third is usually ignored in liquids.

One of the most drastic approximations of fluid mechanics is in the concept of a "perfect fluid," which is assumed to be *homogeneous*,³ *continuous*, *incompressible*, and *inviscid*.⁴ This hypothetical fluid is not concerned with the third and fourth forces; thus the degree to which its equations fit a real fluid depends upon the relative importance of these two forces in determining conditions of equilibrium. If the fluid is viscous, the influence of viscosity is generally confined to a region close to the body called the *boundary layer*, within which the velocity decreases rapidly, becoming zero at the body surface. The velocity gradient, by Eq. (1-26), is responsible for a shearing force that is not accounted for by perfect-fluid theory. The flow pattern outside the boundary layer of a body is predicted fairly accurately by perfect-fluid theory, provided that the actual flow does not become detached or "separated" from the body surface. If such a condition exists, the complete pattern is usually modified to such an extent that the perfect-fluid equations are entirely inadequate to describe the motion. The greater part of aerodynamics studies is con-

¹ Other forces such as surface tension, etc., are not of sufficient interest to include in a text on aerodynamics.

² The terminology used to define the five forces is commonly accepted but nonetheless ambiguous, because it depends upon the point of view. From a molecular viewpoint the second, third, and fourth forces may all be regarded as inertia forces. Usually the context makes the meaning clear.

³ Homogeneity, in the strict sense, implies continuity and incompressibility, but is used here to mean that fluid density is independent of position in a fluid at rest; whereas incompressibility is used to mean that fluid density is independent of static pressure.

⁴ A perfect fluid is frequently assumed to be homogeneous, continuous, and inviscid *but compressible*.

cerned with "streamlined" bodies which are designed specifically to maintain a flow that does not separate; hence, the perfect-fluid theory is valuable for representing these flow patterns. For cylinders, spheres, and other so-called "bluff" bodies, the equations are useful only as approximations up to the point of separation.

In nearly all fluid-dynamic studies, the fluid is assumed to be homogeneous.¹ In most aerodynamic studies it is further assumed to be continuous. The viscous and compressible properties are ignored or included according to their relative importance in a particular problem.

2.2 The Continuity Equation. A continuous tube of fluid (Fig. 2-1) under conditions of steady flow that has no transfer of

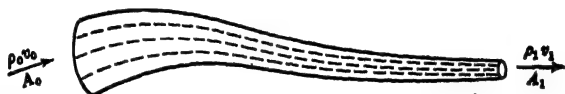


FIG. 2-1. A stream tube.

fluid across its borders is referred to as a *stream tube*. The mass of fluid leaving the stream tube every second must be the same as that entering, or

$$\rho_0 A_0 v_0 = \rho_1 A_1 v_1 \quad (2.1)$$

where A is cross-sectional area of stream tube

v is average velocity

This very important formula is called the *continuity equation*. It applies whether or not the fluid is viscous and compressible. If the fluid is incompressible, Eq. (2.1) may be simplified thus:

$$A_0 v_0 = A_1 v_1 \quad (2.2)$$

The requirement of continuity is really a specialization of the principle of conservation of matter.

2.3 The Bernoulli Equation. Consider an element of the stream tube shown in Fig. 2-2, with cross-sectional area A . If the fluid is assumed incompressible, the contraction of the stream tube in the direction of flow demands an increasing velocity by Eq. (2.2). If, in addition, the fluid is assumed inviscid, the inertia force arising from the above acceleration must be balanced

¹ This assumption is not justified for rarefied air encountered at extreme altitudes and in some supersonic tunnels.

entirely by a differential pressure across the fluid element. Denoting the upstream velocity and pressure by v and p , respectively, and the downstream velocity and pressure by $v + dv$ and $p + dp$,

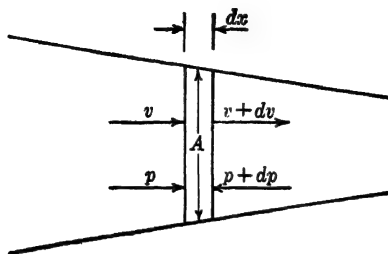


FIG. 2.2. Pressure and velocity relations on the ends of an elemental length of stream tube.

respectively, an equation may be written relating the force arising from the pressure differential and the force from inertia:

$$\begin{aligned} pA - (p + dp)A &= m \frac{dv}{dt} \\ &= \rho A \, dx \frac{dv}{dt} \\ &= \rho A v \, dv \end{aligned}$$

Simplifying the above relation yields

$$dp = -\rho v \, dv \quad (2.3)$$

whence

$$\begin{aligned} p &= -\frac{1}{2}\rho v^2 + C \\ p + \frac{1}{2}\rho v^2 &= C \end{aligned} \quad (2.4)$$

Equation (2.4) may be analyzed by inspection. Since p is a pressure, then $\frac{1}{2}\rho v^2$ and C must also have the dimensions of pressure. The quantity $\frac{1}{2}\rho v^2$ embodies a velocity and is referred to as *dynamic pressure* (also sometimes called *velocity pressure* or *impact pressure*). On the other hand, p is referred to as *static pressure*. Dynamic and static pressure are the only pressures assumed to be present in this system; consequently their sum is defined as the *total pressure*:

$$p + \frac{1}{2}\rho v^2 = H \quad (2.5)$$

or

$$p_0 + \frac{1}{2}\rho v_0^2 = p_1 + \frac{1}{2}\rho v_1^2 \quad (2.6)$$

where H is total pressure. Dynamic pressure occurs so frequently

in aerodynamics that a special symbol q has been assigned to it. In equation form

$$q = \frac{1}{2}\rho v^2 \quad (2.7)$$

where q is dynamic pressure, psf

ρ is fluid density, slug per cu ft

v is velocity, fps

Or if the fluid is air,

$$q = \frac{V^2 \sigma}{391} \quad (2.8)$$

where V is velocity, mph

σ is ratio of air density ρ to standard air density ρ_0 ,
dimensionless

Equations (2.5) and (2.6) may thus be rewritten:

$$p + q = H \quad (2.9)$$

or

$$p_0 + q_0 = p_1 + q_1 \quad (2.10)$$

Equation (2.9) is one form of the *Bernoulli equation*. It states that the sum of static and dynamic pressures is equal to the total pressure and that this total pressure is constant in any stream tube. The equation does not apply to compressible fluids, because the integration leading to Eq. (2.4) assumes that ρ is a constant, nor does it apply if the fluid is viscous, because the equation satisfying equilibrium of forces [Eq. (2.3)] does not contain a viscous force; however, the use of the Bernoulli equation for predicting static pressures on a body or in a short length of pipe involves small error, provided the velocity and velocity gradient are not too large.

A form of the Bernoulli equation that applies to compressible fluids is given in Art. 8.1.

2.4 Implications of Continuity and Bernoulli Equations. In aerodynamic work the compressible property is not important until the velocity in a stream tube is so high that the static pressure is reduced sufficiently to cause an appreciable reduction in air density. Compressible effects, therefore, are associated with comparatively high velocities, around 350 mph or higher. The viscous property of a fluid has its greatest relative importance at low speed. The inertia property is present at all speeds. For a great class of problems, the assumption that the fluid is

incompressible and inviscid does not lead to serious error, and for these problems the continuity and Bernoulli equations may be used with constant density in each.

There are a great many examples of the use of the continuity and Bernoulli equations, but perhaps the simplest and most enlightening one is the *venturi tube*, shown in Fig. 2·3. It consists of a constricted section (throat) followed by a gradual expansion. Fluid passing through the constricted region has a

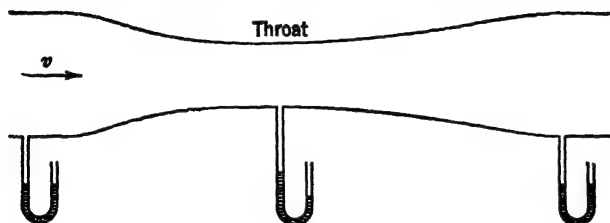


FIG. 2·3. A venturi tube. (The manometers indicate static pressure.)

high velocity, by virtue of the continuity equation, and hence a low static pressure, by the Bernoulli equation. The venturi tube has a great number of uses; for instance, on some aircraft it is used to supply a low-pressure reservoir to actuate gyroscopic instruments. Again, if the areas and difference in pressure between inlet and throat are measured, the velocity at either point may be calculated from a combination of the above two fundamental equations. In this manner the venturi tube is sometimes used to measure velocity and quantity of flow through a pipe.

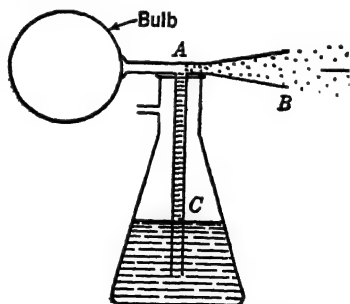


FIG. 2·4. An atomizer.

A second example is the familiar atomizer, shown in Fig. 2·4. Air in the bulb is forced through a contracted section *A* and is discharged from an expanded section *B*. Since the tube area is greater at *B* than at *A*, the velocity must be less at *B* than at *A*. Since the static pressure at *B* is atmospheric, that at *A* must be less than atmospheric. The reduced static pressure at *A* allows atmospheric pressure to force fluid from the reservoir up tube *C*, to be expelled with the air at *B*.

A third example involves finding the efflux velocity of a liquid from a tube in the bottom of a container (Fig. 2-5). The center of the opening is h feet below the free surface of the liquid. The tank

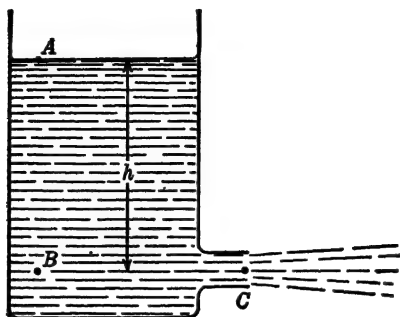


FIG. 2-5. Liquid being ejected from a tank.

is assumed large compared with the opening, so that the velocity at points A and B is assumed to be zero.

$$p_B = p_A + wh \quad (2-11)$$

where p_B is static pressure at B , psf

p_A is static pressure at A , psf

w is fluid density, lb per cu ft

From the Bernoulli equation [Eq. (2-6)] conditions at points B and C may be related, assuming a perfect fluid:

$$p_B + \frac{1}{2}\rho v_B^2 = p_C + \frac{1}{2}\rho v_C^2$$

However, $v_B = 0$; hence

$$p_B = p_C + \frac{1}{2}\rho v_C^2 \quad (2-12)$$

Since $p_A = p_C =$ atmospheric pressure, then from Eqs. (2-11) and (2-12)

$$v_C = \sqrt{2gh} \quad (2-13)$$

A final example is the *pitot tube*, conventionally used on aircraft and in research laboratories for measuring air speed. The instrument, which is shown diagrammatically in Fig. 2-6, consists of a small tube surrounded by a large one. The inner tube is open in the direction of the stream. The stream of air approaching the pitot tube in the direction indicated by v_0 is reduced to zero velocity when it reaches the opening of the small tube at point 1.

It then passes around the outer tube until, at point 2, it has attained essentially its original velocity v_0 . At this point, a hole is located in the outer tube. Applying the Bernoulli equation

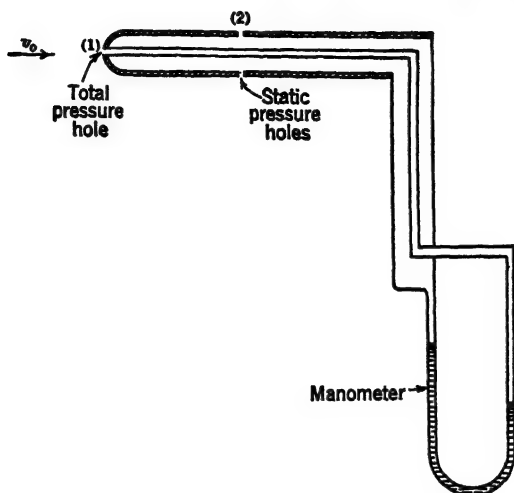


FIG. 2.6. Pitot tube connected to a manometer to indicate dynamic pressure.

to the stream tube, starting at a remote point where the static pressure is p_0 and the velocity is v_0 , gives

$$\begin{aligned} p_0 + \frac{1}{2}\rho v_0^2 &= p_1 + \frac{1}{2}\rho v_1^2 \\ &= p_2 + \frac{1}{2}\rho v_2^2 \end{aligned}$$

From the preceding explanations,

$$v_1 = 0 \quad \text{and} \quad v_2 = v_0$$

hence,

$$p_1 = p_0 + \frac{1}{2}\rho v_0^2 \quad (2.14)$$

$$p_2 = p_0 \quad (2.15)$$

Equation (2.14) shows that the static pressure at point 1 is the same as the free-stream total pressure, while Eq. (2.15) shows that the static pressure at point 2 is the same as the free-stream static pressure. Tubes *A* and *B* may thus be arranged so as to indicate the free-stream static, total, or dynamic pressures. Figure 2.6 shows tubes *A* and *B* connected to a liquid manometer, so as to measure the free-stream dynamic pressure.

2.5 Fluid Forces. The procedure by which a fluid force on a body is computed often depends upon the complexity of the par-

ticular problem. In some instances the total force is obtained by vectorial addition of all the separate forces on the body; on the other hand, it is often more direct to observe the effects the body has on the fluid and to draw conclusions as to the nature of the body forces required to produce them. Both methods of analysis will be used in the following discussions.

Some common nomenclature used to describe fluid forces may be introduced at this time. First, the term *relative velocity* is used to account for the fact that a pressure or force system is dependent, not upon the absolute velocity (how ever it may be defined), but upon the velocity relative to the point or body considered. For instance, the aerodynamic force on an airplane wing is found using the air velocity relative to the wing: it makes no difference whether the air passes over the wing or the wing passes through the air. Second, the terms *remote* and *local* are used to differentiate between conditions far upstream of a point on a body and at the point itself. For instance, air approaching a wing may have a velocity of 200 mph relative to the wing, but the air at various points on the wing surface may have relative velocities greater or less than 200 mph, dependent upon position. The former velocity is called the *remote* velocity, while the latter is called the *local* velocity. Third, on any body there must be at least one point for which the local velocity is zero. This point is called the front (upstream) *stagnation* point. By the Bernoulli equation the static pressure at the stagnation point is seen to have its maximum positive value, which is greater than the remote static by the amount of the remote dynamic; hence,

$$p_s = p_0 + q_0 \quad (2.16)$$

where subscript *s* refers to stagnation and subscript 0 refers to remote condition. For a perfect fluid, a rear stagnation point occurs downstream on the body where the velocity is again zero. For a real fluid, the growing boundary layer ultimately becomes a "wake" of reduced velocity shed from the downstream portion of the body, and the rear stagnation point does not exist.

2.6 Jets. A jet is a stream of fluid with boundaries formed by a fluid of different velocity. The boundary fluid may or may not be the same as that in the jet; for instance, the water ejected from a common garden hose gives a jet and boundary of dissimilar fluids; while a pricked balloon gives a jet and boundary of similar

fluids. A jet may be of interest because it is ejected from, or impinges on, a body; the two examples above represent the former condition while the jet that strikes the blades of a steam or gas turbine represents the latter. At any rate, an inertia force may be produced by either accelerating or decelerating the jet fluid, and this inertia force is responsible directly or indirectly for the propulsion of most fluid-borne vehicles, from tugs to space ships. For convenience in discussion, jets will be con-

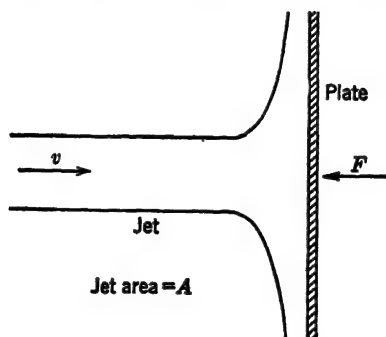


FIG. 2-7. Flat plate and normal jet.

sidered in two groups: decelerated and accelerated. A perfect fluid will be assumed unless otherwise noted.

Decelerated Jets. Let a liquid jet impinge on a stationary infinite flat plate with velocity v , as in Fig. 2-7. The jet is assumed perpendicular to the plate, and the liquid is assumed to flare smoothly along the plate surface. The force on the plate is then obtained by considering its effect in reducing the approaching jet velocity to zero. According to Newton's second law of motion,

$$F = M \Delta v \quad (2-17)$$

where the mass per second is the product of the density and the volume per second, and the change in velocity is from v to 0. The deceleration is toward the plate so that the inertia force must be in the same direction. For equilibrium, a force is required on the plate directed opposite to the approaching stream; therefore,

$$\begin{aligned} F &= (\rho A v)(v) \\ &= \rho A v^2 \end{aligned} \quad (2-18)$$

where A is the jet area. The force on the plate can also be

obtained by considering the effect of the jet in producing a distributed static pressure on the plate (Fig. 2-8). This procedure is unwieldy, however, because first the equation for the pressure distribution must be obtained, and then the product of an elemental area and its local static pressure must be integrated.

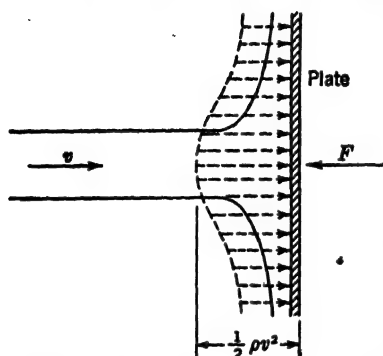


FIG. 2-8. Flat plate and normal jet, showing static pressure distribution.

Its use seems to be unjustified in view of the simplicity of the inertia method. Notice that the force happens to be twice the product of the dynamic pressure and the jet area, but this result could not have been anticipated from consideration of dynamic pressure alone.

If the plate is moving at constant velocity with respect to the ground, the jet force is found by using velocity and mass per second relative to the plate. The ground is only a convenient reference.

Example. A square flat plate is set perpendicular to a jet of water that is moving at 10 mph with respect to the earth. The plate is moving toward the jet with a velocity of 5 mph with respect to the earth. If the jet area is 2 sq ft and the plate area is 100 sq ft, what hydraulic force is acting on the plate?

Solution. The velocity of the jet relative to the plate is 15 mph, or 22 fps. The plate area has nothing to do with the problem, except to show that the plate is large compared to the jet. By Eq. (2-18),

$$\begin{aligned} F &= \rho A v^2 \\ &= (1.94)(2)(22)^2 \\ &= 1880 \text{ lb} \end{aligned}$$

In Fig. 2-9 another situation is depicted: a long ribbonlike jet of area A approaches and leaves a semicircular plate tangentially. The scalar magnitudes of the velocity approaching and leaving the plate are assumed equal. The force can be found in the same manner as in the preceding problem. The change in velocity is from $+v$ to $-v$; hence

$$\begin{aligned} F &= M \Delta v \\ &= (\rho A v)(2v) \\ &= 2\rho A v^2 \end{aligned} \quad (2-19)$$

This problem may also be treated by assuming the approaching stream to be reduced to zero velocity and the returning stream to start from zero velocity; *i.e.*, the inertia force of the approaching stream is directed toward the plate in a direction opposite that of the acceleration (in the same direction as the deceleration), and the inertia force of the returning stream is also directed toward the plate, because it must also be opposite the acceleration. The total force, composed of the vector sum of the two separate forces, is identical to that obtained in Eq. (2-19). This procedure is justified because the over-all force is being found; the history of the particles of fluid from the time they enter the system until they leave is entirely unimportant.

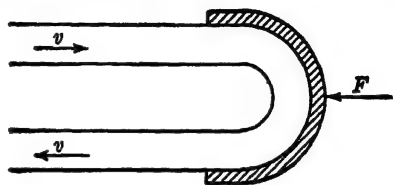


FIG. 2-9. Curved plate and jet.

Consider the system shown in Fig. 2-10. Here the change in velocity is represented most conveniently by vectors (Fig. 2-10a).

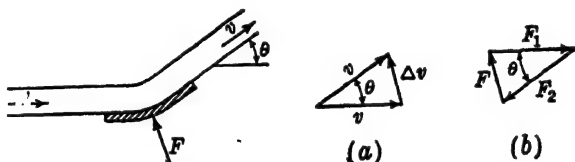


FIG. 2-10. Curved plate and jet.

The leaving stream is in a direction different from the approaching stream, but the change in velocity may be found as a function of the angle between the two. (The scalar magnitudes of the velocity approaching and leaving the plate are again assumed equal.)

$$\begin{aligned}
 F &= (\rho Av)(\Delta v) \\
 &= (\rho Av) \left(2v \sin \frac{\theta}{2} \right) \\
 &= 2\rho Av^2 \sin \frac{\theta}{2}
 \end{aligned} \tag{2-20}$$

The problem can also be solved by assuming that the fluid, originally at velocity v , is reduced to zero velocity, then changes direction and accelerates to velocity v again. Two forces cor-

responding to the two accelerations are determined, and the problem is solved vectorially. Thus, in Fig. 2·10*b*, F_1 is the horizontal force resulting from deceleration of the approaching stream; F_2 is the inclined force resulting from acceleration of the leaving stream; and F is the reaction force required to close the force triangle.

In the two preceding conditions the plate was tangential to the approaching stream. Figure 2·11 shows a different situation:

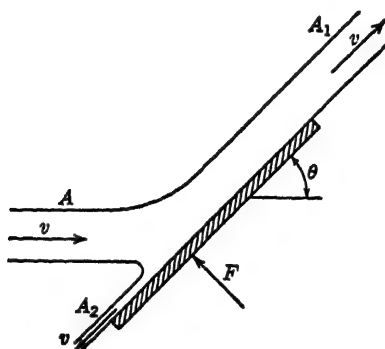


FIG. 2·11. Flat plate and jet.

in order that the sum of all forces parallel to the plate may be zero, some of the fluid must travel in both directions along the plate. Summing forces parallel to the plate gives

$$\begin{aligned}\rho A v^2 \cos \theta + \rho A_2 v^2 &= \rho A_1 v^2 \\ A \cos \theta + A_2 &= A_1\end{aligned}$$

From the continuity equation,

$$\begin{aligned}A v &= A_2 v + A_1 v \\ A &= A_2 + A_1 \\ A \cos \theta + A_2 &= A - A_2\end{aligned}$$

$$A_2 = \frac{A}{2} (1 - \cos \theta) \quad (2\cdot21)$$

$$A_1 = \frac{A}{2} (1 + \cos \theta) \quad (2\cdot22)$$

From the above equations, the areas of the two jets, A_1 and A_2 , are seen to be a function only of the initial area and the

angle of inclination of the plate. The force on the plate is obtained by summing forces that are perpendicular to the plate:

$$F = \rho A v^2 \sin \theta \quad (2.23)$$

Decelerated jets may also arise because no fluid is perfect; i.e., a bluff or streamlined body immersed in a moving stream of real fluid sheds a wake that may be regarded as a decelerated jet. The inertia force on the body is called *drag*. The drag on a bluff

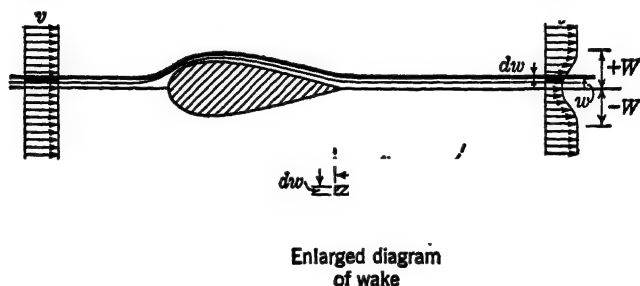


FIG. 2-12. Flow over a streamlined strut or wing showing the velocity distribution within the wake.

body is not always amenable to simple solution by investigation of the wake, because the wake velocity is frequently periodic, but on a streamlined body the drag is readily obtained by integration (Fig. 2-12).

$$\begin{aligned} D &= \int dM \Delta v \\ &= b \rho \int_{-W}^{+W} v_w (v - v_w) dz \end{aligned} \quad (2.24)$$

where D is drag, lb

b is span of body (into the paper), ft

dM is differential mass flow, slug per sec

v is remote velocity (constant), fps

v_w is wake velocity (variable), fps

dw is differential wake width corresponding to v_w , ft

The principal use of the above drag relation is in experimental applications. A wing, for instance, may be tested in a wind tunnel or in flight, and the distribution of velocity in the wake may be found by using a number of total-pressure tubes (the static pressure being assumed constant across the wake). The drag may then be found from Eq. (2.24) by graphical integration.

A word of caution must be inserted regarding the choice of station for which the wake measurements are to be made: This analysis is not concerned with the actual shearing and pressure forces that act on the body surface; it is an indirect procedure by which the effect of the body on the fluid is investigated. The particular force being determined is an inertia force; hence if the wake static pressure is not equal to the remote static pressure, the resulting pressure differential is responsible for a force that must be accounted for in the calculations. *The complication may be avoided by always choosing the wake or jet station sufficiently far downstream so that the static pressure is essentially equal to the remote value.*

The preceding discussion might appear to conflict with the Bernoulli equation since the wake can have a transverse velocity gradient but constant static pressure downstream of the body, and, at the same time, have a constant velocity and static pressure upstream. The explanation lies in the fact that the Bernoulli equation applies strictly to a perfect fluid, but the wake contains all the manifestations of fluid viscosity. From the standpoint of equilibrium of forces, there can be no transverse static-pressure gradient through the wake unless some other force exists coincidentally, *i.e.*, a centrifugal force arising from curvature of the flow. The sum of the static and dynamic pressures does show that the total pressure is least in the center of the wake, as might have been anticipated, since the viscous effects are predominant in that region.

Accelerated Jets. Let a jet be exhausted with velocity v_j from a container that contains all its constituents; the jet discussed in the third example in Art. 2·4 and that ejected from a rocket are two simple examples. The force on the container, called the *thrust*, results from acceleration of the jet fluid, and is given in a manner similar to the preceding examples. If the transverse jet velocity is assumed constant,

$$\begin{aligned} T &= M \Delta v \\ &= \rho A v_j^2 \end{aligned} \quad (2\cdot25)$$

where T is thrust, lb

A is jet area, sq ft

v_j is jet velocity with respect to container, fps

The same remarks regarding the necessity for choosing a station

for which the static pressure is equal to the remote value should be made here; for example, let water in the tank of Fig. 2-13 be ejected from a sharp-edged orifice. The water is unable to execute the 90-deg turn at the orifice; consequently it is exhausted in a tube of decreased area. This is called a *vena contracta* or region of reduced area. The velocity at the reduced area is a maximum, and this maximum velocity must be used in Eq. (2-25), along with the minimum area.

It is interesting to notice that the static pressure on the boundary of the jet is constant and is equal to the atmospheric pressure, but that it must increase from the boundary to the center of the jet if the streamlines are curved, *e.g.*, near the orifice. This variation in static pressure is required to balance the centrifugal force on each fluid particle. Evidently, as soon as the fluid boundaries become parallel, both the velocity and static pressure must be constant across the jet. It is clear that computation of the jet force is simplified by choosing a station so far removed from the orifice that the jet velocity is constant.

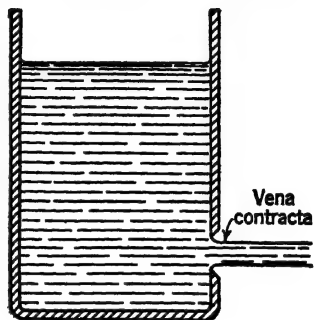


FIG. 2-13. Liquid being ejected from a tank through a sharp-edged orifice to illustrate a vena contracta.

If the container had been moving with constant velocity with respect to the ground, the thrust given by Eq. (2-25) would be unchanged, provided that the mass flow and velocity were chosen with respect to the container. If the container had been immersed in a tank of an arbitrary gas, the thrust would again be computed by Eq. (2-25). An important conclusion may, therefore, be stated: The thrust arising by expulsion of fluid from a container is independent of the relative velocity and physical characteristics of the fluid medium through which the container moves. This statement assumes that the change in medium properties is not accompanied by a change in the pressure difference between the inside and outside of the container.

Attention is now directed to the type of jet that arises from acceleration of the fluid medium in which the body is immersed. A propeller and a jet-propulsion unit are two familiar examples. This problem is the antithesis of the wake problem discussed

earlier: here energy is added to the fluid where previously it was subtracted.

Let a propeller operate in a moving fluid as shown in Fig. 2-14. The purpose of the propeller is to accelerate a quantity of air per second; hence, the slip-stream velocity v_s is greater than the remote velocity v_0 . The affected air is represented by a tube, having a constant velocity at any cross section, whose area

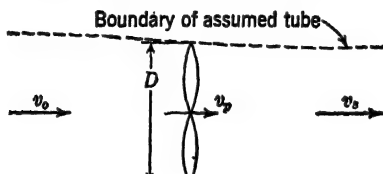


FIG. 2-14. Representative tubular flow of air assumed to be affected by a propeller.

decreases in the direction of flow according to the continuity equation. The thrust on the propeller is obtained by

$$T = \rho A v (v_s - v_0) \quad (2-26)$$

The mass flow represented by $\rho A v$ can be calculated at any convenient station, but usually is given in terms of the propeller disk area and velocity

$$T = \rho A_p v_p (v_s - v_0)$$

or

$$T = \rho \frac{\pi D^2}{4} v_p (v_s - v_0) \quad (2-27)$$

where D is propeller diameter, ft

v is velocity, with subscripts p , s , and 0 indicating propeller disk, slip-stream, and remote, respectively, fps. Here again the slip-stream velocity must correspond to a station for which the static pressure is identical to the remote value.

Let a jet-propulsion unit operate with a velocity v_0 relative to air. If the added exhaust gases are ignored, the thrust equation is the same as Eq. (2-26). The mass flow may be computed at any convenient station, but if the exhaust region is chosen, care must be exercised to account for the change in ρ resulting from

the high exhaust temperature. If the mass flow of the added exhaust gases is not ignored, it can be accounted for as an expulsive jet; hence

$$T = M_a(v_s - v_0) + M_f v_s \quad (2\cdot28)$$

where M_a is mass flow of air, slug per sec

M_f is mass flow of fuel, slug per sec

Once again the static pressure at the chosen station in the slip stream must be the same as the remote value.

2·7 Body Pressure Distribution for a Perfect Fluid. The

forces produced by jets have been determined by use of Newton's second law of motion. Each problem presented could have been solved by computing the shearing and static-pressure forces acting at all points on the body and integrating to find the total force, but the method obviously presents tremendous difficulties.

Nevertheless, it is only through an appreciation of the distribution of pressure and shearing stress that the variation of dynamic forces with changes in body configuration and fluid properties may be understood. As an introduction to this phase of the study, pressure distributions on certain simple bodies immersed in a perfect fluid will be discussed. Explanations of fluid phenomena will frequently be simplified by considering two-dimensional flow, *i.e.*, flow in which all particles of fluid remain in parallel planes as they pass over the body. Thus the flow over a cylinder whose axis is perpendicular to the remote velocity is two-dimensional except at the ends, whereas the flow over a sphere is three-dimensional everywhere.

Cylinder Pressures. Let a stationary cylinder be immersed in a moving perfect fluid, the flow pattern of which is depicted in Fig. 2·15. The spacing of the streamlines indicates the magnitude of the velocity; *i.e.*, by the continuity equation velocity is inversely proportional to area in a stream tube; hence closely spaced streamlines indicate a high velocity, and vice versa.

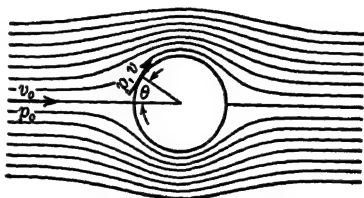


FIG. 2·15. Streamlined flow over a cylinder in a perfect fluid.

Theoretically, the velocity at any point on the surface of a cylinder is given by

$$v = 2v_0 \sin \theta \quad (2-29)$$

where v_0 is remote velocity

θ is angle measured from the front stagnation point, deg

According to the Bernoulli equation,

$$p_0 + \frac{1}{2}\rho v_0^2 = p + \frac{1}{2}\rho v^2 \quad (2-30)$$

or

$$p - p_0 = \frac{1}{2}\rho(v_0^2 - v^2) \quad (2-31)$$

Substituting Eq. (2-29) in Eq. (2-31) yields

$$p - p_0 = q_0(1 - 4 \sin^2 \theta) \quad (2-32)$$

Equation (2-32) gives the pressure differential from the remote value as a function of position on the cylinder surface. A graphical representation is given in Fig. 2-16. Vectors pointing toward the surface indicate positive pressures,¹ and vectors pointing away from the surface indicate negative pressures. Vector lengths represent pressure magnitudes. Since the static pressure is symmetrically distributed, no force acts on the cylinder; *i.e.*, integration of all pressure forces gives zero resultant force. The existence of a force in a real fluid is directly chargeable to its viscosity, which not only causes fluid shear at the surface but also modifies Eq. (2-29), causing dissymmetry of the pressure distribution.

Equation (2-32) can be put in nondimensional form:

$$C_p = \frac{p - p_0}{q_0} = 1 - 4 \sin^2 \theta \quad (2-33)$$

where C_p is a dimensionless *pressure coefficient*. The advantage of the coefficient is that its magnitude depends only upon the surface position on the cylinder; hence, it is unaffected by changes in ρ or v_0 . At the same time it shows the same variation with θ that $p - p_0$ shows at constant q_0 . This nondimensional form of equation will be used repeatedly throughout the text, because the coefficients so formed reduce the number of variables in an equation. Usually, as in the present case, the nondimensional

¹ It is customary to refer static pressures to the remote static pressure; thus a positive pressure means a pressure rise.

coefficient may be thought of as a ratio of two quantities having the same dimensions.

Sphere Pressures. The flow on a cylinder has been given as an example of the procedure used to obtain pressure distribution on a body. It was chosen because of its two-dimensional flow characteristics. If a sphere had been chosen, the pressure distribution could have been obtained in a similar manner from the equation for velocity at any point on the sphere surface:

$$v = \frac{3}{2} v_0 \sin \theta \quad (2.34)$$

Streamlined-body Pressures. The cylinder and sphere are examples of bodies for which simple mathematical expressions define the surface velocity and pressure distribution for perfect-fluid flow. Such bodies are rare. The procedure necessary to define the pressure distribution on most bodies is unusually complicated when approached from a purely theoretical standpoint. For this reason experimental evidence is relied upon very heavily. The symmetrical streamlined airfoil depicted in Fig. 2-17 has front and rear stagnation points for

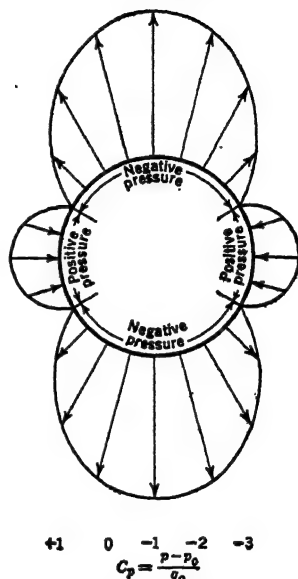


Fig. 2-16. Pressure distribution on a cylinder in a perfect fluid.



Fig. 2-17. Streamlined flow over an airfoil in a perfect fluid.

which the relative velocity is zero and the static pressure is equal in magnitude to q_0 , like the cylinder. Unlike the cylinder, however, the highest velocity, and hence the lowest static pressure, does not necessarily occur at the point of maximum thickness. It may occur forward or rearward depending upon the section

shape. Figure 2-18¹ shows the velocity and pressure distribution for a typical airfoil section. Figure 2-19 shows the static-pressure distribution plotted on the airfoil surface in a manner similar to that used for the cylinder. The resultant force on the streamlined body is again zero for the perfect-fluid condition considered.

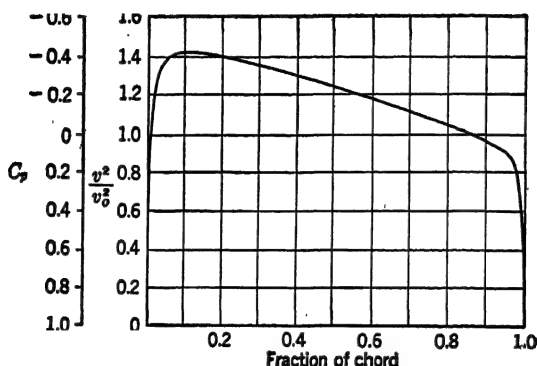


FIG. 2-18. Pressure and velocity distribution on an airfoil in a perfect fluid. (NACA 0012 airfoil from WR L-560.)

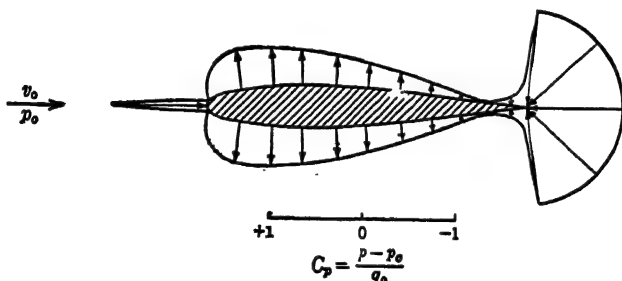


FIG. 2-19. Pressure distribution on an airfoil in a perfect fluid (from Fig. 2-18).

2-8 Body Pressure Distribution for a Real Fluid. Perfect-fluid theory gives a foundation for the study of real fluids. The principal deviation from the characteristics of a perfect fluid is caused by fluid viscosity at relatively low speed and by gaseous compressibility at relatively high speed (above 300 to 400 mph for air at sea level).

Fluid viscosity is responsible for a thin layer of retarded flow, called the boundary layer, that is immediately adjacent to a

¹ Figures 2-18 and 2-19 are based on actual calculations for a conventional wing section.

wetted¹ surface. Through this boundary layer the fluid shearing stress is transmitted, producing a force called *skin friction* on the body. The boundary layer further causes a modification to the flow pattern that disrupts the static-pressure equilibrium predicted by perfect-fluid theory, and thereby produces a pressure force called *form drag*. Streamlined bodies are characterized by a larger proportion of skin friction than form drag (about 70 to 90 per cent for the usual strut or wing section), whereas bluff bodies are characterized by a relatively large proportion of form drag. A flat plate parallel to the remote-velocity vector is an example of pure skin friction, while in the perpendicular or normal attitude it is an example of pure form drag. Some bodies, notably cylinders, spheres, thick strut sections, etc., may act like either streamlined or bluff bodies, depending upon the combination of some very important variables to be discussed later (Art. 2-9); hence, a pattern of the streamlines and the corresponding

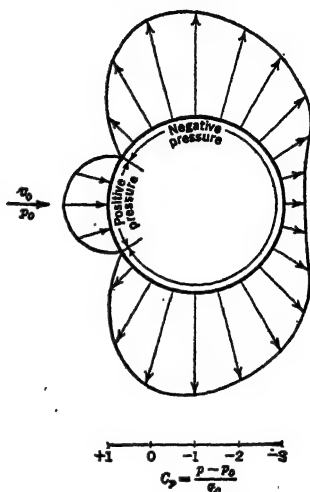


FIG. 2-20. Pressure distribution on a cylinder in an actual fluid.

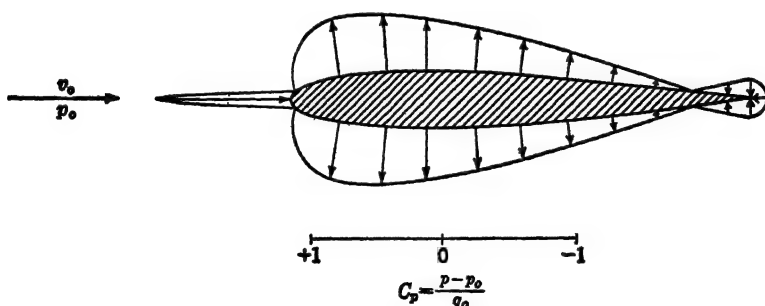


FIG. 2-21. Pressure distribution on an airfoil in an actual fluid.

pressure distribution may be shown only for a particular set of conditions. In Fig. 2-20 is shown a representative pressure

¹ The word "wetted" may be used irrespective of whether the fluid is liquid or gaseous.

distribution for a cylinder operating in a real fluid; the difference in the character of flow as compared with a perfect fluid (Fig. 2-16) is apparent. Figure 2-21 shows the pressure distribution on the wing section of Fig. 2-19, for a real fluid. The major discrepancy is seen to occur at the wing trailing edge, where the pressure fails to rise to the stagnation value shown in Fig. 2-19.

Gaseous compressibility causes variations in density corresponding to changes in static pressure. Large changes in static pressure are characteristics of high speed, and fortunately in this region viscous phenomena are of secondary importance; hence, viscous effects may be ignored temporarily, in order to focus attention on compressible phenomena alone.

The complete equation of continuity is, from Eq. (2-1),

$$\rho_0 A_0 v_0 = \rho_1 A_1 v_1 \quad (2-35)$$

where subscripts merely indicate two stations along a particular stream tube that might be part of the flow through a pipe, or past a wing, etc. Let such a stream tube be considered in which the downstream velocity v_1 is large compared with the upstream velocity v_0 . Since dynamic pressure is dependent upon the square of the velocity, q_1 is also relatively large; hence by the Bernoulli equation, static pressure p_1 is correspondingly small, and this implies a low density.¹ In Eq. (2-35), therefore, ρ_1 is less than ρ_0 when v_1 is greater than v_0 . A peculiar situation arises when v_1 reaches sonic speed (speed of sound): for any further increase in velocity downstream of station 1, the density decreases so rapidly that the area must *increase* to compensate. In other words, *for supersonic conditions* (above the speed of sound), *stream tubes must expand for increasing velocity*. Consider the wing in Fig. 2-22 for which the remote velocity v_0 is subsonic (less than the speed of sound) but of just sufficient magnitude to produce sonic speed a at point A. The shape of the wing is such that it produces expanding stream tubes downstream of point A, which by the previous reasoning *could* give supersonic flow. Let v_0 be increased (but still be subsonic) so as to produce this condition. Ultimately, regardless of supersonic conditions on the wing, there must be a return to the original subsonic flow downstream from the wing. The incompatibility of the super- and subsonic conditions results in an abrupt transformation, through a region of discontinuity

¹ This is a very loose argument. A rigorous analysis is given in Art. 8-2.

of density, pressure, temperature, and velocity, called a *shock wave*. Naturally the pressure distribution, and consequently the force system on the wing, is considerably modified by the *compressibility burble*, or region of disturbed flow, produced by the shock. Compressible effects are present at all speeds and should properly be accounted for, but their predominant importance is not felt until some point on a body reaches the speed of sound,

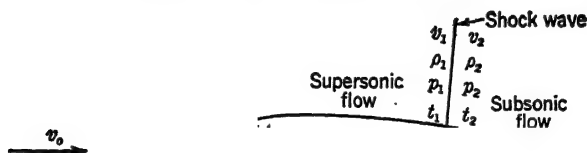


FIG. 2-22. Shock-wave formation on an airfoil at high subsonic speed.

because only under these circumstances is the flow likely to break down.

When the remote velocity itself is supersonic, a head wave similar to the bow wave on a boat is set up at the most forward point on the body. The velocity of the body is greater than that with which pressure waves are propagated through the atmosphere; consequently there is a superimposition of compression waves near the leading edge of the body that produces a refraction of the flow pattern and gives a flow that is radically different from that predicted by perfect-fluid theory.

The history of events on a wing or streamlined section from subsonic, through transonic, to supersonic¹ conditions depends primarily upon the shape of body. The optimum shape for each of the three regimes is, unfortunately, different, the blunt leading edge being characteristic of subsonic design (e.g., a conventional wing), and the sharp leading edge being characteristic of supersonic design (e.g., a rocket).

2-9 The General Force Equation. The general equation for force on any body immersed in a moving fluid is dependent upon several variables. A possible form for the equation is suggested by a mathematical procedure called *dimensional analysis*.

¹ Subsonic, transonic, and supersonic flows are frequently specialized to mean, respectively, conditions on a body for which the velocity is everywhere less than the speed of sound, partially greater than the speed of sound, and everywhere greater than the speed of sound.

In any physical equation, the dimensions on both sides of the equal sign must be the same. For most problems in aerodynamics, these dimensions may be expressed in terms of mass, length, and time, symbolized by M , L , and T , respectively. For instance, in the simple equation

$$\tau = \mu \frac{dv}{dy}$$

the dimensions for the variables are

$$\tau : \frac{M}{LT^2}$$

$$\mu : \frac{M}{LT}$$

$$\frac{dv}{dy} : \frac{1}{T}$$

hence the dimensions on both sides of the equality are identical. This principle applies regardless of the type of equation. For instance, if the equation is a summation, the dimensions of the quantities added together must be identical. Or, again, if the equation is in differential or integral form, the dimensions must be consistent on both sides of the equation, with due regard for the possibility of certain constants being dimensional. The principle allows solution of an equation for which the general form, but not the exponents, is known. The following example will illustrate the method.

To determine the equation for frequency of a simple pendulum, the variables involved that would be expected to enter into the equation are length and mass of the pendulum and acceleration of gravity. A general but arbitrary relationship may be written.

$$\nu = Kl^a m^b g^c \quad (2-36)$$

where ν is frequency, with dimension $1/T$

K is a constant, dimensionless

m is mass of pendulum bob, with dimension M

l is length of pendulum, with dimension L

g is acceleration of gravity, with dimension L/T^2

a, b, c are unknown exponents, dimensionless

Because the dimensions must be identical on the two sides of the equation,

$$\left[\frac{1}{T} \right] = \left[L^a \right] \left[M^b \right] \left[\frac{L^c}{T^{2c}} \right]$$

Equating the exponents of like variables gives

$$\begin{aligned} M : b &= 0 \\ T : 1 &= 2c \\ c &= \frac{1}{2} \\ L : a &= -c = -\frac{1}{2} \end{aligned}$$

hence the desired equation is

$$v = K \sqrt{\frac{l}{g}}$$

By experiment, K could be shown to have the value 2π . Of course, in the particular example, this method of solution is hardly justified, since the frequency of a simple pendulum is much more readily determined by other mathematical means that give not only the general equation but also the exact value for the constant. Notice that the assumption as to the form of the original equation limits the possible type of solution; *e.g.*, Eq. (2-36) could not lead directly to a summation or to a trigonometric or logarithmic equation.

In the above example there were three unknown exponents corresponding to the three fundamental units; *i.e.*, the exponents of the three variables l , m , and g could be solved because there are three fundamental units: mass, length, and time. In a more complicated problem there may be more than three variables, hence more than three exponents, and consequently more unknown quantities than there are equations to determine these unknowns. In this case, one or more exponents must remain unknown in the final equation. The three exponents that are to be obtained absolutely as fractions or integers in the final equation are usually the exponents of the three *most important* variables. With these general statements, attention may be directed to the solution of the general fluid-force equation in which inertia, viscous, and compressible effects are all present. The following equation may be assumed, with exponents to be determined:

$$F = K \rho^a l^b v^c \mu^d a^e \quad (2-37)$$

where K is a constant that depends on shape of body, dimensionless

ρ is mass density, slug per cu ft

l is a characteristic length of body, ft

v is relative fluid velocity, fps

μ is coefficient of viscosity, slug per ft-sec

a is speed of sound, fps

Substituting dimensions, as before, and equating gives

$$\left[\frac{ML}{T^2} \right] = \left[\frac{M^\alpha}{L^{3\alpha}} \right] \left[L^\beta \right] \left[\frac{L^\gamma}{T^\gamma} \right] \left[\frac{M^\delta}{L^\delta T^\delta} \right] \left[\frac{L^\epsilon}{T^\epsilon} \right]$$

Equating exponents of like variables yields

$$\left. \begin{aligned} M : 1 &= \alpha + \delta \\ L : 1 &= -3\alpha + \beta + \gamma - \delta + \epsilon \\ T : 2 &= \gamma + \delta + \epsilon \end{aligned} \right\} \quad (2.38)$$

Since fluid forces are usually expressed in terms of ρ , l , and v , their exponents will be determined absolutely. By simultaneous solution of Eqs. (2.38) in terms of δ and ϵ ,

$$\left. \begin{aligned} \alpha &= 1 - \delta \\ \gamma &= 2 - \delta - \epsilon \\ \beta &= 2 - \delta \end{aligned} \right\} \quad (2.39)$$

Substituting Eq. (2.39) in Eq. (2.37) and separating known and unknown exponents gives

$$F = K \rho v^2 l^2 \left(\frac{\rho v l}{\mu} \right)^{-\delta} \left(\frac{v}{a} \right)^{-\epsilon} \quad (2.40)$$

Equation (2.40) is one form of the general force equation. It shows that in addition to being dependent upon ρ , v^2 , and l^2 as might have been anticipated, the fluid force is also dependent upon two nondimensional parameters raised to unknown exponents. The first combination of terms is called *Reynolds number* R after Osborne Reynolds, who originated it, and the second is called the *Mach number* M after Ernst Mach, for the same reason; hence

$$R = \frac{\rho v l}{\mu} = \frac{v l}{\nu} \quad (2.41)$$

$$M = \frac{v}{a} \quad (2.42)$$

where ν is kinematic coefficient of viscosity. Substituting Eqs. (2-41) and (2-42) in Eq. (2-40) yields

$$F = K\rho\nu^2 R^{-\delta} M^{-\epsilon} \quad (2-43)$$

In order to simplify notation, Eq. (2-43) is written in the following form:

$$\begin{aligned} F &= C_F (\frac{1}{2}\rho\nu^2 l^2) \\ &= C_F q A \end{aligned} \quad (2-44)$$

where C_F is nondimensional force coefficient that depends upon body shape, Reynolds number, and Mach number

q is dynamic pressure, psf

A is representative area, sq ft

Experience has taught that Reynolds number is the important criterion for low-speed operation and that Mach number is important for high-speed operation; consequently, the two influences may be discussed separately.

First consider low speeds, for which compressible phenomena are unimportant; therefore C_F is independent of M and is dependent on K and δ . If these latter two constants can be found either mathematically or experimentally, the force equation for the body is solved. Usually the mathematical solution presents great difficulties, so that experiment is relied upon almost without exception. The experimental information is usually plotted as $\log C_F$ vs. $\log R$, from which K and δ can be simply extracted. Of considerable importance is the fact that *a curve of this sort is universally applicable for all fluids at all speeds, for any body that is geometrically similar to the one used to establish it.* For example, C_F is the same for a 2-in. sphere in water as it is for a 10-ft sphere in air, *provided the Reynolds number is the same.* This single important fact provides the basis for a considerable portion of all hydro- and aerodynamic testing.

In setting up the original force equation, an unjustified assumption was made as to its general form [Eq. (2-37)]. There was no particular reason, for instance, to assume that it should not be in the form of a summation. This implies that the constant K and the exponent δ could themselves be functions of R ; furthermore, they might even be discontinuous functions; consequently, the actual variation of C_F with R might consist of curved lines or even be discontinuous. These peculiarities actually do show

up in experimental data, but this does not contradict the principles involved, because the discontinuities, for instance, show up in all fluids for all geometrically similar bodies at the same Reynolds number.

Next consider high speeds, for which viscous phenomena are relatively unimportant, so that C_F may be considered independent of R . The same remarks that were made for the Reynolds number criterion may be made for Mach number; *i.e.*, a plot of C_F vs. M for a particular body is applicable to all bodies of that shape in any gas. For instance, C_F is the same for a 10-in. model of a guided missile tested in a wind tunnel in Freon gas as for the full-scale missile at 20,000 ft altitude, *provided the Mach number is the same*. This fact is the basis for all high-speed aerodynamic testing.

It should be noted that dimensional analysis produces an equation whose form could be anticipated by inspection. For instance, in Eq. (2-40), the group of terms $\rho v^2 l^2$ has the same dimensions as F , and the other two groups of terms $\rho v l / \mu$ and v/a are both nondimensional.

The form of the nondimensional groups could be anticipated because each contains one and only one variable not contained in the dimensional group, namely, μ and a in the above example. Furthermore, the exponent of this variable becomes the exponent of the nondimensional group (δ and ϵ in the example). Frequently, therefore, the final equation can be written by inspection. For example, the original equation [Eq. (2-37)] could be extended by considering the general force equation for a body that is subjected not only to all the forces given but also to that of gravity. This would lead to

$$F = K' \rho^\alpha l^\beta v^\gamma \mu^\delta a^\epsilon g^\eta \quad (2-45)$$

where g is acceleration of gravity, fps per sec

η is unknown exponent, dimensionless

By inspection, the only possible combination of p , v , and l that has the same dimensions as g is v^2/l ; hence the solution is

$$F = K' \rho v^2 l^2 \left(\frac{\rho v l}{\mu} \right)^{-\delta} \left(\frac{v}{a} \right)^{-\epsilon} \left(\frac{v^2}{l g} \right)^{-\eta} \quad (2-46)$$

The last parameter is called *Froude number* G .

$$G = \frac{v^2}{l g} \quad (2-47)$$

The Froude number generally has little aerodynamic interest but is of considerable importance in ship design, where gravitational (wave) forces are the primary determinant of the total force.

Any dimensionless quantity may be regarded as a ratio of two quantities having the same dimension. For example, Reynolds number may be given physical significance by multiplying numerator and denominator by vl :

$$R = \frac{\rho v^2 l^2}{\mu vl} \quad (2·48)$$

The numerator is then proportional to the *inertia* force, while from Eq. (1·26) the denominator may be shown proportional to the *viscous* force on the body; hence

$$R \propto \frac{\text{inertia force}}{\text{viscous force}} \quad (2·49)$$

Tests run on two geometrically similar bodies, tested perhaps in different fluids at different speeds, must have the same ratio of inertia to viscous forces if the Reynolds number is the same in the two tests. This implies that the flow pattern on the two bodies is geometrically similar at the same Reynolds number, so that, for instance, photographs of the flow patterns about the two bodies would be identical when reduced to the same scale.

Similar statements could be made regarding Mach number:

$$M \propto \frac{\text{inertia force}}{\text{compressive force}} \quad (2·50)$$

and regarding Froude number:

$$G \propto \frac{\text{inertia force}}{\text{gravitational force}} \quad (2·51)$$

The Froude-number criterion is associated with aerodynamic phenomena that are outside the realm of everyday aerodynamics, and is therefore not included in the general force equation.

2·10 The General Moment Equation. Of considerable interest is the moment about some arbitrary point produced by the general force given by Eq. (2·43). The moment equation may be stated without proof from dimensional considerations.

$$M = K'' \rho v^2 l^3 R^{-\lambda} M^{-\Gamma} \quad (2·52)$$

where K'' is new shape coefficient, dimensionless

λ and Γ are new exponents of Reynolds number and Mach number

The dimensionless quantities in Eq. (2-52) may be combined.

$$M = C_m q A l \quad (2-53)$$

where C_m is nondimensional moment coefficient like the force coefficient C_F

l is representative length

2-11 Principal Aerodynamic Forces and Moments. In order to determine conditions of static equilibrium on an arbitrary body immersed in a moving fluid, three mutually perpendicular aerodynamic force and moment components must be known. Of

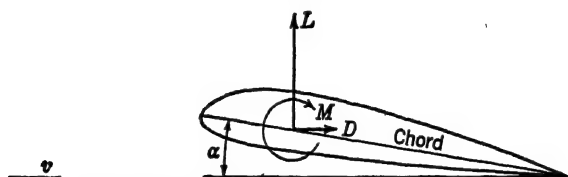


FIG. 2-23. Positive lift, drag, pitching moment, and angle of attack on an airfoil.

these six components, three have particular significance: the *lift* force L , perpendicular to the remote-velocity vector; the *drag* force D , parallel to the remote-velocity vector; and the *pitching moment* M , in the plane that contains the lift and drag. Positive-sign convention is shown in Fig. 2-23, where the lift, drag, and moment are shown on an airfoil. On an airplane the three components have particular significance, because in level flight the lift counteracts its weight, the drag counteracts its thrust, and the moment about the center of gravity (cg) is zero. Equations (2-44) and (2-53) may be used to define the following equations for a wing or airplane:

$$L = C_L q S \quad (2-54)$$

$$D = C_D q S \quad (2-55)$$

$$M = C_m q S c \quad (2-56)$$

where C_L is lift coefficient, dimensionless

C_D is drag coefficient, dimensionless

C_m is pitching moment coefficient, dimensionless

q is dynamic pressure, psf

S is projected wing area, sq ft

c is wing chord, ft or in.

The choice of wing area and chord as representative area and length in these equations is entirely arbitrary but thoroughly standardized (for exact definitions of wing area and chord, see Art. 3-3).

Lift, drag, and pitching moment and the corresponding coefficients depend upon the shape, Reynolds number, and Mach number of the particular body considered. For an airfoil section these variables may be listed as follows:

1. Shape
 - a. Angle of attack, α
 - b. Airfoil section
 - c. Plan form
 - d. Aspect ratio [see Eq. (3-2) for definition]
2. Reynolds number
3. Mach number

The influence of all variables except lc and d must generally be obtained from experiments. Tests on a particular wing or airfoil are customarily conducted in a wind tunnel at constant air speed or dynamic pressure which, for constant temperature and static pressure in the test section, implies constant Reynolds number and Mach number. The data are customarily given in the form of C_L , C_D , and C_m vs. α , or C_D , α , and C_m vs. C_L , according to convenience.

In the next two chapters nomenclature and experimental facilities will be described; Chap. 5 will then return to a discussion of the use of the aerodynamic coefficients developed in this chapter.

PROBLEMS

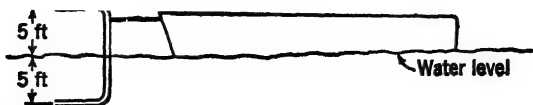
2-1. Find the quantity of air (lb per sec) passing through the test section of a 10-ft-diameter wind tunnel, if the temperature $t = 115^\circ\text{F}$, the pressure $p = 30.5$ in. of mercury, and the velocity $V = 250$ mph. (Standard $\rho = 0.002378$ slug per cu ft.)

2-2. Find the dynamic pressure in the test section of Prob. 2-1.

2-3. A tube contracts from a cross-sectional area $A_1 = 600$ sq ft to $A_2 = 120$ sq ft. The corresponding static pressures are $p_1 = 16.0$ psi and $p_2 = 14.7$ psi. Find the velocity v_2 (fps) at the contracted section. Assume standard air density, and assume a perfect fluid.

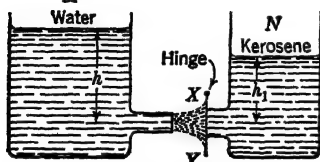
2-4. To the front end of a boat is attached a U-shaped hollow tube, partly submerged, so that the lower end of the tube faces forward into the water, and the upper end faces forward into the air as shown. The

upper and lower ends of the tube are 5 ft above and below the water surface, respectively. If the boat is moving forward at 10 mph with respect



to the water, what is the level of the water in the tube with respect to the external water level? Assume standard conditions.

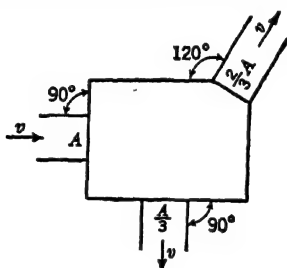
2-5. Two tanks, *M* and *N*, contain water and kerosene, respectively, as shown in the accompanying figure.



A plate *XY*, which is hinged at *X*, is held against the outlet of tank *N* by the water ejected from tank *M*. If outlet area of *M* is 2 sq ft, and outlet area of *N* is 2.5 sq ft, find the maximum height of kerosene, h_1 , that can

be supported by a height of water, $h = 10$ ft. (Kerosene $sg = 0.80$.)

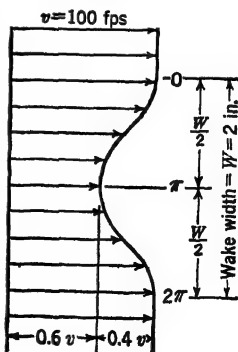
2-6. A jet of water is sent into a mechanism that shoots out two jets



as shown. Assuming all losses negligible, find the resultant force on the mechanism, in magnitude and direction, $F = f(A, v)$.

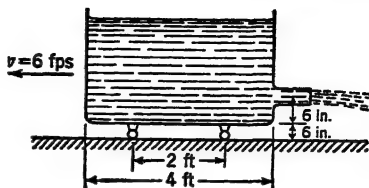
2-7. The velocity distribution in the wake of a wing tested in a wind tunnel is found to be closely represented by a cosine curve, as shown in the accompanying diagram. The minimum wake velocity is three-fifths the remote velocity. If the wake width $W = 2$ in., and remote velocity $v = 100$ fps, find the drag of the wing per foot of span. Assume standard conditions. HINT: This problem may be solved by either mathematical or graphical integration of Eq. (2-24).

2-8. A car partly filled with water is discharging through an orifice, as shown. Weight of car is 1000 lb. Weight of water at moment considered is 2500 lb. The center of gravity of



the car plus water is assumed to act at the same height as that of the water, and midway between the wheels. Discharge velocity is 16 fps with respect to the car, and discharge quantity is 3 cfs. Car velocity is 6 fps to the left. Neglecting hydraulic and mechanical friction, and assuming the water level in the tank remains horizontal,

- Find the width of the car (ft).
- Find the acceleration of the car (fps per sec).
- Find the front and rear wheel reactions R_F and R_R (lb).



2-9. A 3000-lb rocket ejects a

stream of hot gases at $M = 1.0$ at standard pressure but at 1650 F. Assume the exhaust gases have the same constituents as air. If the rocket is fired vertically upward, find its initial acceleration (fps per sec). Jet area is 2 sq ft.

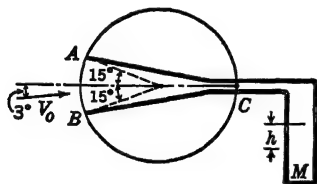
2-10. A 28,000-lb rocket discharges 19,400 lb of burned gases at a constant rate for 70 sec with a relative velocity of 6500 fps. It is fired vertically upward. Ignoring the drag force, and assuming the acceleration of gravity independent of altitude, find

- The maximum velocity attained by the rocket (mph).
- The total time to reach maximum altitude (sec).

2-11. Compute the slip-stream velocity (fps), at 10,000 ft altitude, for a propeller having 7-ft diameter, if thrust $T = 500$ lb, remote velocity $v_0 = 264$ fps, and the relation between slip-stream velocity v_s and propeller velocity v_p is given by

$$v_s - v_0 = 2(v_p - v_0)$$

2-12. An instrument is constructed to show angular inclination of an air stream. It consists of a cylinder



(see diagram) with holes drilled at A and B. The drilled holes, if extended, would pass through C. Tubes lead from holes A and B to a U-tube vertical manometer M containing kerosene ($sg = 0.80$). What height h of kerosene (ft) corresponds to a 3-deg inclination of

the air stream if $V_0 = 200$ mph? Assume standard conditions.

2-13. A Quonset hut (assume it to be a half-circular cylinder) 100 by 24 ft is built in the middle of a large plain. Maximum anticipated wind velocity perpendicular to the hut axis is 80 mph. Maximum and minimum recorded temperatures for the region are $t = 95$ F and $t = -10$ F, while maximum and minimum recorded pressures are $p = 31$ in. of mercury and $p = 28.5$ in. of mercury, respectively. Find the maximum

anticipated lifting force on the hut, assuming that perfect-fluid equations may be used to establish velocity distribution. Ignore end effect (consider it a two-dimensional problem), and assume the static pressure within the hut is equal to the remote static pressure.

2-14. The wing of an airplane operating at 10,000 ft altitude has a maximum positive pressure that is 100 psf higher than atmospheric pressure, and a maximum negative pressure that is 200 psf lower than atmospheric pressure.

a. What is the airplane velocity (fps)?

b. What is the maximum tangential velocity on the wing surface (fps)?

2-15. By dimensional analysis find the general equation for thrust of a propeller

$$T = K \rho^\alpha n^\beta D^\gamma f(v, n, D)$$

where ρ is mass density, slug per cu ft

n is rotational speed, rps

D is diameter, ft

v is forward velocity, fps

α, β, γ are exponents to be determined

2-16. A model airplane was tested in a wind tunnel: $t = 85^\circ\text{F}$; $\rho = \text{standard}$; $c = 10$ in.; $R = 2 \times 10^6$ (based on the length c in feet).

a. What was the air speed of the test (mph)?

b. What was the Mach number for the test?

2-17. A full-scale airplane has a design altitude of 13,000 ft and cruising speed of 240 mph. A 1:10 scale model is constructed to test in a wind tunnel at 180 mph at 78 F. How many atmospheres of pressure is required in order to obtain the same R as that of the full-scale airplane? (1 atm = 14.7 psi.)

CHAPTER 3

AERONAUTICAL NOMENCLATURE

This chapter will be concerned primarily with the description and classification of aircraft and aircraft components. There will be no attempt to enter into any detail, nor will the study be complete,¹ but it will serve a useful purpose in clarifying subsequent discussions.

3-1 Aircraft Types. The word aircraft applies to all man-made craft that are supported by the air. Airships of all types are statically supported by buoyancy, but nearly all other aircraft are supported dynamically by relative air motion. Only the latter *heavier-than-air* craft will be considered in this text.

Heavier-than-air craft may be subdivided into those whose wings are fixed, such as the *airplane* and *flying wing*, and those whose wings are movable, such as the *helicopter* and *autogiro*. The helicopter and autogiro both have wings that rotate in a horizontal plane; the former having its wings continuously driven by an engine and the latter having its wings driven by the relative motion of the air. Both the autogiro and the airplane must have propellers to provide thrust, but the helicopter obtains thrust from its rotating wings. A separate type of aircraft that has no engine is called a *glider*. A glider that has a very high ratio of wing area to weight may be so light that it will rise when it encounters an atmospheric upgust (thermal). If designed specifically to soar for long periods of time in these upgusts, it is called a *sailplane*.

Of all the types of aircraft mentioned above, the one of primary aerodynamic interest is the airplane. Airplanes may be classified in several ways: according to the number of wings employed, as monoplanes, sesquiplanes, or biplanes (Fig. 3-1); according to wing position, as parasol, high-wing, midwing, or low-wing airplanes (Fig. 3-1); or according to the number of engines, as single-engined, twin-engined, or multiengined. Other classifications

¹ A fairly complete list of standardized nomenclature is given in TR 474.

could be made, dependent upon type of landing gear, propellers, engines, etc. One general classification, however, seems to overshadow all the foregoing, and that is the classification according to the purpose for which the airplane is built: bomber, cargo,

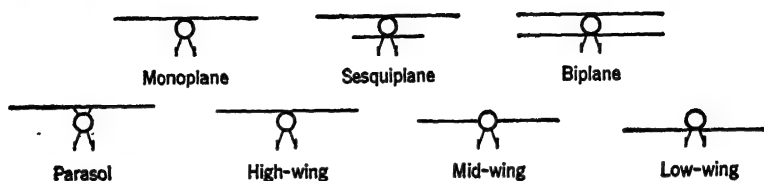


FIG. 3-1. Conventional wing and fuselage combinations.

pursuit, transport, trainer, etc. The Army and Navy of the United States have both adopted symbols for defining the utility of all military aircraft. The code letters and numbers specify the duty for which the airplane is designed, its model number, etc. In the commercial field, companies generally assign individual code numbers to their airplanes, but the method varies considerably between companies; hence, their numbers are significant only when compared with other numbers of the same company.

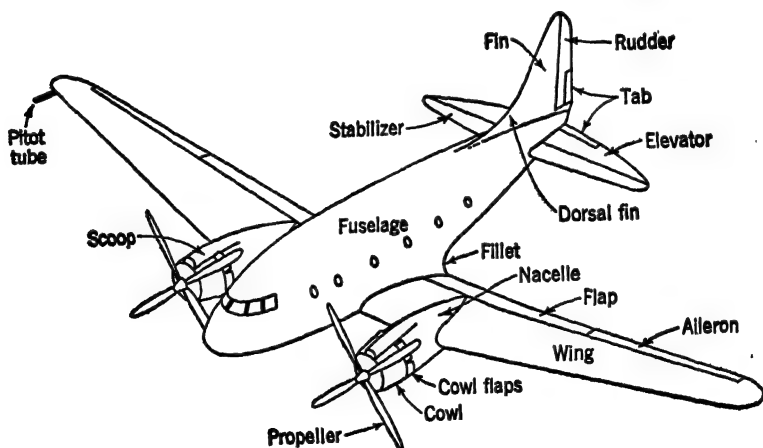


FIG. 3-2. Airplane nomenclature.

3-2 Airplane Components. Customarily an airplane has the following major components: a wing or wings for aerodynamic support of the weight of the airplane; a fuselage to hold the passengers, cargo, etc.; a jet unit or propeller and engine to supply

motive force; landing gear for support while on the ground; an empennage (tail group) to aid stability; and control surfaces to regulate the flight attitude. Figure 3-2 shows these main components. In the following pages these components will be defined and described.

3-3 Wing. The wing of an airplane is the component that is primarily responsible for sustaining it during flight. The maximum projected area of the wing is defined as the *wing area* S . If a nacelle or fuselage obscures part of the wing, the wing leading and trailing edges are graphically extended to pass through them.

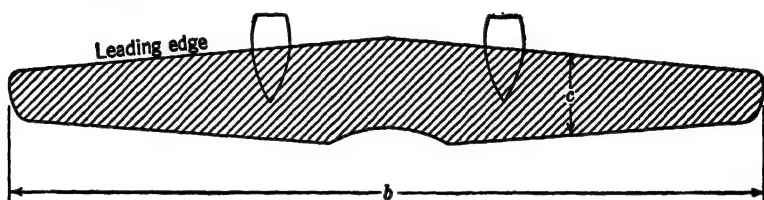


FIG. 3-3. Wing-planform definitions of area, span, and chord.

On the other hand, if a portion of the wing is cut out, say to improve vision, the cut out area is not included in the definition of S . These principles are clarified in Fig. 3-3, where the cross-hatched lines indicate the wing area, according to the above definition. The maximum lateral wing dimension is called the *span* b , and the distance from wing leading edge to trailing edge is called the *chord* c (Fig. 3-3). The chord of a wing is seldom constant, so that an average chord is frequently defined, but the same symbol c is generally used; usually the equation in which the symbol appears makes its intended meaning clear; thus

$$c = \frac{S}{b} \quad (3-1)$$

where c is average chord, ft

S is wing area (maximum projected area), sq ft

b is span, ft

Aspect ratio is the ratio of span to average chord, and from Eq. (3-1) may be expressed in terms of area also.

$$A = \frac{b}{c} = \frac{b^2}{S} = \frac{S}{c^2} \quad (3-2)$$

Wings may have a great variety of *plan forms* (Fig. 3.4), whose principal geometric characteristic is the taper ratio λ :

$$\lambda = \frac{c_t}{c_r} \quad (3.3)$$

where λ is taper ratio, dimensionless

c_t is tip chord, ft

c_r is root chord, ft

A wing that does not have straight leading and trailing edges, such as an elliptical plan form, may be represented by an "effective" straight tapered plan form for many calculations.

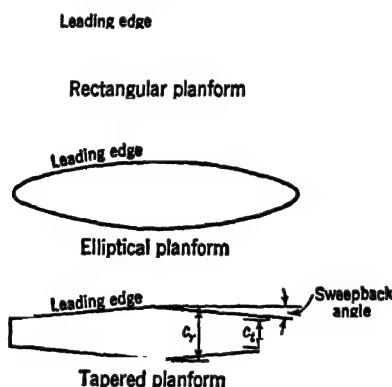


FIG. 3.4. Common wing planforms.

Wing *sweepback* is given by the angle the leading or trailing edge makes with a perpendicular to the root chord, or by the per cent chord that forms a straight line from wing tip to tip; *i.e.*, if the 25 per cent chord is straight, it has all points corresponding to the 25 per cent chord falling on one line on both sides of the root chord. Wing *dihedral* is usually defined as the angle formed by a line passing through the 25 per cent chord of all wing sections in a spanwise direction and the line joining the two wing tips. A twisted wing has *washout* if the angle of attack (see page 61) at the tip is less than that at the root, and *washin* if the angle of attack at the tip is greater. By *aerodynamic washout* is meant that the zero-lift chord (see next paragraph) at the tip is at a smaller angle of attack than at the root.

A wing section or *airfoil section*¹ is formed by a streamlined contour as shown in Fig. 3-5. The line that is equidistant from the upper and lower surfaces is called the *mean line*, *median line*, or *mean-camber line*. The straight line joining the intersections of the mean line with the airfoil surface defines the *chord*.² The angle between the chord and the remote-velocity vector v is called the *angle of attack*, α , and the deviation of the mean line from the chord line is called *camber*; i.e., a highly cambered airfoil section has an excessively curved mean line. When the airfoil is at such an angle of attack that there is no force perpendicular to the remote-velocity vector (no *lift*), the line parallel to the remote-velocity vector that passes through the trailing edge is called the

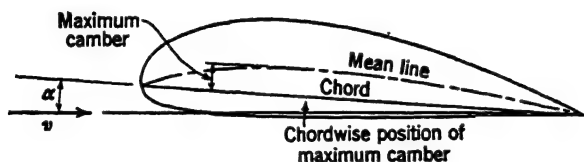


FIG. 3-5. Geometric properties of an airfoil section.

zero-lift chord. For a symmetrical airfoil section, the chord and the zero-lift chord are coincident, and the camber is zero.

Early planes were built according to the mistaken belief that the thinnest possible wings, accompanied by numerous external bracing wires and struts, were the best. Modern practice is to build the wing thick enough to include all necessary bracing internally, whenever possible. The geometric proportions of an airfoil section are conveniently expressed in terms of three main variables:

1. Shape of the mean line
2. Thickness
3. Thickness distribution

A great number of airfoil sections have been developed by experi-

¹ "Airfoil" is technically a synonym for wing, although it is seldom used in this sense at present except in the phrase airfoil section. "Airfoil" is often used to designate a test specimen of a wing.

² The chord is only an arbitrary reference. It is also frequently defined as the line joining leading and trailing edges, or as the line tangent to the lower surface at two points. The latter definition is used primarily for propeller-blade sections.

menters in the United States and elsewhere. In order to provide a reliable basis for design, the NACA, in 1929, started development of a systematic series of sections that have since provided clear proof of the influence of changes in shape of the mean line and changes in thickness of the airfoil on aerodynamic characteristics. Basing the series upon the assumption that the thickness distribution is the least important of the three previously mentioned variables, the NACA chose the average thickness distributions from two well-known, successful airfoil sections as a basis for a major part of their early tests: they were the Clark Y (U.S.A.) and the Göttingen 398 (German). By varying the per cent thickness and shape of the mean line but keeping the thickness distribution fixed, two series of airfoil sections were developed. These sections, along with the later "low-drag" and "high-speed" airfoils, comprise the major part of the sections used in this country at the present time.

The first *four-digit* series is based upon a mean line defined by two second-degree parabolas that are tangent at the point of maximum camber (Fig. 3-5). Changes in shape of the mean line are accomplished by varying only the position and magnitude of the maximum camber. Changes in thickness are accomplished only by increasing or decreasing all ordinates from the mean line by proportionate amounts. The code used to define the resultant contour of the airfoil is composed of four digits: the first gives the *amount* of maximum camber in per cent of chord, the second gives the *position* of the maximum camber in tenths of chord,¹ and the last two give the *maximum thickness* in per cent of chord. The following example may clarify the preceding explanation:

2415

Maximum camber is
two-hundredths of chord

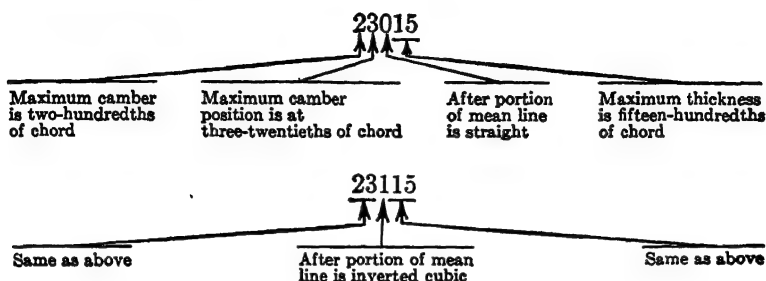
Maximum camber position
is at four-tenths of chord

Maximum thickness is
fifteen-hundredths of chord

The second *five-digit* series has the same thickness distribution as the four-digit series but is based upon a mean line defined by a cubic in the forward part of the airfoil, which becomes tangent either to a straight line or to an inverted cubic that forms the after

¹ Chordwise positions are invariably measured from the *leading edge* of a wing or airfoil.

portion. The designation for the five-digit series is somewhat similar to that for the four-digit series and may be shown by the following examples:



Test results of the above four- and five-digit airfoils may be found in *TR* 460, 586, 610, 669,¹ etc.

Theoretical considerations have indicated that by having the most negative pressure on an airfoil occur closer to the trailing edge than on the four- or five-digit series and by reducing the absolute value of the most negative pressure (Fig. 3-6), the drag

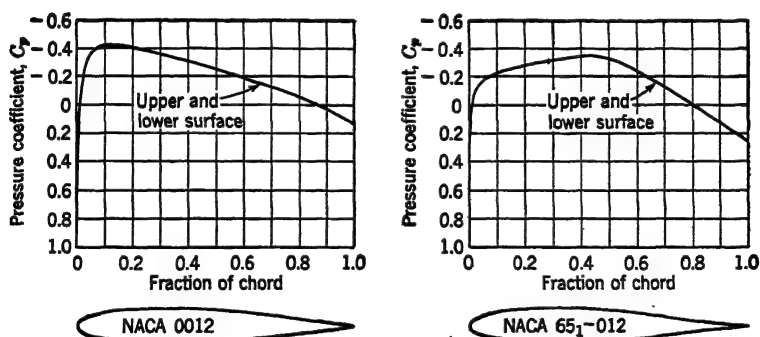


FIG. 3-6. Comparison of pressure distribution on a four-digit and low-drag symmetrical airfoil at zero angle of attack. (From *WR L-560*.)

may be reduced and the high-speed characteristics improved. This has led to several new airfoil series that are characterized by a maximum thickness occurring somewhere in the vicinity of the mid-chord.

¹ *TR* 669 contains correction factors that must be applied to all prior NACA airfoil tests run in the Variable-Density Tunnel.

One of the earliest of this type was originally designed for desirable high-speed characteristics. It is a modified four-digit series in which the first four digits have their usual meaning, while a group of digits following a dash indicates thickness distribution. The first digit within this group indicates leading-edge radius according to the following:

- 0 designates sharp leading edge.
- 3 designates one-fourth normal four-digit radius.
- 6 designates normal four-digit radius.
- 9 designates three times normal four-digit radius.

The second digit gives the position of the maximum thickness in tenths of chord. For example,¹

2409-04

Same as four-
digit series

Sharp leading edge

Maximum thickness
at four-tenths chord

More extensive tests were subsequently run on other airfoils designed primarily for low drag characteristics, the most successful of which were the 1-series, 6-series, and 7-series. The numbering system is somewhat similar for these three groups, but each will be discussed separately.

The 1-series Airfoils. This group is defined as a symmetrical airfoil having a minimum (most negative) pressure occurring well back from the leading edge. Changes in airfoil characteristics within the series are then accomplished by changing the thickness and the shape of the mean line as in the four- and five-digit airfoils, the difference being that the airfoil is designed to give low drag at a particular angle of attack or lift coefficient. The second digit refers to the position of minimum pressure for the basic symmetrical section at zero lift, in tenths of chord. The digit after the hyphen refers to the design lift coefficient in tenths, and the last two digits refer to the maximum thickness in per cent of chord. For example,

16-218

1-series airfoil

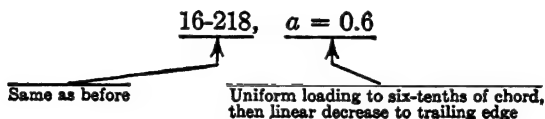
Minimum pressure
at six-tenths of chord
for symmetrical basic
section at zero lift

Design lift coeffi-
cient is 0.2

Maximum thickness
is eighteen-hundredths
of chord

¹ For further information and test results, see *TR 492*, *WRL-143*, *TN 976*, etc.

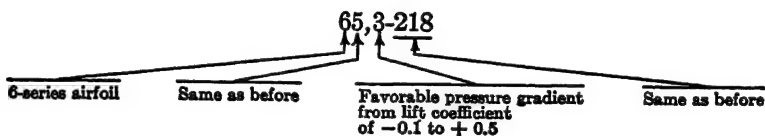
The mean line is usually curved in such a manner that it produces an approximately constant chordwise difference in pressure between upper and lower surfaces at the design lift coefficient, which produces an approximately constant load per inch on the chord. However, the mean line may be curved so as to produce an approximately constant load from the leading edge to the 60 per cent chord, say, and then a linearly decreasing load to the trailing edge. This change in "loading" is indicated after the airfoil designation:



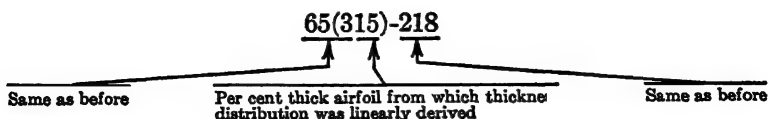
Frequently, if the loading is uniform so that $a = 1.0$, the load designation is deleted.

One of the most useful 1-series airfoils is the 16-() series, which is usually referred to as the 16-series.

The 6-series Airfoils. The system of designation is similar to that for the 1-series airfoils, but additional information is given by another number that shows the range of lift coefficients, in tenths, above and below the design lift coefficient, for which a favorable pressure gradient¹ exists on both surfaces.



In contrast to all the preceding airfoils discussed, the thickness distribution of the above airfoil depends upon its maximum thickness. A second subgroup with a thickness distribution obtained by linearly varying all ordinates in proportion to the maximum thickness is designated as in the following example:



¹ The pressure gradient is favorable if the pressure becomes increasingly negative in the direction of flow. The theory will be discussed in Chap. 7.

A third subgroup is based upon a theoretical rather than individually derived (first subgroup) or linearly specified (second subgroup) variation in thickness distribution with maximum thickness. All digits have the same meaning as in the first subgroup. For example,

653-218

Again the above airfoil has a distribution of thickness that depends upon its maximum thickness. A fourth subgroup obtained by a linear variation like the second subgroup is specified like the second subgroup

65(315)-218

All the 6-series airfoil symbols may be followed by a loading term as in the 1-series.

The 7-series Airfoils. This series was designed to produce a minimum pressure at different per cent chord on the upper and lower surfaces. For example,

747 A 218

7-series airfoil	Favorable pressure gradient for four-tenths chord on upper surface at design c_l	Favorable pressure gradient for seven- tenths chord on lower surface at design c_l	Serial letter to indicate thickness distribution and mean line	Same as
---------------------	---	---	---	---------

All the 7-series airfoils have thickness distributions that are individually derived, hence do not vary linearly with maximum thickness.¹

Supersonic flight poses problems that are entirely different from subsonic. A series of airfoils, based on theoretical considerations, has been developed by NACA. All airfoils are characterized by a knife-edge leading edge. The numbering system may best be illustrated by an example.²

1S-(50)(03)-(50)(03)

Series number 1
designates wedge

2 designates
circular-arc

Supersonic

Maximum thickness of upper
surface is at 50 per cent chord

Maximum thickness of
lower surface is
three-hundredths of chord

Maximum thickness of lower
surface is at 50 per cent
chord

Maximum thickness of upper surface
is three-hundredths of chord

¹ For further information and experimental results on the 1-, 6-, and 7-series airfoil sections, see *WR L-560*.

² For further information and test results, see *TN 1211*.

Examples of some common airfoils of the various groups described are depicted in Fig. 3-7.

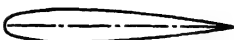
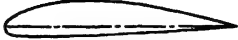
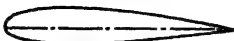
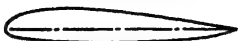
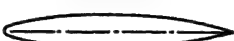

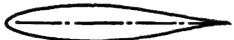
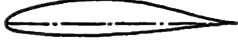
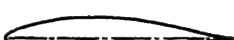

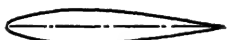

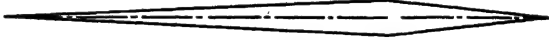
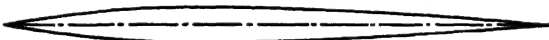
Four-digit series airfoils	 NACA 0015	 NACA 4415
Five-digit series airfoils	 NACA 23015	 NACA 23115
1-series airfoils	 NACA 16-015	 NACA 16-515
6-series airfoils	 NACA 65, 2-015	 NACA 65(216)-415 $\alpha=0.5$
	 NACA 65 ₂ -415	 NACA 65(421)-415
7-series airfoils	 NACA 747A015	 NACA 747A415
Supersonic airfoils	 NACA 1S-(70)(03)-(70)(03)	
	 NACA 2S-(30)(03)-(30)(03)	

FIG. 3-7. Examples of common airfoil sections. (From TR 537, WR L-560, TN 976, and TN 1211.)

3-4 Fuselage. The fuselage or body of an airplane is primarily designed to hold the passengers, cargo, etc. It also provides a structural link between the wing and tail. In some airplanes these two separate functions are accomplished by booms and a cab (Fig. 3-8). Fuselages are made as streamlined as possible, but a certain amount of irregularity in the vicinity of the windshield is generally a necessary evil. Smooth airflow in the juncture between the wing and fuselage is often accomplished by means of a *fillet*, which is a nonstructural sheet that gives a gradual curvature from the fuselage to wing instead of the abrupt angular transition that would occur without it. A fuselage may have any convenient cross section consistent with structural and cargo specifications

except that if it is to be pressurized, a circular or multiple-circular section is generally used. It should be smoothly faired and have no sharp corners that might cause flow separation.

The fuselage of a seaplane is called a *hull* when it serves a dual purpose by providing buoyant support while on the water.

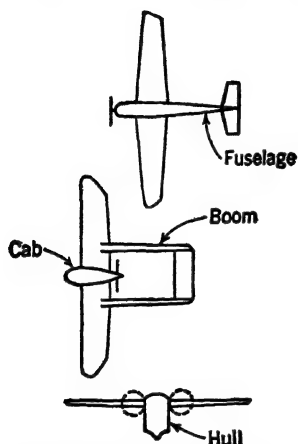


FIG. 3-8. Fuselage configurations.

3-5 Power Plant. The power plant consists of the complete propulsive unit, including the engine. It may be classified either as a propeller and reciprocating engine or as a jet unit. There is some overlapping in the two categories, but this will be pointed out in the course of the discussion.

Propeller and Reciprocating Engine.

In a conventional power plant the propeller may be in front of the engine, in which case the airplane is called a *tractor*, or it may be behind, in which case it is called a *pusher*. A propeller may have any number of blades from one to five on a single hub, or may have four, six, or eight blades contra-rotating on two separate hubs. Engines may be *in-line*, *radial*, *multiple-bank radial*, etc. They may be *liquid-cooled* or *air-cooled*. They may be *unsupercharged*, *supercharged* by either a gear-driven supercharger or turbosupercharger, or

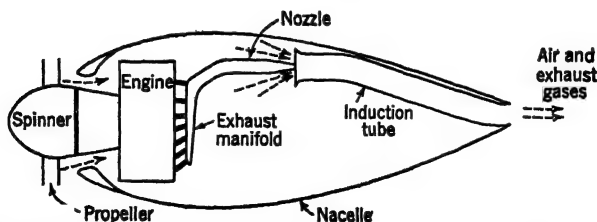


FIG. 3-9. Diagrammatic representation of an exhaust-aspirated cooling system.

compounded with an exhaust turbine attached to the crankshaft. The engine may be mounted on the front of the fuselage in a single-engined airplane, so that the fuselage itself provides the streamlining, or it may be mounted within an enclosed fairing or *nacelle*,

as on a multiengined airplane. In order to provide proper cooling and increase efficiency, the propeller may be provided with a *spinner* on the hub and a *cowl* on the forward section of the nacelle or fuselage. The cowl is a separate ring-shaped fairing that guides the air over the engine and allows it to flow smoothly over the nacelle or fuselage. *Cowl flaps* (Fig. 3-2) are frequently used to control the rate of flow of cooling air over the engine, although

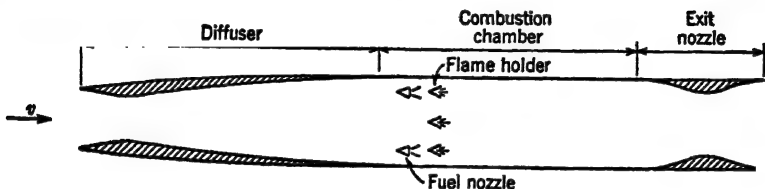


FIG. 3-10. Diagrammatic representation of a ram-jet. (From TN 1349.)

in some installations the exhaust gases from the engine are used to "induce" cooling flow (Fig. 3-9). This procedure obviates the necessity for having cowl flaps. Cooling flow is sometimes increased by the fan action of a *cuff*, which consists of an airfoil-shaped sheetmetal fairing that surrounds the propeller shank.

Jet Unit. A jet unit may be classified according to whether it consists of a simple tube relying upon *ram*¹ for compression of the combustible mixture, or whether it uses a mechanical compressor for this purpose. The former device, shown in Fig. 3-10, is called

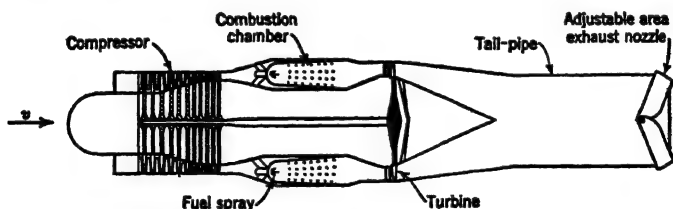


FIG. 3-11. Diagrammatic representation of a turbo-jet. (From TN 1349.)

a *ram-jet* or *athodyd* (aero-thermo-dynamic-duct). The latter, shown in Fig. 3-11, is called a *turbo-jet*, since the compressor is driven by a gas turbine.

Combined Units. There are several interesting combinations of the above systems. For instance, the exhaust stacks of the

¹ Ram is the pressure rise that occurs at the front end of a body moving with a velocity relative to the air.

reciprocating engine may be connected to nozzles to increase exhaust velocity and hence produce an appreciable thrust increment. Again a conventional propeller may be combined with the turbo-jet. The combination is called a *turbo-propeller* (Fig. 3-12). Again, a small-diameter propeller may be enclosed within the shell of the *turbo-jet* just forward of the compressor to increase the mass

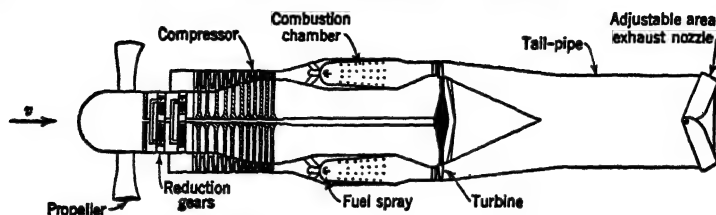


FIG. 3-12. Diagrammatic representation of a turbo-propeller.

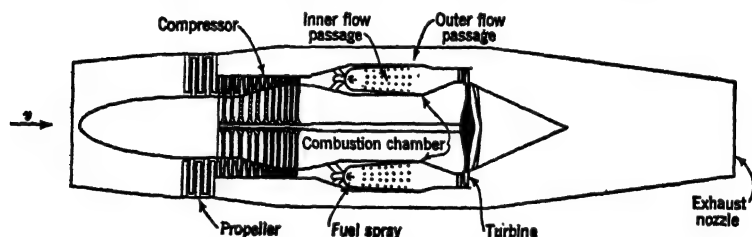


FIG. 3-13. Diagrammatic representation of a ducted propeller.

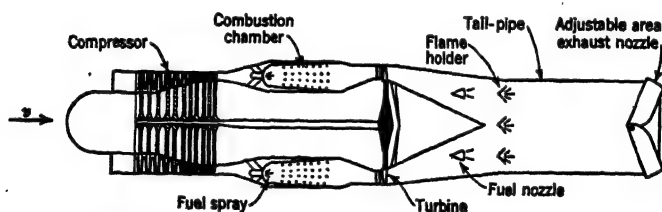


FIG. 3-14. Diagrammatic representation of a turbo-ram-jet.

flow of air (Fig. 3-13). This arrangement is called a *ducted propeller*, and it is effective in increasing the static thrust and reducing the high fuel consumption of the conventional turbo-jet. Again, the ram-jet principle may be used to advantage in a *turbo-ram-jet* (Fig. 3-14) by injecting fuel in the high-speed stream of the tail pipe. This system is called *afterburning*, and it is an effective method for increasing thrust of the turbo-jet even though it does result in a considerable increase in fuel consumption.

3-6 Landing Gear. The landing gear is used to provide mobile support for the airplane on the ground. It may be a conventional type with two *main wheels* forward and a *tail wheel* in the after section of the fuselage; it may be a *tricycle landing gear* with the two main wheels further aft and a *nose wheel* near the forward section of the fuselage; or it may be a *bicycle landing gear* consisting of two main wheels on the fuselage center line and an auxiliary wheel outboard on each wing. Part or all of the landing gear is frequently retractable into the nacelle, wing, or fuselage to improve performance of the aircraft.

3-7 Empennage. The empennage or tail group aids in stabilizing and controlling the airplane. It usually consists of a single horizontal surface, and anywhere from one to three vertical surfaces. The horizontal surface consists of a *stabilizer* and *elevator*, and the vertical surface consists of a *fin* and *rudder*. If twin vertical tails are used they are usually mounted near the tips of the stabilizer, so that the stabilizer approximately bisects them. The horizontal and vertical surfaces may be combined in one surface called a *V tail*, which is essentially a horizontal surface with extreme dihedral. A *dorsal fin* is a forward extension of the usual vertical surface and is used particularly on multiengined airplanes (Fig. 3-2).

3-8 Control Surfaces. Control surfaces are used to regulate the flight of the airplane. The main surfaces are *ailerons* mounted on the wing-tip trailing edges to provide control in "rolling" the airplane (motion about the longitudinal axis of the airplane), *rudder* mounted on the fin trailing edge to provide control in "yawing" the airplane (motion about the vertical axis), and *elevators* mounted on the stabilizer trailing edge to provide control in "pitching" the airplane (motion about the lateral axis of the airplane). These three control surfaces appear on conventional aircraft as separate entities but may be combined so as to have one surface perform two or even all three functions, as in the V tail and in some versions of flying wings.

Auxiliary controls include *flaps* mounted inboard of the ailerons on the wing trailing edge and *slots* on the wing leading edge. Both controls are used primarily to reduce landing speed. An auxiliary surface that is sometimes incorporated with an aileron, rudder, or elevator is called a *tab* (Fig. 3-2). Its purpose is either to relieve pilot fatigue by shifting the neutral stick position from that cor-

responding to zero control-surface deflection to some other value, in which case it is called a *trim tab*, or to aid in deflecting the control surface, when it is called a *servo tab*.¹ A large deflection of the control surface is accomplished by a relatively small deflection of the tab.

3-9 Aircraft Instruments. Of all the instruments used to indicate the functioning of the various parts of the airplane and the performance of the airplane itself, one of the most important to the aerodynamicist is the air-speed indicator. It is essentially a pressure gage connected to a pitot tube, and it is calibrated in velocity units instead of pressure units. The calibration is done so as to correspond to standard sea-level conditions according to the equation

$$v_i = \sqrt{\frac{2q}{\rho_0}} \quad (3-4)$$

where v_i is indicated air speed, fps

q is dynamic pressure, psf

ρ_0 is standard sea-level mass density, slug per cu ft

The indicated air speed is, therefore, a function of dynamic pressure, so that at altitude, for instance, the air-speed indicator does not indicate true air speed. True air speed is obtained from

$$v = \sqrt{\frac{2q}{\rho}} \quad (3-5)$$

where ρ is the mass density for the particular operating conditions considered. True air speed may be obtained from indicated air speed by combining Eqs. (3-4) and (3-5):

$$v = \frac{v_i}{\sqrt{\sigma}} \quad (3-6)$$

$$V = \frac{V_i}{\sqrt{\sigma}} \quad (3-7)$$

The indicated air speed is seen to be a fictitious air speed arising from the inability of an air-speed indicator to compensate for variations in density of the atmosphere.

¹ Not all tabs used for this purpose are called servo tabs (see Art. 15-6).

Equations (3-6) and (3-7) are technically correct only under very restricted circumstances. For instance, even at moderate speeds, say about 300 mph, air compressibility must be accounted for (see Art. 8-4). Furthermore, the pitot tube is invariably mounted in a position on the airplane for which the velocity and static pressure are not identical to the remote values. This is frequently called *position error*, and it is not usually constant with

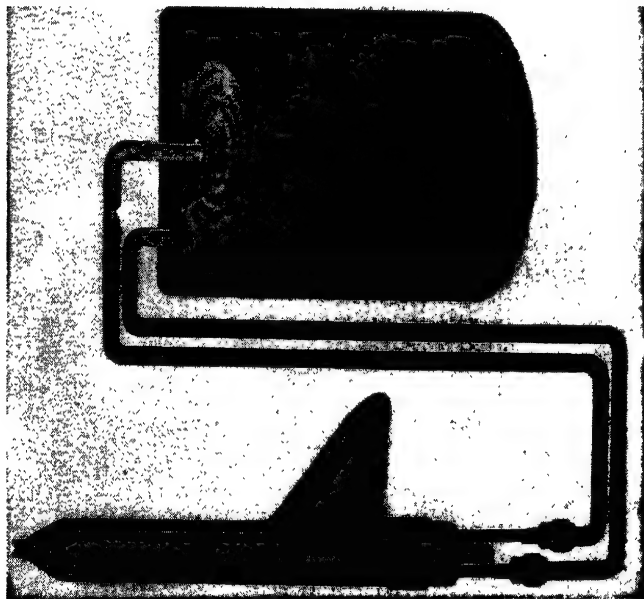


FIG. 3-15. Pitot tube and air-speed indicator. (*Kollsman Instrument Division of Square D Company.*)

angle of attack of the airplane. Superimposed on these effects is the possibility of slight mechanical defects in the construction of the pitot tube or the air-speed indicator.

Calibration of the installation in a particular airplane is commonly accomplished by making several flights at different air speeds between pylons. From the distance between pylons and the time of flight the ground speed may be computed. The runs are always made in both directions at a particular air speed to nullify effect of wind, so that the average ground speed is equal to the true air speed. From the true air speed, the reading of the air-speed indicator, the atmospheric temperature and pressure,

and the mathematical correction due to compressibility, the correction factor due to position error and mechanical defect may be computed.

A diagrammatic representation of a pitot tube and air-speed indicator is shown in Fig. 3-15.

PROBLEMS

3-1. An airplane at 40,000 ft is operating at a Mach number $M = 0.5$ and Reynolds number $R = 10,000,000$. If the aspect ratio $A = 12$, what is the wing area S (sq ft)?

3-2. An airplane leaves an airport at 3 p.m. with a full gas tank. It flies toward a point that is due west into a 20-mph head wind (relative to ground). What time must it turn back if it is to arrive with 20 gal of fuel still in the tank? The whole flight is made at constant indicated air speed $V_i = 100$ mph.

Altitude = 15,000 ft

Fuel consumption = 0.5 lb per bhp-hr

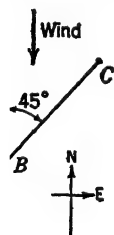
Gas weight = 6 lb per gal

Average bhp = 1000 bhp

Tank capacity = 350 gal

3-3. In Prob. 3-2, a 20-mph wind is blowing from the northwest instead of a 20-mph head wind. Solve the problem again.

3-4. An airplane at sea level flies a 23-mile straight course at 150-mph ground speed with a 15-mph tail wind. Reynolds number $R = 10,000,000$; density $\rho = 0.0022$ slug per cu ft; aspect ratio $A = 12$; standard pressure. Find the Mach number, wing span, and indicated air speed (mph).



3-5. An airplane at sea level flies north from A to B into a 40-mph head wind, as shown, then northeast from B to C (the wind is still from the north). From a map of the terrain, $AB = BC$. Time of flight on leg BC is 2 hr. If constant indicated air speed $V_i = 200$ mph is maintained for both legs, find time for leg AB .

3-6. An airplane equipped with a mechanically accurate pitot tube and air-speed indicator is flown north and south over a 2.5-mile course in order to find the position error for the instrument. Outgoing time $T_o = 45$ sec, and return time $T_r = 54$ sec. Temperature $T = 80$ F, and atmospheric pressure $p_a = 28$ in. of mercury. The air-speed indicator shows a constant reading of 180 mph for the two legs of the flight. Ignoring effects of compressibility, find

a. The magnitude of the wind, assuming no east-west component (mph).

b. The position error ΔV (mph) to be added to the dial reading of the

air-speed indicator at this speed, in order to obtain the correct indicated air speed.

3.7. An air-speed indicator is calibrated by flying an airplane over a square course 20 miles on a side. An air speed of 160 mph is shown by the indicator and is held constant for the complete flight. A ground observer records the time on each of the four legs: AB , $t = 7.06$ min; BC , $t = 7.74$ min; CD , $t = 7.50$ min; DA , $t = 6.86$ min. Mass density ratio = 0.80.

a. Find the correction factor F_c by which the dial reading of the air-speed indicator must be multiplied, in order to obtain the correct indicated air speed. Ignore compressibility effects.

b. If AB is north and BC is west, find the direction of the axis of the airplane on leg AB .

CHAPTER 4

EXPERIMENTAL FACILITIES

The evolution of an airplane, from its preliminary design through its final assembly, is aided materially by numerous experiments to check the theoretical and empirical calculations relating to its aerodynamic characteristics. In this chapter, equipment used in experimental testing will be discussed, with particular emphasis on wind tunnels.

4-1 Early Testing Techniques. One of the earliest types of equipment used for measuring aerodynamic forces was a whirling arm on the end of which the model was mounted (Fig. 4-1).

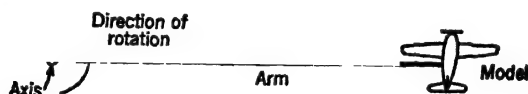


Fig. 4-1. Whirling-arm method for determining aerodynamic characteristics.

This crude device had the disadvantage of making the model operate in the wake resulting from its preceding revolution; also the model was in a continual state of curved flight. Other early equipment included cars that ran on tracks, pendulum arrangements that were used primarily for testing symmetrical or asymmetrical bodies, droptesting equipment in which the model was usually restrained by means of a vertical wire, and miscellaneous systems utilizing the natural velocity of the wind.

Most of the above systems have proved unsatisfactory for one reason or another and have been replaced by the wind tunnel, whose principal feature is a tube through which air is drawn, in order to produce an artificial relative velocity with respect to a stationary body suspended in its stream. Its development has been almost entirely empirical, because there is no completely reliable theory to predict characteristics of flow in a tube of arbitrary shape even for low speeds.

4-2 Classification of Wind Tunnels. Wind tunnels and their components may be classified in the following manner:

- | | |
|------------------------|------------------------------------|
| A. Air path | c. Hexagonal |
| 1. Direction | d. Elliptical |
| a. Horizontal | e. Rectangular |
| b. Vertical | D. Flow improvement |
| c. Inclined | 1. Bellmouth |
| 2. Speed | 2. Honeycomb |
| a. Subsonic | 3. Expansion section |
| b. Supersonic | 4. Corner vanes |
| B. Circuit | 5. Prerotation and antiswirl vanes |
| 1. Open circuit | 6. Screens |
| 2. Closed circuit | E. Model support |
| a. Single return | 1. Wire |
| b. Double return | 2. Strut |
| c. Annular return | F. Force measurement |
| C. Test section | 1. Mechanical |
| 1. Throat | 2. Electromechanical |
| a. Open throat | 3. Strain gage |
| b. Closed throat | 4. Hydraulic |
| 2. Shape | 5. Pressure |
| a. Circular | |
| b. Square | |

Each of the above divisions and subdivisions will be discussed briefly.

A. Air Path. Wind tunnels are generally built so that the flow through the test section is horizontal, although in some tunnels where space is an important consideration, the vertical tunnel may be the only answer. A vertical flow is necessary in a *free-spinning tunnel* (Fig. 4-2), for which a flying model is built with appropriate weight and moment of inertia¹ and is allowed to "spin" freely in the vertical flow of air. Model flight characteristics in the spin may then be used to predict characteristics of the full-scale airplane. Vertical flow is also necessary in the *gust tunnel*, in which a flying model is catapulted horizontally through the test section in order to observe its behavior upon encountering a sharp-edged gust (Fig. 4-3). Its characteristics

¹ Flying models, and models whose structural elasticity may be important, are the only ones requiring scaled weight and moment of inertia; for all other tests these characteristics have no particular significance.

may then be used to predict the response of a full-scale airplane to gusty air. An inclined flow is required for a *free-flight tunnel* (Fig. 4-4), in which a flying model simulates "gliding" in the test section, accomplished by maintaining a velocity equal to the

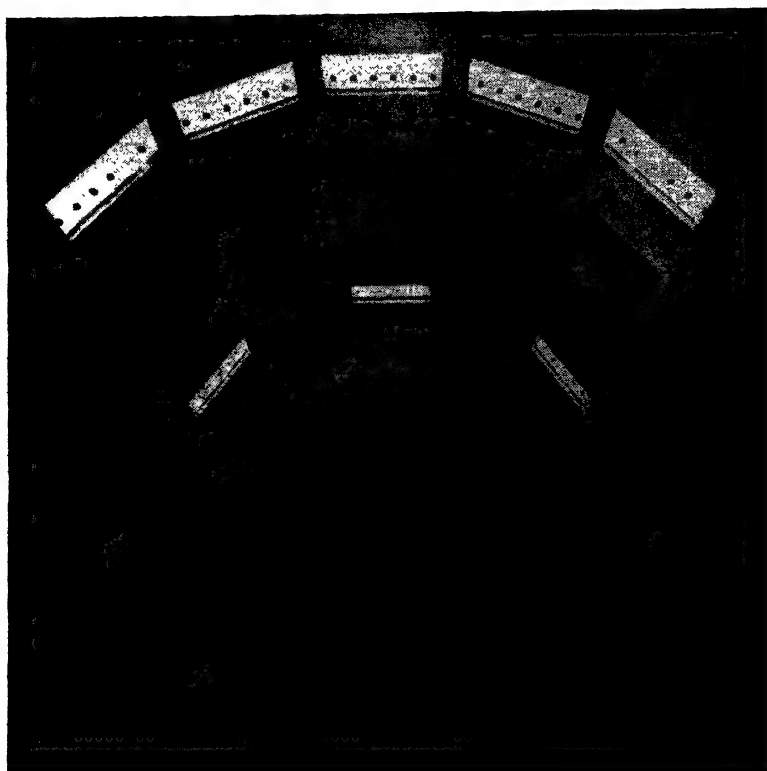


FIG. 4-2. Twenty-Foot Free-Spinning Tunnel of the NACA (Langley Field). The spinning model is launched by the operator on the right. The middle operator records the spinning characteristics by means of a motion-picture camera. The operator on the left controls the air speed. (NACA photograph.)

glide velocity and by tilting the tunnel axis through an angle corresponding to the glide angle. The model is equipped with control surfaces electrically operated through fine wires leading from the aft section of the fuselage, and the "pilot" is able to control its flight.

The velocity of air through the test section of a wind tunnel may be less than the speed of sound (*subsonic*) or greater than the speed



FIG. 4-3. NACA Gust Tunnel (Langley Field). The model is shot from the catapult to pass over the vertical jet of air and is caught in a net to the left. A camera takes speed-flash photographs in rapid succession to record its flight. (NACA photograph.)

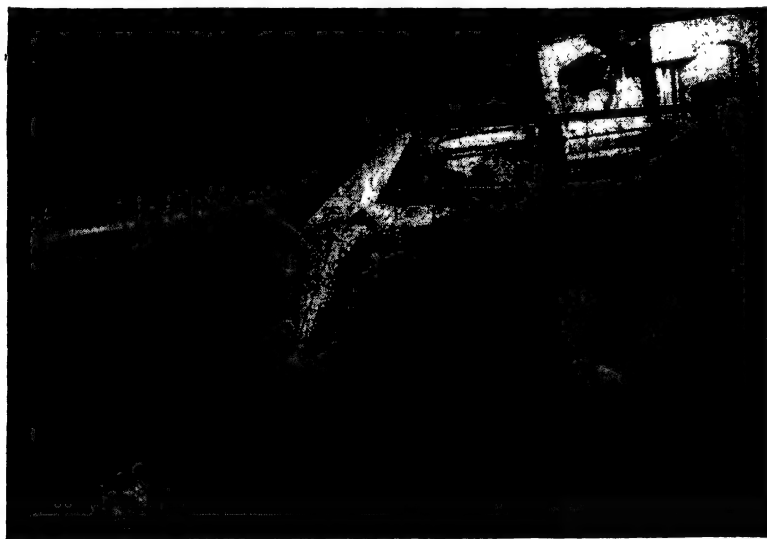


FIG. 4-4. Free-Flight Tunnel of the NACA (Langley Field) showing the model controlled by the "pilot" at the lower left and the tunnel operators at the right. (NACA photograph.)

of sound (*supersonic*). In the former category, wind tunnels may be classed as *low-speed* if they operate at less than about 400 mph, and *high-speed* if they operate above this speed. The low-speed tunnels are used primarily for predicting the aerodynamic characteristics (performance, stability, and control) of an airplane in a range of speeds for which compressibility of the air is not appreciable. The high-speed tunnels are used primarily to show the effect of compressibility on the characteristics. Power required to operate a wind tunnel increases radically with increase in speed; e.g., the 8½ by 12-ft Consolidated Vultee tunnel gives about 300 mph with 2250 hp, while the 8½ by 12-ft Cornell tunnel gives about 700 mph with 14,000 hp.

Supersonic tunnels are constructed so as to have a constricted section upstream of the test section. With increase in speed of the tunnel, the speed in the constricted section increases until the speed of sound is attained. Further power input can produce no speed increase at the constricted section, but a shock wave forms downstream. Sufficient power is applied to make the shock wave occur downstream of the test section; then the constricted region has a Mach number of 1, the test section has a Mach number greater than 1, and the velocity downstream of the shock wave is subsonic. For a particular ratio of constriction area to test-section area, only one Mach number is possible in the test section. In Fig. 4-5 a model is shown mounted in a supersonic tunnel.

B. Circuit. Some tunnels are built in the form of a single tube with the air drawn into an intake and exhausted downstream at the exit, with no provision for guiding the air back into the intake. Most tunnels are built so that the air is recirculated through a *return tube*. The former type is referred to as an *open-circuit tunnel*, and the latter is referred to as a *closed-circuit tunnel*. The former takes less room and is cheap to construct, but generally has large circuit losses; consequently, it is seldom used for tunnels having large power consumption.

The closed-circuit type of tunnel usually has a single return tube but may have the air split in two directions after leaving the expansion section, to return to the test section by two separate tubes. The former type, called a *single-return tunnel* (Fig. 4-6), has less chance for dissymmetry of flow in the test section and fewer adjusting mechanisms than the latter, which is called a

double-return tunnel (Fig. 4-7). It is frequently more expensive to build, however.

Figure 4-8 shows the NACA Variable-Density Tunnel (VDT) that has been of considerable value for showing effect of varying Reynolds number. It is no longer used for testing purposes. It consists of a hermetically sealed tank with circular cross section and hemispherical ends to withstand the large changes in pressure used to vary the density. The circular test section is suspended

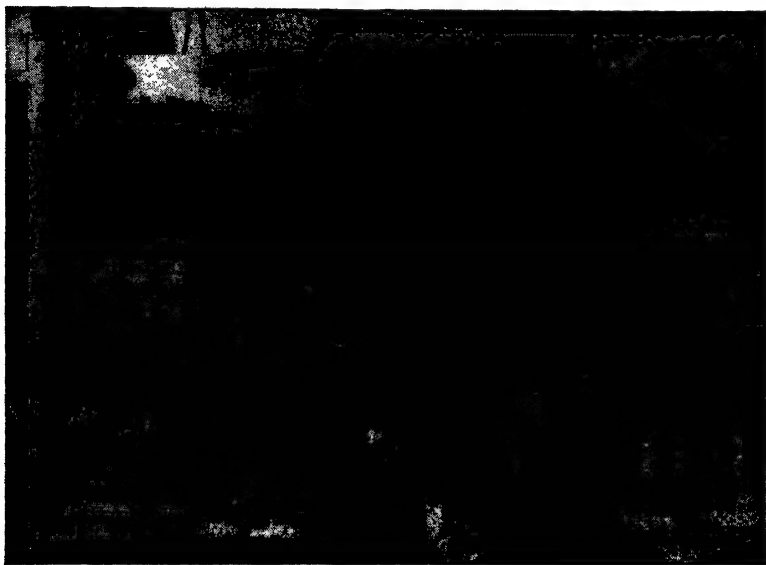


FIG. 4-5. NACA 9-in. Supersonic Tunnel (Langley Field). The model shown in the test section may be tested at Mach numbers from 1.4 to 2.4. Four additional models are shown at the lower left. (NACA photograph.)

in the center of the tank, with the flow in the direction of its longest axis. Return of the air from the end of the expansion is accomplished annularly around the shell that forms the test section and expansion section. This type of tunnel is called an *annular-return tunnel*.

The Variable-Density Tunnel is one of several tunnels in which the air may be pressurized (positively or negatively) in order to simulate a wide range of Reynolds numbers. This procedure involves certain complications in the design of the tunnel. In order to have a balance system that is contained outside the walls of the tunnel but still has structural connection with the model-



FIG. 4-6. Cutaway view of a single-return tunnel. (Boeing Airplane Co. Edmund T. Allen Memorial Aeronautical Laboratory.)

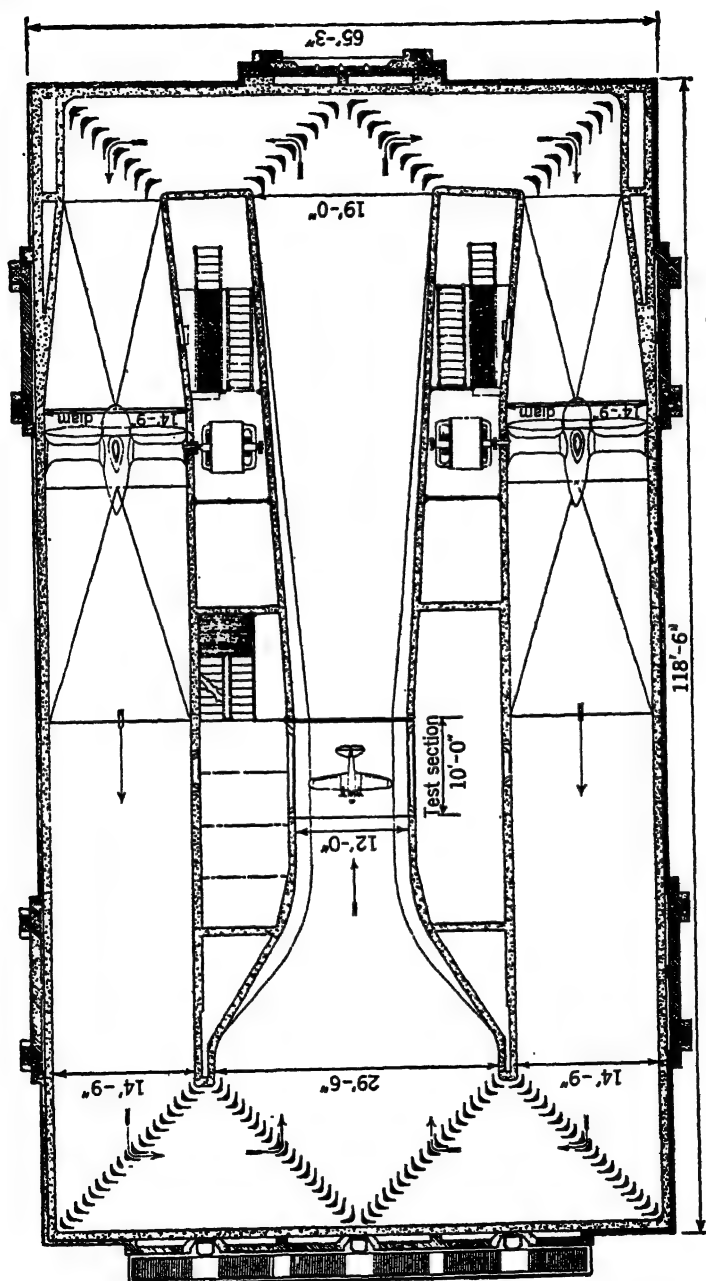


FIG. 4-7. Plan view of a double-return tunnel (UWAL Kirsten tunnel).

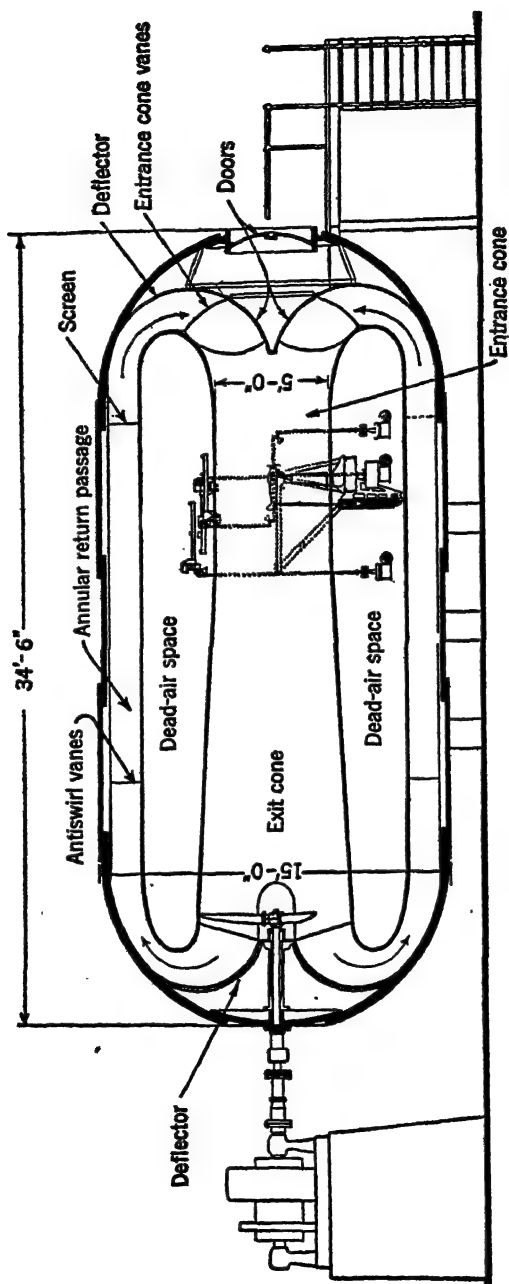


Fig. 4-8. Elevation of an annular-return tunnel (Variable-Density Tunnel) of the NACA at Langley Field. (From TR 416.)

supporting mechanism, a chamber must be built that can be maintained at the same pressure as that in the test section. If the pressures are either very high or very low, men may not work in the balance chamber; hence, all the balance system must be operated by remote control.

A nonpressurized, closed-circuit tunnel must have some point in its circuit vented to the atmosphere. This is usually accomplished at the test section by means of an *atmospheric slot* down-



FIG. 4-9. Air exchanger. The cool air enters the louvers at the top of one tower and the warm air is exhausted out the other (United Aircraft Corp. 18-ft main wind tunnel).

stream of the model. The test section then operates at atmospheric pressure, and none of the complications described above are present. For high-speed subsonic tunnels, or in tunnels used for testing engines, the dissipation of heat through the walls may not be sufficient to keep the air relatively cool. Some of the heat may be removed by running water through the corner vanes (see Sec. *D* below) or wall surface of the tunnel, but if this is insufficient, part of the air must be exhausted for every complete circuit around the tunnel. (In engine tests it is mandatory that some of the air be exhausted to carry away the burned gases from the engine.) An *air exchanger* is installed in the low-velocity region of the tunnel for this purpose (Fig. 4-9). It is usually

adjustable so that from 0 to 25 per cent of the air is exchanged in each cycle. Its installation requires that the test section operate under reduced pressure, and again a sealed chamber must be provided to house the balance system. For a subsonic tunnel the pressure reduction is not sufficient to prevent men working in the balance chamber (usually the pressure conditions correspond to a maximum of about 15,000 ft altitude), but it requires



Fig. 4-10. Open-throat wind tunnel (NACA Full-Scale Tunnel at Langley Field). (NACA photograph.)

a system of locks to allow men to pass in and out during a test. Again the balance system may be operated by remote control, however, in which case the locks are not necessary.

C. Test Section. Most wind tunnels are *closed-throat*, by which is meant that the test section is completely enclosed by the tunnel walls. In some tunnels, the test section may be *open-throat*, which means that there are no walls at the test section. Design of the latter type (Fig. 4-10) has inherent characteristics that limit the length of test section; also, there is some possibility of extraneous vortices and crosscurrents entering the stream from the room itself.

The shape of the test section must be determined primarily by

the type of bodies to be tested. In a tunnel that is to be used for testing bodies of arbitrary shape, the test section should probably be about as wide as it is high, and hence a circular, hexagonal, or square test section is desirable. For a wind tunnel in which airplane-model tests constitute a major portion of the work, a

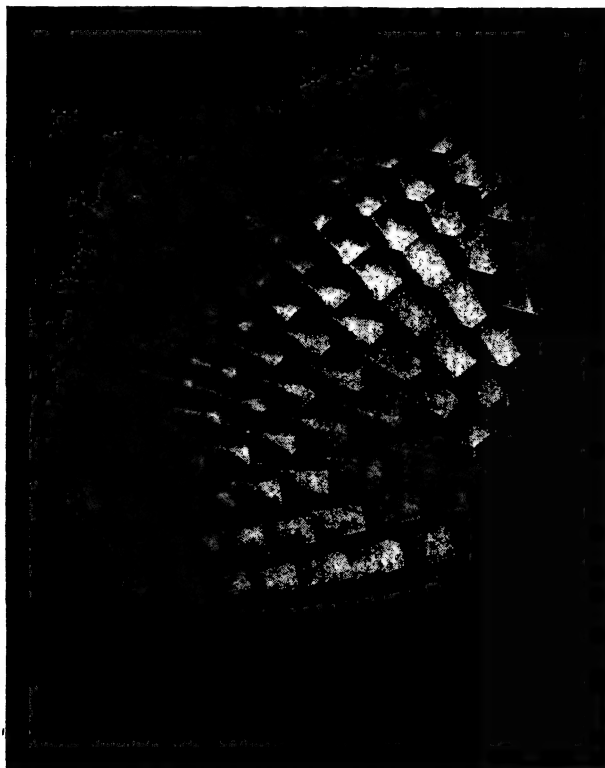


FIG. 4-11. Bellmouth and honeycomb installation in an open-circuit tunnel (UWAL 30-in. hexagonal tunnel).

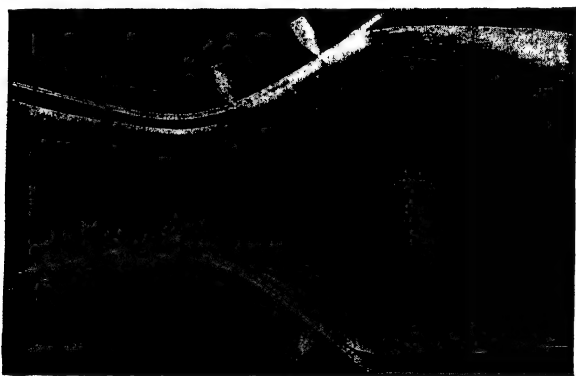
test section wider than it is high is dictated from the standpoint of most effective use of the cross-sectional area for minimum interference of the wall on the model; hence an approximately elliptical or rectangular section produces the best results. A flat floor is particularly desirable because it is handier from the standpoint of work on the model and allows incorporation of a model-supporting system that may be rotated on a horizontal table (see Sec. E). A *two-dimensional* tunnel is built with a narrow

but high test section, and the short-span airfoil is mounted horizontally between the walls.

D. Flow Improvement. The flow characteristics of a wind tunnel may be improved by any means that succeeds in reducing



(a)



(b)

FIG. 4-12. Prevention of separation in an expanding tube through the use of boundary-layer control: (a) no suction, (b) with suction. (*Reproduced by permission of Engineering Societies Monograph Committee from "Applied Hydro- and Aeromechanics," by L. Prandtl and O. G. Tietjens, McGraw-Hill Book Company, Inc., 1934.*)

the periodic or circulatory pattern inserted by a propeller, contraction, expansion, corner, etc.

An open-circuit wind tunnel is always built with a large *bell-mouth* to prevent the formation of a *vena contracta* (region of separated flow in which the air is unable to execute the sharp

corner at the intake). The bellmouth is frequently followed by a *honeycomb* (Fig. 4-11). Its purpose is to break down large vortices into a great number of small ones that dissipate more rapidly. The individual sheets of the honeycomb are sometimes adjustable to control direction of the flow. Honeycombs are seldom used in closed-circuit tunnels, because the contraction upstream of the test section is very effective in damping out excessive turbulence.

Downstream of the test section an expansion is generally built with approximately 7-deg equivalent cone angle¹ in order to

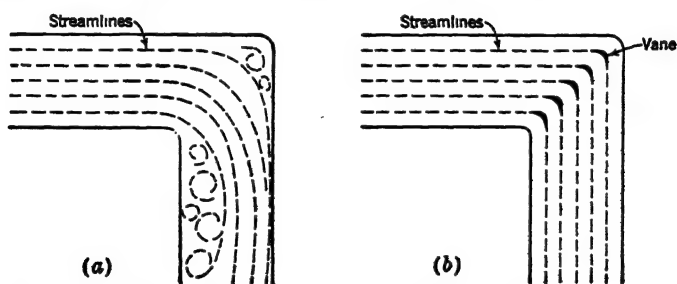


FIG. 4-13. Prevention of separation at the corner of a duct: (a) without vanes—separated, (b) with vanes—unseparated.

prevent separation from the walls. *Boundary-layer control*, or some energy-addition device, may be used to improve tunnel performance by preventing separation in the expansion tube downstream of the test section (Fig. 4-12).

A closed-circuit tunnel must have *corner vanes* to prevent flow separation, as shown in Fig. 4-13. The vanes are usually hollow streamlined airfoils through which water may be circulated for cooling of the air. *Prerotating* vanes are installed before, or *antiswirl* vanes behind, a single-rotating propeller to counteract the rotational flow imposed by the propeller (Fig. 4-14).

Excessive turbulence of the air stream may be reduced by using a large contraction ratio and by using a great number of short-chord vanes. The vanes break down the size of the individual vortices in a manner similar to the honeycomb described earlier.

¹ The length of expansion necessary for a noncircular section may be estimated by representing its section by an equivalent circle of the same area, then computing the length of truncated cone required to give a 7-deg cone angle. This procedure is empirical and is not reliable for slender cross sections.

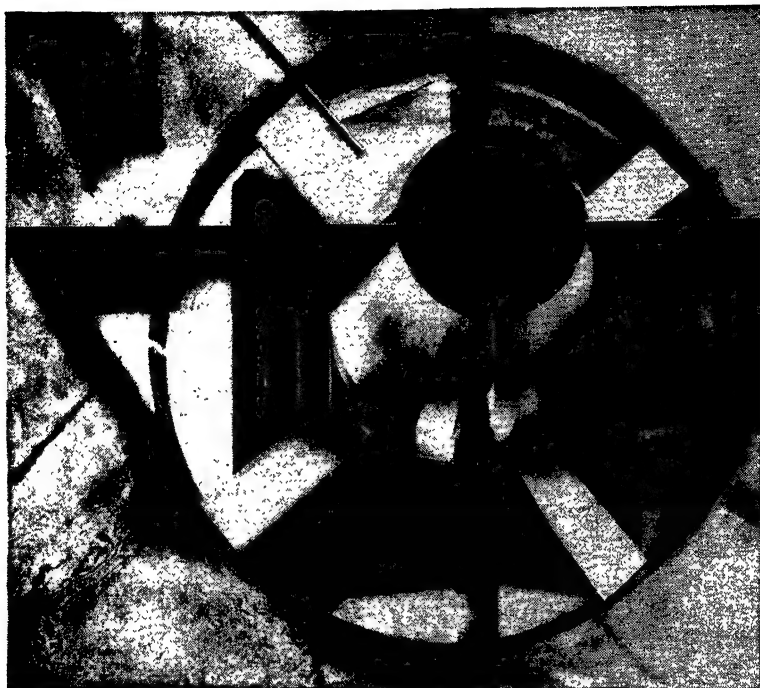


FIG. 4-14. Antiswirl vanes installed downstream of a wind-tunnel propeller (United Aircraft Corp. 4- by 6-ft pilot wind tunnel).

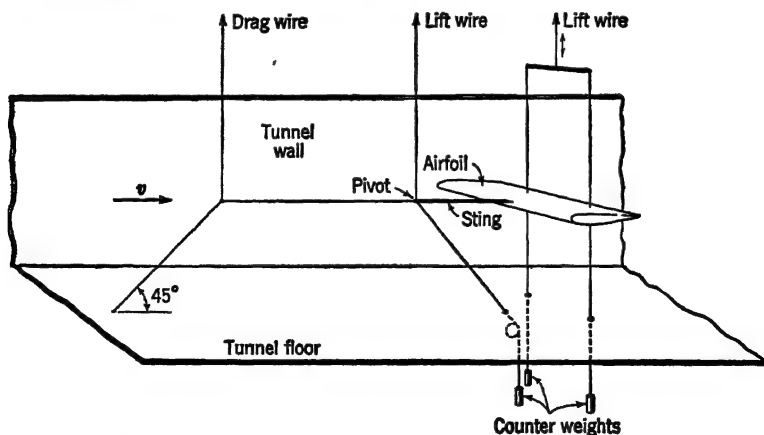


FIG. 4-15. Typical three-component wire system for supporting a model in a wind tunnel. The angle of attack of the wing may be changed by raising or lowering the downstream lift wires.

For a *low-turbulence tunnel* in which the eddies are to be kept to an absolute minimum, single or multiple *screens* may be installed in the low-velocity region upstream of the test section. They consume a considerable amount of power.

E. Model Support. Model support may be accomplished either by a wire or a strut system. In the wire system it is advisable to have the model inverted in order to reduce the size of necessary counterweights and hence keep wire dimensions to a minimum.



FIG. 4-16. Single strut and fork system for model mounting. The strut is a stationary windshield that houses the columns to which the three forks are attached (Lockheed Aircraft Corp. wind tunnel).

The system is critically dependent upon its alignment, and large errors in determining drag of a model result if the lift wires are inclined even slightly from the vertical (Fig. 4-15). The major disadvantage of a wire system is the complexity associated with the installation and removal of a model, caused by the numerous wires and model fittings.

The strut system allows rapid installation and removal of a model, because generally only three attachments are used. This system may consist of a single strut from which *forks* project (Fig. 4-16) that allow rotation of the model in two planes, *i.e.*, pitching and yawing; or it may consist of three struts from which *bayonets* project. These struts are attached to a common table

so arranged that its rotation in the horizontal plane produces yaw, and raising and lowering of the rear bayonet produces pitching of the model (Fig. 4-17). The advantages of this latter arrangement are considerable because of the adaptability of the system to models of any span and to bodies of any type, since the individual struts may be shifted laterally and up- and downstream on the table.

F. Force Measurement. In a mechanical system, the force to



FIG. 4-17. Three-strut and circular-table system for model mounting. The three struts are windshields that line up with the air stream when the model is yawed. They house the columns to which the bayonets are attached. (Boeing Airplane Co. Edmund T. Allen Memorial Aeronautical Laboratory.)

be measured is transmitted to a conventional balance in which a sliding weight on the beam, or number of fixed pan weights, produce the balance (Figs. 4-18a and b). With an electromechanical arrangement, the balancing of the forces is accomplished electromagnetically (Fig. 4-18c). Equilibrium in either system may be established automatically by electrical devices; *i.e.*, a motor may be arranged to drive the moving weight in Fig. 4-18a, or add and subtract pan weights in Fig. 4-18b, or a photocell circuit may be arranged to change the current in Fig. 4-18c.

Forces may also be measured with mechanical or electrical *strain*

In a mechanical strain gage the deflection or "strain" of a

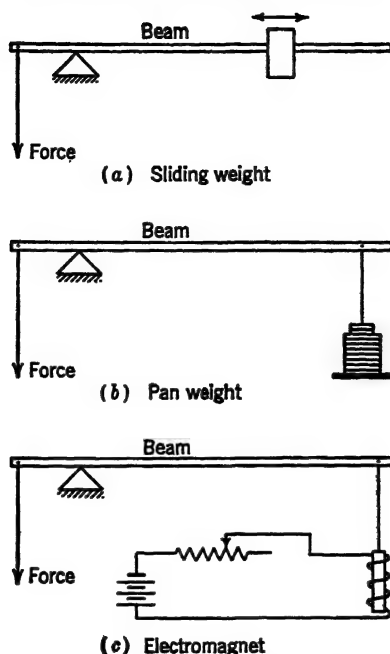


FIG. 4-18. Typical mechanical and electromechanical systems used to indicate model forces.

structural element supporting the model is multiplied by a gear train for easy reading on a dial. The electrical strain gage indicates the deflection by a change in electrical resistance of a fine wire pasted to the structural element.

A *hydraulic capsule* may be used to measure force in the following manner: The load is transmitted to a diaphragm as in Fig. 4-19; a constant pressure source produces a pressure in the cell that depends upon the size of gap between the diaphragm and the outlet. Equilibrium is established when the internal force arising from the pressure in the cell

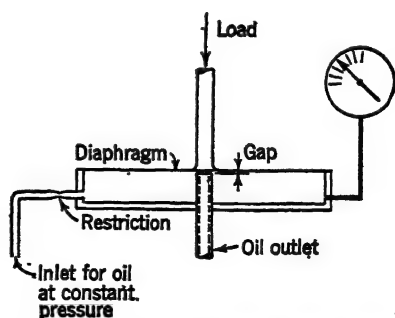


FIG. 4-19. Hydraulic-capsule method used to indicate model forces. (Reproduced by permission, with minor modifications, from "Wind Tunnel Testing," by Alan Pope, published by John Wiley & Sons, Inc., 1947.)

balances the load. The cell pressure is indicated on a pressure gage and may be calibrated in terms of the load.

Some of the most elaborate wind tunnels are equipped with automatic recorders to register continuous force and moment readings with a stylus, oscillograph, or card-punching mechanism.

Indirect determination of forces is accomplished by measuring body static pressures, tunnel-wall static pressures, or wake total pressures. Each method requires integration to obtain the force, but although an integrating manometer may be used and great accuracy is possible, the methods have a very restricted application.

4-3 Visual Flow Aids. Qualitative indications of the flow pattern on a body may be obtained in a number of ways. Usually the body must be tested in a two-dimensional tunnel in which the height of the test section is much greater than its width and the model completely spans the tunnel. For low speeds and slight expense, there are a number of methods by which flow may be observed that involve the introduction of some foreign material into the air stream. Unfortunately, some of the best agents are irritating if not toxic. Titanium tetrachloride and fuming stannic chloride produce dense white clouds of smoke but are very irritating to the nostrils. Furthermore they are likely to be injurious to mechanical equipment because of the presence of hydrochloric acid. Dry ice gives a weak smoke that may be made denser by heating with water; however, condensation is a major problem in this method. Sometimes smoke from burning wood, etc., or fumes from heated oil or kerosene are used, but these methods require special equipment and are generally somewhat dangerous. Talc or other fine inert powder agitated with air provides one of the cheapest and safest methods for this type of flow visualization.

The flow may also be shown by painting the surface of the body, or the walls of the tunnel next to the body, with a mixture of kerosene and lampblack. The streaks produced by the passing air show the pattern. Another frequently used method is to attach tufts of thread to the surface of the body by means of cellulose tape so as to allow the thread to assume the direction of the local flow. Both methods show conditions only within the boundary layer.

For very high speeds, subsonic and supersonic, one of three methods is commonly used: the *shadow* method, the *schlieren* or *striae* method, or the *interferometer* method. Each procedure takes advantage of the changes in density that accompany changes in static pressure on an airfoil or other similar body in a flow field.

The shadow method uses a small but intense light source, a lens to make the light rays parallel, and a screen or photographic plate on which the light rays are caught (Fig. 4-20a). The model is situated between the lens and screen. A density gradient on the model produces deflection of the light rays but produces no change in light intensity on the screen. A *change* in density gradient

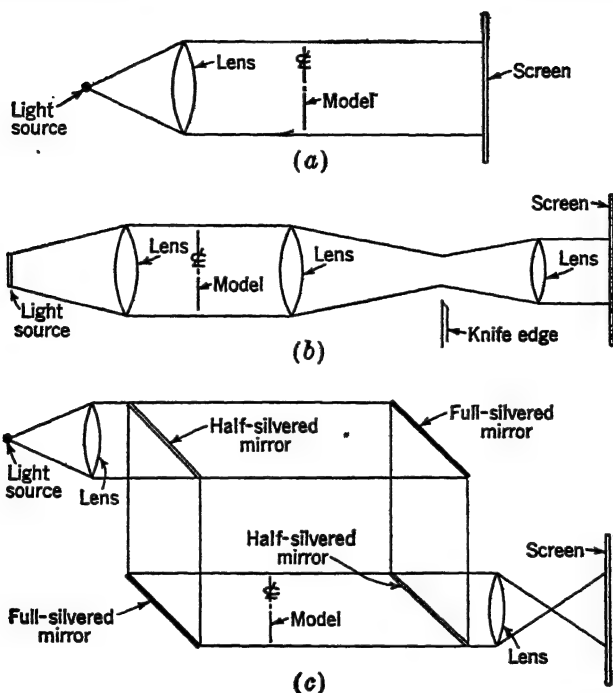


FIG. 4-20. Simplified diagram of (a) shadow, (b) schlieren, and (c) interferometer setups.

causes the light rays to either converge or diverge, and hence produces either an increase or a decrease in light intensity on the screen. The method is not very satisfactory unless the flow contains steep density gradients. These gradients occur, for instance, in passing through a shock wave, as shown in the shadowgraph in Fig. 8-6.

The schlieren method is represented diagrammatically in Fig. 4-20b by a large light source whose light rays pass through a set of lenses, and are finally caught on a screen or photographic plate. If a knife-edge is inserted part way into the light beam

at the focal point of the second lens, the illumination of the whole screen is uniformly reduced. If now a model is inserted between the first two lenses, as shown, a density gradient at some point on the model may produce, say, a downward deflection of the light rays. These rays are intercepted by the knife-edge, and thus the light intensity is reduced locally on the screen. Conversely, upward deflection produces a local increase in light intensity on the screen. Photographs obtained by the schlieren method are



FIG. 4-21. General view of a schlieren setup for a supersonic tunnel (NACA 1- by 3-ft supersonic tunnel at Moffett Field). (*NACA photograph.*)

characterized by light and dark areas as in Fig. 8-10, but the interpretation of these areas depends upon the orientation of the knife-edge; *i.e.*, it depends upon whether the knife-edge is inserted at the left or right, or top or bottom of the light beam. Figure 4-21 shows a typical schlieren setup for a supersonic tunnel.

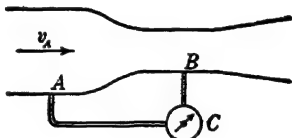
The interferometer method is shown diagrammatically in Fig. 4-20c. Monochromatic light passes in parallel rays by two paths through a set of full-silvered and half-silvered mirrors and is finally caught on a screen or photographic plate. A model inserted in one of the paths may produce a density locally that is different from that in the other path. Since speed of light is a function of the density of the medium through which it passes,

the two paths produce light waves that are out of phase. This results in characteristic "interference fringes" or lines of high and low light intensity on the screen. The difference in density between two points in the air stream is proportional to the number of fringes between the two corresponding points on the screen.

PROBLEMS

4-1. A circular, single-return tunnel is constructed with a 2.45:1 diameter ratio of contraction. The minimum area is at the test section. What error in test-section dynamic pressure results from assuming it is equal to the difference in static pressure between the maximum and minimum sections? Assume a perfect fluid.

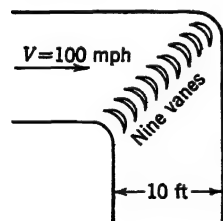
4-2. A mechanically accurate air-speed indicator C is connected to two static-pressure leads, A and B , in the side of a circular tube, through which air is passing. Diameter of tube at A is 2 ft. Diameter of tube at B is 1 ft. Air density in the tube $\rho = 0.0018$ slug per cu ft. If the air-speed indicator reads 150 mph, what is the true air speed at B ? Assume no losses occur from A to B .



4-3. A student ran a wind-tunnel test to find the lift coefficient of an airfoil. He read the lift balance and computed the lift coefficient as $C_L = 0.28$, but unfortunately, made two errors during the test:

1. He thought the slant-tube manometer by which he measured dynamic pressure was inclined at 30 deg, but it had slipped to 25 deg.
2. He assumed the barometric pressure was standard. It was 30.5 in. of mercury.

Find the correct lift coefficient.



4-4. Corner vanes in a wind tunnel are used to deflect the air through 90 deg. Nine vertical vanes are used in a tunnel that has a cross section 10 ft across and 20 ft high (see diagram). If the velocity $V = 100$ mph, find the magnitude and direction of the aerodynamic load on each vane. Assume perfect fluid and standard conditions.

4-5. An airplane has aspect ratio $A = 8$ and wing area $S = 1250$ sq ft. It is designed to cruise at 10,000 ft at an indicated air speed $V_i = 220$ mph. A geometrically similar model is to be tested in a wind tunnel at the same Reynolds number as that for the cruising condition of the full-scale airplane. Model chord $c = 9$ in.; test velocity $V = 250$ mph at temperature $t = 80$ F. What should the pressure be in the test section (atm)? (1 atm = 14.7 psi.)

CHAPTER 5

AIRFOIL CHARACTERISTICS

It is fitting that the aerodynamic properties of airfoil sections and wings be the subject of rather intensive study in this and subsequent chapters, for these characteristics are important, not only in so far as the wing itself is concerned, but also because they determine successful operation of the stabilizer, fin, propeller, etc. The force system on an airfoil arises directly from an unbalanced static pressure that is distributed normal to the surface and an unbalanced shearing stress that is distributed tangential to the surface. The pitching moment arises from an unbalanced couple produced by these same influences.

In this chapter only airfoil and wing characteristics are considered, but some problems involving complete airplanes will be discussed, in which case the airplane lift will generally be assumed equal to the wing lift, the airplane drag will be assumed equal to the wing drag plus a constant, and the aerodynamic moment will be assumed to arise only from the wing lift and moment and from the tail lift.

5-1 Force Representation. The complete force system on a wing may be represented in magnitude by a resultant force R ; in direction by an angle γ ; and in position by the point at which the resultant intersects the chord, called the *center of pressure* (cp), measured in fraction of chord from the leading edge (Fig. 5-1a).

For aerodynamic purposes, the foregoing system is not too satisfactory; a second method of representation involves resolution of the resultant into two components: the first, called *lift* L , perpendicular to the remote velocity, and the second, called *drag* D , parallel to the remote velocity. Both forces are assumed to pass through the center of pressure (Fig. 5-1b).

A third method involves transferring the force system to a reference point on the chord (say n per cent chord) and accompanying the transfer by the necessary pitching moment M_n about the point n , a positive value of which is defined as a "climbing" moment (Fig. 5-1c).

A fourth method is similar to the third but has the two force vectors perpendicular and parallel to the chord instead of to the remote-velocity vector. They are called the *normal force* N and *chordwise force* C , respectively (Fig. 5-1d). Use of this method is restricted almost completely to structural analyses.

The four systems are shown in Fig. 5-1 for positive forces and moments. They are equivalent, and one system may always be derived from another. The resultant is reduced to components

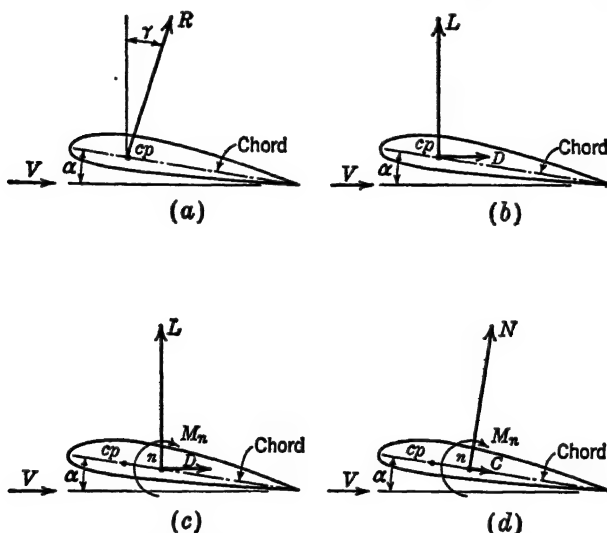


FIG. 5-1. Various equivalent methods for representing the force system on an airfoil.

because for steady level flight, the lift directly balances the weight, and the drag balances the thrust. The force system is transferred to a fixed reference point, in the third and fourth methods, because the cp is a variable quantity. Frequently used references are the 25 per cent chord and the airplane center of gravity (cg); since the cg occurs close to the wing chord on most aircraft, it is frequently defined as the point *on the chord* through which the weight acts.

Pressure drag or *form drag* and viscous drag or *skin friction* together constitute *profile drag* of a wing or *parasite drag* of an airplane. The difference between parasite drag and profile drag is called *residual drag*. *Induced drag* is present even for a perfect fluid in which there is no profile or parasite drag, and it arises from

the rearward inclination of the resultant vector on a lift-producing body. Lift, induced drag, and pitching moments are predictable by perfect-fluid theory provided there is no separation of flow from the body surface. Profile and parasite drag, which are a direct result of fluid viscosity and compressibility, are not predictable from this theory and must be derived from semiempirical relations.

The equations for lift and drag shown in Chap. 2 are repeated here:

$$\left. \begin{aligned} L &= C_L S \left(\frac{1}{2} \rho v^2 \right) \\ &= C_L S \frac{V^2 \sigma}{391} \\ &= C_L S q \end{aligned} \right\} \quad (5.1)$$

$$\left. \begin{aligned} D &= C_D S \left(\frac{1}{2} \rho v^2 \right) \\ &= C_D S \frac{V^2 \sigma}{391} \\ &= C_D S q \end{aligned} \right\} \quad (5.2)$$

5.2 Lift. Any arbitrary body set unsymmetrically with respect to the remote velocity may be expected to produce some amount of lift. An airfoil is specifically designed to produce a large amount of lift but at the same time give only a small drag. It accomplishes its purpose by deflecting a large quantity of air with a minimum retardation of velocity.

Another effective method for producing a large amount of lift is to rotate a cylinder at constant rpm in a stream of air; however, because the drag produced by such a system is prohibitive for aircraft use, it is only of academic interest. This same *Magnus effect* accounts for the flight curvature produced by cut of a tennis ball, slice or hook of a golf ball, and curve or drop of a baseball, and it serves as an introduction to the concept of *circulatory flow*.

A fluid element in a perfect fluid that, by some means, is rotated about a fixed center, has a centrifugal force that is exactly balanced by a static-pressure force. Consider a fluid element having unit depth (into the paper) and dimensions dr and ds in the plane of rotation (Fig. 5-2). The centrifugal force is

$$dF_c = (\rho \, dr \, ds) \frac{v_t^2}{r} \quad (5.3)$$

where r is radius from the center of rotation to particle, ft
 v_t is tangential velocity, fps

and the pressure force is

$$dF_p = dp \, ds \quad (5-4)$$

where dp is the radial pressure differential across the element in pounds per square foot. Equating Eqs. (5-3) and (5-4) gives

$$\frac{dp}{dr} = \frac{\rho v_t^2}{r} \quad (5-5)$$

The Bernoulli equation may be differentiated:

$$dp = -\rho v_t \, dv_t \quad (5-6)$$

Substituting Eq. (5-6) in Eq. (5-5) yields

$$\frac{dv_t}{v_t} = -\frac{dr}{r} \quad (5-7)$$

Thus

$$v_t = \frac{K}{r} \quad (5-8)$$

where K is a constant. *The tangential velocity is seen to vary inversely with the radius.* It will be recalled that the discussion refers to a perfect fluid, which, of course, is inviscid. In a real fluid the tangential velocity at the center must be zero rather than infinite in order to preclude the possibility of having infinite shearing stresses. The influence of viscosity in modifying Eq. (5-8) decreases with radial distance however, and for most practical problems in aerodynamics this equation may be used directly.

The circulatory flow may be investigated further by introducing the concept of the *circulation* Γ . If an arbitrary closed path is considered in any flow field, such that it forms a single loop, the circulation is defined as the integral of the product of the tangential velocity component and the differential path length. The integral is taken around the closed path or line and is properly called a *line integral*, indicated by the symbol \oint ; hence

$$\Gamma = \oint v_t \, ds \quad (5-9)$$

where Γ is circulation, sq ft per sec

v_t is tangential velocity component, fps

ds is elemental path length, ft

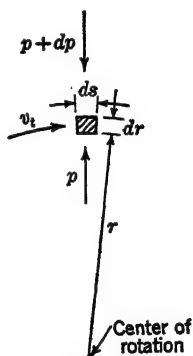


FIG. 5-2. Fluid element in circulatory flow.

The line integral may be unfamiliar to the student, but it should be recalled that an integral sign is a symbol that means "sum," even though the elements of the sum are infinitesimals. Just as the equation

$$z = \int_a^b y \, dx$$

means "add up all the elements that measure y by dx between $x = a$ and $x = b$," so the above line integral means "add up all the elements that measure v_t by ds on the closed path." Referring

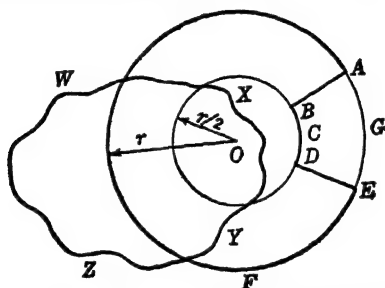


Fig. 5-3. Alternate paths in circulatory flow.

now to the specific problem, the circulation about a circular path having radius r and constant tangential velocity v_t is

$$\begin{aligned} \Gamma &= \oint v_t \, ds \\ &= v_t \oint ds \\ &= v_t (2\pi r) \end{aligned} \tag{5-10}$$

By comparison with Eq. (5-8), the circulation is seen to be *constant* for any circular path about the fixed center. This result may be extended. In Fig. 5-3, consider the path $ABCDEFA$, where BCD is the arc of a circle having half the radius of the circle AEF , while AB and ED are radial. Since the arc length BCD is half AGE but has double its tangential velocity, the circulation along the path $ABCDEFA$ must be equal to that around $AGEFA$. From this it is intuitively concluded that the circulation is the same for all paths that include the fixed center O (such as $WXYZ$, for instance). Also the circulation about any path that does not include the fixed center is *zero* (such as $AGEDCBA$, for instance). It is important to realize the significance of these results because the concept of circulatory flow allows solution of the ideal flow around a rotating cylinder, airfoil, etc., and provides a firm founda-

tion for an appreciation of some of the phenomena to be described in the remaining chapters.

A fortunate characteristic of the circulatory flow is that it may be combined with other types of flow, and the velocity at a point can then be obtained by simple vector addition of the contributing velocity components. This is the so-called *principle of superposition*. It will be illustrated now by an infinite cylinder that rotates in a moving perfect fluid. The influence of the cylinder on the streamlines is obtained by composition of the *rectilinear* and *circulatory* flow. The former flow is shown in Fig. 5-4 as a series of streamlines that have their direction unchanged by passage over the cylinder, while the latter is shown as a series of streamlines for which the circulation is constant; hence the velocity varies inversely as the radius.¹

The surface value of the rectilinear velocity has been given in Art. 2-7 and is repeated here:

$$v = 2v_0 \sin \theta \quad (5-11)$$

The surface value of the circulatory flow is given by Eq. (5-10), with $r = R$.

$$v_i = \frac{\Gamma}{2\pi R} \quad (5-12)$$

The total surface velocity is obtained by vector addition of the velocities from Eqs. (5-11) and (5-12); however, since they are in the same direction (tangent to the surface), the addition may be accomplished algebraically; thus

$$\begin{aligned} v_0 &= v + v_i \\ &= 2v_0 \sin \theta + \frac{\Gamma}{2\pi R} \end{aligned} \quad (5-13)$$

¹ A natural question arises here because it seems inconsistent to speak of a rotating cylinder being able to cause the perfect fluid to rotate. The present discussion is concerned only with the state of affairs *after* the fluid has been rotated by some means. After it has been started, it will rotate indefinitely. In a real fluid, the circulation is maintained by friction between the fluid and cylinder.

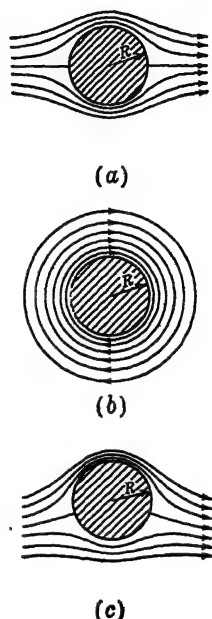


FIG. 5-4. Flow patterns on an infinite circular cylinder: (a) rectilinear, (b) circulatory, (c) combined rectilinear and circulatory.

For the chosen directions of flow shown in Fig. 5·4, the velocity on the upper surface is increased, while the lower surface velocity is decreased; furthermore, the front stagnation point moves rearward on the lower surface, and the rear stagnation point moves

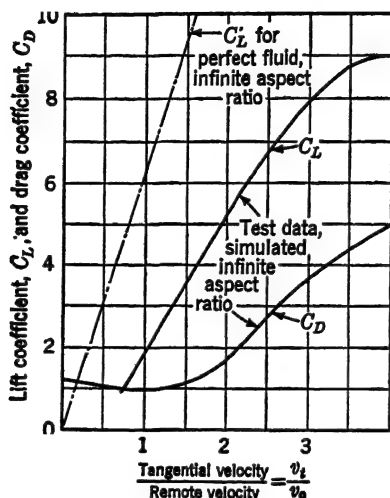


FIG. 5·5. Aerodynamic characteristics of a rotating cylinder. (Replotted by permission from "Elementary Mechanics of Fluids," by H. Rouse, published by John Wiley & Sons, Inc., 1947.)

forward. By combining the Bernoulli equation and Eq. (5·13), the lift per unit span on the infinite cylinder is given by

$$\frac{L}{b} = \rho v_0 \Gamma \quad (5·14)$$

Equation (5·14) is called the *Kutta-Joukowski lift equation*. For the cylinder considered it may also be written

$$\frac{L}{b} = \rho v_0 (2\pi R v_t)$$

and may be expressed in terms of the lift coefficient, using Eq. (5·1),

$$C_L = 2\pi \frac{v_t}{v_0}$$

This theoretical value of the lift coefficient is much larger than is realized experimentally (Fig. 5·5), primarily because of the major importance of viscosity, which is responsible for the large wake

shown in Fig. 5-6. Experimental data for a rotating sphere are presented in Fig. 5-7 for comparison with the cylinder data.

Attention is now directed to the flow of a perfect fluid on an



FIG. 5-6. Flow pattern on a rotating cylinder in a real fluid. Peripheral velocity is double the remote velocity. (Reproduced by permission of Engineering Societies Monograph Committee from "Applied Hydro- and Aeromechanics," by L. Prandtl and O. G. Tietjens, McGraw-Hill Book Company, Inc., 1934.)

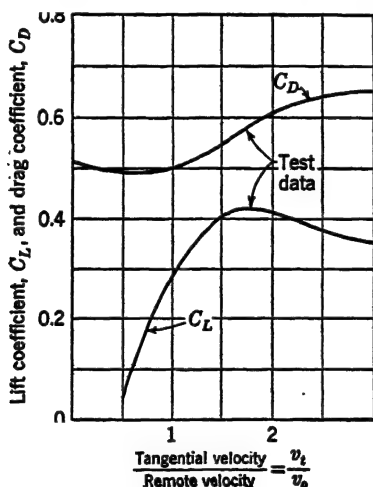


FIG. 5-7. Aerodynamic characteristics of a rotating sphere. (Replotted by permission from "Elementary Mechanics of Fluids," by H. Rouse, published by John Wiley & Sons, Inc., 1947.)

airfoil of infinite aspect ratio. The principle of superposition is again applied, as shown in Fig. 5-8. The circulatory flow does not follow concentric circles because of the shape of the airfoil;

however, at a sufficiently great distance from the airfoil, the flow does approach a circular path, and Eq. (5.14) may again be used. (Recall that the circulation about a path with infinite radius is identical to that around the airfoil itself.) The shape of the circulatory flow pattern *in the immediate vicinity* of the airfoil may be established by distributing along the mean line a series of

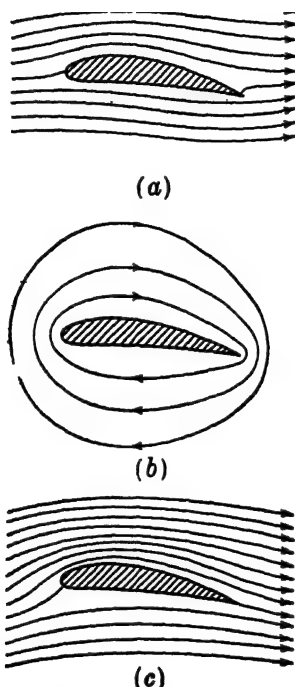


FIG. 5-8. Flow pattern on an infinite airfoil: (a) rectilinear, (b) circulatory, (c) combined rectilinear and circulatory. (From TR 116.)

vortices similar to the single vortex used to represent the cylinder. By a more elegant procedure, the cylinder of Fig. 5.4 may be "transformed" into the airfoil of Fig. 5.8 by means of transformation equations that allow solution of the complete flow pattern. This process of *conformal transformation* is beyond the scope of this text, but it is interesting to observe that the apparently complicated flow about an airfoil lends itself to mathematical solution. The solution obtained in this manner is, of course, more representative of the flow in an actual fluid than is the solution obtained

for the cylinder, because of the characteristically smaller wake. The circulation on the airfoil must be just sufficient to move the rear stagnation point in Fig. 5-8a to the trailing edge, as in Fig. 5-8c. This limitation is necessary in order to exclude the possibility of an infinite velocity around the sharp trailing edge.

Equation (5-14) may be combined with Eq. (5-1) to obtain a relation between lift coefficient and circulation that will have considerable value in later analyses.

$$L = \rho b v \Gamma = C_L b c \frac{1}{2} \rho v^2$$

$$C_L = \frac{2\Gamma}{cv} \quad (5-15)$$

Recall that Eq. (5-15) applies only to a wing having infinite aspect ratio.

The lifting force on either the cylinder or airfoil must arise entirely from a pressure differential between the lower and upper surface.¹ For low angles of attack, of the airfoil, the pressure differential arises from an upper-surface pressure that is more negative than the lower. For high angles of attack, it arises from a large negative pressure on the upper surface and positive pressure on the lower surface. The Bernoulli equation requires a high velocity for large negative pressures and low velocity for positive pressures, so that the amount of circulation required to produce the required lift varies with angle of attack. The fundamental difference between the cylinder and airfoil is then seen to be in the manner by which a velocity (or pressure) difference is obtained on the two surfaces: the cylinder must be rotated to shift the front and rear stagnation points below the horizontal diametral planes, whereas the airfoil, which has its rear stagnation point fixed at the trailing edge, needs only an increment in angle of attack to shift the front stagnation point rearward along the lower surface. Both systems produce a velocity on the lower surface that is less than it would be without circulation and a velocity on the upper surface that is greater than it would be without circulation; hence, each surface of both systems contributes to the total lift.

From theoretical considerations, the lift derived from an airfoil at constant velocity is linearly dependent upon the angle of attack. From test data on airfoils, a linear variation in C_L with α is usually

¹ The discussion is limited to a perfect fluid.

shown for a considerable range of angles (Fig. 5-9a). Ultimately, however, the airfoil reaches such an attitude that separation occurs somewhere on the upper surface (Fig. 5-10). The resulting deviation from linearity increases with increase in angle of attack until the maximum C_L value ($C_{L_{\max}}$) is obtained. Beyond the maximum value, C_L decreases, sometimes gradually, sometimes abruptly. The phenomenon is called *stalling*, and the angle corresponding to $C_{L_{\max}}$ is called the *stall angle*, the *burble angle*, or the *angle for maximum lift*. Since separation usually starts well below the

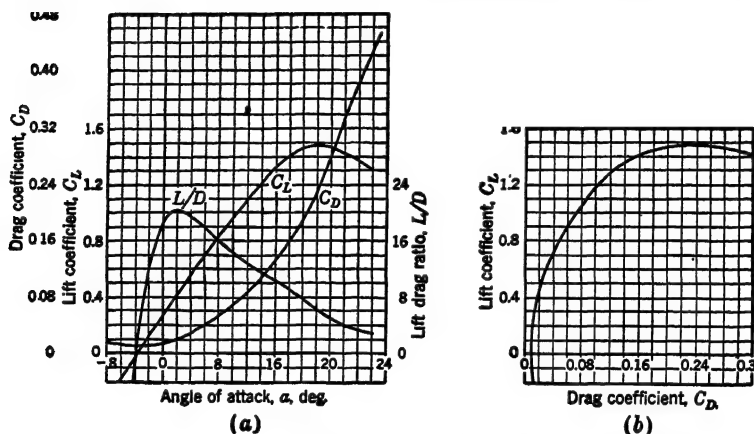


FIG. 5-9. Aerodynamic characteristics of an NACA 4418 airfoil of aspect ratio 6 at Reynolds number of 8,180,000. (From TR 669.)

angle corresponding to $C_{L_{\max}}$, the first two names are technically misnomers, but stalling has become associated with $C_{L_{\max}}$ through long use.

The angle corresponding to $C_L = 0$ is called the *angle of zero lift*, α_{L_0} . It is always zero for a flat plate or symmetrical airfoil section and becomes more negative with increasing camber.

For most airfoils the lift curve may be represented by the linear equation

$$C_L = \left(\frac{dC_L}{d\alpha} \right) (\alpha - \alpha_{L_0})$$

$$C_L = a(\alpha - \alpha_{L_0}) \quad (5.16)$$

where a is lift-curve slope, per deg

α is angle of attack, deg

α_{L_0} is angle of zero lift (usually negative), deg



(a)



(b)

FIG. 5-10. Flow pattern on an airfoil in a real fluid: (a) low angle of attack—unstalled, (b) high angle of attack—stalled. (Reproduced by permission from "The Physics of Solids and Fluids," by P. P. Ewald, Th. Pöschl, and L. Prandtl, Blackie & Sons, Limited, 1936.)

An equation similar to Eq. (5-16) may be written for radian measure:

$$C_L = m(\alpha - \alpha_{L_0}) \quad (5-17)$$

where m is lift-curve slope, per radian

α is angle of attack, radians

α_{L_0} is angle of zero lift, radians

The above equations are obviously not applicable in the stall region where the curve is no longer linear. The slope, a or m , depends primarily upon aspect ratio and Mach number. The angle of zero lift, α_{L_0} , depends upon airfoil section and Mach number, while $C_{L_{\max}}$ depends upon all the variables listed in Art. 2-11 except l_a .

For an airplane in steady (unaccelerated) level flight, the lift must equal the weight; hence

$$\begin{aligned} W &= L = C_L S \frac{V^2 \sigma}{391} \\ V &= 19.78 \sqrt{\frac{W}{C_L S \sigma}} \end{aligned} \quad (5-18)$$

The *stalling speed* V_s corresponds to $C_{L_{\max}}$; thus

$$V_s = 19.78 \sqrt{\frac{W}{C_{L_{\max}} S \sigma}} \quad (5-19)$$

The stalling speed is the absolute lower limit for which level flight may be maintained; hence the advisability of securing a large value of $C_{L_{\max}}$ is apparent. The ratio W/S is frequently referred to as the *wing loading* l_w , and it ranges in value from about 6 to 12 psf for light planes to a maximum of about 50 to 100 psf for heavily loaded cargo planes or bombers.

Example. A flying wing has the following specifications: $l_w = 15$ psf, $V_s = 75$ mph at 10,000 ft. Find $C_{L_{\max}}$.

Solution. From Eq. (5-19),

$$\begin{aligned} C_{L_{\max}} &= \frac{391W}{SV_s^2 \sigma} \\ &= \frac{391l_w}{V_s^2 \sigma} \\ &= \frac{(391)(15)}{(75)^2(0.738)} \\ &= 1.41 \end{aligned}$$

5-3 Drag. Below the stall, for conventional airfoils, the drag curve (C_D vs. α) has an approximately parabolic shape (Fig. 5-9a), but near the stall its shape depends on the severity of the stall. The drag coefficient is comparatively small (the *minimum* C_D is usually about one two-hundredth of the *maximum* C_L), and to allow easier reading, it is plotted to a larger scale than is C_L . Also, C_L and C_D are not usually drawn to scale on a vector diagram such as Fig. 5-1. It is important to realize that the comparative relationship is obscured by these procedures.

In a wind-tunnel test, data are usually recorded for constant values of α , since it specifies model attitude; for this reason, experimental curves are often plotted vs. α . However, when applying the information to aerodynamic problems, particularly those concerned with performance, the lift coefficient is a much more important variable, for it is an immediate indication of airplane speed. The graph of C_L vs. C_D is called a *polar curve* (Fig. 5-9b), because a vector from the origin to any point on the curve represents magnitude and direction of the *resultant* coefficient, provided the coordinates are plotted to the same scale. The drag coefficient is ordinarily plotted to a larger scale than C_L , so again the relative importance of the two coefficients is obscured.

A parabolic shape of C_D vs. α requires a parabolic shape of C_D vs. C_L , because of the linearity of the lift curve. The equation for the parabola is put in the form

$$C_D = A + BC_L^2 \quad (5-20)$$

where A is a constant that depends mostly upon the airfoil section and its Reynolds number and Mach number, and B is a constant that depends mostly upon the wing aspect ratio. The mathematical representation of the polar curve by such an equation does not have great significance when applied to a wing by itself but is of particular importance in the complete airplane, because it allows considerable simplification of the computation of airplane performance.

Curves of C_L and C_D vs. α for an NACA 23015 airfoil are included in Fig. I, Appendix B.

5-4 Lift/Drag Ratio. A commonly used term is obtained by dividing lift by drag, or lift coefficient by drag coefficient. The resulting ratio is called the L/D ratio, and it is usually plotted vs. α as in Fig. 5-9a.

For a power-off glide in still air (flying wing), the lift must equal the weight (assuming $\cos \theta = 1.0$); then from Fig. 5-11 the glide angle θ may be found.

$$\theta = \cotan^{-1} \left(\frac{L}{D} \right) = \tan^{-1} \left(\frac{D}{L} \right) \quad (5.21)$$

The minimum glide angle is seen to correspond to the maximum L/D , written $(L/D)_{\max}$, which is found from the peak of the curve in Fig. 5-9a, or at the point of tangency of a line from the origin

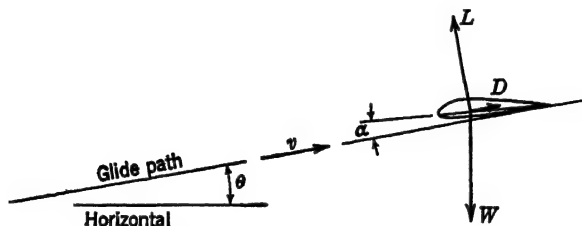


FIG. 5-11. Geometric characteristics of a wing in a glide.

to the curve in Fig. 5-9b. The same reasoning applies to a complete airplane, of course, except that the L/D curve and polar for the complete airplane must be used.

In still air, maximum ground distance is obtained at a speed corresponding to $(L/D)_{\max}$; however, in a head wind the airplane must fly at slightly greater speed, and in a tail wind it must fly at a slightly lesser speed, than that corresponding to $(L/D)_{\max}$. For these latter conditions, the *ground* distance is dependent not only on the glide angle with respect to the *air* ($\tan^{-1} D/L$), but also on the *time* the airplane is in the air; thus a head wind necessitates flying faster in order to reduce the time during which the wind has an opportunity to blow the airplane back toward the starting point. Conversely, a tail wind necessitates flying slower in order to be assisted by the wind in increasing the ground distance (see Prob. 5-5).

5-5 Pitching Moment. In order to discuss the pitching moments on an airfoil, it is important first to appreciate the fact that the lift of an airfoil arises principally from the static pressure which is distributed along its upper and lower surfaces. (The

influence of skin friction may be ignored.) This static pressure arises from three separate influences:

1. That due to angle of attack
2. That due to camber
3. That due to thickness

For the first influence, consider a flat plate at a low positive angle of attack in a perfect fluid. The requirement that the flow in the vicinity of the trailing edge be parallel to the plate trailing edge is fundamental in specifying the required amount of circulation. This has already been discussed in relation to Fig. 5-8. The front stagnation point is downstream from the leading edge on the lower surface, and the pressures are distributed so that the lift always acts at exactly the 25 per cent chord (see Fig. 15-19). For the second influence, consider a cambered flat plate *at zero lift*. In order for the cambered plate to have a total lifting force that is zero, the plate angle of attack must be negative. This implies that the leading-edge region must have a negative lift and the trailing-edge region must have a positive lift. Figure 15-20a shows this effect for a plate having a sharp break at the 70 per cent chord. The pressure distribution would be somewhat similar for a continuously curved plate except that there would be no infinite upper-surface negative pressures. The important point is that an aerodynamic *moment* is introduced by the down lift and up lift at the leading edge and trailing edge, respectively. It is important to realize that the moment produced about the leading edge, say, is exactly the same as the moment produced about any other point on the chord line or in space. *This in turn means that the moment coefficient due to camber is independent of position on the chord.* The third influence may be dispensed with, because the pressure distribution due to thickness alone produces identical changes in pressure on the top and bottom surface and hence adds nothing to either the lift due to angle of attack or the moment due to camber.

The three influences are additive. Since the lift coefficient due to (1) acts at the 25 per cent chord, the moment coefficient about the 25 per cent chord due to (1) is zero (it is not zero for any other point on the chord). Since the moment coefficient due to (2) is the same for any point on the chord, it may be chosen to act at the 25 per cent chord. There is no moment or lift associated

with (3); thus it may be discarded from present considerations. The important conclusion is that the moment coefficient about the 25 per cent chord is constant for all lift coefficients, and its magnitude depends only upon the shape of the mean line.

The discussion has been concerned with a perfect fluid, but even in a real fluid, these same principles hold with surprising accuracy. In a real fluid the lift due to angle of attack does not act at exactly the 25 per cent chord, but its point of action is rarely less than the 23 per cent chord and rarely greater than the 28 per cent chord.

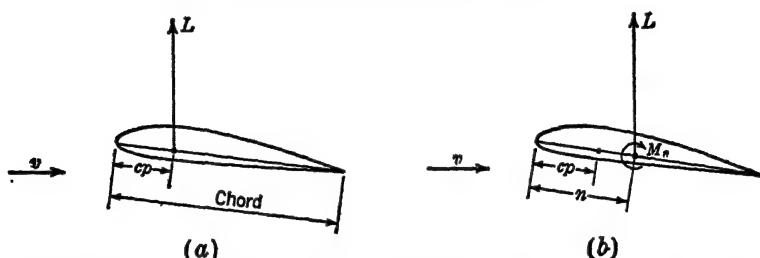


FIG. 5-12. Equivalent methods for representing force system on an airfoil, exclusive of the drag: (a) lift at the center of pressure cp , (b) lift at an arbitrary point n accompanied by a moment about point n .

This reference point is called the *aerodynamic center* (ac), and the corresponding moment coefficient is called the *moment coefficient about the aerodynamic center*, C_{mac} . From the preceding statements, both the ac and C_{mac} are fixed characteristics of a particular airfoil section (see Figs. 9-14 and 9-15, and Table III, Appendix A).

It is frequently convenient to represent the force system on an airfoil by a single force acting at the center of pressure, as in Fig. 5-1a. Since the present discussions are concerned with moments, the drag may be ignored, and the cosine of the angle of attack may be assumed equal to 1 (Fig. 5-12a). An expression may be obtained for the moment about any point n in terms of the lift and center of pressure (Fig. 5-12b):

$$M_n = L(n - cp)c \quad (5-22)$$

where M_n is pitching moment at point n , lb-in.

L is lift, lb

cp is center of pressure, fraction of chord

n is arbitrary point, fraction of chord

c is chord, in.

Both sides of Eq. (5-22) may be divided by qSc in order to produce a nondimensional moment coefficient:

$$C_{m_n} = \frac{M_n}{qSc} \quad (5.23)$$

$$\begin{aligned} &= \frac{L}{qS}(n - cp) \\ &= C_L(n - cp) \end{aligned} \quad (5.24)$$

Equation (5-24) may be rearranged

$$cp = n - \frac{C_{m_n}}{C_L} \quad (5.25)$$

In Eq. (5-25) n is perfectly arbitrary, but if it is chosen as the aerodynamic center, then $C_{m_n} = C_{m_{ac}}$, and

$$cp = ac - \frac{C_{m_{ac}}}{C_L} \quad (5.26)$$

However, since ac and $C_{m_{ac}}$ are *constants*, the center of pressure is seen to be a hyperbolic function of the lift coefficient. This is

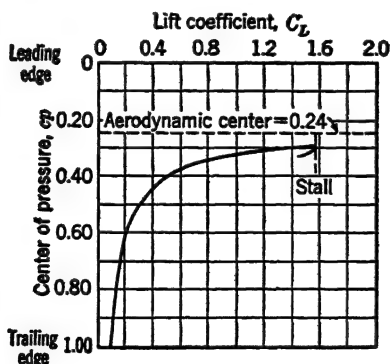


FIG. 5-13. Approximate center-of-pressure variation with lift coefficient for an NACA 4418 airfoil section. (Based on data from TR 669.)

verified by the experimental data shown in Fig. 5-13. In this figure, evidently the distance from the leading edge to the horizontal asymptote is the ac , while the distance from the horizontal asymptote to any point on the curve is $-C_{m_{ac}}/C_L$. Equation (5-26)

may be linearized by choosing $1/C_L$ as a variable instead of C_L ; hence

$$cp = ac - C_n \cdot \left(\frac{1}{C_L} \right) \quad (5-27)$$

The data of Fig. 5-13 have been plotted in Fig. 5-14. Here the intercept is ac , and the slope is $-C_{m_{ac}}$, in accordance with Eq. (5-27). These two curves show that for $C_L = 0$, $cp = +\infty$, which means that the center of pressure moves off the airfoil to infinity down-

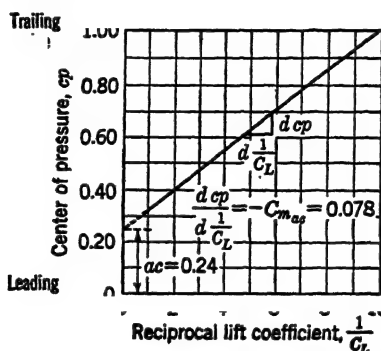


FIG. 5-14. Approximate center-of-pressure variation with lift-coefficient reciprocal for an NACA 4418 airfoil section. (Based on data from TR 669.)

stream as C_L approaches 0. This peculiar condition is a consequence of trying to represent a couple by a single force.

A relationship may now be established for the moment coefficient C_{m_n} about any arbitrary point n and the moment coefficient about the aerodynamic center $C_{m_{ac}}$. From Eqs. (5-25) and (5-26), at a particular C_L

$$\begin{aligned} cp \quad n - \frac{C_{m_n}}{C_L} &= ac - \frac{C_{m_{ac}}}{C_L} \\ C_{m_n} &= C_{m_{ac}} + (n - ac)C_L \end{aligned} \quad (5-28)$$

Figure 5-15 shows the data of Fig. 5-13 plotted for $n = 0.27$. According to Eq. (5-28), the intercept is $C_{m_{ac}}$, and the slope is $n - ac = 0.03$. Since $n = 0.27$, then $ac = 0.24$.

Figures 5-13, 5-14, and 5-15 show three methods for presenting the same aerodynamic data. The latter method is by far the most useful, because it will be shown later that the slope of this curve

is the criterion for stability, whether the curve corresponds to a flying wing or complete airplane.

These discussions may be clarified by examples.

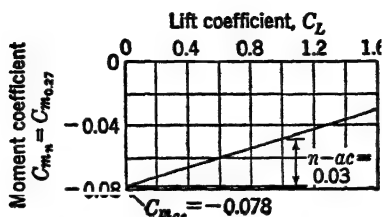


FIG. 5-15. Approximate variation of moment coefficient $C_{m_{30}}$ with lift coefficient for an NACA 4418 airfoil section. (Based on data from TR 669.)

Example 1. For a symmetrical wing, the aerodynamic center is 0.23. What is $C_{m_{0.30}}$ at $C_L = 1.0$?

Solution. Since $C_{m_{ac}}$ must be zero, the pitching moment coefficient at the 30 per cent chord is obtained by substitution in Eq. (5-28).

$$\begin{aligned} C_{m_n} &= C_{m_{ac}} + (n - ac)C_L \\ C_{m_{0.30}} &= 0 + (0.30 - 0.23)1.0 \\ &= 0.07 \end{aligned}$$

This mathematical solution should be compared with its graphical significance as in Fig. 5-15.

Example 2. Find the moment about the 30 per cent chord of an airfoil when $C_L = 0.5$, if for $C_L = 0.5$, $C_{m_0} = -0.20$. Dynamic pressure $q = 100$ psf; span $b = 10$ ft; and chord $c = 2$ ft.

Solution. An equation similar to Eq. (5-28) may be developed in terms of any two arbitrary positions, m and n , instead of in terms of n and ac .

$$C_{m_m} = C_{m_n} + (m - n)C_L$$

Let $m = 0.30$ and $n = 0$.

$$\begin{aligned} C_{m_{0.30}} &= C_{m_0} + (0.30 - 0)C_L \\ &= -0.20 + (0.30)(0.5) \\ &= -0.05 \end{aligned}$$

The moment may be obtained from Eq. (5-23).

$$\begin{aligned} M_n &= C_{m_{0.30}} q S c \\ &= (0.05)(100)(20)(2) \\ &= 200 \text{ lb-in.} \end{aligned}$$

The moment is seen to be a diving moment.

Example 3. The following data are computed from wind-tunnel tests on an airfoil:

$$\text{When } C_L = 0, \quad C_{m_{0.25}} = -0.126$$

$$\text{When } C_L = 0.6, \quad C_{m_{0.20}} = -0.15$$

Find ac and $C_{m_{ac}}$.

Solution. Substitution of the first relation in Eq. (5-28) yields

$$C_{m_{ac}} = -0.126$$

Equation (5-28) may be rearranged to solve for ac :

$$ac = n + \frac{C_{m_{ac}} - C_{m_n}}{C_L}$$

Substituting the second relation given in the problem, along with the $C_{m_{ac}}$, in this equation gives

$$ac = 0.20 + \frac{(-0.126) - (-0.15)}{0.6}$$

$$ac = 0.24$$

Notice that if the first relation in the stated problem had been substituted in the equation for ac , it would have been indeterminate, for when $C_L = 0$, C_m for any point is equal to $C_{m_{ac}}$; hence

$$\frac{C_{m_{ac}} - C_{m_n}}{C_L} = \frac{0}{0}$$

The ac of most airfoils is at approximately the 25 per cent chord and is changed only slightly by changes in the variables listed in Art. 2-11. The $C_{m_{ac}}$ becomes more negative with increasing camber, but is unaffected by all other variables except Mach number.

Wind-tunnel test data are frequently presented with the moment coefficient about the 25 per cent point, $C_{m_{0.25}}$, plotted vs. C_L because the center of gravity of a complete airplane is usually fairly close to the wing ac .

5-6 Airfoil Balance and Stability. In order for a wing to maintain steady flight by itself with no tail, it must be *balanced* and *stable*; i.e., all aerodynamic and gravitational forces and moments must total zero, and the wing must return to equilibrium if disturbed by some influence, such as a gust.

A cambered wing can be balanced in flight only if the center of gravity is behind the ac a distance¹ $C_{m_{ac}}/C_L$, as in Fig. 5-16a.

¹ The distance is dimensionless, like ac and cp .

However, a slight increase in angle of attack leaves the C_{mac} and weight coefficient¹ C_W unchanged but increases C_L , thereby causing a further increase in α ; hence, the wing is unstable.

A cambered wing that is inverted can be balanced only if the cg is ahead of the ac a distance C_{mac}/C_L as in Fig. 5-16b. An increase in angle of attack in this case produces a restoring moment; hence the wing is stable.

A symmetrical wing can be balanced only if the cg is coincident

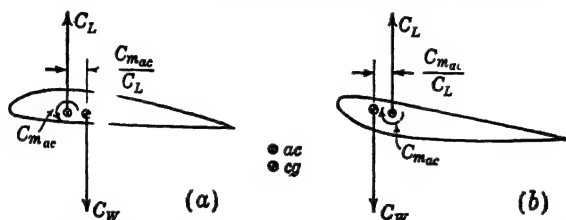


FIG. 5-16. Dimensionless force representation on a conventional airfoil: (a) upright—balanced and unstable, (b) inverted—balanced and stable.

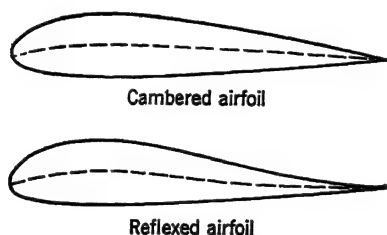


FIG. 5-17. Cambered and reflexed airfoil.

with the ac, because $C_{mac} = 0$. This condition is neutrally stable; i.e., there is no unbalanced moment produced by an increase in α to cause further increase or reduction in α .

A cambered airfoil may be made stable by reflexing the trailing edge, as in Fig. 5-17. Flying wings must be stable without the use of a tail; hence, they are generally constructed with a reflexed airfoil section.

The above airfoil characteristics may be shown by means of a curve of $C_{m_{cg}}$ vs. C_L . If the cg of a cambered airfoil is placed forward of the ac, it will be stable but unbalanced. If the cg of

¹ The weight coefficient $C_W = W/qS$ is not standardized nomenclature but is useful here to make the diagram completely nondimensional.

an inverted-camber or reflexed wing is placed behind the ac, it will be both unstable and unbalanced, as shown in Fig. 5-18. On this graph a curve is labeled balanced if it is possible to balance at some positive C_L , even though for all other C_L no balance is possible without deflection of a control surface.

The stable and unstable characteristics of airfoils may be verified

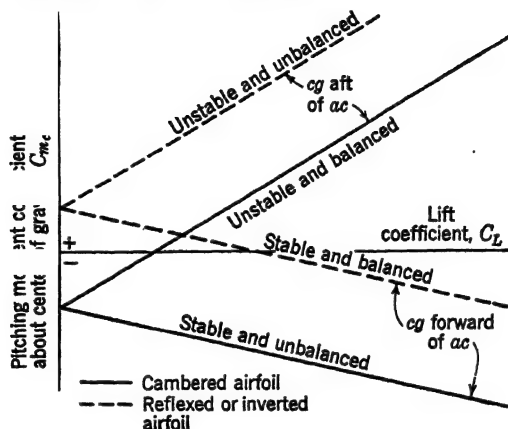


FIG. 5-18. Illustration of four possible conditions of balance and stability for a cambered and reflexed (or inverted) airfoil.

approximately¹ by ballasting a cambered card with paper clips, then inverting it, then reflexing it. The position of the paper clips in a chordwise direction determines the lift coefficient at which the card will fly, and therefore also determines the glide angle.

PROBLEMS

5-1. Prove the Kutta-Joukowski lift equation [Eq. (5-14)].

5-2. The landing speed of an airplane is 9 mph greater than its stalling speed. Landing $C_L = 1.24$; stalling $C_L = 1.5$. Find the stalling speed.

5-3. An airplane has the following characteristics: maximum lift coefficient $C_{L_{\max}} = 1.4$; angle of zero lift, $\alpha_{L_0} = -2.0$ deg; lift curve slope $a = 0.075$ per deg; stalling speed, $V_s = 60$ mph at 3000 ft. At what velocity will it fly at sea level, if the angle of attack, α , = 1.0 deg?

5-4. A wing having an NACA 23015 airfoil (see Fig. I, Appendix B) is glided from a tower into a 30-mph horizontal head wind, landing 500 ft from the base. Total time of flight is 20 sec. Aspect ratio $A = 6$;

¹ A card is not well streamlined, particularly when inverted, and it is the leading-edge stall that makes the card very stable in this attitude; nevertheless, the principles are illustrated.

chord $c = 3.5$ ft; weight $W = 500$ lb. Assuming the cosine of the glide angle is 1.0, find the angle of attack of the wing and the height of the tower.

5-5. A wing is glided from a height h into a horizontal head wind of magnitude V_w mph. If the wing loading is l_w psf, find an equation for horizontal distance d (ft) that the wing travels before striking the ground. Put equation in following form:

$$d = (h) \left(\frac{C_L}{C_D} \right) [1 - f(l_w, V_w, \sigma, C_L)]$$

where distances are in feet and velocity is in mph. Assume the cosine of the glide angle is 1.0.

5-6. Find the maximum possible ground distance, *with* and *without* horizontal head wind, that a wing may glide from a height of 100 ft. NACA 23015 airfoil; $l_w = 8$ psf, $V_w = 40$ mph, $A = 6$, $\sigma = 0.7$. Also find true air speed with and without wind. Assume the cosine of the glide angle is 1.0.

5-7. A wing having an NACA 23015 airfoil section is glided from a 30-ft tower into a 30-mph head wind. The wing lands 1000 ft from the base of the tower in 40 sec. $A = 6$, $S = 50$ sq ft, $W = 300$ lb. Find the inclination of the wind from the horizontal. Is the wind directed up or down? Assume cosine of glide angle and wind angle = 1.0.

5-8. When the velocity is 200 mph at sea level, the wing lift on an airplane is 3000 lb, and the center of pressure is 2.4 ft aft of the wing leading edge. If the span $b = 36$ ft and the chord $c = 6$ ft, find the pitching moment coefficient about the leading edge, C_{m_0} .

5-9. From wind-tunnel tests on an airfoil, the following data were taken:

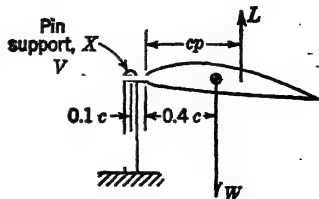
$$\text{When } C_L = 0.2, \quad C_{m_{0.25}} = -0.040$$

$$\text{When } C_L = 0.6, \quad C_{m_{0.25}} = -0.036$$

Find a_c and $C_{m_{ac}}$, and find the c_p when $C_L = 0.5$.

5-10. From wind-tunnel tests on an airfoil, the following data were obtained: $V = 100$ mph; $t = 45^\circ\text{C}$; $p = 28$ in. of mercury; lift = 10 lb; drag = 0.6 lb; moment about a point 3 in. upstream of the leading edge = -42.5 lb-in. If the wing span is 30 in. and the wing chord is 5 in., find C_L , C_D , $C_{m_{0.25}}$, and Reynolds number.

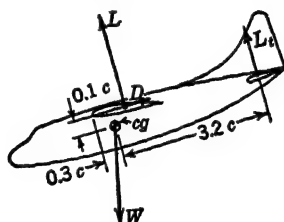
5-11. A wing having $l_w = 6$ psf is free to rotate about a point one-tenth chord ahead of the leading edge (point X in the diagram). Velocity $V = 60$ mph; $a_c = 0.24$; c_g is at the 40 per cent chord. When $C_L = 0.5$, $C_{m_x} = -0.25$. Find the lift coefficient at which the wing



balances in the air stream and the center of pressure corresponding. Assume standard conditions.

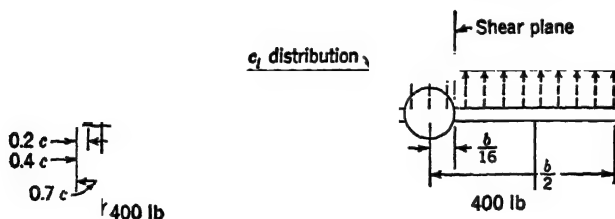
5-12. An airplane weighing 9000 lb is in a power-off vertical dive accelerating at a rate of $\frac{3}{8} g$. The distance from wing ac to tail cp is $3.0c$; total airplane $C_D = 0.025$; wing $C_{m_{ac}} = -0.03$. If cg is coincident with ac, and C_D passes through ac, what is the wing lift (lb)?

5-13. An airplane is in a power-off glide such that the slope of the glide path is 1:20; wing ac = 0.25. When wing $C_L = 0.3$, $C_{m_{0.25}} = -0.006$. Drag of complete plane is assumed to act at cp of wing. Center of



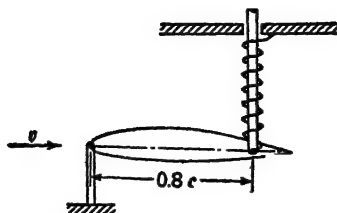
gravity of complete airplane acts below the chord line as shown. Assume cosine of small angles is 1.0. Assume tail lift L_t acts perpendicular to V . Find L_t if $W = 10,000$ lb.

5-14. A wing is tested in a wind tunnel, and the following data are obtained: $ac = 0.25$; $\alpha_{L_0}^* = -1.24$ deg; $a = 0.07$ per deg; $C_{m_{ac}} = -0.01$. The model wing area is 5 sq ft, but the aspect ratio is unknown. An airplane is built using the above wing but with a scale ten times that of the model. The complete plane weighs 8000 lb. Front spar is at $0.2c$, and rear spar is at $0.7c$. The wing weight outboard of the wing-



to-wing fuselage junction is 400 lb and acts at $0.4c$. The wing is rectangular in plan form and has a constant c_l across the span as shown. Find shear in pounds (parallel and normal to chord) existing at the wing-to-fuselage junction on the front and rear spars of the wing for an airplane flying level at 200 mph at sea level (wing $L/D = 15$). Assume the shear parallel to the chord is divided evenly between the two spars. Assume cosine of small angles = 1.0. How would the solution be modified if the airplane had been in a 5-deg climb?

5.15. A wing is supported in a wind tunnel by a pin joint at its leading edge, and by a frictionless spring and rod arrangement at $0.8c$, in such a



way that the spring may take compression or tension, as shown.

$dC_L/d\alpha = 4.8$ per radian; $dC_{m_{0.20}}/dC_L = 0.03$; $\frac{d \text{ cp}}{d (1/C_L)} = 0.05$, $q = 20$ psf; $c = 1$ ft; $b = 10$ ft; $\alpha_{L_0} = -5.0$ deg; spring constant = 500 lb per in. deflection. With wind off, the wing angle of attack, $\alpha = -1.0$ deg. Wing weight may be neglected.

- a. Find α . Is the spring in tension or compression?
- b. Find α with the spring and rod disconnected.

CHAPTER 6

ASPECT RATIO AND PLAN-FORM INFLUENCES

The geometric shape of a wing, as seen in plan view, is specified mainly by the aspect ratio, taper ratio, and sweepback. The influence of these variables on lift and drag will be the subject of this chapter.

The flow over a wing may be discussed from several points of view. The fact that a wing is able to produce a lift implies by Newton's second law of motion that acceleration of the air stream must occur in the opposite direction. Using this principle, the *momentum theory of lift* allows certain general statements to be made regarding the flow pattern near the wing. Use of the theory is restricted in the same sense that the momentum principle is restricted when used to compute the thrust of a propeller; *i.e.*, the over-all influence of the unit on the air stream may be anticipated, but such factors as pressure distribution on the wing or propeller blades, flow pattern in the immediate vicinity of the unit, and rotational components of the air stream must be established by other means. The *circulation theory* is the tool by which these effects are predicted.

Some of the most complicated theoretical analyses in the field of aerodynamics are concerned with the accurate representation of the flow over an arbitrary wing at an arbitrary Reynolds number and Mach number. In this text only the simplest approach to these problems will be presented, and only low-speed subsonic flow will be considered. The momentum theory will be used to develop certain basic relations; then the circulation theory will be used to support and amplify the conclusions drawn from the former discussions.

6-1 The Momentum Theory. Consider a wing at positive angle of attack, so that it has a positive lift coefficient. A perfect fluid is assumed; hence the profile drag is zero. The resultant force on the wing arises from deflection of the air in a direction opposite to the resultant. This deflection occurs asymptotically

above and below the wing, but may be represented by a *constant* deflection throughout a tube of air having a diameter equal to the span of the wing (Fig. 6-1). If the lift is assumed essentially

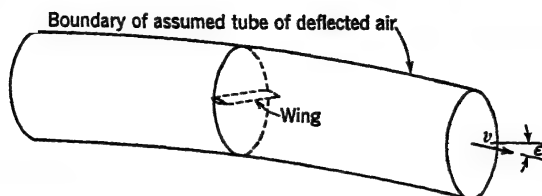


FIG. 6-1. Representative tube of air assumed to be deflected through an angle of downwash ϵ for a wing of finite aspect ratio.

equal to the resultant, Newton's second law of motion gives¹

$$\begin{aligned} L &= (\text{mass per second})(\text{change in velocity}) \\ &= (\rho av)(v\epsilon) \end{aligned} \quad (6-1)$$

$$= \rho \frac{\pi b^2}{4} v^2 \epsilon \quad (6-2)$$

where a is cross-sectional area of tube, sq ft

ϵ is down-wash angle at a distance downstream from wing,
radians

b is wing span, ft

Now let a slightly different condition be considered: the same

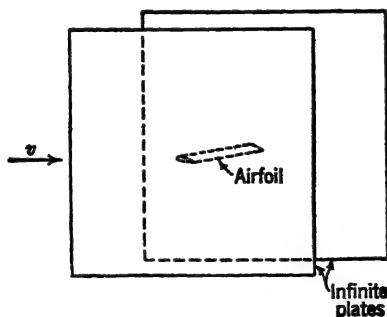


FIG. 6-2. Airfoil contained between infinite end plates.

wing is placed between two plates, as in Fig. 6-2, so that it touches them and allows no leakage of air at its tips between lower and upper surfaces. The plates are assumed to extend to infinity in

¹ Remember that $2 \sin (\epsilon/2) \approx \sin \epsilon \approx \epsilon$ in radians, if ϵ is a small angle.

all directions in the vertical plane. In order to obtain positive lift on the airfoil, the air must again be deflected through an angle, but the problem here is to determine the magnitude of this angle. If a perfect fluid is again assumed, the laminations of air extending to infinity above and below the airfoil must all

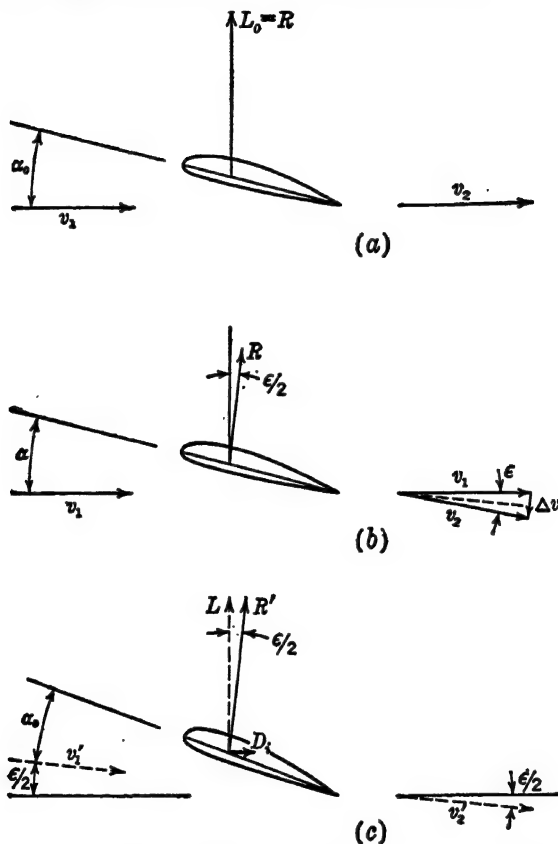


FIG. 6-3. Airfoil force representations: (a) infinite aspect ratio, (b) finite aspect ratio, (c) representative flow for finite aspect ratio.

be deflected through the angle ϵ . According to Eq. (6 1), however, since the area a becomes infinite and the lift on the wing is neither zero nor infinite, *the down-wash angle ϵ must approach zero.*

Now let a new condition be considered: the original span wing is assumed to be extended so as to have an infinite span but the

same chord as before. For this case, the three-dimensional flow at the tips influences only a very small proportion of the wing. The flow over the major portion must be similar to that depicted in Fig. 6-2, because the air is affected infinitely far above and below the wing. The average down-wash angle must again approach zero.

The results of the foregoing illustrations lead to an important conclusion: for finite aspect ratio, the average down-wash angle has definite, measurable magnitude, but for infinite aspect ratio (finite chord but infinite span), the average down-wash angle goes to zero. Furthermore, an airfoil contained between vertical planes simulates infinite-aspect-ratio characteristics.

The momentum theory is used to investigate flow conditions in the immediate vicinity of a wing. Admittedly the flow is merely *representative* of the true conditions on the wing, but several important facts nevertheless may be obtained. Consider an airfoil of infinite aspect ratio at angle of attack α_0 , as in Fig. 6-3a. From the foregoing discussion, the lift is equal to the resultant force on the wing and is, of course, perpendicular to the remote velocity. If, instead, the airfoil has a finite aspect ratio, the resultant force is inclined rearward through an angle $\epsilon/2$, because its direction is specified by the change in velocity Δv . Now if the curved flow pattern that starts with v_1 and ends with v_2 (Fig. 6-3b) is replaced by the local linear flow that starts with v'_1 and ends with v'_2 , as in Fig. 6-3c, this latter condition can be analyzed similarly to the infinite-aspect-ratio condition of Fig. 6-3a, except that the whole diagram is rotated through an angle $\epsilon/2$. In other words, in order to produce a resultant R' in Fig. 6-3c that has the same scalar magnitude as the lift L_0 in Fig. 6-3a, the angle of attack must be larger by $\epsilon/2$. This angle is of considerable importance and is called the *induced angle of attack* α_i .

$$\alpha_i = \frac{\epsilon}{2} \quad (6-3)$$

$$\alpha = \alpha_0 + \alpha_i \quad (6-4)$$

where α is angle of attack for finite aspect ratio, radians
 α_0 is angle of attack for infinite aspect ratio, radians
 α_i is induced angle of attack, radians

The lift on a wing is given by Eqs. (5.1) and (6.2) as

$$L = C_L S \frac{1}{2} \rho v^2 \quad (6.5)$$

$$= \frac{\pi b^2}{4} \rho v^2 \epsilon \quad (6.6)$$

Combining these two equations with Eq. (6.3), and noting that $A = b^2/S$, gives

$$\alpha_i = \frac{C_L}{\pi A} \quad (6.7)$$

where A is aspect ratio. Since ϵ in Eq. (6.6) is in radians, α_i in Eq. (6.7) must also be in radians. The corresponding equation in degrees is

$$\alpha_i = 18.24 \frac{C_L}{A} \quad (6.8)$$

Wind-tunnel tests on a wing of finite aspect ratio may be used to compute infinite-aspect-ratio characteristics by plotting C_L vs. α and obtaining the required data simply by subtracting α_i at every C_L . For instance, if the tests were run with aspect ratio of 6, Eqs. (6.4) and (6.8) give

$$\alpha_0 = \alpha_6 - 18.24 \frac{C_L}{6}$$

where subscripts 0 and 6 refer to aspect ratio infinity and 6, respectively. Correspondingly, curves for other aspect ratios may be obtained by adding the proper α_i onto the curve for infinite aspect ratio again; *e.g.*, the curve for aspect ratio 9 may be obtained from

$$\alpha_9 = \alpha_0 + 18.24 \frac{C_L}{9}$$

Instead of computing the curve for infinite aspect ratio in order to get from aspect ratio 6 to 9, a direct procedure may be used; thus

$$\alpha_0 = \alpha_9 - \alpha_{i_9} \quad (6.9)$$

$$\alpha_0 = \alpha_6 - \alpha_{i_6} \quad (6.10)$$

If C_L is the same in the two equations, then α_0 is the same; hence

$$\begin{aligned}\alpha_9 &= \alpha_6 - \alpha_{i6} + \alpha_{i9} \\ &= \alpha_6 - 18.24C_L \left(\frac{1}{6} - \frac{1}{9} \right)\end{aligned}$$

An experimental curve for $A = 6$ is shown in Fig. 6-4a, and curves for $A = 9$ and $A = \infty$ have been superimposed, using the

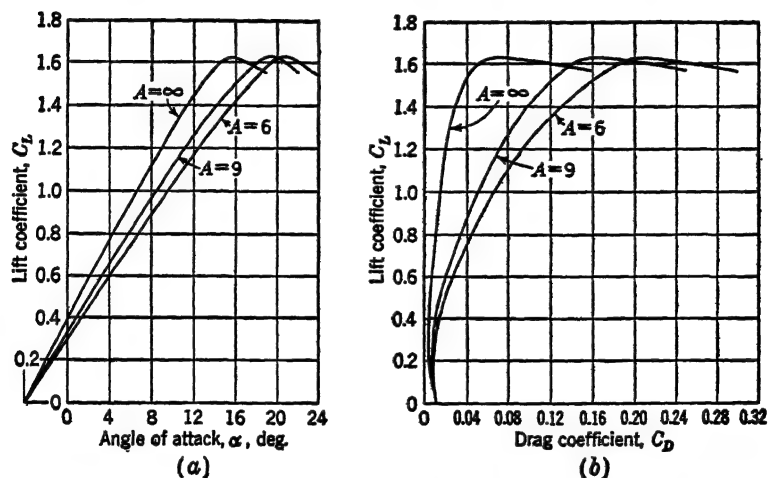


FIG. 6-4. Airfoil characteristics showing effect of aspect ratio changes. (Uncorrected data for an NACA 4412 airfoil from TR 669.)

above relations. In general, for any combination of aspect ratios,

$$\alpha_x = \alpha_y - 18.24C_L \left(\frac{1}{A_y} - \frac{1}{A_x} \right) \quad (6-11)$$

The corresponding equation for slope of the lift curve may be obtained by differentiating Eq. (6-11) with respect to C_L .

$$\begin{aligned}\frac{d\alpha_x}{dC_L} &= \frac{d\alpha_y}{dC_L} - 18.24 \left(\frac{1}{A_y} - \frac{1}{A_x} \right) \\ a_x &= \frac{a_y}{1 - 18.24a_y[(1/A_y) - (1/A_x)]} \quad (6-12)\end{aligned}$$

where a_x and a_y are slopes of the lift curve $dC_L/d\alpha$, per degree, for aspect ratios A_x and A_y , respectively.

The rearward inclination of the resultant vector in Fig. 6-3c produces a component parallel to the remote velocity called the *induced drag* D_i .

$$D_i = L\alpha_i \quad (6-13)$$

or

$$C_{D_i} = C_L\alpha_i \quad (6-14)$$

where α_i is in radians. Substituting α_i from Eq. (6-7) in Eq. (6-14) yields

$$C_{D_i} = \frac{C_L^2}{\pi A} \quad (6-15)$$

By reasoning similar to that used for the angle of attack relationship in Eq. (6-4),

$$C_D = C_{D_0} + C_{D_i} \quad (6-16)$$

where C_D is total wing drag coefficient, dimensionless

C_{D_0} is drag coefficient for infinite aspect ratio, called *profile drag coefficient*, dimensionless

C_{D_i} is induced drag coefficient, dimensionless

Again, an equation allowing computation of the drag coefficient for any aspect ratio from that for another aspect ratio may be obtained in a manner similar to Eq. (6-11).

$$C_{D_x} = C_{D_y} - \frac{C_L^2}{\pi} \left(\frac{1}{A_y} - \frac{1}{A_x} \right) \quad (6-17)$$

Example. Find the angle of attack and drag coefficient of an NACA 23015 airfoil of aspect ratio 12, at $C_L = 0.5$.

Solution. From Fig. I, Appendix B, $\alpha_8 = 5.45$ deg, and $C_{D_8} = 0.0225$ at $C_L = 0.5$. From Eq. (6-11),

$$\begin{aligned} \alpha_{12} &= \alpha_8 - 18.24C_L \left(\frac{1}{A_8} - \frac{1}{A_{12}} \right) \\ &= 5.45 - (18.24)(0.5) \left(\frac{1}{8} - \frac{1}{12} \right) \\ &= 4.70 \text{ deg} \end{aligned}$$

From Eq. (6-17),

$$\begin{aligned} C_{D_{12}} &= C_{D_8} - \frac{C_L^2}{\pi} \left(\frac{1}{A_8} - \frac{1}{A_{12}} \right) \\ &= 0.0225 - \frac{(0.5)^2}{\pi} \left(\frac{1}{8} - \frac{1}{12} \right) \\ &= 0.0159 \end{aligned}$$

In Fig. 6-4b, polar curves are shown for aspect ratios of 6, 9, and infinity, like those of Fig. 6-4a. In this graph it is apparent that the infinite-aspect-ratio characteristics are the best attainable for a particular airfoil section, because under these conditions the least possible drag coefficient occurs at a given lift coefficient. Usually in commercial airplanes, the final aspect ratio chosen is the result of a compromise between structural and aerodynamic considerations, so that wing aspect ratios of less than 6 or more than 15 are seldom used. The factor that determines the aspect ratio for a particular airplane is the duty for which the airplane is designed. For instance, racing planes and pursuit ships usually are designed with low-aspect-ratio wings, because induced drag is unimportant at high speed (low lift coefficient); gliders and cargo ships are usually designed with high-aspect-ratio wings, because induced drag is important at low speed (high lift coefficient).

6-2 Plan-form Effects. The equations derived in the preceding article could also have been developed from the circulation theory. As a matter of fact, some of the results of the circulation theory were necessary to make the momentum theory valid. In particular, the choice of a circular tube of air having diameter equal to the wing span was not arbitrary but was dictated by the circulation theory. The momentum theory is useful because it can be used to develop the fundamental equations relating the characteristics of wings with different aspect ratios. It has little use beyond this stage, however, and the shape of the streamlines near the wing must be obtained from other considerations. Before introducing the circulation theory, certain physical characteristics of the flow may be discussed.

A wing at positive lift coefficient must have a pressure differential from lower to upper surface, as shown in Fig. 6-5a.¹ At the tips of the wing, the air tends to flow laterally from the lower to upper surface in an attempt to alleviate the differential; thus, a transverse flow exists that is superimposed on the two-dimensional flow. For a rectangular wing, the transverse flow is most predominant at the tips and then decreases inboard, until at the wing center line it is nullified by an equal and opposite

¹ The lower-surface average pressure need not be positive; it must only be less negative than the upper surface. The positive pressure is shown only to prevent ambiguity.

flow generated by the opposite wing tip. Figure 6-5b shows the direction of flow on the upper and lower surfaces of a wing resulting from a combination of the longitudinal and transverse velocity components. The wing is shown as viewed from the top, with solid lines denoting flow on the upper surface, and dotted lines denoting flow on the lower surface. The air immediately behind the wing has a swirling motion, most predominant at the tips but with smaller swirls or *vortices* inboard resulting from the shearing imposed by the transverse components above and below the

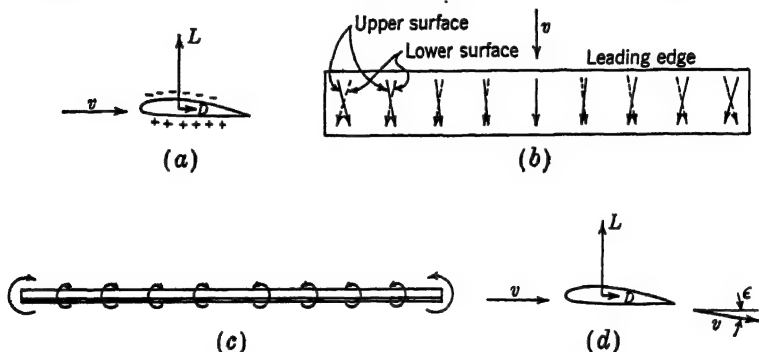


FIG. 6-5. Three-dimensional flow over a rectangular wing at positive lift coefficient: (a) average upper and lower surface pressures, (b) upper and lower surface velocity directions, (c) upstream view showing vortex distribution near wing trailing edge, (d) average downward inclination ϵ of flow passing over airfoil.

wing. Thus, the air immediately behind the wing has *trailing vortices*, as shown in an upstream view in Fig. 6-5c. The effect of these vortices is to give an *average* downward inclination to the air leaving the wing, as in Fig. 6-5d. The average angle through which the velocity vector is rotated is the same angle ϵ discussed in the previous article.

On most practical wings, the angle of down-wash is not constant across the span. It depends upon the plan form of the wing considered; a rectangular wing would be expected to have a much higher concentration of vortex action at the wing tip, where the chord is large, than a tapered wing, whose tip chord is relatively small. From theoretical considerations it may be shown that the only kind of wing that produces a constant angle of down-wash across the span is one having an elliptical plan form. These concepts will be clarified in the next articles.

6-3 The Circulation Theory. From the statements of Art. 5-2 it was apparent that the velocity component arising from the circulatory flow about a cylinder, say, could be added vectorally to the rectilinear component in order to establish the resultant velocity at any point in the flow field. This principle of superposition allows investigation of the purely circulatory flow about *any* vortex filament¹ without regard for the rectilinear flow; then a composition of the two flows produces the required solution. As an introduction to this concept, first picture a taut piano wire in still air, on which are mounted several small spools. If one of the spools is somehow rotated at constant rpm, it would be

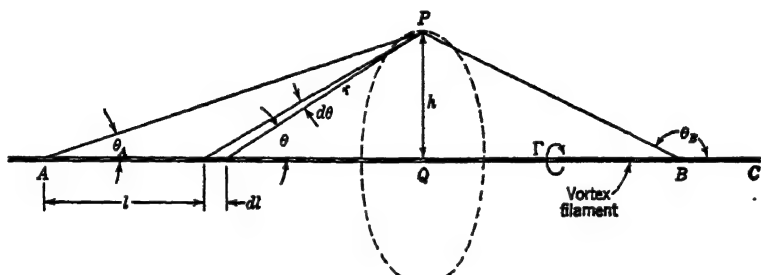


FIG. 6-6. Nomenclature diagram for circulatory flow about a vortex filament.

expected to cause a rotation of the complete mass of air surrounding the spool (viscous effects are ignored except in so far as they are required to initiate the motion). Now if another spool is rotated at the same rpm as the first one, it too will produce a rotation of the complete mass of air surrounding it; furthermore, the velocity components arising from each spool are additive. The procedure may be extended to any number of spools. These conclusions are admittedly intuitive, but they provide a background for understanding the behavior of air surrounding a vortex filament. Consider such a filament of length AB (Fig. 6-6) having circulation Γ and elemental length dl . Actually the filament AB cannot exist as an independent unit, but must be part of a filament having constant circulation Γ that either forms a closed path or is continuous to infinity in both directions; however, in many aerodynamic problems it is convenient to

¹ A vortex filament is the core of the circulatory flow, assumed to have an infinitesimal diameter.

consider a filament to be composed of a number of sections, and it is on this basis that the finite length AB is analyzed.

The element dl produces a tangential velocity dw (into the paper) at an arbitrary point P , expressed by

$$dw = \frac{\Gamma}{4\pi r^2} \sin \theta \, dl \quad (6.18)$$

Equation (6.18) is called the *Biot-Savart law*, and it is very important for predicting the flow over a wing, wind-tunnel wall interference, ground effect, etc. The total tangential velocity at P arising from all the elements between A and B is

$$w = \frac{\Gamma}{4\pi} \int \frac{\sin \theta}{r^2} \, dl \quad (6.19)$$

Equation (6.19) may be integrated if r and dl are expressed in terms of θ and $d\theta$, respectively:

$$w = \frac{\Gamma}{4\pi} \int_{\theta_A}^{\theta_B} \frac{\sin \theta \, d\theta}{h} \quad (6.20)$$

By integration,

$$w = \frac{\Gamma}{4\pi h} (\cos \theta_A - \cos \theta_B) \quad (6.21)$$

where h is perpendicular distance from AB to P

θ_A is angle between PA and AB

θ_B is angle between PB and BC

Evidently, if the filament is infinitely long in both directions, $\theta_A = 0$, and $\theta_B = 180$ deg; then

$$w = \frac{\Gamma}{2\pi h} \quad (6.22)$$

Also, if the filament starts at Q and extends to infinity in only one direction,

$$w = \frac{\Gamma}{4\pi h} \quad (6.23)$$

The above principles were used by Prandtl (TR 116) to represent the flow on a wing of finite aspect ratio. Consider a hypothetical wing having *constant* lift per foot of span. The flow about such a wing may be represented by a *bound* vortex contained

between the wing tips and two *free* or *trailing* vortices shed from the wing tips (Fig. 6-7). The resulting system is aptly called a *horseshoe vortex*. The velocity at any point in space is obtained from the vector sum of the components arising from each of the three sections of the filament, in accordance with Eq. (6-21).

A wing having constant lift per foot of span is not a physical reality. On any wing, the lift per foot of span must gradually

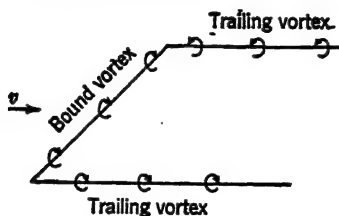


FIG. 6-7. A horseshoe vortex.

decrease to zero at the wing tip. Thus the simple horseshoe vortex does not always lead to practical results. It serves two important purposes, however. First, there are some problems in which it is sufficiently accurate to represent a wing by a simple horseshoe vortex as in Fig. 6-8. (The vortex span is usually assumed about eight-tenths of the geometric span.) For instance, in computing the effect of presence of the ground on a wing, the wing is represented by a simple horseshoe vortex, while the

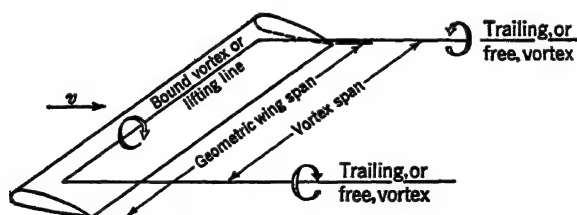


FIG. 6-8. Representation of a rectangular wing by a horseshoe vortex.

ground is represented by an *image* horseshoe vortex, having circulation in a sense which is opposite that of the wing (Fig. 6-9). The influence of the image vortex on the flow field around the wing may then be computed using Eq. (6-21). It is apparent that the image trailing vortices produce an *up-wash* over the wing, which effectively increases the wing aspect ratio, while the image bound vortex produces a flow curvature and velocity

reduction. Notice that the image vortices, in combination with the wing vortices, satisfy the condition that there must be no flow through the ground. Second, the simple horseshoe vortex provides a foundation for further discussion, because the lift

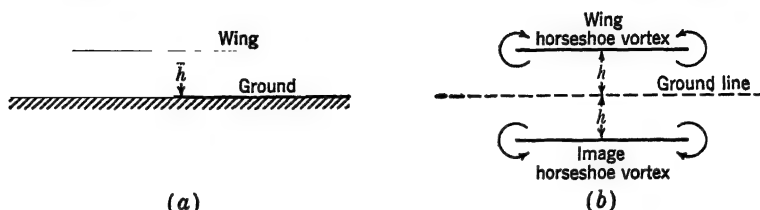


FIG. 6-9. Representation of an actual wing near the ground by a wing horseshoe vortex and image horseshoe vortex.

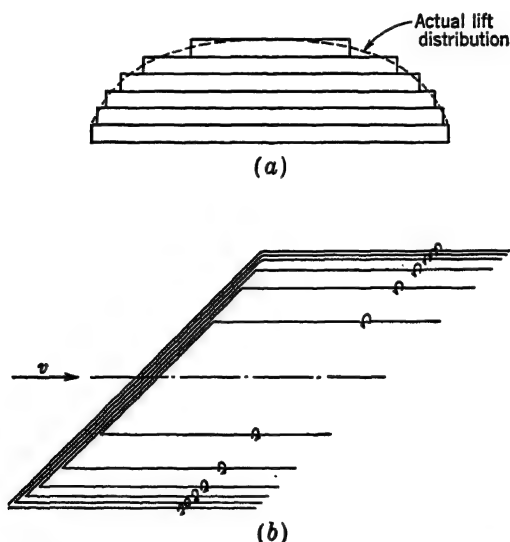


FIG. 6-10. Representation of the actual lift distribution on a wing by a number of strips having constant circulation, showing the corresponding system of horseshoe vortices.

distribution on a wing may be represented by a number of span-wise strips of constant lift per unit span, each having its corresponding horseshoe vortex (Fig. 6-10). As the number of strips is increased, the actual lift distribution is represented more and more closely, and the number of horseshoe vortex systems

increases. In the limit the system becomes a *sheet* of trailing vortices. The influence of each bound and trailing vortex in the system contributes to the resultant velocity vector at any point in space, in accordance with Eq. (6-21). For instance, in Fig.

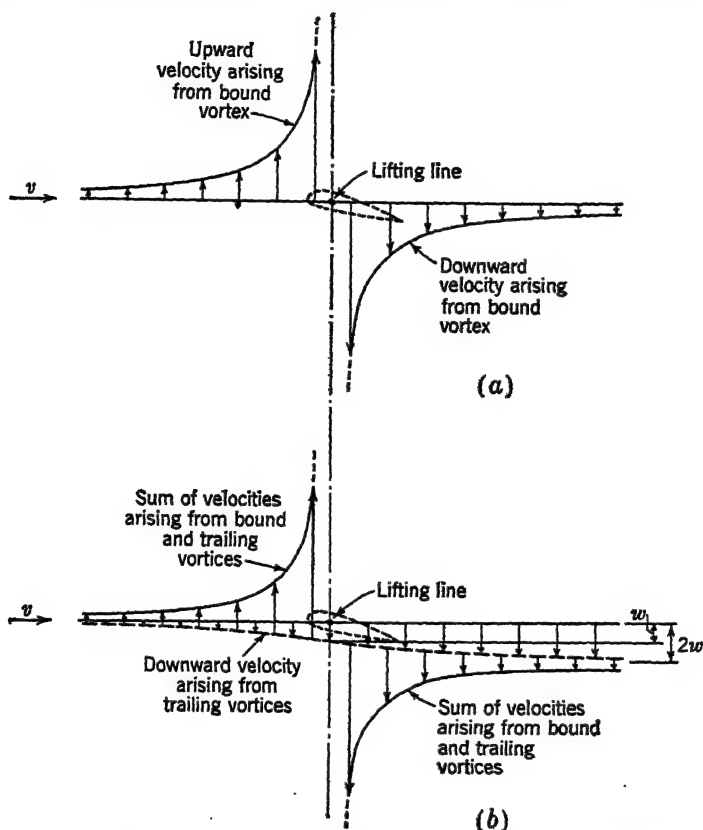


FIG. 6-11. Vertical component of velocity introduced up- and downstream of a wing at the mid-span; showing: (a) that due to the bound vortex and, (b) that due to the trailing vortices plus the bound vortex.

6-11 the velocity components introduced up- and downstream of a wing by the bound and trailing vortices are shown for a vertical plane midway between the trailing vortices. The bound vortex is seen to contribute an up-wash upstream and a down-wash downstream of the wing, while the trailing vortices together contribute a down-wash of increasing magnitude with increasing

distance downstream. From Eqs. (6-22) and (6-23) the down-wash at the wing *due to the trailing vortices* is seen to be half that at infinity downstream; hence upon addition of the rectilinear velocity component, the angular deflection of the air at the wing is half that at infinity downstream. This was also shown for the *average* down-wash by the momentum theory; *i.e.*, $\alpha_i = \epsilon/2$.

It is apparent that any type of lift distribution may be accurately represented by judicious choice of a sufficient number of horseshoe vortices. The spanwise variation in down-wash is dependent upon the type of lift distribution being represented. An elliptical wing gives an elliptical lift per unit span and produces a constant spanwise down-wash distribution. A rectangular wing gives its greatest down-wash at the wing tips. A highly tapered wing gives its greatest down-wash at the wing root.

In these discussions the horseshoe vortices may be assumed to have their bound vortices coincide with the center of pressure. This gives a so-called *lifting line*. A more accurate procedure is to have the horseshoe vortices distributed in a chordwise direction; however, this multiplies the analytical difficulties.

The circulation theory is a very powerful tool for studying aerodynamic phenomena. It will be referred to frequently in later sections of the text.

6-4 Section Characteristics. The total lift, drag, and moment coefficients on a wing depend upon the effective angle of attack of each section of the wing. In order to differentiate between coefficients that refer to a section of a wing and those that refer to the complete wing, lower-case symbols are used; *i.e.*,

c_l is section lift coefficient, dimensionless.

c_d is section drag coefficient, dimensionless.

c_m is section moment coefficient, dimensionless.

Section characteristics are usually obtained by testing a short-span airfoil of constant chord between vertical walls in a wind tunnel in order to simulate two-dimensional flow. The results correspond very closely to infinite-aspect-ratio characteristics computed from finite-aspect-ratio tests on elliptical wings.

Section characteristics may also be anticipated from tests on rectangular wings by a combination of theoretical and empirical correction factors. The equations for induced effects must be modified to account for a variable spanwise section lift coefficient, and the profile drag must be corrected for end effect and for

variable spanwise angle of attack. The computed characteristics agree fairly well with those obtained in two-dimensional tests. Table III, Appendix A, shows section characteristics of several airfoils derived from three-dimensional wind-tunnel tests.

6-5 Spanwise Lift Distribution. The method by which spanwise lift distribution is represented by an infinite number of horse-shoe vortices has particular importance in defining the lift distribution corresponding to a particular wing plan form. The trailing-vortex distribution, down-wash distribution, lift-coefficient

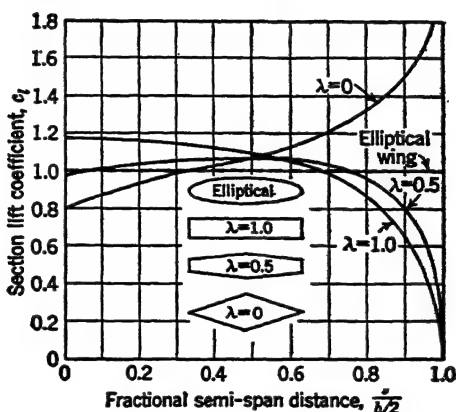


FIG. 6-12. Spanwise variation of section lift coefficient for several wing plan forms having aspect ratio $A = 6$ and total lift coefficient $C_L = 1.0$. (Based on data from TR 572.)

distribution, and lift distribution across the span are mutually dependent. A concentration of trailing vortices near the wing tips, for instance, produces also a concentration of down-wash near the tips, which in turn gives a relatively low section lift coefficient at the tips. The span loading then depends upon the relative size of the chord at the tips. A rectangular wing has just such a concentration of trailing vortices near the wing tips, and the resulting reduction in lift coefficient is clearly shown in Fig. 6-12. Since the chord of a rectangular wing is constant across the span, the lift distribution has a similar appearance (Fig. 6-13). An elliptical wing has the trailing vortices distributed in a manner that gives a constant down-wash and hence a constant lift-coefficient distribution across the span. Since the chord is elliptically distributed, the lift distribution is also elliptical. A highly tapered wing has the trailing vortices distributed more

inboard than they are with an elliptical wing, and for the diamond-shaped wing shown in Fig. 6-12, the lift coefficient rises sharply near the wing tips. This wing has a wing chord that decreases linearly with distance from the wing center line, and the lift distribution reduces in the manner shown in Fig. 6-13. A wing

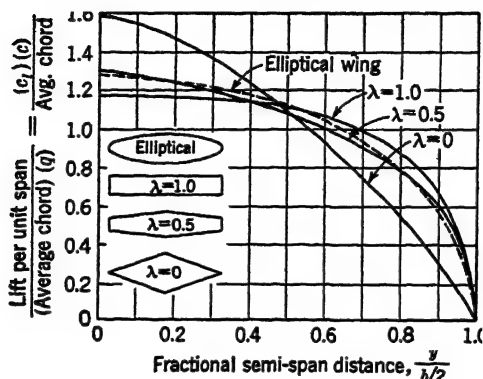


FIG. 6-13. Spanwise variation of lift loading for several wing plan forms having aspect ratio $A = 6$ and total lift coefficient $C_L = 1.0$.

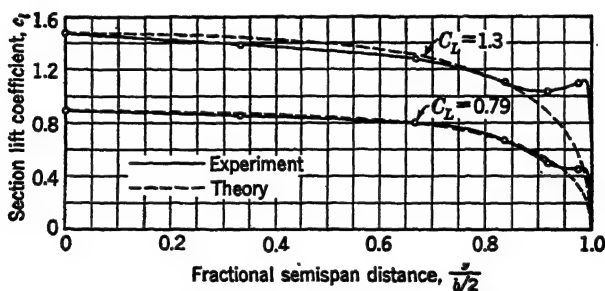


FIG. 6-14. Comparison of theoretical and experimental section-lift-coefficient variation across the span of a rectangular wing having aspect ratio of 6. (From TN 606.)

with taper ratio of about $\lambda = 0.5$ has a lift distribution somewhat similar to that of an elliptical wing. All the curves shown on these two figures were obtained from theoretical considerations, assuming wings of constant airfoil section with no washout. Experimental data verify the general trends of all these curves, although the rectangular wing has a peculiar rise in lift coefficient at the wing tip (Fig. 6-14), apparently caused by the tip vortices

rolling up into one single strong vortex whose center is inboard of the wing tip.

The spanwise distribution of down-wash is not of great importance in itself (except as it affects the flow over the tail of the airplane), but it defines the distribution of effective angle of attack and hence of lift-coefficient distribution across the span. The lift-coefficient distribution is very important, for it specifies how the wing will stall. A rectangular wing has its highest lift coeffi-

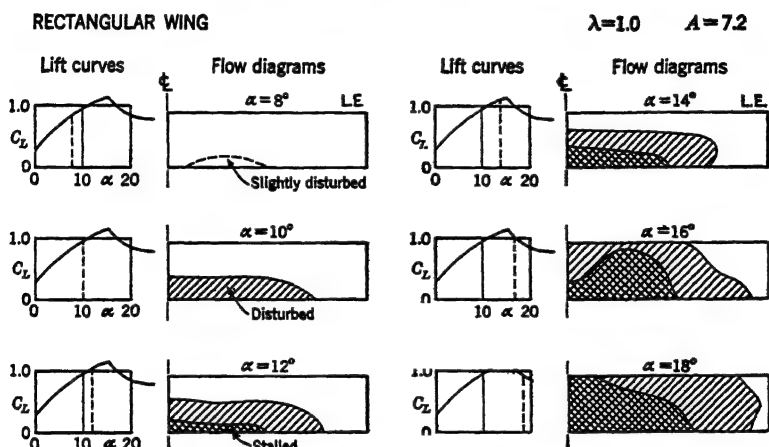


FIG. 6.15. Stalling characteristics of a rectangular wing of aspect ratio $A = 7.2$. Single crosshatch lines indicate disturbed region. Double crosshatch lines indicate stalled region. (From R&M 1796. Reproduced with permission of the Controller of His Britannic Majesty's Stationery Office.)

cient at the wing root and therefore stalls here first.¹ An elliptical wing has a constant lift coefficient across the span and thus stalls evenly across the span. A highly tapered wing has its first stall at the wing tip. A wing with sweepback acts similarly to a wing with more taper. A swept-forward wing acts like a wing with less taper.² These statements are verified by the experimental results shown in Figs. 6.15 to 6.18.

¹ In these discussions it is assumed that there is no washout, that a constant airfoil section is used, and that Reynolds-number effects are negligible.

² These discussions take no account of spanwise flow within the boundary layer, which sometimes has a tremendous influence on stalling characteristics. For large angles of sweepback, the boundary-layer flow aggravates the tip-stalling tendencies. For large angles of sweepforward, the boundary-layer flow promotes root stalling.

ELLIPTICAL WING

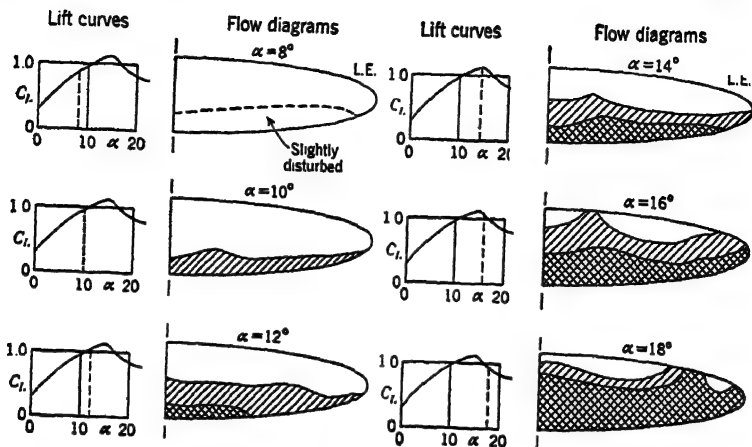
 $A=6$ 

FIG. 6-16. Stalling characteristics of an elliptical wing of aspect ratio $A = 6$. Single crosshatch lines indicate disturbed region. Double crosshatch lines indicate stalled region. (From R&M 1796. Reproduced with permission of the Controller of His Britannic Majesty's Stationery Office.)

TAPERED WING

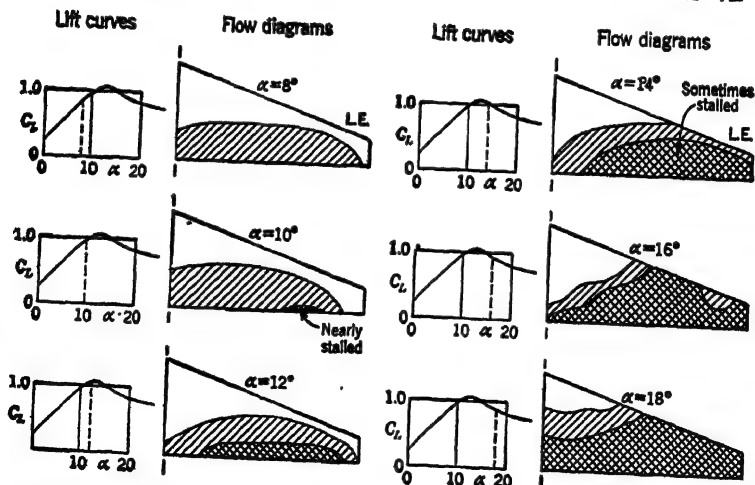
 $\lambda=0.25 \quad A=7.2$ 

FIG. 6-17. Stalling characteristics of a swept-back wing of aspect ratio $A = 7.2$ and taper ratio $\lambda = 0.25$. Single crosshatch lines indicate disturbed region. Double crosshatch lines indicate stalled region. (From R&M 1796. Reproduced with permission of the Controller of His Britannic Majesty's Stationery Office.)

The tendency of a wing to stall first at the tips is very undesirable because it promotes lateral instability (see Art. 15-4). One obvious method of preventing tip stall is to avoid highly tapered plan forms; however, for structural reasons, this plan form is the most desirable in cantilevered construction. If the tip section of a wing is constructed so as to have a reduced angle of attack, by gradually twisting the wing in a spanwise direction,

TAPERED WING

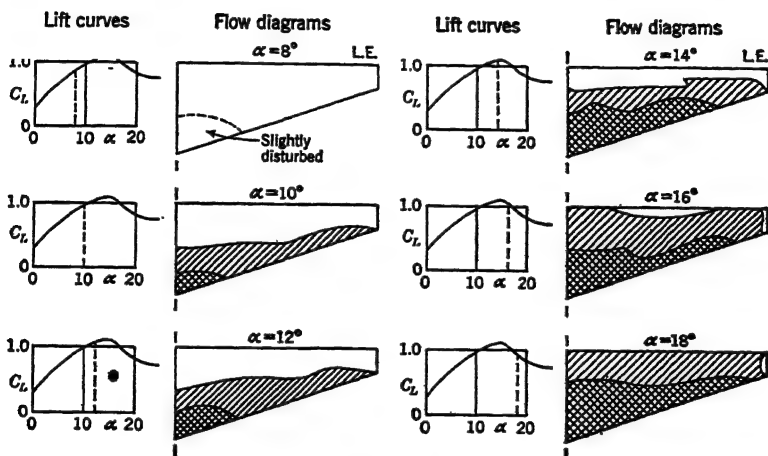
 $\lambda=0.25$ $A=7.2$ 

FIG. 6-18. Stalling characteristics of a swept-forward wing of aspect ratio $A = 7.2$ and taper ratio $\lambda = 0.25$. Single crosshatch lines indicate disturbed region. Double crosshatch lines indicate stalled region. (From *R&M* 1796. Reproduced with permission of the Controller of His Britannic Majesty's Stationery Office.)

the wing may be made to stall gradually from root to tip. This *washout* is one of the most effective methods for preventing tip stall. Another method is to change the airfoil section at the tip to one that is more cambered and hence has a larger $c_{l_{\max}}$ (see Art. 9-5). Such a wing may or may not have aerodynamic washout. A final method is to install *slots* (see Art. 10-2) in the outboard wing panel, thereby giving the tip area a greater stall angle than the root area. These methods frequently lead to an appreciable drag increase and hence must not be used to excess.

6-6 Modifications to Induced-drag and Angle-of-attack Formulas. The equations for α_i and C_{D_i} developed in Art. 6-1 are strictly applicable only to a wing having an elliptical plan form.

For other plan forms the equations should theoretically be modified, because of the spanwise variation in section lift coefficient.

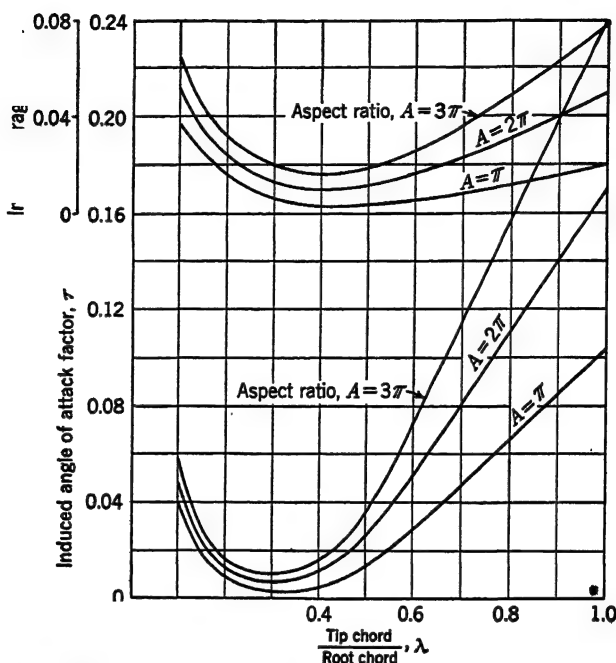


FIG. 6-19. Mathematically determined correction factors for induced angle of attack and induced drag coefficient. (Based on calculations by H. Glauert, *R&M* 1226.)

cient. The following equations, suggested by Glauert,¹ use the lifting-line theory mentioned in Art. 6-3:

$$\alpha_i = \frac{C_L}{\pi A} (1 + \tau) \quad (6-24)$$

$$C_{Di} = \frac{C_L^2}{\pi A} (1 + \delta) \quad (6-25)$$

where α_i is in radians. The factors τ and δ are plotted in Fig. 6-19.

Equations (6-24) and (6-25) have a tendency to give corrections that are too large. First, the lifting-line theory is admittedly an approximation for a lifting surface and is particularly inexact for small aspect ratios. Second, the vortices near the tip of some

¹ GLAUERT, H., "The Elements of Aerofoil and Airscrew Theory," Cambridge, London, 1947.

wings combine together to form a single large vortex that tends to produce an *up-wash* over the extreme outboard portion of the wing. Third, fluid viscosity distorts the anticipated vortex flow. Many attempts have been made to correlate theoretical

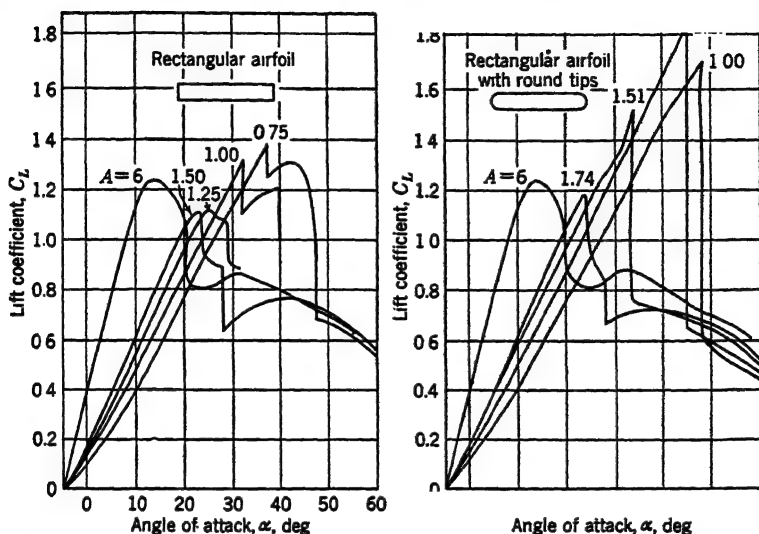


FIG. 6-20. Comparison of lift curves at low aspect ratio. (From TR 431.)

and experimental results. The present status of the investigations is not such that any particular method has received universal acceptance. In this text, Eqs. (6-24) and (6-25) will be used with τ and $\delta = 0$ for aspect ratios greater than 6. For aspect ratios less than 6, an empirical equation suggested by K. D. Wood¹ will be used for slope of the lift curve

$$m = 2\pi \left(\frac{A}{A+3} \right) \quad (6-26)$$

or

$$a = 0.1095 \left(\frac{A}{A+3} \right)$$

The latter specification produces a slight lack of correlation with Eq. (6-12) at $A = 6$, but this is not serious, because all conventional wings have aspect ratios greater than 6, while stabilizers and fins usually have aspect ratios less than 6.

¹ Wood, K. D., "Technical Aerodynamics," McGraw-Hill, New York, 1947.

The effect of aspect ratio on $C_{L_{\max}}$ must generally be obtained by experiment. The tendency is toward a decrease in $C_{L_{\max}}$ with decreasing aspect ratio, presumably caused by the increased curvature of the flow field associated with reduction in aspect ratio; *i.e.*, the airfoil has an effective camber that is less than the geometric camber because the down-wash produces a flow pattern that is curved in the same direction as the mean line of the airfoil. For extremely low aspect ratios, the boundary layer is considerably affected by the strong tip vortices, and separation is delayed to a very high angle of attack (see Fig. 6-20); thus the maximum lift coefficient *increases* with decrease in aspect ratio.

6-7 Airplane Efficiency Factor. The induced drag of a wing arises only when the wing has a positive or negative lifting force. The total wing drag is composed of induced drag and profile drag. In coefficient form,

$$C_D = C_{D_0} + C_{D_i} \quad (6-27)$$

where C_D is wing drag coefficient, dimensionless

C_{D_0} is profile drag coefficient, dimensionless

C_{D_i} is induced drag coefficient, dimensionless

The total drag of an airplane is composed of wing drag and residual drag. In coefficient form,¹

$$C_D = C_{D_0} + C_{D_i} + C_{D_r} \quad (6-28)$$

where C_D is airplane drag coefficient, dimensionless

C_{D_r} is residual drag coefficient, dimensionless

The sum of the profile drag and residual drag is called *parasite drag*. Again in coefficient form,

$$C_{D_p} = C_{D_0} + C_{D_r} \quad (6-29)$$

and

$$C_D = C_{D_p} + C_{D_i} \quad (6-30)$$

where C_{D_p} is parasite drag coefficient.

The induced drag coefficient may always be computed by Eq. (6-15), using the wing lift coefficient and aspect ratio. The residual drag coefficient is then seen to include any induced effects on the fuselage, tail, etc. This is merely a matter of definition and is done for the sake of simplicity.

The induced drag coefficient is proportional to the square of the lift coefficient, and for most wings and airplanes it is primarily responsible for the parabolic shape of the drag curve. The profile

¹ The symbol C_D is used for both the wing and airplane drag coefficient. The equation always makes its meaning apparent.

drag coefficient and residual drag coefficient usually have a somewhat parabolic shape and for mathematical manipulation may be represented by exactly parabolic curves.

Conventionally, C_D and C_{D_0} or C_{D_p} are plotted vs. C_L^2 in a form similar to Fig. 6-21, and the experimental curves are then repre-

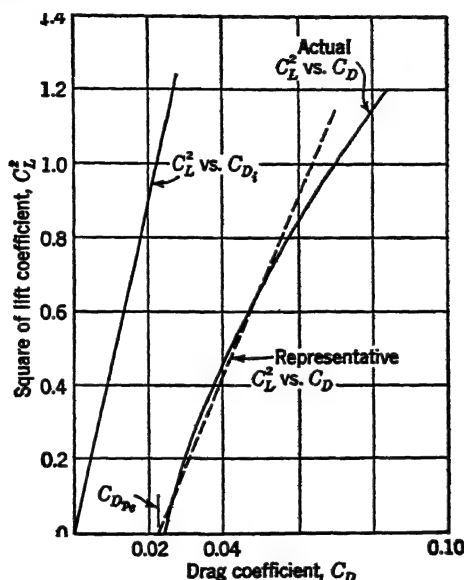


FIG. 6-21. Representation of an airplane polar curve by a parabolic equation. The deviation is greatly exaggerated for clarity.

sented by straight lines. In order to provide good representation, the straight lines may be constructed to coincide with the experimental data at $C_L = 0.3$ and $C_L = 0.8$. The equation for profile drag coefficient¹ is then

$$C_{D_0} \doteq C_{D_{0_e}} + \left(\frac{dC_{D_0}}{dC_L^2} \right) C_L^2 \quad (6\ 31)$$

where $C_{D_{0_e}}$ is "equivalent" profile drag coefficient corresponding to intercept of curve

$\frac{dC_{D_0}}{dC_L^2}$ is slope of the C_{D_0} vs. C_L^2 curve (the subscript e is deleted since this slope is seldom used in any other sense)

¹ There seems to be no commonly accepted symbol corresponding to C_{D_0} , or C_{D_p} . These symbols are used here to avoid ambiguity.

Correspondingly,

$$C_{D_p} = C_{D_{p_0}} + \left(\frac{dC_{D_p}}{dC_L^2} \right) C_L^2 \quad (6.32)$$

From Eqs. (6.30) and (6.32),

$$C_D = C_{D_{p_0}} + \left(\frac{dC_{D_p}}{dC_L^2} + \frac{1}{\pi A} \right) C_L^2 \quad (6.33)$$

Equation (6.33) is one form of the parabolic equation for the polar curve of an airplane.

A comparison factor frequently used in performance computation is called the *airplane efficiency factor*,¹ defined by the following equation:

$$e = \frac{dC_{D_p}/dC_L^2}{dC_D/dC_L^2} \quad (6.34)$$

or by differentiating Eq. (6.30) and substituting in Eq. (6.34), an alternate form is obtained:

$$e = 1 - \frac{dC_{D_p}/dC_L^2}{dC_D/dC_L^2} \quad (6.35)$$

The factor e is thus seen to show the relative importance of the parasite drag characteristics in determining the slope of the polar curve. Values of e generally range from about 0.8 to 1.0.

The parabolic form of the drag equation may now be written in terms of the airplane efficiency factor. Writing Eq. (6.34) in another form yields

$$e = \frac{1}{1 + \pi A (dC_{D_p}/dC_L^2)} \quad (6.36)$$

and, by substitution in Eq. (6.33),

$$C_D = C_{D_{p_0}} + \frac{C_L^2}{\pi A e} \quad (6.37)$$

Equation (6.37) is the conventional parabolic equation for the polar curve of an airplane. This equation will have particular

¹ Also called the *span efficiency factor* and the *Oswald efficiency factor*, after its originator.

importance in performance calculations. In many cases, it is sufficiently accurate to replace C_{D_p} by $C_{D_{p_{\min}}}$, because the latter drag coefficient usually occurs at a very low lift coefficient.

Example. An airplane with aspect ratio $A = 8$ has $e = 0.90$ and $C_{D_{p_{\min}}} = 0.0200$. Find L/D when $C_L = 0.60$, and find dC_{D_p}/dC_L^2 .

Solution. From Eq. (6-37),

$$\begin{aligned} C_D &= 0.0200 + \frac{(0.6)^2}{(8)(0.90)} \\ &= 0.0200 + 0.0159 \\ &= 0.0359 \end{aligned}$$

$$\frac{L}{D} = \frac{0.60}{0.0359} = 16.7$$

From Eq. (6-36),

$$\begin{aligned} \frac{dC_D}{dC_L^2} &= \frac{1}{\pi A} \left(\frac{1}{e} - 1 \right) \\ &= \frac{1}{(\pi)(8)} \left(\frac{1}{0.90} - 1 \right) \\ &= 0.0044 \end{aligned}$$

Frequently it is convenient to consider a wing efficiency factor e_w , which is defined in exactly the same manner as that for the airplane, except that C_{D_p} is always replaced by C_{D_0} ; *e.g.*,

$$\begin{aligned} C_D &= C_{D_0} + \frac{C_L^2}{\pi A e_w} \\ &= C_{D_{0_{\min}}} + \frac{C_L^2}{\pi A e_w} \end{aligned} \quad (6-38)$$

$$e_w = \frac{1}{1 + \pi A (dC_{D_0}/dC_L^2)} \quad (6-39)$$

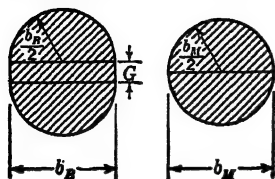
PROBLEMS

6-1. For an elliptical wing, $\alpha_i = 2.5$ deg, $b = 100$ ft, $V = 130$ mph. Find lift L at sea level.

6-2. Plot C_L vs. α for $A = 6, 10$, and ∞ for an NACA 23015 rectangular airfoil, using Fig. I, Appendix B, and check the slopes by Eq. (6-12).

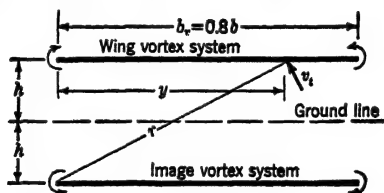
6-3. Plot C_D vs. α and the polar for $A = 6, 10$, and ∞ for an NACA 23015 rectangular airfoil, using Fig. I, Appendix B, and record $(L/D)_{\max}$, and C_L for $(L/D)_{\max}$ for each aspect ratio.

6-4. A biplane has span $b_B = 42$ ft; gap $G = 6$ ft, and chord $c_B = 7$ ft. Find the span of a monoplane having the same weight, induced drag, and velocity, but with chord $c_M = 6$ ft. Repeat with $c_M = 8$ ft, and comment on the significance of the two answers. Assume the mass deflected is based on the areas shown.



6-5. A wing having an NACA 23015 airfoil section is sailed down a 2.0-deg hill, up which a 10-mph wind is blowing. A pitot tube on the wing indicates $q = 9$ psf. Weight $W = 400$ lb; span $b = 33$ ft; chord $c = 3$ ft. The wing is riveted, so that the drag coefficient is higher than would be expected with a smooth wing. Find the increment in C_D due to the rivets.

6-6. A wing is represented by a horseshoe vortex having vortex span $b_v = 0.8b$. It is flying at a height h above the ground, as shown. Find the ratio of effective aspect ratio A_E to geometric aspect ratio A as a



function of the ratio of span b to height h , $A_E/A = f(b/h)$. Also find A_E/A for $b/h = 3.0$. Use the following information:

1. The actual c_t distribution over span b is represented by a constant c_t over span b_v ; hence $L = \rho b_v \Gamma v = C_L S \frac{1}{2} \rho v^2$.
2. The image trailing vortices that represent the ground both produce an up-wash over the wing vortex system. The up-wash at a point y arising from one image vortex is a component of the tangential velocity v_t , and is thus a function of y . The influence of the bound vortex may be ignored.
3. The product of the average up-wash \bar{w} and the vortex span b_v is equal to the integral of the product of the up-wash at a point y and the differential span dy . The expression for average up-wash can be used to find the effective aspect ratio.



6-7. A wing, tail, and tail boom are in a steady glide at 100 mph at sea level, with the boom parallel to the flight path as shown. Wing

characteristics: NACA 23015 airfoil, $A = 6$, $S = 50$ sq ft. Incidence $i_w = 7$ deg with respect to the boom. Tail characteristics: *inverted* NACA 23015 airfoil, $A = 6$, $S = 10$ sq ft. Stabilizer angle $i_s = 2$ deg, measured with respect to the boom. Assuming boom drag $= 0$ lb, cosine of small angles $= 1.0$, and assuming that the tail acts in a circular tube of downswep air from the wing ($\epsilon = 2\alpha_i$), find the sinking speed or vertical rate of descent, v_v (fpm).

6-8. A pursuit plane weighing 5000 lb is in a terminal-velocity vertical dive at 3000 ft with propellers fully feathered. The wing has an NACA 23015 section; $A = 8$, $S = 250$ sq ft, $C_{m_{ac}} = -0.008$. The ac and cg are coincident. The distance from cg to tail cp is 20 ft. $C_{D_e} = 0.0195$. Find the following, ignoring effects of compressibility and assuming zero elevator deflection:

a. Wing C_L

b. Tail load required for equilibrium (lb)

c. Terminal velocity V_T (mph)

d. Tail lift coefficient C_{L_t} , if tail area is 50 sq ft

e. Tail angle of attack (deg), if the tail has an *inverted* NACA 23015 section with $A = 5$. (A positive tail angle of attack is defined in the same direction as a positive wing angle of attack, regardless of airfoil section.)

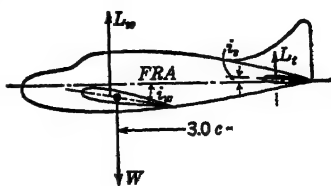
6-9. An airplane weighing 3500 lb has an NACA 23015 airfoil of aspect ratio $A = 8$. Stalling speed at sea level, $V_s = 60$ mph; $C_{D_e} = 0.0130$ (independent of C_L). Cruising speed $V_c = 140$ mph at 5000 ft altitude. A new wing having the same airfoil section but 10 per cent greater wing area is installed on the airplane. What must the aspect ratio be to give the same cruising speed and total drag as the original configuration, but at 10,000 ft instead of 5000 ft? What is the new sea-level stalling speed (mph)?

6-10. Airfoil data: $A = 6$, $m_0 = 5.5$ per radian, $dC_{D_0}/dC_L^2 = 0.0060$. When $\alpha = 10$ deg, $C_L = 0.7$, and $C_D = 0.0650$.

a. A flying wing cruises at $C_L = 0.7$. $W = 400$ lb; $A = 12$; same airfoil section. Find α , D , L/D .

b. A flying wing cruises at $\alpha = 10$ deg. $W = 400$ lb; $A = 12$; same airfoil section. Find C_L , D , L/D .

6-11. A 30,000-lb cargo airplane has its fuselage reference axis (FRA) horizontal, as shown, at a design cruising speed of 150 mph at 7000 ft. Find incidence angle i_w and stabilizer angle i_s , referred to the fuselage reference axis, to balance the airplane at this speed. Assume the tail is in the effective circular tube of downswep air from the wing ($\epsilon = 2\alpha_i$). Ignore the moments arising from the thrust



and drag. Wing area $S = 1000$ sq ft; tail area $S_t = 200$ sq ft; wing aspect ratio $A = 8$; tail aspect ratio $A_t = 2.5$; slope of lift curve for wing (infinite aspect ratio), $m_0 = 5.5$ per radian. Distance from cg to tail cp is 3.0c. The cg is at 0.35c, and the wing ac = 0.23. The wing and tail have symmetrical airfoil sections.

6-12. An airplane weighs 70,000 lb and has a wing loading $l_w = 50$ psf. The wing is rectangular, with aspect ratio $A = 10$, and has an NACA 23015 airfoil section. The residual drag coefficient $C_{D_r} = 0.0120$, and is independent of C_L .

a. Plot C_{D_p} vs. C_L^2 from $C_L = 0$ to $C_L = 1.0$ (see Prob. 6-3).

b. Determine C_{D_p} and e by matching the mathematical and experimental data at $C_L = 0.3$ and $C_L = 0.8$.

6-13. The drag coefficient of a complete airplane is $C_D = 0.0450$ when $C_L = 0.8$. For the wing, $e_w = 0.83$; $b = 80$ ft; $A = 10$. Find C_{D_p} for the complete airplane at $C_L = 0.5$, if $dC_{D_r}/dC_L^2 = -0.0022$.

6-14. For a wing at $C_L = 0.7$: $C_{D_0} = 0.01$; $\alpha_{10} = 8.0$ deg; $C_{m_{0.30}} = -0.01$. Knowing that $dC_{D_0}/dC_L^2 = 0.005$, $\alpha_{L_0} = -0.5$, and that $d\text{ cp}/d\frac{1}{C_L} = 0.04$, find $C_{D_{10}}$ at $C_L = 0.3$, α_0 at $C_L = 0.8$, $C_{m_{0.30}}$ at $C_L = 0.3$, e at $C_L = 0.8$ for $A = 10$, and e_w for $A = 10$.

CHAPTER 7

VISCOSITY PHENOMENA

The resultant aerodynamic force on an airplane is composed of the individual forces on all its components. The force system is sufficiently complicated when each component is considered independently, but the mutual *interference* that arises between components makes accurate force predictions impossible without large reliance on experimental evidence. Nevertheless, an understanding of the principles that govern fluid behavior is necessary for intelligent interpretation of experimental results. Of particular interest is the role played by the thin but ever-present boundary layer, which is the consequence of fluid viscosity. Changes in the character of this layer with Reynolds number produce changes in body force coefficients that are referred to as *Reynolds-number effects* or *scale effects*.

7.1 The Boundary Layer. The boundary layer has been mentioned previously as a region of retarded flow immediately adjacent to the surface of a body subjected to relative fluid motion. The shearing stress τ_0 on the body surface is related to the physical characteristics of the boundary layer through the velocity gradient at the body surface.

$$\tau_0 = \mu \left(\frac{du}{dy} \right)_0 \quad (7-1)$$

where τ is shearing stress, psf

μ is coefficient of viscosity, lb-sec per sq ft

du/dy is velocity gradient, per sec

Subscript 0 refers to the body surface; hence, in general, the thinner the boundary layer (with constant μ), the larger is the shearing stress or skin friction.

The boundary layer has additional importance because it produces a deviation of the streamlines from that predicted by perfect-fluid theory. This gives rise to a pressure field surrounding the body that is also different from that anticipated from perfect-fluid

theory. One of the interesting characteristics of a boundary layer (or any other kind of parallel flow) is that it transmits static pressures undiminished; hence the modified pressure field is conveyed to the body itself. This unbalances the body pressure distribution and causes a *form drag*, which is comparatively small if the flow is unseparated, but may be very large if the flow is separated. The modified pressure field also causes a reduction in the lift that is predicted by the circulation theory, which is comparatively

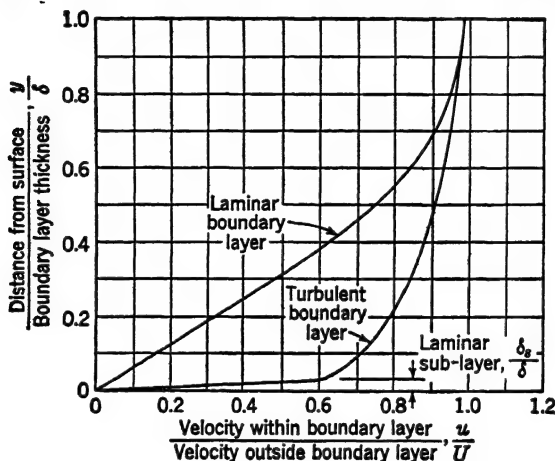


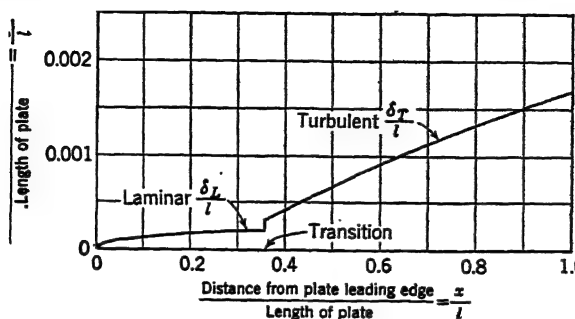
FIG. 7-1. Dimensionless laminar and turbulent boundary-layer profiles.

small for unseparated flow but may be very large if the flow is separated. These and other effects will be studied in the following articles.

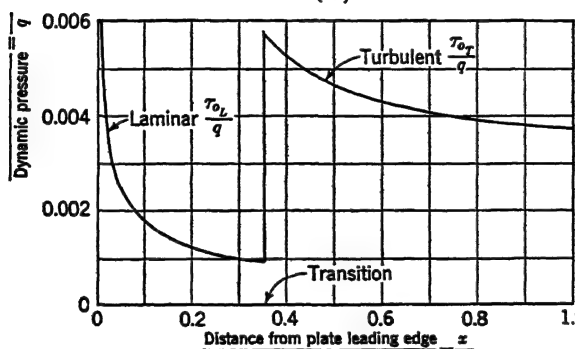
Because of the asymptotic nature of a boundary-layer velocity profile, a definition of its thickness must necessarily be arbitrary. One common definition of the thickness δ is the distance from the surface for which the velocity u within the boundary layer is 99 per cent of the velocity U outside the boundary layer (Fig. 7-1). In the following discussions, all equations involving boundary-layer thickness will be based on this definition.

7-2 Laminar Boundary Layer. Flow on a smooth flat plate set parallel to the remote velocity provides an example of boundary-layer phenomena in their simplest environment; *i.e.*, linear flow (ignoring deviation caused by boundary-layer growth), smooth body surface, zero static-pressure gradient, and no initial stream turbulence. The flow within the boundary layer immediately

downstream from the leading edge contains only molecular velocity fluctuations and is referred to as *laminar flow*: correspondingly, the boundary layer is called a *laminar boundary layer*. Growth



(a)



(b)

Fig. 7-2. Example of dimensionless thickness and shearing stress on a smooth flat plate in the absence of pressure gradient or external turbulent: (a) boundary-layer thickness growth, (b) shearing-stress distribution.

of this boundary layer may be shown to take place according to the following equation:

$$\delta_L = 4.9 \sqrt{\frac{\mu x}{\rho U}} \quad (7-2)$$

where δ_L is laminar-boundary-layer thickness, ft

μ is coefficient of viscosity, lb-sec per sq ft

x is distance from plate leading edge, ft

ρ is mass density, slug per cu ft

U is velocity outside the boundary layer, here equal to the remote velocity v , fps

Equation (7.2) shows that the boundary-layer thickness increases parabolically with distance from the leading edge, as shown in Fig. 7.2a, and decreases with increasing velocity.

A fortunate property of the laminary velocity profile is that it has the same "shape" (as shown in Fig. 7.1) for all points on the plate even though its thickness varies; hence, since the boundary layer is thin near the leading edge, $(du/dy)_0$ is large. From Eq. (7.1) the shearing stress τ_0 must, therefore, also be large; the actual variation may be obtained from the following equation:

$$\tau_{0L} = 0.332 \sqrt{\frac{\mu \rho U^3}{x}} \quad (7.3)$$

where τ_{0L} is plate shearing stress in pounds per square foot. A typical variation in shearing stress with distance along the plate is shown in Fig. 7.2b.

Since a major part of the air deceleration takes place near the leading edge of the plate, as shown by the shearing-stress curve, the drag coefficient might be expected to decrease with increasing Reynolds number; i.e., if a particular plate has its length doubled, thereby doubling the Reynolds number and the area, the drag does not double, because less shear occurs on the added section; hence by Eq. (5.2), C_D decreases. This supposition is borne out by the following equation, which may be derived from Eq. (7.3) by integration:

$$c_{dL} = \frac{2.656}{\sqrt{R_l}} \quad (7.4)$$

where c_{dL} is laminar drag coefficient, dimensionless

R_l is Reynolds number based on the length l of the plate, dimensionless

Equation (7.4) is plotted as the lower curve in Fig. 7.3.

7.3 Turbulent Boundary Layer. If the plate is sufficiently long, *transition* occurs, and a *turbulent boundary layer* ensues. For mathematical definition of the characteristics of the turbulent layer, however, it is convenient to consider transition occurring at the plate leading edge. The discussions then lead to very specialized results. The more general problem is discussed in Art. 7.4. Within the turbulent boundary layer, the air particles oscillate longitudinally and transversely, but in such a manner that the time average of the velocity is essentially constant at any given point past which the fluid is flowing. This may be compared

with the molecular fluctuations in a laminar profile that produce no appreciable change in the velocity with time, the difference being only a matter of the "scale of operation." The laminar shearing stress arises from molecular transfer of momentum from the low-speed region adjacent to the plate to the outer edge of the boundary layer, and vice versa, as was shown in Art. 1-4. The same process is present in a turbulent boundary layer, except that the mass of the agent involved is much larger; *i.e.*, *particles* of air moving with relatively low velocity at the plate surface migrate to the outer extremities of the boundary layer, and vice versa. This interchange of particles introduces an additional shearing stress that is superimposed upon the expected viscous shearing stress. In the region immediately adjacent to the plate, and well within the turbulent boundary layer, the transverse fluctuations are very small because of the proximity of the plate. Indeed, in this region the particle fluctuations are assumed to be zero, and the flow is truly laminar in nature. This leads to the existence of a so-called *laminar sublayer* within the turbulent boundary layer, shown as δ_s in Fig. 7-1.

The shearing-stress equation for a turbulent boundary layer is the same as that for laminar flow [$\tau = \mu(du/dy)$] *only* in the laminar sublayer. For the remainder of the boundary layer, the stress is larger for a particular du/dy because of the additional stress imposed by the particle fluctuations. The shearing equation for turbulent flow is frequently written

$$\tau_r = \epsilon \frac{du}{dy} \quad (7-5)$$

where ϵ is a variable, usually many times larger than μ , called the *exchange coefficient*. From the preceding statements, as y decreases to the value δ_s , ϵ approaches μ . The greater shearing stress that is characteristic of a turbulent boundary layer is clearly demonstrated by the greater value of $(du/dy)_0$ within its laminar sublayer as compared with that of the laminar boundary layer.

For a plate on which only turbulent flow is presumed to exist, the variation in boundary-layer thickness is given empirically by

$$\delta_r = 0.37 \left(\frac{\mu x^4}{\rho U} \right)^{1/4} \quad (7-6)$$

Equation (7-6) shows that the turbulent boundary layer grows

more rapidly than does the laminar. The corresponding shearing-stress equation is

$$\tau_{0,T} = 0.0296 \left(\frac{\rho^4 U^3 \mu}{x} \right)^{1/2} \quad (7.7)$$

This relation shows that the shearing stress decreases less drastically with distance from the leading edge than for laminar flow.

By the above remarks, c_d for a turbulent boundary layer should decrease with increasing Reynolds number, but not so rapidly as

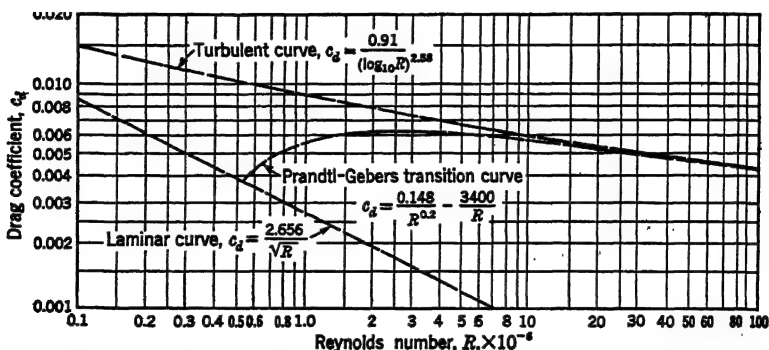


FIG. 7-3. Drag coefficient variation with Reynolds number on a smooth flat plate in the absence of pressure gradient and external turbulence. (From TR 586.)

for laminar flow. The equation for turbulent drag coefficient corresponding to Eq. (7.7) is

$$c_{dT} = \frac{0.148}{(R_1)^{1/2}} \quad (7.8)$$

All the equations for laminar flow are based upon theoretical considerations. The equations for turbulent flow are based upon experiment, and therefore are not unique. The NACA has adopted the following equation in preference to the simpler expression in Eq. (7.8), because it gives closer agreement with experimental data at high Reynolds numbers:

$$c_{dT} = \frac{0.910}{(\log_{10} R_1)^{2.58}} \quad (7.9)$$

Equation (7.9) is plotted in Fig. 7-3 as the upper line.

7.4 Transition. It was explained in Art. 7-3 that laminar flow must ultimately convert to turbulent flow at a point called the

transition. This transition actually probably fluctuates over a considerable length of plate, and the laminar and turbulent velocity profiles in the near vicinity are probably adulterated somewhat in the transition process; nevertheless, for mathematical convenience, transition is assumed to occur instantaneously, with a "pure" laminar profile preceding and a "pure" turbulent profile following. This assumption leads to certain physical inconsistencies that may not be discussed here because of the complexity of the problem. Assuming transition to occur at a point on the plate, the turbulent boundary layer may be shown to increase suddenly¹ as in Fig. 7-2a, while the shearing stress increases suddenly as in Fig. 7-2b.

Under ideal experimental conditions, in which the turbulence content of the stream is itself very low, the transition occurs when the Reynolds number, based on the distance x from the plate leading edge reaches 530,000, or

$$R_x = \frac{\rho U x}{\mu} = \frac{\rho v x}{\mu} = 530,000$$

Hence, for example, for a plate Reynolds number of 1,060,000, based on the plate length, transition occurs at the mid-chord. For a plate like that depicted in Fig. 7-2, the drag coefficient must be weighted according to the length of plate subjected to each type of flow. According to Prandtl and Gebbers, the following equation gives the variation in c_d with Reynolds number for a plate above $R_i = 530,000$:

$$c_d = \frac{0.148}{(R_i)^{1/2}} - \frac{3400}{R_i} \quad (7-10)$$

Equation (7-10) is shown as the middle curve in Fig. 7-3.

In recapitulation: a smooth flat plate in the absence of pressure gradient and external stream turbulence has a drag coefficient indicated by Eq. (7-4) at low Reynolds number, until the critical Reynolds number of 530,000 is reached. With Reynolds number increasing beyond the critical, the plate has a transition point that moves forward, causing increased drag coefficient according to Eq. (7-10). Ultimately, at high Reynolds number, it becomes

¹ Remember that the boundary-layer thickness definition is arbitrary. It could possibly *decrease* using some other definition.

asymptotic to Eq. (7-9), which is representative of the fully turbulent condition.

7-5 Separation. Flow on a thick body differs from that on a flat plate, principally because the thickness of the body causes velocities that are different from the remote velocity, and this, in turn, causes negative and positive pressure gradients on the forward and rearward sections of the body, respectively. Unfortunately, characteristics of a boundary layer are changed not

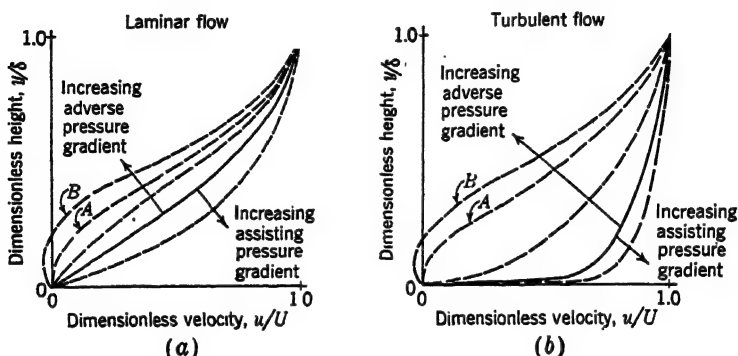


FIG. 7-4. Effect of static-pressure gradient on boundary-layer profile: (a) laminar, (b) turbulent. The curves in Fig. 7-4b labeled *A* and *B* are not verified by experimental data. They have been estimated to simplify explanations. (*Modified curves based on data in TR 497 and WR L-382.*)

only by the changes in local velocity (changes in local Reynolds number) but also by the pressure gradient. The change in profile shape with change in pressure gradient is shown nondimensionally in Figs. 7-4a and b for laminar and turbulent conditions, respectively. A large or continual adverse pressure gradient causes a reduction in velocity throughout the boundary layer but gives the greatest *percentage* reduction next to the surface, where the velocity is the lowest. Under extreme circumstances $(du/dy)_0$ may become zero (curves *A*) or even negative (curves *B*). The former condition mathematically defines *separation*, and the latter indicates *flow reversal*.

7-6 Scale Effect on a Sphere. A good example of transition and separation phenomena is the flow over a sphere. At very low Reynolds numbers, there is no separation; the drag is almost entirely skin friction, and the drag coefficient follows Stokes' law for completely laminar flow (Fig. 7-5):

$$C_D = \frac{24}{R} \quad (7.11)$$

where C_D is based on cross-sectional area of sphere, dimensionless
 R is based on diameter, dimensionless

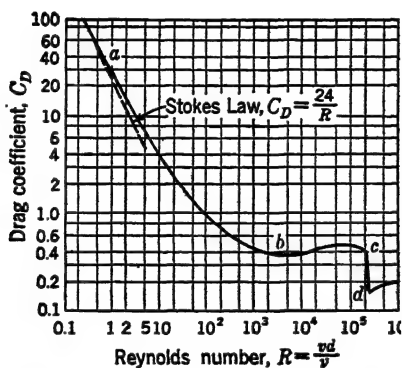
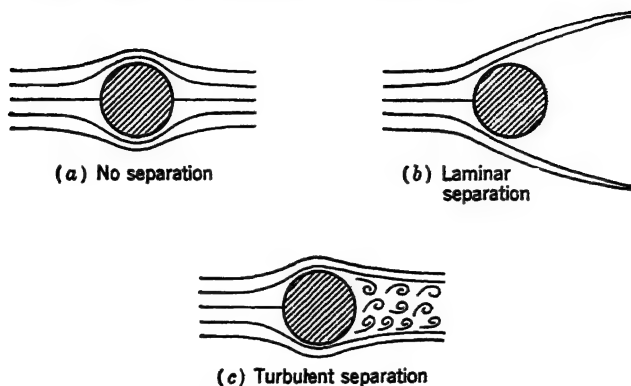


FIG. 7-5. Variation in flow pattern and drag coefficient with Reynolds number on a sphere. (Drag-coefficient variation with Reynolds number replotted by permission of Engineering Societies Monograph Committee from "Applied Hydro- and Aeromechanics," by L. Prandtl and O. G. Tietjens, McGraw-Hill Book Company, Inc., 1934.)

When R is about 1.0 (point a), laminar separation begins near the rear stagnation point. With increasing Reynolds number, the separation point moves forward on the rear surface of the sphere, until at about $R = 2000$ (point b) it reaches the diametral plane. It remains in this general vicinity until transition occurs in the separated wake at about $R = 300,000$ (point c). The transition

point moves toward the diametral plane and reaches it at about $R = 400,000$ (point d). With further increase in Reynolds number, the transition point remains relatively stationary. (The transition point is not likely to move forward of the most negative pressure point on the sphere, because it would then be in a region of assisting pressure gradient, which tends to maintain laminar flow. Transition can be forced to occur forward of the most negative pressure point by roughening the sphere surface.)

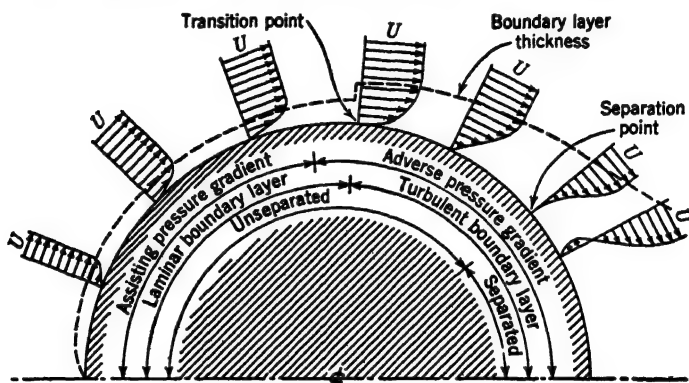


Fig. 7-6. Diagrammatic representation of boundary-layer growth on a sphere for $R > 550,000$. (The boundary layer thickness is exaggerated for clarity.)

At point a the flow is similar to that predicted by perfect-fluid theory, except for that within the boundary layer, and the drag is entirely due to skin friction. At point b the laminar separation causes a large wake, which gives a very large pressure drag and a consequent large deviation from the Stokes curve. At point c a transition forms in the separated wake of the sphere and rapidly moves to the diametral plane; however, the resulting turbulent boundary layer has a characteristically greater velocity near the surface of the sphere, which allows the air to resist the adverse pressure gradient more successfully. Separation (now turbulent) is delayed until the air stream is well back on the downstream side of the sphere. At point d this separation is established at its rearmost position and remains relatively stationary for a considerable range of Reynolds numbers. The boundary-layer changes that take place prior to turbulent separation are shown diagrammatically in Fig. 7-6, and a corresponding typical turbulent separation is shown in Fig. 7-7. The Reynolds number for which

C_D suddenly decreases is called the *critical Reynolds number*, arbitrarily defined as the R for which $C_D = 0.3$.

The laminar boundary layer is inherently unstable as it approaches the critical Reynolds number, and it apparently converts to a turbulent boundary layer in sympathetic response to certain external disturbing frequencies and amplitudes imposed by noise, stream turbulence, or surface roughness. For instance, a sphere



FIG. 7-7. Typical turbulent separation on a curved surface. (Reproduced by permission of Engineering Societies Monograph Committee from "Applied Hydro- and Aeromechanics," by L. Prandtl and O. G. Tietjens, McGraw-Hill Book Company, Inc., 1934.)

towed through the stagnant atmosphere indicates the standard reference critical Reynolds number of 385,000, but a sphere tested in the usually turbulent stream of a wind tunnel always indicates less than this value. Indeed, the ratio of these two Reynolds numbers is called the *turbulence factor* (TF), and it is commonly used as an indication of the degree of stream turbulence in a wind tunnel.

$$TF = \frac{385,000}{\text{tunnel critical } R} \quad (7-12)$$

This same turbulence factor is used to define an "effective" Reynolds number R_e for comparison of airfoil or airplane characteristics obtained from wind tunnels.

$$R_e = (R_t)(TF)$$

where R_t is test Reynolds number, dimensionless

TF is turbulence factor, dimensionless

The data presented by NACA in its various reports are nearly always plotted as a function of effective Reynolds number rather than test Reynolds number.

Addition of a conical afterbody to a sphere reduces the adverse pressure gradient and allows the flow to continue to the trailing edge without separating. The drag coefficient is considerably reduced, the amount depending upon the *fineness ratio*, or ratio of length to maximum diameter. For a particular cross-sectional area, a fineness ratio of 2 or 3 gives the minimum drag. Of course,

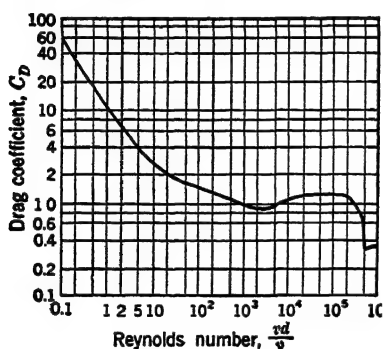


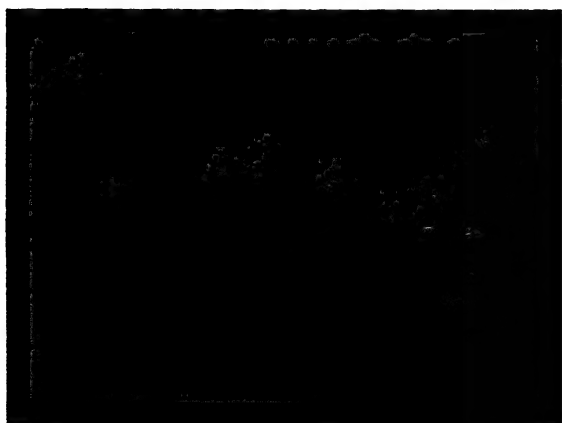
FIG. 7-8. Variation in drag coefficient with Reynolds number on an infinite cylinder. (Replotted by permission of Engineering Societies Monograph Committee from "Applied Hydro- and Aeromechanics," by L. Prandtl and O. G. Tietjens, McGraw-Hill Book Company, Inc., 1934.)

for the ultimate in streamlining, the forebody and afterbody are formed by one continuous convex surface.

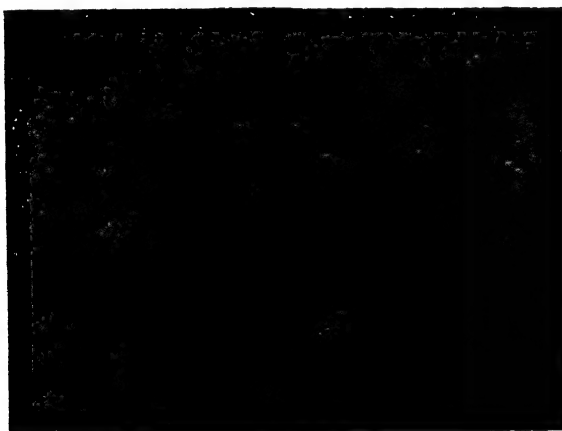
7-7 Scale Effect on a Cylinder. The separation and transition phenomena on a circular cylinder are somewhat similar to those for a sphere, as may be seen in Fig. 7-8. In the region from $R \approx 100$ to $R \approx 100,000$ the separated flow in the wake may not be characterized by a random vortex pattern but may assume a periodic nature as in Fig. 7-9b.

The individual vortices rotate in opposite directions from the two sides of the cylinder and give a staggered arrangement that extends for a considerable distance downstream before decomposing. von Kármán was able to give a mathematical expression for the spacing of the vortices; hence the pattern is commonly called the *Kármán vortex trail*. He was further able to predict the drag coefficient of such a cylinder with surprising accuracy. The periodic shedding of vortices implies a periodic transverse force on the cylinder, which may cause it to vibrate, unless restrained. The "singing" of electric transmission lines and oscillation of tall smokestacks in natural winds is directly attributable to this phenomenon. The disastrous collapse of the Tacoma Narrows suspension bridge was also caused, in part, by a similar phenomenon.

7-8 Scale Effect on a Normal Flat Plate. Except for extremely low Reynolds numbers, the flow on a flat plate perpendicular to



(a)



(b)

FIG. 7-9. Flow patterns behind an infinite cylinder showing two possible wake configurations: (a) Reynolds number = 1.5, and (b) Reynolds number = 250. (Reproduced by permission of Engineering Societies Monograph Committee from "Applied Hydro- and Aeromechanics," by L. Prandtl and O. G. Tietjens, McGraw-Hill Book Company, Inc., 1934.)

the stream is always separated at the plate edges. This produces a wake of fairly constant size, which in turn gives a fairly constant drag coefficient, having a value based on the plate area of about

$C_D = 1.28$. The same Kármán vortex formation within the wake is apparent in Fig. 7-10.

7-9 Scale Effect on an Airfoil. The effect of Reynolds number on the aerodynamic characteristics of an airfoil is more complicated than any yet discussed, because of the variation of airfoil characteristics with angle of attack. The two force components, lift and drag, may best be discussed separately. (There is no appreciable scale effect on pitching moment.) Reference will be made



FIG. 7-10. Flow pattern behind a normal flat plate. Reynolds number = 250. (Reproduced by permission of Engineering Societies Monograph Committee from "Applied Hydro- and Aeromechanics," by L. Prandtl and O. G. Tietjens, McGraw-Hill Book Company, Inc., 1934.)

only to section characteristics, to exclude the effects of aspect ratio and plan-form shape.

Lift. For low angles of attack, c_l may usually be assumed independent of Reynolds number, but considerable variation takes place in the value of $c_{l_{max}}$. The reason is that at low Reynolds number (point *a*, Fig. 7-11), laminar separation takes place at a comparatively low angle of attack, but with increasing Reynolds number (point *b*), transition moves forward on the upper surface and produces a turbulent boundary layer that is able to withstand the adverse pressure gradient and hence to delay separation. Ultimately, when the transition point is well forward on the upper surface (point *c*), further increase in Reynolds number causes no appreciable change in $c_{l_{max}}$, because turbulent flow is well established over most of the airfoil. Of course, the particular variation in $c_{l_{max}}$ is primarily dependent upon the airfoil section, because the surface contour defines the velocity and pressure distributions. Curves of scale effect for several airfoils are shown in Fig. 7-12.

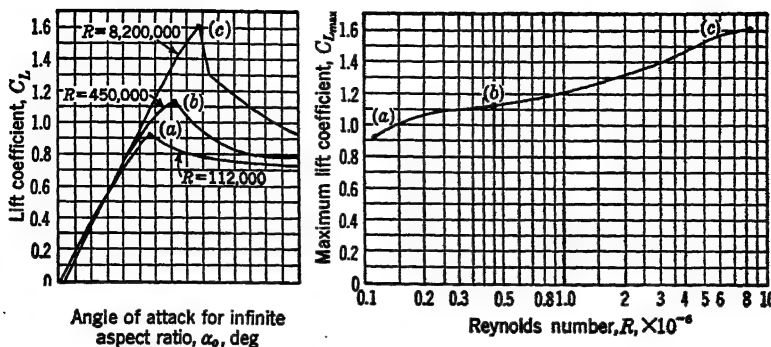


FIG. 7-11. Effect of Reynolds number on the lift curve of an NACA 23012 airfoil. (Uncorrected data from TR 586.)

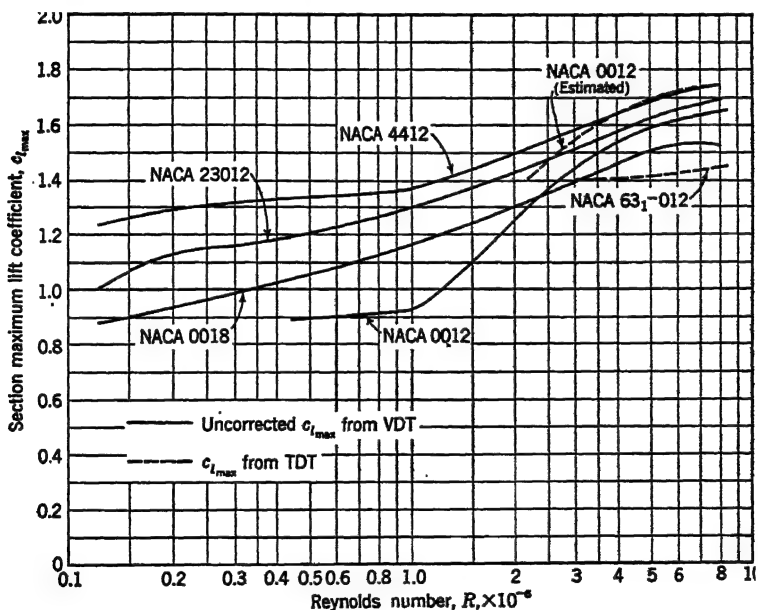


FIG. 7-12. Scale effect on section maximum lift coefficient for several representative NACA sections. (Uncorrected data from TR 586 and WR L-560.)

Drag. The effect of Reynolds number on c_{d_0} is usually indicated by showing its influence on $c_{d_0_{min}}$: the trend is approximately the same for other low lift coefficients (Fig. 7-13a). The curve of $c_{d_0_{min}}$ is usually superimposed on a similar one for a flat plate, as in Fig. 7-13b. This allows comparison of an airfoil having zero

camber and thickness (flat plate) with airfoils having various amounts of camber and thickness.

At low Reynolds number (point *a*, Fig. 7-13*b*), an airfoil generally has laminar separation occurring upstream from the trailing edge, and the large wake produces a relatively large form drag, which in turn gives a large drag coefficient. As the Reynolds number is increased (point *b*), transition appears on the airfoil downstream of the laminar separation point, and the wake width decreases in a manner similar to that shown for the sphere (Art. 7-6). At higher

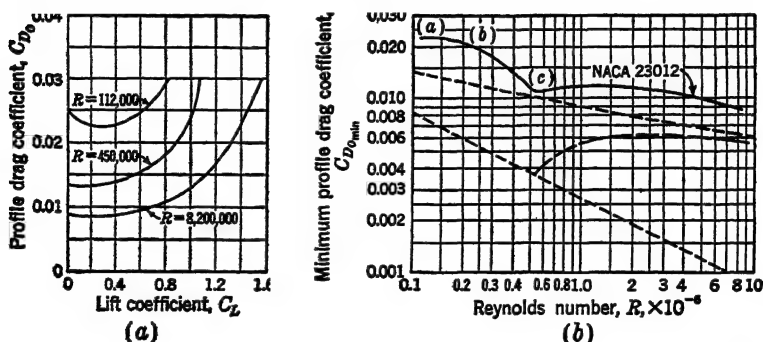


FIG. 7-13. Effect of Reynolds number on the drag curve of an NACA 23012 airfoil. (Uncorrected data from TR 586.)

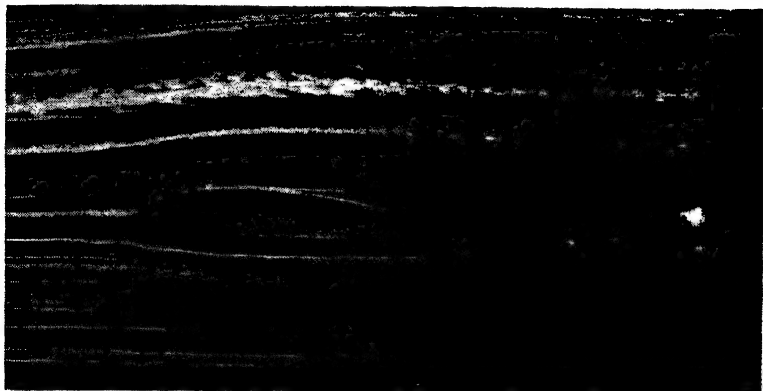
Reynolds numbers (point *c*), transition has moved forward and passed the expected laminar separation point, and the afterbody turbulent flow is now able to resist the adverse pressure gradient without separating. The magnitude of the drag coefficient from point *c* on is therefore determined primarily by skin friction.¹

In Fig. 7-14, the flow pattern is shown for two low Reynolds numbers, to illustrate laminar separation and the influence of transition in restoring the flow to the airfoil surface. Both conditions correspond to a low angle of attack.

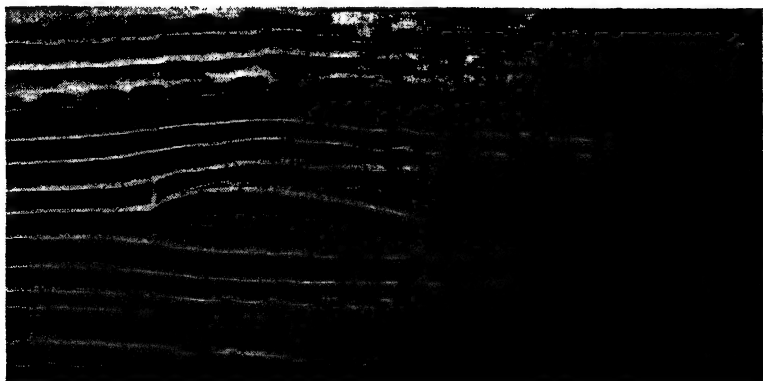
The particular variation of $c_{d_{0,min}}$ with R is dependent upon airfoil section, as shown in Fig. 7-15.

¹ Some British tests on conventional airfoils, reported in *R & M* 1838, indicate that form drag varies linearly with per cent airfoil thickness at high Reynolds numbers, and that it constitutes (very approximately) the same per cent of total drag as its per cent thickness; i.e., an airfoil 10 per cent thick may be expected to have about 10 per cent form drag and about 90 per cent skin friction.

7-10 Scale Effect on Low-drag Airfoils. For a conventional airfoil of average thickness, laminar flow is almost impossible to maintain over a major portion of the upper surface. At low Reynolds numbers, there is a tendency toward laminar separation,



(a)



(b)

FIG. 7-14. Effect of Reynolds number on the flow pattern of an NACA 0012 airfoil at a low angle of attack: (a) low Reynolds number, showing laminar separation, (b) higher Reynolds number, showing laminar separation followed by reattachment of flow caused by transition. (*NACA photographs.*)

while at high Reynolds numbers, transition to turbulent flow occurs. Both cause drag increments over that expected from unseparated laminar flow. The chordwise location of the transition point is a function of Reynolds number and pressure gradient;

hence it varies considerably between airfoils. Conventional four- and five-digit airfoils have a minimum pressure on the upper surface that is close to the leading edge, and the adverse pressure gradient from this point to the trailing edge makes laminar flow almost impossible to maintain at high Reynolds numbers. An airfoil so constructed that an assisting gradient exists over the forward part of its surface delays transition and allows a con-

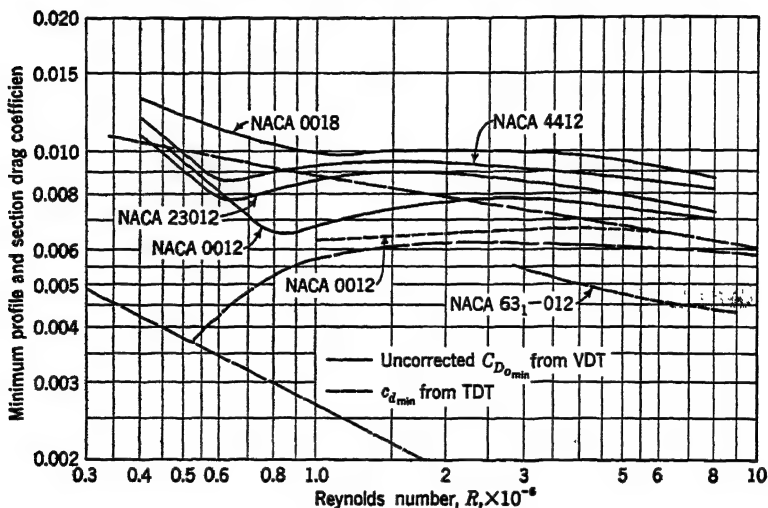


FIG. 7-15. Scale effect on minimum drag coefficient for several representative NACA sections. (Uncorrected data from TR 586 and WR L-560.)

siderable reduction in drag coefficient, because of the lower shearing stresses characteristic of the laminar boundary layer. Figure 7-15 compares the drag coefficient of a typical low-drag airfoil section with some common four- and five-digit sections.

Low-drag airfoils are characterized by a relatively sharp leading edge and by a maximum thickness that is well aft, to produce the desired pressure distribution, and the drag curve has a characteristic *bucket* or region of reduced c_d (Fig. 7-16).

The low-drag airfoil depends for its success upon maintaining laminar flow over a good portion of the airfoil but is so designed that the peak negative pressure does not occur beyond the point where transition takes place; otherwise the adverse pressure gradient on the downstream side of the peak pressure point is *more likely* to produce turbulent separation. Use of a low-drag section

on a wing of practical construction depends for its success on a smooth, inflexible surface and nonturbulent initial stream. Conventional factory methods are generally unsatisfactory for their construction, and they do not exhibit their desirable qualities in a propeller slip stream or in the relatively disturbed flow at the wing tips. For this reason, they seem to have some possibilities for success on jet-propelled airplanes having a "skin" of large moment

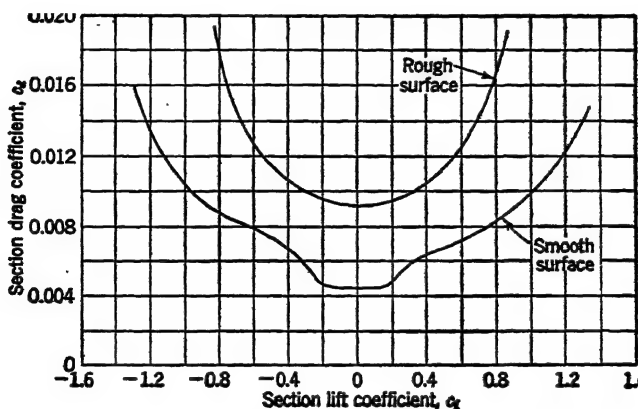


FIG. 7-16. Aerodynamic characteristics of an NACA 63₁-012 airfoil at a Reynolds number of 6,000,000. (From *WR L-560*.)

of inertia. Figure 7-16 verifies that the desirable low-drag characteristics are completely lost if the airfoil surface is rough. Similar results would be exhibited with large external stream turbulence. Roughness may be due to factory methods, but even with a satisfactory finish it can be introduced artificially by oil, dust, splattered flies, etc.

PROBLEMS

7-1. From Eq. (7-3) prove Eq. (7-4).

7-2. Using Eq. (7-2), find a general equation for laminar-boundary-layer thickness δ_L (in.) at the transition point on a smooth flat plate, in the absence of pressure gradient, as a function only of remote velocity in miles per hour. Assume standard conditions and no stream turbulence (hence the critical Reynolds number is 530,000).

7-3. Compute the drag coefficient of a circular flat plate having diameter d when at zero angle of attack at a Reynolds number (based on the diameter) $R_d = 500,000$. Assume there is no pressure gradient and no stream turbulence. **HINT:** Choose an element of plate parallel to the remote velocity, and apply Eq. (7-4). The resulting equation may be integrated either graphically or by using the binomial theorem. Comment on the fact that the computed drag coefficient does not correspond to any of the theoretical lines on Fig. 7-3.

7-4. Discuss the effect on the stalling of a tapered wing of the variation in section maximum lift coefficient $c_{l_{\max}}$ with Reynolds number; *i.e.*, does this variation tend to nullify, or aggravate, the tip-stalling characteristics?

CHAPTER 8

COMPRESSIBILITY PHENOMENA

The growing importance of high-speed flight has required intensive mathematical and experimental investigation of the properties of compressible fluids. Experimental work has been hampered considerably by the excessive power required to create artificially a high-speed jet of air in which to conduct model tests; consequently, most data have been obtained from relatively small scale models, from which only trends of aerodynamic properties may be established. Many novel and ingenious procedures have been used to obviate the necessity of using a supersonic wind tunnel, but with all present techniques either the model used is very small or the necessary equipment is usually complicated and expensive to operate.

For purposes of segregating the problems of high-speed flight, three main regimes are defined for describing the velocity at a point in a fluid. The subsonic region corresponds to a velocity less than the speed of sound; sonic corresponds to the speed of sound, and supersonic means greater than the speed of sound; hence, in terms of the Mach number,

Subsonic: $M < 1$

Sonic: $M = 1$

Supersonic: $M > 1$

When describing the field of flow over an airfoil or any other body, part of the flow may be subsonic, part sonic, and part supersonic. In order to describe the type of flow, subsonic is taken here to indicate that the velocity is *everywhere* less than the speed of sound, and supersonic means that the flow is *everywhere* greater than the speed of sound.¹ The intermediate region is called transonic; here either the remote velocity is subsonic and a

¹ Actually an impossibility because of the existence of a boundary layer even in supersonic flow; however, the definition refers to conditions outside the boundary layer and wake.

local velocity on the body is supersonic, or the remote velocity is supersonic and some local velocity is subsonic; hence

$$\begin{aligned}
 \text{Subsonic: } & \begin{cases} M < 1 \\ M_L < 1 \end{cases} \\
 & M > 1 \\
 & M_L < 1 \quad \text{for some point on body} \\
 \text{Transonic: } & \text{or} \\
 & \begin{cases} M < 1 \\ M_L > 1 \end{cases} \quad \text{for some point on body} \\
 \text{Supersonic: } & \begin{cases} M > 1 \\ M_L > 1 \end{cases}
 \end{aligned}$$

where M is remote Mach number, and M_L is local Mach number.¹

For subsonic flow, some semiempirical equations have been developed that allow fairly accurate prediction of high-speed aerodynamic characteristics from low-speed data. In the supersonic region, the characteristics can again be predicted with fairly good accuracy. The transonic region, because of the mixed nature of its flow, does not lend itself to simple mathematical treatment; experiment is the most satisfactory method by which it may be investigated at present.

A complete understanding of compressible phenomena requires appreciation not only of the classical hydrodynamic theories but those of thermodynamics as well. In this elementary text only the most general problems will be stated, along with some of the more important mathematical and experimental conclusions. Unless otherwise noted, all viscous effects will be ignored.

8-1 Continuity and Bernoulli Equations. In the previous statement of the continuity equation and in the development of the Bernoulli equation (Arts. 2-2 and 2-3), the density ρ was assumed to be independent of static-pressure changes arising from changes in velocity in a stream tube. This simplification does not involve serious error, provided the velocity is everywhere small compared with the speed of sound, but when the velocity in the stream tube is allowed to approach the speed of sound, the effect of changes in density must be taken into account.

The continuity equation for compressible fluids, from Eq. (2-1), is

$$\rho A v = K \quad (8-1)$$

¹ The upper boundary of the transonic region is sometimes defined to correspond to a remote Mach number of 1. See Art. 8-7.

where K is a constant. The Bernoulli equation for compressible fluids is developed from its differential form [Eq. (2-3)]:

$$\frac{dp}{\rho} = -v \, dv \quad (8-2)$$

Within the stream tube, changes in density are assumed to occur adiabatically, because the changes occur too rapidly for any appreciable heat to flow; thus, from Eq. (1-17),

$$\frac{p}{\rho^\gamma} = C_1 \quad (8-3)$$

$$= \left(\frac{p}{C_1} \right)^{1/\gamma} \quad (8-4)$$

where C_1 is a constant. Equation (8-2) may be integrated, after substituting ρ from Eq. (8-4):

$$C_1^{1/\gamma} \frac{dp}{p^{1/\gamma}} + v \, dv = 0 \quad (8-5)$$

$$\frac{\gamma}{\gamma - 1} \frac{p}{\rho} + \frac{v^2}{2} = C_2 \quad (8-6)$$

where C_2 is a constant. Equation (8-6) is the more general form of the Bernoulli equation. Although the equation was developed from Eqs. (8-2) and (8-3), each of which assumes no dissipative forces are present, it could have been developed from much more general considerations which would show that this particular form of the Bernoulli equation applies to *any* flow of a compressible fluid in which there is no heat flow through the stream-tube boundaries; *i.e.*, it applies to any adiabatic flow whether isentropic or not.

8-2 Implications of the Continuity and Bernoulli Equations. The continuity and Bernoulli equations may be expanded and combined to show some of the important properties of compressible flow. First, consider a venturi tube. The variation in velocity v with area A may be obtained in the following manner: The derivative of the logarithm of Eq. (8-1) yields

$$\frac{dA}{A} + \frac{dv}{v} + \frac{dp}{\rho} = 0 \quad (8-7)$$

which, of course, is merely another way of stating the continuity equation. From Eqs. (1-20) and (1-23)

$$\frac{dp}{dV} = -\frac{\rho a^2}{V} \quad (8-8)$$

However,

$$\begin{aligned}\Gamma &= \frac{1}{\rho g} \\ \frac{d\Gamma}{d\rho} &= -\frac{1}{\rho^2 g}\end{aligned}\quad (8.9)$$

Equations (8.8) and (8.9) may be combined to give

$$dp = a^2 d\rho \quad (8.10)$$

From the differential form of the Bernoulli equation [Eq. (8.2)]

$$\rho = -\frac{dp}{v dv} \quad (8.11)$$

Equation (8.10) is substituted in Eq. (8.11):

$$\rho = -\frac{a^2 d\rho}{v dv} \quad (8.12)$$

Equation (8.12) is substituted in Eq. (8.7):

$$\frac{dA}{A} + \frac{dv}{v} - \frac{v dv}{a^2} = 0 \quad (8.13)$$

Finally, Eq. (8.13) is rearranged as follows:

$$\frac{dv}{v} = \frac{dA}{A} \frac{1}{M^2 - 1} \quad (8.14)$$

where M is the Mach number corresponding to area A and velocity v . Equation (8.14) shows a great deal about the properties of a stream tube in compressible flow. For instance, when $M = 0$,

$$\frac{dv}{v} = -\frac{dA}{A}$$

therefore,

$$Av = \text{a constant}$$

Hence, as the Mach number approaches zero, the fluid properties approach more and more closely those of an incompressible fluid, for which an increase in stream-tube area requires a corresponding decrease in velocity. More important, however, it shows that when $0 < M < 1$, an increase in area requires less decrease in velocity, until when $M > 1$, an increase in area requires an *increase in velocity*. These peculiar conditions are brought about by the

reduction of density, which at subsonic speed occurs less rapidly than the area increases, and at supersonic speed occurs more rapidly than the area increases.

A pressure equation corresponding to Eq. (8-14) may be obtained by writing, from Eq. (8-2),

$$\frac{dv}{v} = -\frac{dp}{\rho v^2} \quad (8-15)$$

and from Eqs. (1-22) and (1-23),

$$\rho = \frac{\gamma p}{a^2} \quad (8-16)$$

Substituting Eq. (8-16) in Eq. (8-15) and the result in Eq. (8-14) gives

$$\frac{dp}{p} = \gamma \frac{dA}{A} \frac{M^2}{1 - M^2} \quad (8-17)$$

The important aspect of Eq. (8-17) is that it shows, for a fixed Mach number, that an increase in area (positive dA) requires a pressure rise (positive dp) for $M < 1$ and a pressure drop (negative dp) for $M > 1$.

8-3 Compressible Flow in a Laval Nozzle. The physical significance of these relationships may be clarified diagrammatically as in Fig. 8-1, where a portion of a Laval nozzle in the form of a symmetrical venturi tube is shown, with three reference stations: two stations are located up- and downstream where the areas are the same, and the third corresponds to the axis of symmetry where the area is a minimum. If the flow through the tube is completely subsonic (Fig. 8-1a), the reduction in area in the throat of the tube requires an increase in velocity and reduction in pressure; then the increase in area in the downstream section requires a decrease in velocity and increase in pressure. Scalar conditions in the tube are perfectly symmetrical up- and downstream from the throat. Now let the initial velocity v_i be increased; the velocity in the throat v_t and the final velocity v_f must also increase. Ultimately, with sufficient increase in v_i , v_t reaches the local speed of sound, or reaches $M = 1$. *No further increase in Mach number upstream of the constricted section and at the constricted section itself is possible*, but according to Eq. (8-14), the velocity may become supersonic downstream of the throat. When this condition prevails, the flow becomes unsymmetrical (Fig. 8-1b), and the large downstream

kinetic energy must somehow revert to potential energy in the form of static pressure. The reduction in velocity occurs abruptly through a *normal shock wave*, on the upstream side of which the

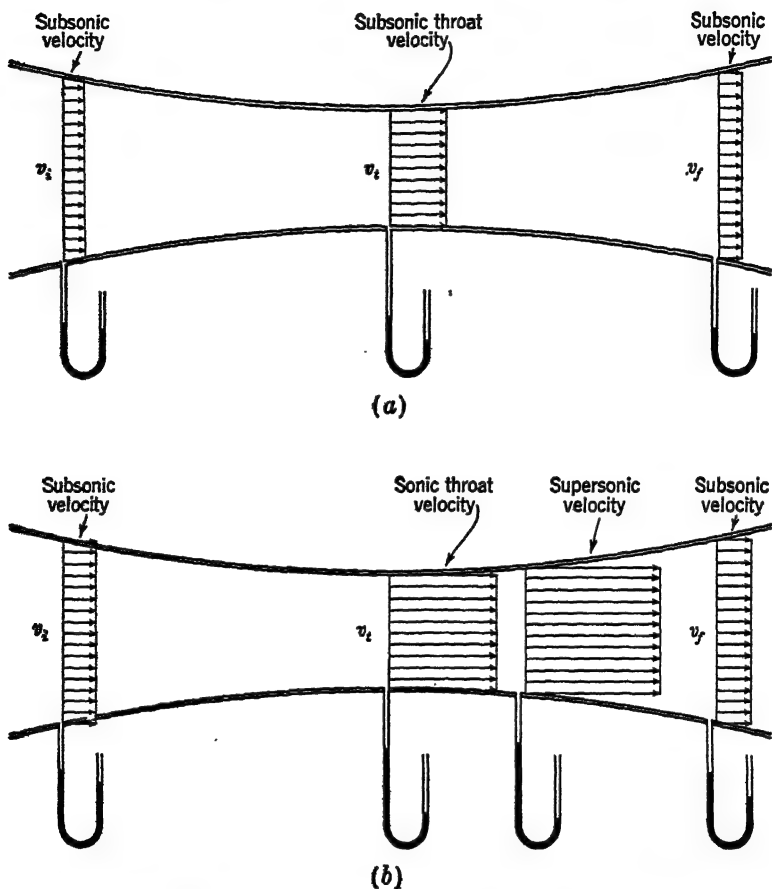


FIG. 8-1. Comparison of flow through a Laval nozzle for: (a) subsonic, and (b) supersonic conditions.

velocity is supersonic and the static pressure is very low. On the downstream side the velocity is about the same as the initial velocity, while the static pressure is less than its initial value. Supersonic speed may be attained, then, by mechanically reducing the static pressure in the downstream station by means of a suction

pump of some sort.¹ Increasing the amount of suction merely causes the shock wave to move downstream. It is of considerable interest that a *unique value of the Mach number corresponds to each station upstream of the shock*; this value is determined only by the geometry of the tube. Furthermore, an upstream constriction in which the velocity is sonic is *necessary* for the production of supersonic flow. This is the reason why supersonic tunnels are built with the test section downstream from a constriction, and this fact also explains why most supersonic tunnels have only one possible test-section Mach number, unless the walls are flexible so as to change the ratio of areas between the constriction and the test section.

8-4 Subsonic Airfoil Flow—Two-dimensional. The changes in density accompanying changes in static pressures on an airfoil reflect back to produce a pressure distribution that is different from that predicted for an incompressible fluid by perfect-fluid theory. The development of equations to show modifications to the incompressible pressure distribution is, in general, a rather elaborate procedure. Only the results will be shown here.

For an incompressible fluid, the pressure at the stagnation point is greater than the remote static pressure by the amount of the dynamic pressure q (see Art. 2-5); hence

$$C_{p_s} = \frac{\Delta p_s}{q} = 1 \quad (8-18)$$

where C_{p_s} is pressure coefficient at stagnation point, dimensionless

Δp_s is change in static pressure at stagnation point, from remote value, psf

q is remote dynamic pressure, psf

For a compressible fluid, the pressure at the stagnation point is augmented according to the following equation,² which incidentally is derived directly from the Bernoulli equation:

$$C_{p_s} = 1 + \frac{1}{4} M^2 + \frac{2 - \gamma}{24} M^4 + \dots \quad (8-19)$$

¹ It should be noted that the ratio of inlet to outlet pressure in the tube is the determinant of flow conditions within the tube. A high positive pressure at the intake and atmospheric pressure at the exhaust would work just as well.

² This same equation may be used to correct a pitot-tube reading in a compressible fluid: $q_{\text{correct}} = q_{\text{read}}/C_{p_s}$.

In the above convergent series, no appreciable error is involved if only the first two terms are retained; hence

$$C_p \approx 1 + \frac{M^2}{4} \quad (8-20)$$

where M is the remote Mach number.

For the remaining pressure on the airfoil, two commonly accepted equations are used. Neither applies accurately where

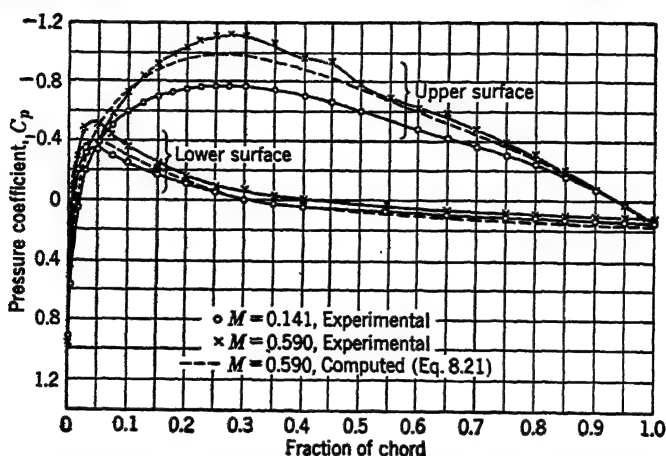


FIG. 8-2. Comparison of experimental and computed pressure coefficient on an NACA 4412 airfoil at $\alpha = -0.25$ deg. (Experimental data from TR 664.)

the local velocity on the airfoil is considerably different from the remote velocity; hence they do not apply at the stagnation point or on the upper and lower surfaces of an airfoil at high angle of attack. The Prandtl-Glauert equation has had wide use, but the Kármán-Tsien equation gives slightly closer correlation with experimental data. The Prandtl-Glauert equation is

$$C_p = \frac{C_{p0}}{\sqrt{1 - M^2}} \quad (8-21)$$

and the Kármán-Tsien equation is

$$C_p = \frac{C_{p0}}{\sqrt{1 - M^2} + \left(\frac{M^2}{1 + \sqrt{1 - M^2}} \right) \frac{C_{p0}}{2}} \quad (8-22)$$

where C_p is pressure coefficient for compressible flow, dimensionless

C_{p0} is pressure coefficient for incompressible flow ($M \rightarrow 0$), dimensionless

M is remote Mach number, dimensionless

In Fig. 8-2 the pressure distribution about a four-digit airfoil is shown. Experimental data are compared with those obtained by using Eq. (8-21) for $M = 0.59$; the correlation is seen to be reasonably good.

Lift Coefficient. The lift coefficient of a wing is dependent upon the pressure-coefficient distribution, according to the following analysis. Let an element of surface, ds , be chosen on the airfoil

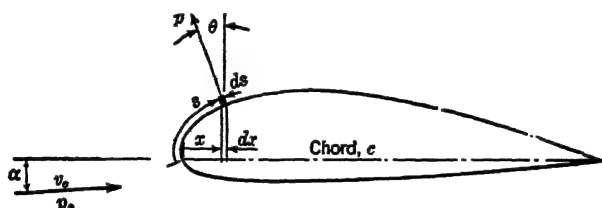


FIG. 8-3. Orientation of surface element ds used in establishing Eq. (8-24).

shown in Fig. 8-3. The lift on the element may be obtained by first finding the differential normal force.

$$dN = -b(p - p_0) ds \cos \theta$$

From the geometry of the wing

$$dx = ds \cos \theta$$

and, neglecting the small chordwise force component,

$$dL = dN \cos \alpha \quad (8-23)$$

Thus the total lift may be obtained by integrating over the upper and lower surfaces:

$$L = -b \cos \alpha \left(\int_0^c (p - p_0)_U dx - \int_0^c (p - p_0)_L dx \right)$$

where subscripts U and L designate upper and lower surfaces, respectively. The lift coefficient may be obtained by dividing through both sides by $q_0 bc$:

$$c_L = -\cos \alpha \int_0^1 (C_{pU} - C_{pL}) d\left(\frac{x}{c}\right) \quad (8-24)$$

On a plot of pressure coefficient vs. fraction of chord, such as Fig. 8·2, the lift coefficient from Eq. (8·24) may be obtained as the product of $\cos \alpha$ and the area contained between the upper-surface and lower-surface curves, with due regard for signs. For example, just by eye the lift coefficient at $M = 0.141$ on Fig. 8·2 may be estimated as about $c_l = 0.4$.

Since the lift coefficient depends upon the pressure coefficients, which in turn depend upon the Mach number, the equations used to predict the variation in C_p with M may be applied directly for a similar prediction of c_l . For instance, by use of Eq. (8·21),

$$c_l = \frac{c_{l_0}}{\sqrt{1 - M^2}} \quad (8·25)$$

where the subscript has the same meaning as before. Figure 8·4 shows experimental data compared with the lift coefficient computed by Eq. (8·25).

The slope of the lift curve is, of course, determined according to an equation similar to that used for the lift coefficient:

$$a = \frac{a_0}{\sqrt{1 - M^2}} \quad (8·26)$$

The influence of increasing Mach number may be given a geometric interpretation that has particular value in estimating the drag coefficient and pitching moment coefficient, as will be shown in the next sections. The thickness, and the camber and angle of attack *measured from zero lift*, are all assumed to be increased by $1/\sqrt{1 - M^2}$; thus

$$t = \frac{t_0}{\sqrt{1 - M^2}} \quad (8·27)$$

$$\xi = \frac{\xi_0}{\sqrt{1 - M^2}} \quad (8·28)$$

$$\alpha' = \frac{\alpha'_0}{\sqrt{1 - M^2}} \quad (8·29)$$

where t is thickness, fraction of chord

ξ is camber, referred to zero-lift chord, fraction of chord

α' is angle of attack measured from zero lift, deg

The subscript 0 refers to the incompressible conditions ($M \rightarrow 0$). Neither thickness nor camber affect the lift of the wing, but an increase in angle of attack produces a corresponding increase in

lift coefficient and lift-curve slope. This has already been shown in Eqs. (8-25) and (8-26).

Drag Coefficient. The geometric approach allows solution of the drag coefficient for a high subsonic Mach number, using incom-

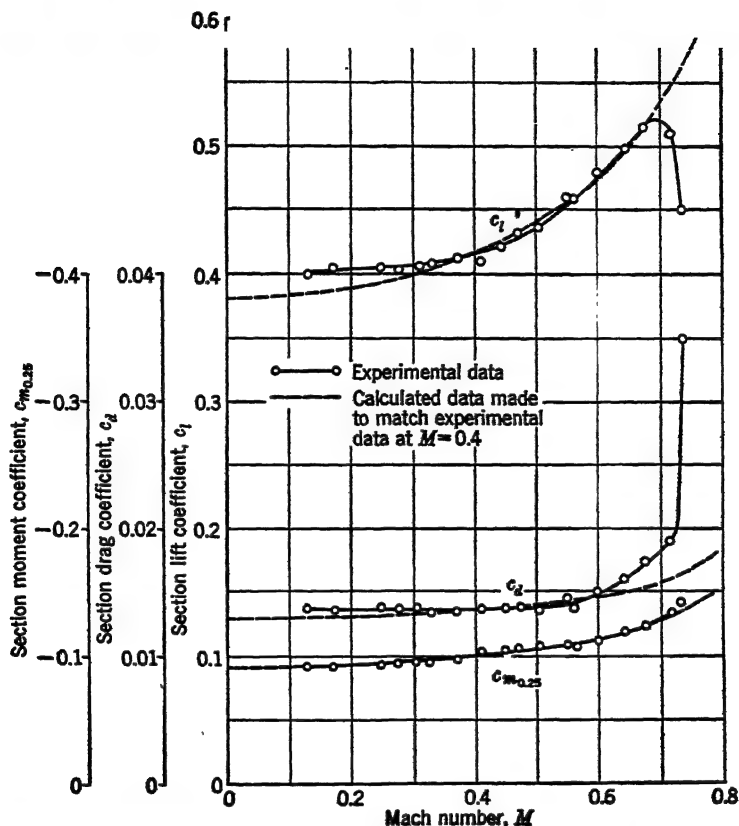


FIG. 8-4. Comparison of experimental and computed variations of aerodynamic coefficients with Mach number for an NACA 4412 airfoil at $\alpha = -0.25$ deg. (Experimental data from force tests in TR 646.)

pressible data. The method involves choosing c_d for an airfoil whose lift coefficient, thickness, and camber have all been increased by $1/\sqrt{1-M^2}$. This requires low-speed data that show not only the conventional variations of c_l and c_d vs. α but also the effect of thickness and camber. The method for determining c_d is thus seen to be partly empirical; even so, the correlation between experiment and theory is fairly good, as shown in Fig. 8-4.

Pitching Moment Coefficient. Pitching moment coefficients are conventionally plotted to correspond with either the 25 per cent chord or the aerodynamic center; consequently, the variation of c_m with c_i is usually negligible. Since c_{mac} may be shown theoretically to be linearly dependent upon amount of camber and independent of thickness, then by Eq. (8-28)

$$c_{mac} = \frac{c_{mac_0}}{\sqrt{1 - M^2}} \quad (8-30)$$

The curves presented in Fig. 8-4 show good correlation between experiment and theory.¹

In all these subsonic discussions, the effects of viscosity, as represented by the Reynolds number, have been ignored. This is fortunately permissible, provided that all discussions are limited to relatively large Reynolds numbers where the aerodynamic characteristics do not vary appreciably with Reynolds number alone.

8-5 Supersonic Airfoil Flow—Two-dimensional. In order to discuss supersonic flow, a different approach may be used, in that a single particle is assumed to move through a stationary fluid; the resulting pressure waves may then be studied.

Consider a particle moving to the left at *subsonic* speed in a stationary fluid. In the time interval t , it moves from a to e (Fig. 8-5a). During the same time interval, the pressure wave that started at a reaches $ABCD$. The circles of decreasing radius represent the positions of pressure waves at time t that originated at b , c , and d ; for instance, the radius of the circle whose center is at c is one-half of the largest circle, because ec is one-half of ea . The interesting fact about this motion is that the particle itself always remains within the confines of all previously produced waves; furthermore, each wave must remain within the confines of all waves previously produced. A point x , far ahead of the moving particle, then experiences a gradually increasing intensity of disturbance as the particle approaches, and a gradually decreasing intensity after it passes. This condition is somewhat analogous to the familiar *Doppler effect* produced by the horn of an approach-

¹ The correlation shown in the three curves in Fig. 8-4 may be slightly misleading because of the method of plotting; i.e., mathematical and experimental data have been matched at $M = 0.4$. This was done because of unknown Reynolds-number effects at low Mach number.

ing automobile: the pitch and intensity increase gradually, reach a maximum, then decrease as the automobile passes.

Now let the particle move at supersonic speed, and again consider the wave front produced by the particle traveling left through point *a* (Fig. 8-5*b*). By the time it has reached point *e*, the wave front, which does not travel so fast, has enlarged only to *ABCD*. Again the wave produced by the particle in passing through point *c*, halfway between *a* and *e*, grows to half the size of the wave, *ABCD*. Here, evidently, conditions are radically different from the subsonic case. The particle is *never* within the boundaries of any previous wave, nor is any wave completely enclosed by a preceding one. Furthermore, the tangent to all waves produces a conical envelope whose apex is coincident with the particle. The envelope forms a *Mach wave*, and the *Mach angle* μ is seen to be related to the particle velocity and Mach number:

$$\begin{aligned}\mu &= \sin^{-1} \frac{a}{v} \\ &= \sin^{-1} \overline{M}\end{aligned}\quad (8-31)$$

where *a* is speed of sound, fps

v is particle velocity, fps

A point *x* ahead of the moving particle experiences nothing until the Mach wave is encountered; then the sudden disturbance decreases gradually. If, instead of a single particle, an infinite number of particles forming an infinite filament into the paper is considered, the same statements may be made regarding the formation of Mach waves. Here, however, the flow would be two-dimensional.

In Fig. 8-5*b* a moving particle in a stationary fluid was con-

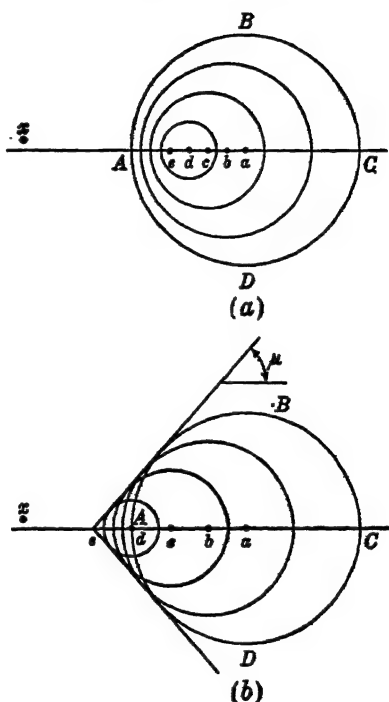


FIG. 8-5. Pressure waves produced *t* seconds after a particle passes left through point *a*: (a) subsonic, (b) supersonic.

sidered. By a change in reference axes, the fluid may be considered to pass by the particle at supersonic speed, producing a standing wave. Since the wave front in Fig. 8-5b had a sonic normal velocity, the component of the remote supersonic velocity that is normal to the standing wave must also be sonic.

The point source of disturbance just described always produces a weak type of wave that has been defined as a Mach wave. If the

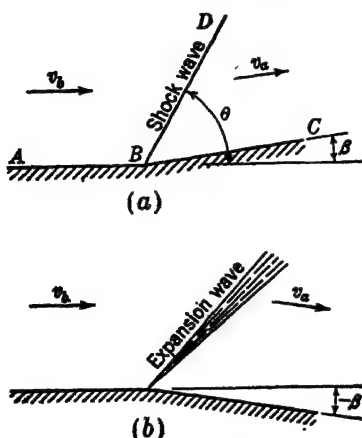


FIG. 8-6. Supersonic flow patterns showing: (a) convergent flow with shock wave, and (b) divergent flow with expansion wave.

two types of waves are similar in that the final velocity vector is supersonic and parallel to the wall, but the oblique shock wave is generally very thin, and the changes in velocity and static pressure occur abruptly upon passing through it. On the other hand, the expansion wave is generally not thin, and the changes in velocity and static pressure occur gradually through a characteristic fanlike region. (This latter phenomenon is frequently called a *Prandtl-Meyer expansion*.) For a particular supersonic remote velocity, there is a maximum positive β for which the shock wave will occur as described above (e.g., at $M = 3.0$ $\beta_{\max} = 34$ deg). For any larger β , the shock wave moves forward at point B, giving a *detached shock wave*. Again, for a particular supersonic remote velocity, there is a maximum negative β for which an expansion wave will occur as described above. For any larger β , the flow will separate at the point B.

disturbance consists of a solid wall which produces a change in the direction of flow as in Fig. 8-6, a Mach wave results only if β is infinitesimal. For finite positive β , an *oblique shock wave* is produced (Fig. 8-6a). The velocity vector v_b rotates through the angle β and reduces to v_a abruptly upon passing through the shock, while the static pressure increases. For finite negative β , an *expansion wave* is produced (Fig. 8-6b). Here the velocity vector v_a again rotates through the angle β but increases to v_b while the static pressure decreases. The

The photograph shown in Fig. 8-7 illustrates some of these principles. The shock wave at the leading edge, the expansion wave at the first break in the body surface, the expansion wave at the trailing edge, and the separated wake are all clearly defined.

Lift Coefficient. Let a thin flat plate be inclined at an angle α to the air stream, as in Fig. 8-8a. The streamlines deflect in



FIG. 8-7. Supersonic flow over a bullet at Mach number = 1.58. The shock wave originating at the leading edge, the expansion wave at the first break in the bullet contour, the expansion wave at the trailing edge, and the boundary layer and wake are all clearly shown. (Shadowgraph taken by Dr. A. G. Charters at the Aberdeen Proving Ground. Reproduced by permission.)

passing through the expansion and shock wave and follow the shape of the plate to the trailing edge, where they again pass through a shock and expansion wave. The pressure decrement and increment on the upper and lower surfaces are equal, as in Fig. 8-8b. Integration of the pressure forces in the vertical direction allows computation of the lift coefficient. The final result (due to Ackeret), assuming α is a small angle, is

$$c_l = \frac{4\alpha}{\sqrt{M^2 - 1}} \quad (8-32)$$

where α is the angle of attack in radians defined by a chord joining the leading and trailing edges of the plate.

For thin, slightly cambered airfoils, the lift coefficient may be estimated by a more elaborate procedure,¹ but Eq. (8-32) gives an approximate result even for these airfoils, provided that they have sharp leading edges and that no separation occurs.

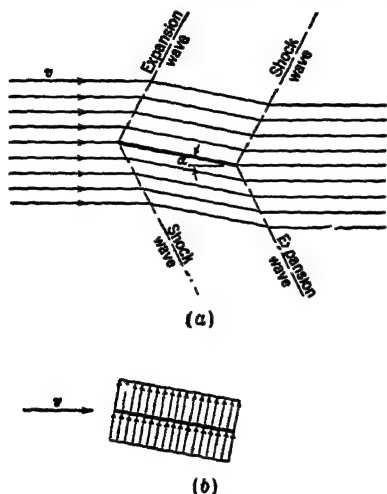


FIG. 8-8. Supersonic flow characteristics of a flat plate: (a) streamline pattern, (b) pressure distribution.

Drag Coefficient. On the same plate in Fig. 8-8, D/L is evidently approximately equal to the angle of attack in radians; hence

$$c_d = \frac{4\alpha^2}{\sqrt{M^2 - 1}} \quad (8-33)$$

It is interesting to notice that the relation $c_d = c_i \alpha$ used to establish Eq. (8-33) is required because the pressures act perpendicular to the plate surface. The same requirement is true for a flat plate in subsonic flow also, but in this case the infinite velocity around the infinitely thin leading edge gives a negative drag force

that precisely counteracts the drag due to the normal force.

The effects of viscosity on c_d must be accounted for by separate calculations but may be estimated, in the absence of test data, to be the same as for unseparated subsonic flow at the same Reynolds number. The drag computed using Eq. (8-33) is generally called *wave drag*, to differentiate it from the skin friction and form drag due to viscosity.

For airfoils having finite thickness Eq. (8-33) must be modified. Two of the simplest examples are the circular-arc (lenticular) and double-wedge (diamond) airfoils. For the circular-arc airfoil the drag coefficient given by Eq. (8-33) must be increased by

$$\Delta c_d = \frac{16}{3\sqrt{M^2 - 1}} \left(\frac{t}{c} \right)^2 \quad (8-34)$$

¹ See TN 1143 and TN 1179.

and for the double-wedge airfoil it must be increased by

$$\Delta c_d = \frac{4}{\sqrt{\gamma M^2}} \left(\frac{t}{c} \right)^2 \quad (8-35)$$

These results are again due to Ackeret. It is important to notice that the drag due to airfoil thickness is proportional to the square

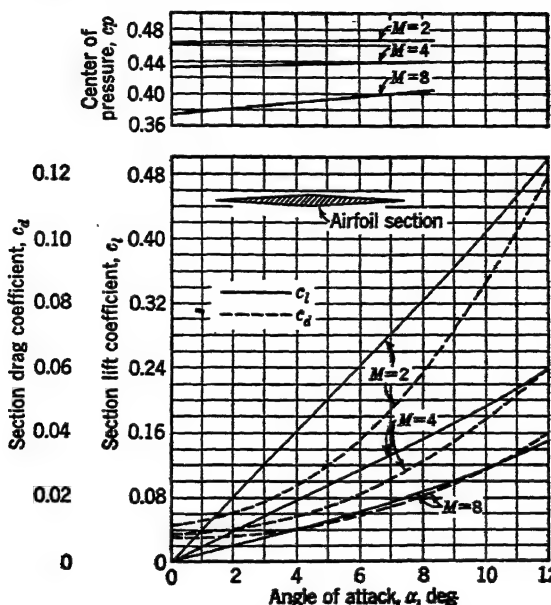


FIG. 8-9. Supersonic aerodynamic characteristics of a 5 per cent thick double-wedge airfoil. (From TN 1179.)

of the thickness ratio. This is a characteristic of all supersonic airfoils and is the reason that thin airfoil sections are so much more important for supersonic than for subsonic airplanes.

Pitching Moment Coefficient. According to Ackeret, the center of pressure of a thin uncambered supersonic airfoil remains fixed at the 50 per cent chord regardless of airfoil section, hence $ac = 0.50$ and

$$C_{m_{0.50}} = 0 \quad (8-36)$$

In Fig. 8-9 the characteristics of a 5 per cent thick double-wedge airfoil are shown as a function of Mach number and of angle of attack. The curves were obtained from a more exact method than

that suggested by Ackeret, and the drag curves include an estimate of the effects of viscosity.

8-6 Transonic Airfoil Flow—Two-dimensional. The transonic regime divides the sub- and supersonic regimes of flow. It begins when some point on the airfoil surface attains sonic speed, and ends when the complete flow pattern is supersonic. The pressure coefficient corresponding to sonic speed on the airfoil is

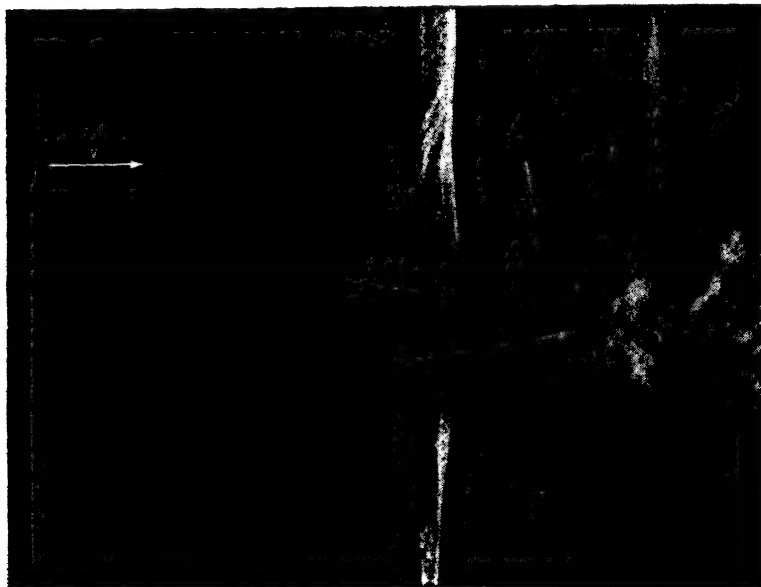


FIG. 8-10. Schlieren photograph of flow past a 12-per-cent-thick circular-arc airfoil at $M = 0.902$ and $\alpha = 0$. (Reproduced by permission from *Shock-wave Oscillations in Wind Tunnels*, by H. W. Liepmann and H. Ashkenas, JAS, May, 1947.)

called the *critical pressure coefficient*. The lowest remote Mach number for which sonic speed can be attained locally on the airfoil is called the *critical Mach number*.

While the critical Mach number is defined by the attainment of sonic speed somewhere on the airfoil, this may not actually correspond to any "critical" condition on the airfoil, except that it represents a limit below which no shock waves can occur. Local speeds greater than that of sound may, and frequently do, exist for a considerable distance along the surface of an airfoil; usually, however, the same difficulty is encountered as for the venturi tube

described in Art. 8-3. The after region of an airfoil, by its geometry, requires an expansion of stream tubes, which may produce supersonic velocities, dependent on the magnitude of the remote Mach number. The conversion of this very high speed air to the low speed necessary at the trailing edge produces a shock wave similar to that in the venturi tube. Unfortunately, the sudden rise in pressure frequently causes separation of the flow, and the two effects together lead to a general decay of the aerodynamic characteristics of the airfoil, as shown at about $M = 0.7$ in Fig. 8-4. No reliable theory has been advanced to predict the exact variation in airfoil characteristics caused by this *compressibility burble*; consequently, experimental evidence must be analyzed very carefully in order to extract the principal variables involved.¹

It has been found that the shock-wave formation at low Reynolds numbers, in which the flow is completely laminar, is considerably different from that at high Reynolds numbers, for which the flow is at least partly turbulent. The mutual interaction between shock waves, expansion waves, and the boundary layer is understood only in a qualitative way at present. Figure 8-10 shows a close-up of the shock-wave and boundary-layer formation on a circular-arc airfoil at high Mach number, and Fig. 8-11 shows a series of schlieren photographs of the flow pattern on an NACA 23015 airfoil at several Mach numbers.

The onset of compressibility burble is clearly shown in the above photographs, and is shown graphically in Fig. 8-12, where pressure coefficient is plotted for the NACA 4412 airfoil of Fig. 8-4. The sudden increase in pressure coefficient (positively) on the upper surface at about the 65 per cent chord is indicative of a relatively strong shock wave. The maximum negative pressure coefficient was considerably higher than the critical value, indicating a relatively high supersonic speed, and this speed persisted for a considerable portion of the airfoil upper surface.

The interpretation of the photographs and pressure distribution may be aided by reference to Fig. 8-13, where diagrams depict the flow over an airfoil for several Mach numbers. At $M = 0.7$, a small region of supersonic flow has formed on the airfoil upper surface. The rise in pressure upon passing through the shock wave is insufficient to cause flow separation; hence no appreciable changes in aerodynamic characteristics would be anticipated. At

¹ A good discussion is contained in *TM* 1113.

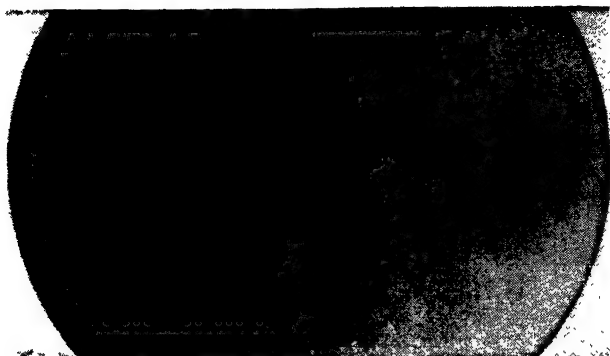
 $M = 0.400$  $M = 0.600$  $M = 0.700$

FIG. 8-11. Schlieren photographs of flow over an NACA 23015 airfoil at various Mach numbers. $\alpha = 3$ deg. (NACA photographs.)

 $M = 0.750$  $M = 0.800$  $M = 0.821$

FIG. 8-11. Schlieren photographs of flow over an NACA 23015 airfoil at various Mach numbers. $\alpha = 3$ deg. (NACA photographs.)

$M = 0.9$, the supersonic region is more extensive on the upper surface, and a small region appears on the lower surface. The upper-surface region not only is more extensive than at $M = 0.7$;

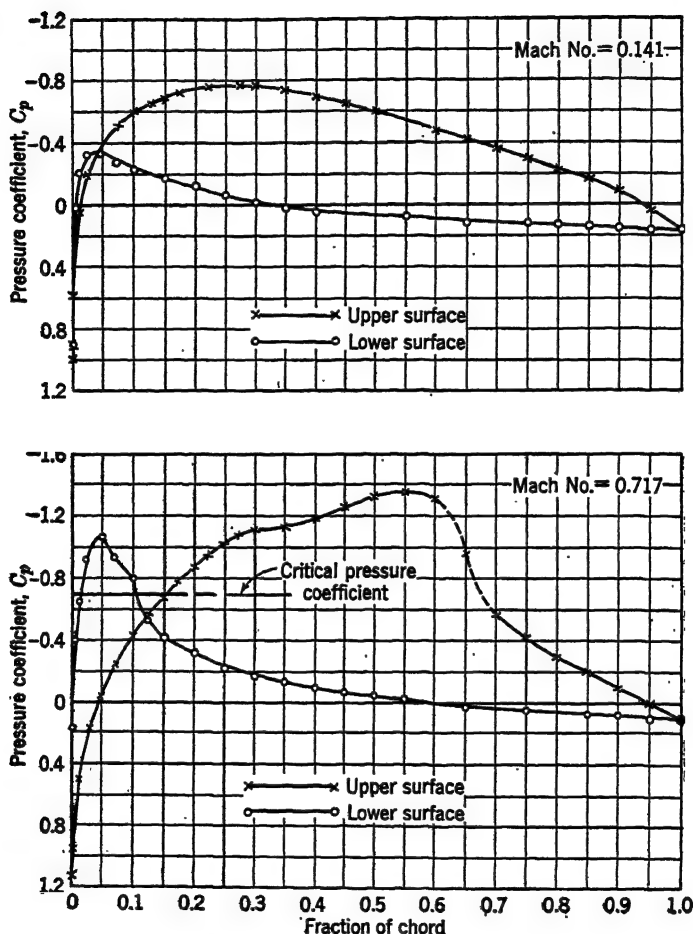


FIG. 8-12. Comparison of pressure coefficient at high and low Mach number on an NACA 4412 airfoil at $\alpha = -0.25$ deg. (From TR 646.)

it represents a higher supersonic velocity and thus a larger pressure rise through the shock wave, sufficient in this case to precipitate separation of the flow, with consequent increase in drag and reduction in lift. The diagrams for $M = 0.95$ and $M = 1.05$ are

somewhat similar, except that the latter shows a weak bow wave ahead of the leading edge, followed by a subsonic region, which in turn is followed by a supersonic region up to the shock wave. At $M = 1.3$ the bow wave approaches more closely to the leading edge, and the subsonic region shrinks. The position of the bow wave with respect to the leading edge and the extent of the sub-

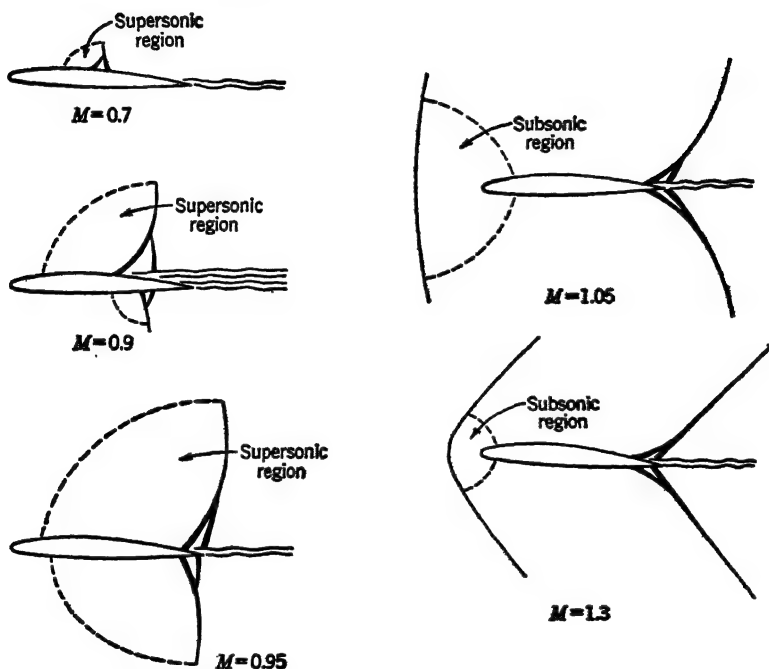


FIG. 8-13. Diagrammatic representation of transonic flow configurations for several Mach numbers. (From *NACA—University Conference on Aerodynamics. A compilation of papers presented, June 21 to 23, 1948.*)

sonic region depend upon the nose shape. For a sharp-edged nose, the bow wave may become attached to the leading edge, and the subsonic region may shrink to zero. The Mach number at which attachment occurs depends upon the wedge angle of the nose.

8-7 Three-dimensional Flow. The problems of three-dimensional flow are considerably more complex than those of two-dimensional flow, and solutions have been obtained for only a few special cases. In this article the results of some of these solutions will be presented. Before discussing three-dimensional flow prob-

lems it will be convenient to introduce a change in definitions of the transonic and supersonic flow regimes. The convention that the division between the transonic and supersonic regimes is defined by the attainment of a remote value of the Mach number equal to unity will be used here.

Subsonic Flow. In two dimensions the Prandtl-Glauert rule was used to predict high-speed airfoil-section characteristics from low-speed test data (Art. 8-4). Similarly, in three dimensions, equations will be shown for predicting high-speed wing characteristics from low-speed test data. The following discussions relate strictly to a thin wing at low angle of attack that has an elliptical plan form without sweepback.

At constant geometric angle of attack, the lift coefficient increases with increasing Mach number according to the following relation:

$$C_{LM} = C_L \left(\frac{m_0 + \pi A}{m_0 + \pi A \sqrt{1 - M^2}} \right) \quad (8-37)$$

where C_{LM} is lift coefficient at Mach number M , dimensionless

C_L is lift coefficient at zero Mach number, dimensionless

A is aspect ratio, dimensionless

M is Mach number, dimensionless

m_0 is slope of lift curve for infinite aspect ratio at $M = 0$, per radian

Correspondingly the slope of the lift curve increases according to

$$a_M = a \left(\frac{m_0 + \pi A}{m_0 + \pi A \sqrt{1 - M^2}} \right) \quad (8-38)$$

where a_M is slope of lift curve at Mach number M , per deg

a is slope of lift curve at zero Mach number, per deg

These equations were suggested by B. Göthert¹ for high aspect ratios (say, $A > 6$). For low aspect ratios the following equation, suggested by H. Multhopp, gives better correlation with available experimental results:

$$a_M = a \left(\frac{1 + \sqrt{1 + \frac{A^2}{4}}}{1 + \sqrt{1 + \frac{A^2}{4}} (1 - M^2)} \right) \quad (8-39)$$

¹ TM 1105.

Two important characteristics of these three equations should be observed. First, if the aspect ratio is infinite, these equations reduce to Eqs. (8-25) and (8-26). Second, if the aspect ratio is zero, there is no effect of compressibility; *i.e.*, the slope of the lift curve, for instance, does not change appreciably with increase in Mach number if the aspect ratio is very low.

The effect of increasing Mach number on profile drag coefficient C_{D_0} is obtained in exactly the same manner as in the two-dimensional case (Art. 8-4). The equation for induced drag coefficient is the same as for the incompressible case studied in Chap. 6.

$$C_{D_{iM}} = \frac{C_{L_M}^2}{\pi A} \quad (8-40)$$

The effect of increasing Mach number on pitching moment coefficient is obtained in exactly the same manner as the two-dimensional case (Art. 8-4).

Transonic Flow. The equations given in the preceding section for predicting compressibility effects in three-dimensional flow take no account of the fact that the aerodynamic properties of a wing decay considerably at a Mach number that is usually slightly higher than M_{cr} . It is important that the critical Mach number be as large as possible. In two dimensions the only variable that may be changed in order to increase M_{cr} is the airfoil section. Since M_{cr} is determined entirely by the magnitude of the maximum local velocity on the wing surface as compared with the remote velocity, it is apparent that the airfoil section should have a shape such that this ratio is as small as possible at the design lift coefficient of the wing. In three dimensions, aspect ratio and sweepback provide additional variables. (Effects of taper and washout are not considered here.)

In Fig. 8-14, changing aspect ratio is shown to be relatively ineffective unless the aspect ratio is less than about three or four. In order to appreciate the influence of sweepback, consider first a wing at positive angle of attack in an air stream. If the wing is moved parallel to its span then, except for end effects and for boundary-layer effects, which may be ignored temporarily, no change in the aerodynamic properties of the wing are to be expected. Notice, however, that the relative velocity is rotated from the direction it had when the wing was stationary.

The above reasoning may be extended to a wing with sweepback. Again the boundary layer and the flow at the tips and root are ignored. If the relative velocity is v , only the component $v \cos \Lambda$ perpendicular to the wing axis determines the aerodynamic characteristics of the wing. This implies that the critical Mach number of a wing with sweepback is increased over one without sweepback according to

$$M_{cr} = \frac{M'_{cr}}{\cos \Lambda} \quad (8-41)$$

where M_{cr} is critical Mach number of wing with sweepback Λ

M'_i is critical Mach number of the same wing without sweepback

Equation (8-41) gives a simple relation between the critical Mach

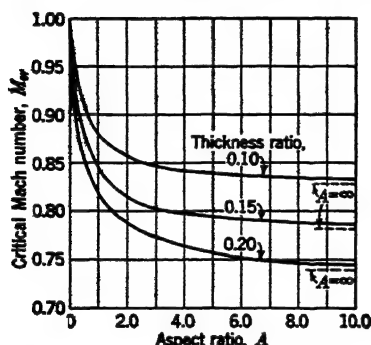


FIG. 8-14. Variation of critical Mach number with aspect ratio for ellipsoids of various thickness ratio. (From TN 1792.)

numbers for a swept and unswept wing. It is not too valuable, however, because first, the airfoil section is generally specified in a plane parallel to the remote-velocity vector rather than normal to the span; second, the flow over the root and tip section may not be analyzed by the reasoning leading to Eq. (8-41); third, the lift coefficient is by no means constant from root to tip; and fourth, there is usually a strong secondary flow from root to tip of the wing within the boundary layer. The net result of these effects is that the critical Mach number of the wing as a whole is determined by the attainment of sonic speed at some point whose spanwise and chordwise position depends upon the particular wing plan form and airfoil section considered. Sweepback is beneficial for increasing the critical Mach number, but Eq. (8-41) is entirely too optimistic for predicting the effect in three-dimensional flow.

Supersonic Flow. In this section the supersonic characteristics of some specific wing shapes will be discussed. These shapes have been investigated because the mathematical equations describing their geometry are very simple. Other more complicated shapes

have also been investigated but are not treated here because only the results can be shown, and the results shown here are sufficient to illustrate some of the more elementary principles involved.

Skin friction and form drag due to viscosity are ignored in the following discussions to simplify the presentation. Estimation of these viscous effects may be carried out as in the two-dimensional case; *i.e.*, the drag coefficient for unseparated subsonic flow at the same Reynolds number may be used in the absence of test data.

Consider an infinitely thin flat-plate wing with constant chord

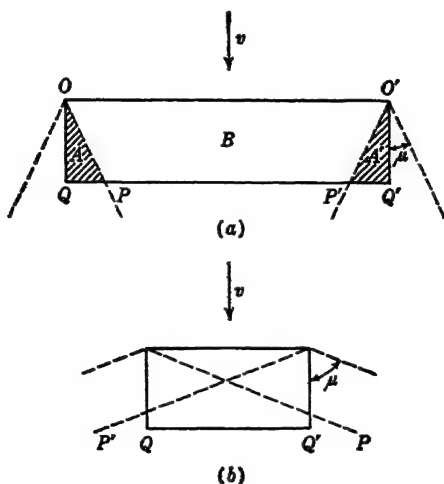


FIG. 8-15. Geometry of Mach cones at the tips of a rectangular wing: (a) high Mach number and high aspect ratio, (b) lower Mach number and lower aspect ratio.

and infinite span in a supersonic stream of air at low angle of attack. This is merely another way of considering two-dimensional flow, hence Eqs. (8-32), (8-33), and (8-36) apply for defining the lift, drag, and pitching moment coefficients, respectively.

For the same wing with finite aspect ratio, a Mach cone is formed at the leading edge of each wing tip, as shown in Fig. 8-15a. The regions *A*, *A'*, and *B* act as three separate lifting surfaces. The region *B* has section characteristics again defined by Eqs. (8-32), (8-33), and (8-36). The regions *A* and *A'* within the Mach cones have pressures that vary from a value along the line *OP* (or *O'P'*) that is equal to the pressure in the area *B*, to zero along the line *OQ* (or *O'Q'*). The exact variation of the pressure in these regions is

not important in this discussion,¹ but the over-all lift, drag, and pitching moment equations have particular interest. They are given as follows:

$$C_L = \frac{4\alpha}{\sqrt{M^2 - 1}} - \frac{2\alpha}{(M^2 - 1)A} \quad (8.42)$$

$$C_D = \frac{4\alpha^2}{\sqrt{M^2 - 1}} - \frac{2\alpha^2}{(M^2 - 1)A} \quad (8.43)$$

$$C_{m_{0.50}} = \frac{\alpha}{3(M^2 - 1)A} \quad (8.44)$$

where α is angle of attack in radians.

The drag coefficient given by Eq. (8.43) is obtained from $C_D = C_L\alpha$ for the same reason as in two-dimensional flow. [See discussion following Eq. (8.33).]

The influence of aspect ratio is contained in the second term of Eqs. (8.42) and (8.43). The drag coefficient may be expressed in terms of the lift coefficient by eliminating α between these two equations.

$$C_D = \frac{C_L^2 \sqrt{M^2 - 1}}{4[1 - 1/(2A\sqrt{M^2 - 1})]} \quad (8.45)$$

For a particular Mach number and aspect ratio the drag coefficient is seen to be parabolically related to the lift coefficient as in subsonic flow, but here the influence of aspect ratio does not appear in the simple form that it did for subsonic flow. For this reason induced drag in supersonic flow loses its significance as a separate entity. If the wing tips are cut off along OP and $O'P'$ so that none of the wing is contained within the Mach cone, and hence there are no induced effects, the wing acts as in two-dimensional flow and Eqs. (8.32), (8.33), and (8.36) apply.

The aerodynamic properties of a three-dimensional wing *due to angle of attack* have been presented. Further discussions will be concerned with a wing at zero angle of attack.

If a rectangular wing having finite thickness and infinite aspect ratio is considered, the drag coefficient at zero angle of attack for, say, a circular-arc airfoil section is given by Eq. (8.34). Surprisingly enough, this same equation applies even for finite aspect

¹ For a complete discussion see *TM 897* and *R&M 2001*, or Sibert, H. W., "High-speed Aerodynamics," Prentice-Hall, New York, 1948.

ratios provided that the points P and P' in Fig. 8-15a lie between Q and Q' . If P and P' lie outside QQ' , as in Fig. 8-15b, then the drag coefficient is less than that given by Eq. (8-34). This is shown graphically in Fig. 8-16.

One of the most important ways in which the drag coefficient of a wing in supersonic flow may be reduced is to employ sweepback. In order to simplify presentation and yet retain as many important variables as possible, consider a wing with a circular-arc airfoil section at zero angle of attack having sweepback Λ . The Mach cone arising from the center-line leading edge may be forward or aft of the wing leading edge (Fig. 8-17). The Mach cone arising from a wing-tip leading edge may or may not enclose part of the opposite wing tip. The three variables that determine the relation between the Mach cones and the geometry of the wing are the sweepback angle Λ , the aspect ratio A , and the Mach number M . The equations relating the drag coefficient to these three variables are very complicated, but the results are shown parametrically in Fig. 8-17. In

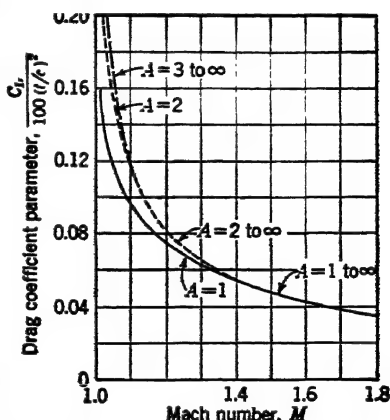


FIG. 8-16. Generalized curves for determining variations of wave drag coefficient with Mach number for rectangular wing. Circular-arc airfoil at zero lift.

(NOTE: For $A > 1$, $M > 1.8$: $\frac{C_D}{100(t/c)^2} = \frac{16}{300\sqrt{M^2 - 1}}$.) (From TN 1449.)

order to appreciate immediately the significance of these curves, consider a wing that has a 45 deg sweepback angle and a 10 per cent thick circular-arc airfoil section. Figure 8-17 then reduces to a plot of C_D vs. $\sqrt{M^2 - 1}$ for various values of A . Now if the Mach angle is also 45 deg, then from Eq. (8-31), $M = \sqrt{2}$, or $\sqrt{M^2 - 1} = 1$. For $\sqrt{M^2 - 1} < 1$, then, the Mach wave arising from the center-line leading edge is forward of the wing leading edge, while for $\sqrt{M^2 - 1} > 1$, the Mach wave is aft of the wing leading edge. The curves show that for all aspect ratios the highest drag coefficient is attained when the Mach wave is coincident with the wing leading edge.

An example of the use of Fig. 8-17 is given in Fig. 8-18, where curves of drag coefficient vs. Mach number for several angles of sweepback are shown. It can be seen that sweepback is beneficial only if the sweepback angle Λ is somewhat greater than the complement of the Mach angle μ . (For the data contained in these two figures, the airfoil section in the direction of the remote velocity was held constant for all Λ .)

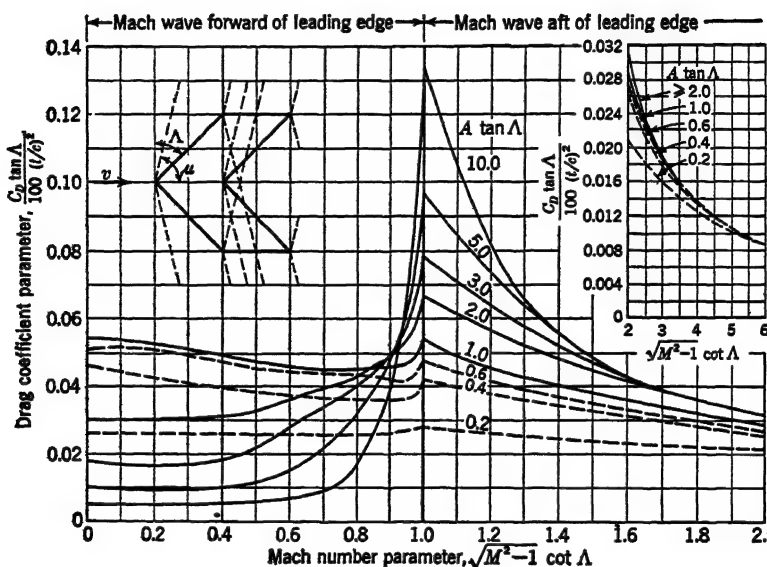


FIG. 8-17. Generalized curves for determining variation of wave drag coefficient with Mach number for untapered swept-back wing. Circular-arc airfoil at zero lift. Λ = sweepback angle, $\mu = \sin^{-1} \frac{1}{M} = \cot^{-1} \sqrt{M^2 - 1}$ = Mach angle. (From TN 1449.)

8-8 Practical Aspects of High-speed Flight. The critical Mach number of an airfoil to be used for high subsonic speeds must be known, in order to anticipate the decay of its aerodynamic properties. Unfortunately, two of the geometric properties of an airfoil that are desirable from a low-speed standpoint, namely, moderate thickness and camber, are undesirable at high speed because they decrease the critical Mach number of the section. Fortunately, the thickness *distribution* that is desirable for low-drag airfoils is also desirable for high-speed airfoils, because of the low peak pressure for a particular lift coefficient (see again Fig.

3-6). The wing that gives the highest critical Mach number should therefore be thin, have camber and thickness distributed¹ to produce a flat pressure curve, and have considerable sweepback. This, of course, assumes no auxiliary means are used to prevent compressibility burble, and also assumes that high speed is one of the primary considerations on the airplane.

The wing is not alone in its compressibility phenomena. The same kind of flow distortions occur on any body at some subsonic speed. The fuselage should generally be long and slender, in order to give a high critical Mach number; otherwise the pains taken to produce a satisfactory wing are at least partly nullified. Any major protuberance or irregularity on the fuselage or wing surface is likely to cause burbling, and hence must be carefully designed or removed. The practical aspect of designing an airplane to operate at very high speed becomes very acute, primarily because the aerodynamic requirement of extreme slenderness and wing sweepback reduces the rigidity of the airplane and makes structural design increasingly difficult.

In Fig. 8-19, polar curves are shown for a typical high-speed, single-engined airplane for several Mach numbers. The drastic change in characteristics at high Mach number is clearly shown. For a particular airplane in level flight at a given altitude, the C_L and Mach number are automatically specified by the velocity. The lowest dotted curve is for an airplane having wing loading $l_w = 40$ psf and gross weight $W = 9000$ lb at sea level. The middle dotted curve is for 25,000 ft, and the upper one is for 50,000 ft. All three curves at high lift coefficient become coincident with the curve for $M = 0.298$. These curves will be used in Chap. 14, where performance of a high-speed airplane with turbo-jet is discussed.

In subsequent chapters all effects of Reynolds number and Mach number on aerodynamic coefficient will be ignored unless

¹ These influences are treated in more detail in Art. 9-13.

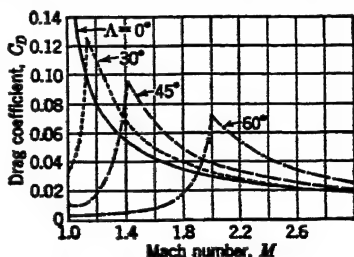


FIG. 8-18. Effect of Mach number on wave drag coefficient for untapered sweptback wing. Ten per cent thick circular-arc airfoil at zero lift. $A = 5.0$. (From Fig. 8-17.)

otherwise specified. This leads to tremendous simplification of the problems discussed, and of course in some cases is entirely

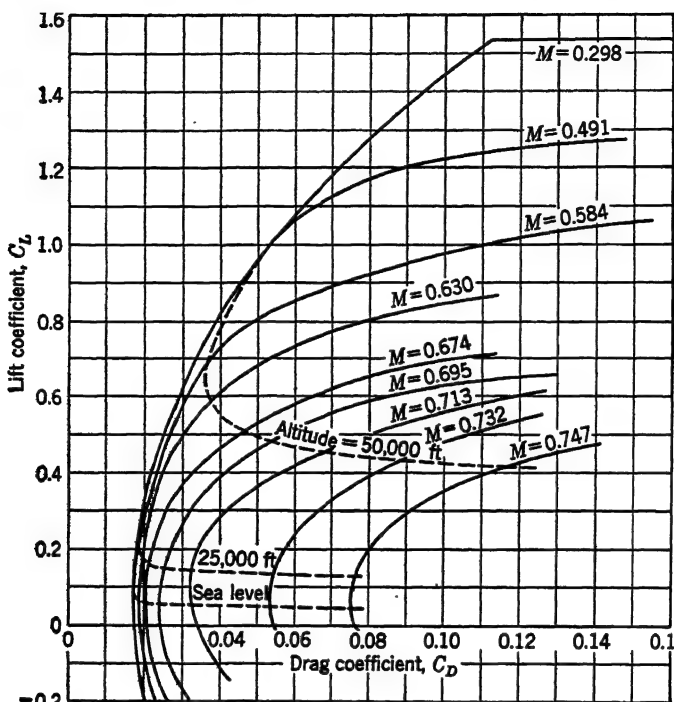


FIG. 8-19. Aerodynamic characteristics of a typical high-speed, single-engined airplane. (Modified from data contained in *WR A-90*.)

unjustified. It is important to be constantly aware of these approximations in the following chapters.

PROBLEMS

8-1. A pitot tube is installed in a high-speed (subsonic) wind tunnel, and has its two leads connected to a vertical U-tube mercury manometer. Test-section temperature $t = 50$ F; pressure $p = 14.9$ psi. Outside conditions are standard. What height h of mercury (ft) corresponds to a test-section velocity of 525 mph?

8-2. Estimate the lift coefficient at $\alpha = -0.25$ for an NACA 4412 airfoil at $M = 0.141$ and $M = 0.717$, using Fig. 8-12, and verify the answers on Fig. 8-4. Notice that the curves shown on Fig. 8-4 are results of force measurements; hence the correlation will not be precise.

8.3. Estimate the moment coefficient about the 25 per cent chord $c_{m_{0.25}}$ at $\alpha = -0.25$ for an NACA 4412 airfoil at $M = 0.141$ and $M = 0.717$, using Fig. 8.12, and verify the answers on Fig. 8.4. **HINT:** Go through an analysis similar to that used to obtain Eq. (8.24). A new set of curves must be plotted for graphical integration, whose coordinates are dictated by the form of the integral obtained.

8.4. Plot curves of c_l , c_d , and $c_{m_{0.25}}$ vs. Mach number from $M = 0$ to $M = 8$ for the symmetrical diamond-shaped airfoil shown in Fig. 8.9 at $\alpha = 4$ deg. Make the following assumptions:

1. At $M = 0$, $dc_l/d\alpha = 0.087$ per deg; $c_d = 0.0350$.
2. The transonic region is from $M = 0.7$ to $M = 1.3$.
3. At $M < 0.7$ the data shown in Fig. 9.12 may be used for estimating the effect of thickness on c_d .
4. At $M > 1.3$, the data from Fig. 8.9 may be used.
5. Reynolds number effects may be ignored at all Mach numbers.

8.5. Show analytically that each of the dotted lines on Fig. 8.19 corresponds to a constant value of $M^2 C_L$.

CHAPTER 9

THE OPTIMUM AIRFOIL

The choice of airfoil section depends upon the type of airplane for which it is to be used. Structural and aerodynamic considerations are often of equal weight. In this chapter some important aerodynamic characteristics of airfoils will be discussed, with a view to deciding their relative importance on the airplane.

Experimental data obtained from the various government, commercial, and collegiate laboratories show some lack of correlation, dependent upon the amount of inherent tunnel stream turbulence, and waviness or roughness of the model surface, and also dependent upon whether the section data were reduced from three-dimensional or two-dimensional tests and whether force or pressure tests were used. This does not destroy the value of the experiments but does restrict accurate comparison of data to a particular tunnel in which turbulence and airfoil surface conditions were closely controlled and duplicated between airfoils.

9-1 Historical Sketch.¹ Prior to extensive investigation of low-drag airfoils, section data were reduced from force tests on rectangular wings by means of theoretical and empirical equations (*e.g.*, see the equations under Table III, Appendix A). Most airfoil tests by the NACA were run in the variable-density tunnel (VDT), in order to secure large Reynolds numbers. Unfortunately, this tunnel had excessive turbulence ($TF = 2.65$), and the resulting data were subject to some question. With the advent of extensive use of the pressure technique for obtaining c_l by integration around the airfoil² and c_{a_0} by integration within the downstream wake, new possibilities for more accurate testing with high Reynolds number and low stream turbulence were opened up. Accordingly, the NACA constructed the two-dimensional low-

¹ Most of the statements contained in Art. 9-1 are based on information in *WR L-560*.

² Integration of pressures on the floor and ceiling of the test section, in two-dimensional tunnels, is also used to obtain c_l .

turbulence tunnel (LTT) and the two-dimensional low-turbulence pressure tunnel (TDT), in each of which the airfoil completely spans the narrow but high test section. In these tunnels the fundamental characteristics of some of the four- and five-digit airfoils were reinvestigated, and a thorough program was begun to determine the properties of the newer low-drag sections. From these tests the effects of stream turbulence and airfoil surface roughness were shown to have a profound influence on the aero-

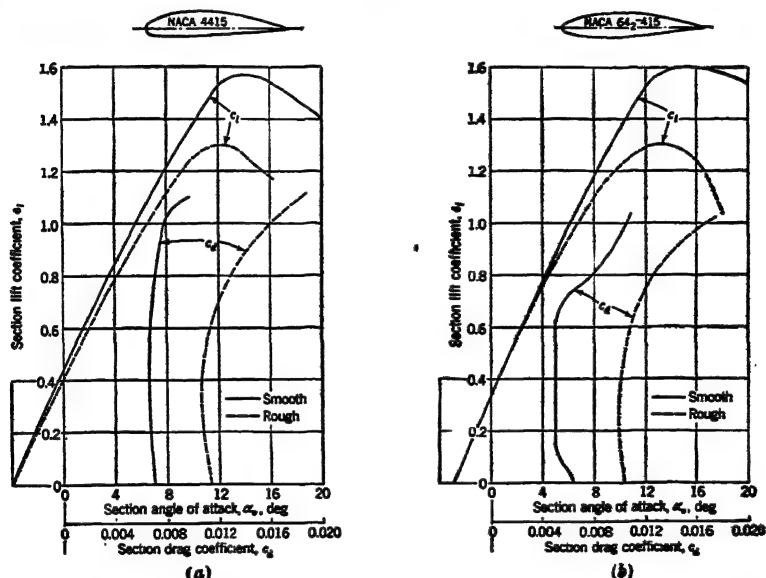


FIG. 9-1. Comparison of the effect of surface roughness on: (a) NACA 4415 airfoil, and (b) an NACA 642-415 airfoil. $R \approx 6 \times 10^6$. (From *WE L-560*.)

dynamic characteristics; increase in either variable was found to produce transition closer to the wing leading edge, which caused an increase in drag and a modification to the magnitude and severity of the peak of the lift curve. The stream turbulence in a practical wing could arise, for instance, from the slip stream of a propeller, while surface roughness could arise from any number of sources. Although indentations like scratches were found to be not too important, any protuberance, even in the form of dust particles, could be sufficiently large, compared to the local boundary-layer thickness, to produce premature transition. The most critical region for the protuberances is the wing leading edge, because the

laminar boundary layer is very thin and, of course, transition here subjects a considerable portion of the wing to turbulent flow. Roughness fairly widely scattered on the wing leading edge was found to produce flow over the entire wing that was largely turbulent, because each projection produced a disturbed region that spread laterally and overlapped the region arising from an adjacent projection.

The low drag coefficients obtained under ideal conditions are therefore not generally obtainable on a conventional airplane because of vibration, propeller wake, dust, etc., and because of limitations imposed by methods of construction. It is only by extreme care in design, construction, and maintenance that full value may be realized from the low-drag sections. In Fig. 9-1 the *percentage change* in characteristics due to roughness is seen to be much more for the low-drag airfoil than for the conventional four-digit airfoil. It should be noted that the amount of roughness used in these tests was unusually large.

9-2 Airfoil Geometry. In Chap. 3 the code used by the NACA for designation of its various airfoil sections was briefly discussed. An additional description of the geometry of airfoils is now in order, as a prelude to comparison of airfoil sections from an aerodynamic standpoint.

According to the Bernoulli equation, the pressure coefficient at any point on an airfoil in incompressible flow is dependent upon the square of the velocity at that point:

$$C_p = 1 - \left(\frac{v}{v_0} \right)^2 \quad (9-1)$$

where v is surface velocity, fps

v_0 is remote velocity, fps

The velocity is assumed to be composed of three independent components:

1. The velocity induced by the thickness of the basic symmetrical airfoil at zero angle of attack, Δv_t
2. The velocity corresponding to the shape of the mean line, Δv_c
3. The velocity corresponding to the change in angle of attack, Δv_a

Fortunately, theoretical and empirical methods are available for predicting each of the three components, so that they may be

added algebraically to obtain the total velocity. The static-pressure distribution is therefore immediately predictable for any arbitrary airfoil at an arbitrary angle of attack. Although this text is not concerned with the methods by which the velocities are established, the results are of considerable interest. Figure 9-2a,

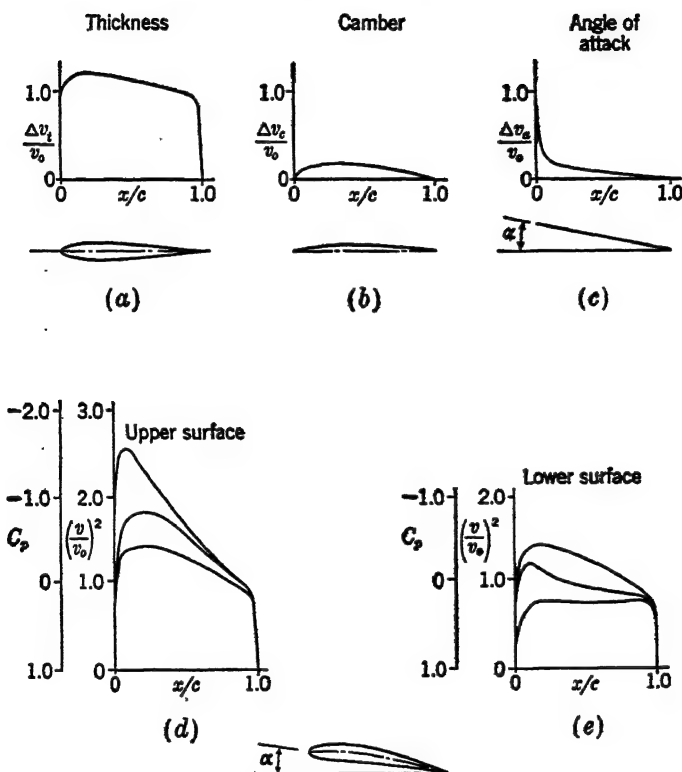


FIG. 9-2. Synthesis of airfoil pressure distribution.

shows a nondimensional curve of velocity induced by airfoil thickness; Fig. 9-2b shows that arising from camber, and Fig. 9-2c shows that arising from positive angle of attack. In Fig. 9-2d, the lower curve shows the square of the velocity ratio from Fig. 9-2a; *i.e.*, it represents the square of the velocity ratio on the upper surface of a symmetrical airfoil at zero angle of attack. The middle curve is obtained from the square of the sum of the ordinates from Figs. 9-2a and b; *i.e.*, it represents the square of the

velocity ratio on the upper surface of a cambered airfoil at zero angle of attack. The upper curve is obtained from the square of the sum of the ordinates from Figs. 9·2a, b, and c; *i.e.*, it represents the square of the velocity ratio on the upper surface of a cambered airfoil at positive angles of attack. Using Eq. (9·1), the pressure coefficient corresponding to the square of the velocity ratio is also shown. Figure 9·2e is similar to Fig. 9·2d but shows curves for the lower surface of the airfoil. Whereas the velocity on the upper airfoil surface is increased by camber and positive angle of attack, it is decreased on the lower surface; thus, for instance, the lower curve in Fig. 9·2e corresponds to the upper curve in Fig. 9·2d.

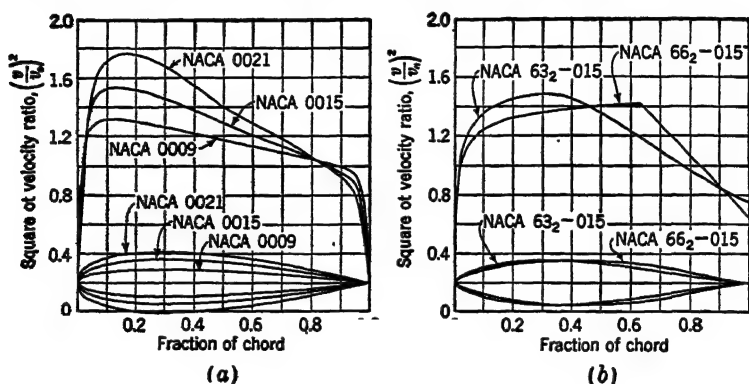


FIG. 9-3. Effect on velocity gradient of: (a) amount of thickness, and (b) position of maximum thickness for some NACA airfoils. (From *WR L-560*.)

The effect of amount of thickness and position of maximum thickness, for actual airfoils, is shown in Figs. 9·3a and b, respectively. The trends shown in these two graphs are characteristic of all airfoils.

The camber of a four- or five-digit airfoil is specified rather arbitrarily by simple mathematical equations. The amount of camber and the position of maximum camber are then described by the first and second digit as shown in Chap. 3. In the low-drag series of airfoils, the *position of maximum camber* is specified indirectly by the shape of the pressure distribution it produces. In Fig. 9·4, mean lines are shown for three values of this *loading factor* α . Each mean line is adjusted to give exactly $c_l = 1.0$. (The amount of camber shown is unusually high: the lift coefficient of unity is chosen only as a convenient reference.) The algebraic

difference between pressure coefficients from the upper and lower surfaces is shown on the same diagram. Obviously, integration of each pressure curve by Eq. (8.24) must give $c_l = 1.0$. The amount of camber is specified indirectly by a design lift coefficient;

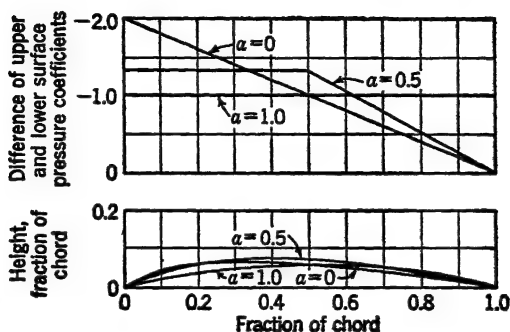


FIG. 9-4. Mean lines for various loading factors to produce $c_l = 1.0$, with the corresponding algebraic difference of pressure coefficients from the upper and lower surfaces. (From WR L-560.)

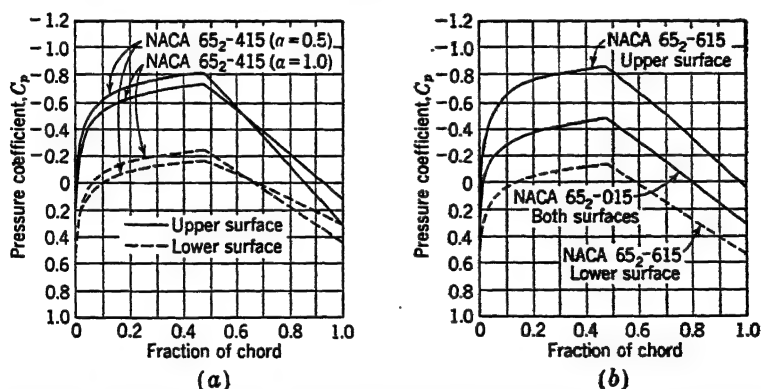


FIG. 9-5. Upper and lower surface pressure coefficients for: (a) two loading factors, and (b) two different amounts of camber, for some low-drag airfoil sections. All curves correspond to the design lift coefficient. (From WR L-560.)

also called *ideal lift coefficient*. The design lift coefficient of all the airfoils shown in Fig. 9-4 is 1.0. If the ordinates of the mean line were reduced to half, the design lift coefficient would be 0.5, etc. By these indirect procedures, the shape of the mean line is given aerodynamic rather than geometric significance. Figure 9-5 shows, for several low-drag airfoil sections, the influence on the

upper- and lower-surface pressure coefficients of changes in the loading factor and the design lift coefficient.

Combining the thickness distribution with the mean line dictates the geometric form of an airfoil. The whole purpose of the low-drag series of airfoils is to produce a favorable pressure gradient over a major portion of the airfoil surface in order to promote laminar flow. This is very simple to obtain *for the design lift coefficient* as shown in Fig. 9-5b. Changes in angle of attack, however, modify the pressure distribution, and at some angle of attack the favorable pressure distribution on one or the other sur-

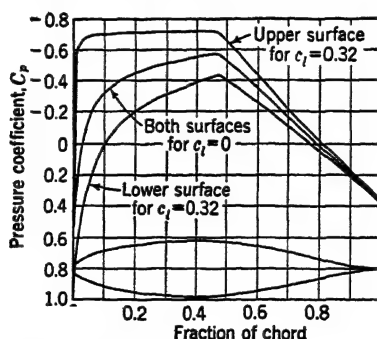


FIG. 9-6. Upper and lower surface pressure coefficients for $c_l = 0$ and $c_l = 0.32$ for an NACA 653-018 airfoil section. (From *WR L-560*.)

face will become unfavorable. In Fig. 9-6 a symmetrical low-drag airfoil is depicted that has a favorable pressure gradient to about the 50 per cent chord at zero lift coefficient, but when the angle of attack is increased to $c_l = 0.32$, the upper surface develops a pressure gradient that is just barely favorable. Further increase in angle of attack would cause a slightly unfavorable gradient and promote transition to turbulent flow. This is verified in Fig. 9-7, where the same airfoil is shown to have a low drag coefficient in the range of approximately $c_l = \pm 0.32$ that increases drastically outside this region because of the onset of turbulent flow. The same basic airfoil section cambered to a design lift coefficient of $c_l = 0.6$ is also shown, and the same conclusions may be drawn regarding the shape of its pressure distribution curves and type of flow.

With these general remarks about the geometry of the low-drag series of airfoils, attention may be turned to the influence of some

important aerodynamic properties of the airfoil on performance and stability of a complete airplane.

In the following discussions, section characteristics will be referred to almost exclusively, because it is on this basis that the more recent data are compared; however, the general statements made about section characteristics also apply to infinite-aspect-ratio characteristics, because the difference between them is usually very small. The four- and five-digit airfoils were not

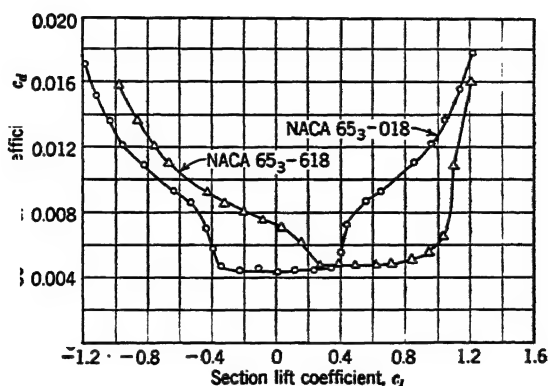


FIG. 9-7. Polar curves for two low-drag airfoils of different camber. $R \approx 6 \times 10^6$. (From *WR L-560*.)

developed on a theoretical basis as were the low-drag sections, but the effects of camber and thickness are illustrated as well by one series as another.

All discussions will be concerned with subsonic speeds below the critical Mach number, unless otherwise specified.

9-3 Angle of Zero Lift, α_{l_0} . The angle of zero lift is defined by the attitude of the chord line when the airfoil has no lift. It has no significance in choice of an airfoil, because it merely indicates that the lift curve is shifted one way or the other. The only effect of a difference in the angle of zero lift of two airfoils is that it requires a difference in incidence on the airplane.

Angle of zero lift is almost completely independent of thickness and Reynolds number but becomes more negative with increasing camber, as shown in Figs. 9-8a and 9-9, and usually becomes more positive with increasing Mach number.

9-4 Lift-curve Slope, $dc_l/d\alpha$. There is very little difference in lift-curve slope among various airfoils having the same aspect ratio (Figs. 9-8a and 9-10), but small differences are important in two respects. First, vertical gusts cause a sudden increase in angle of attack and thereby cause a sudden change in wing lift

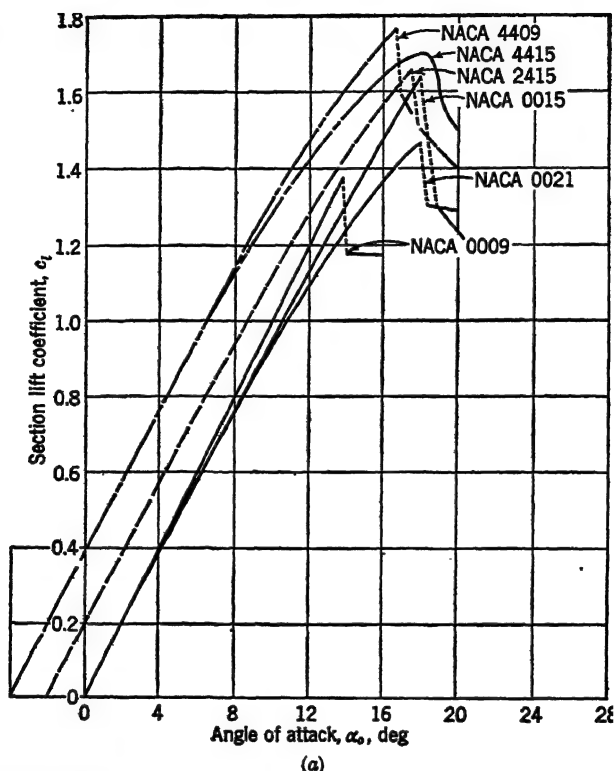
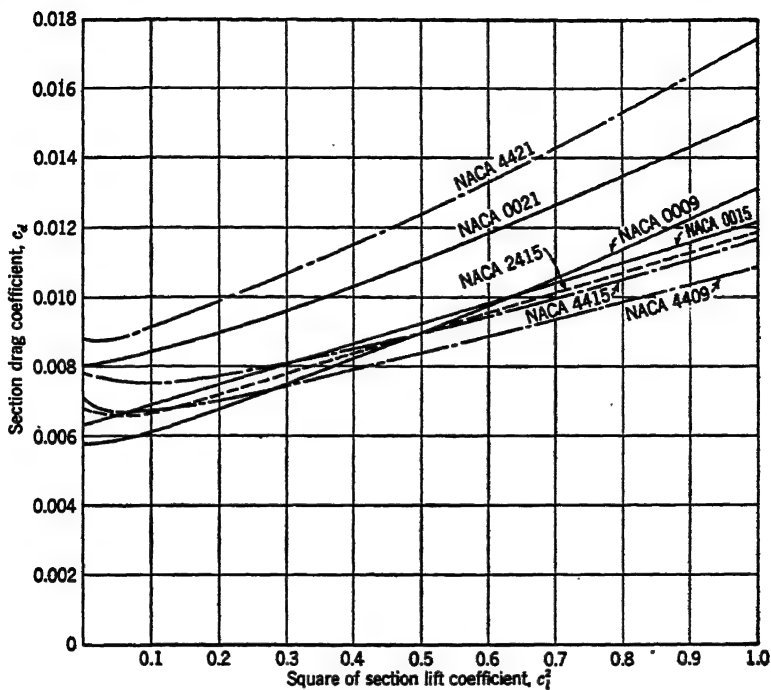


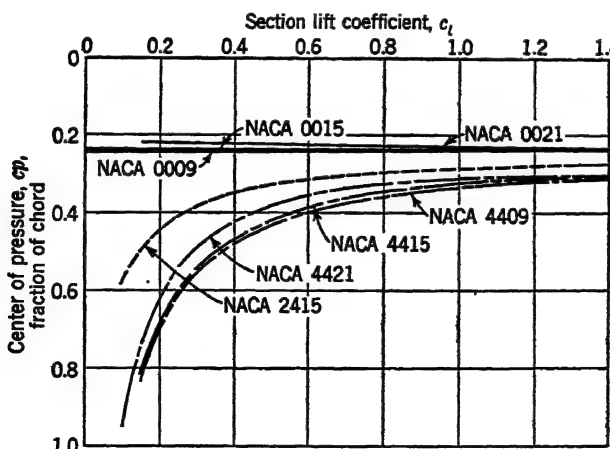
FIG. 9-8. Aerodynamic characteristics of some four-digit airfoils. $R \approx 8 \times 10^6$. (From TR 669.)

that depends upon $dc_l/d\alpha$; hence a large $dc_l/d\alpha$ produces large gust loads on the wing. Second, the longitudinal stability of an airplane will later be shown to depend directly on the section tail lift-curve slope, and inversely on the section wing lift-curve slope.

The theoretical slope of the lift curve is frequently defined as 2π per radian. Using this slope, the *airfoil efficiency factor*, $m_0/2\pi$, is sometimes used as a means for comparing lift-curve slopes between various airfoils. The slope of the lift curve is 2π



(b)



(c)

FIG. 9-8. Aerodynamic characteristics of some four-digit airfoils. $R \approx 8 \times 10^6$. (From TR 669.)

per radian only for an airfoil having zero thickness, however, and it increases for thicker sections as may be seen in Fig. 9-10. Pinkerton¹ has pointed out that the theoretical value is not realized on an actual airfoil, primarily because the difference in

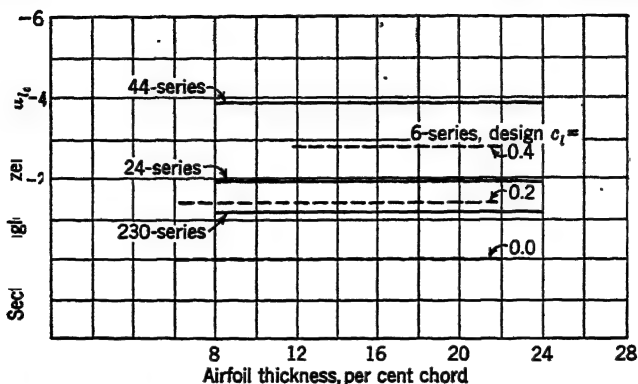


FIG. 9-9. Variation of section angle of zero lift with thickness for four-digit, five-digit, and 6-series airfoils. $R \approx 6 \times 10^6$. (Averaged data from WR L-560.)

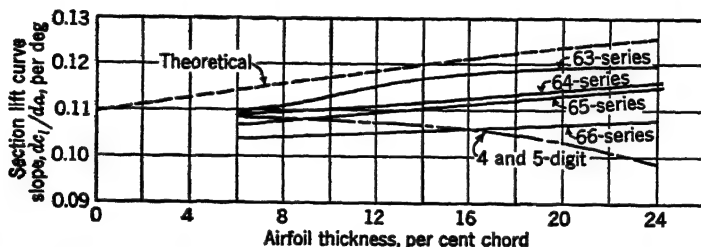


FIG. 9-10. Variation of section lift-curve slope with thickness for four-digit, five-digit, and 6-series airfoils. The theoretical curve is not unique. Actually, each airfoil has a corresponding theoretical curve, but the one shown is representative of most conventional airfoils. It corresponds to the *Joukowski* airfoil, which has considerable mathematical significance in aerodynamic theory. $R \approx 6 \times 10^6$. (Experimental data averaged from WR L-560.)

thickness of the boundary layer on the upper and lower airfoil surfaces causes an effective reflexing of the airfoil that increases with increase in angle of attack. This partially explains the difference in slopes of the various airfoils depicted in Fig. 9-10.

There is a negligible scale effect on $dc_l/d\alpha$, but in general an increase in Mach number gives an increase in lift-curve slope [see Eq. (8-26)].

9-5 Maximum Lift Coefficient, $c_{l_{max}}$. In landing an airplane, the ground speed must be kept as low as possible. Since ground

¹ TR 563.

speed is determined by air speed, the maximum lift coefficient of the wing should be as high as practicable in order to attain a low landing speed. From another point of view, it should be as large as practicable, in order to have the smallest wing area for a chosen acceptable landing speed.

The effect of thickness and camber on $c_{l_{\max}}$ is considerable. A very thin symmetrical airfoil has such a small radius of curvature at the leading edge that it promotes premature leading-edge separation. This effect is considerably reduced if the airfoil is sufficiently cambered. A very thick symmetrical airfoil has such a large adverse pressure gradient on the after portion of the upper surface that separation again occurs prematurely, but here the separation first occurs close to the trailing edge. These effects are shown in Fig. 9-8a and 9-11.

Some airfoils have a large value of $c_{l_{\max}}$, but the curve of c_l vs. α has a sharp peak or even a sudden break (Fig. 9-8a). If all other characteristics are comparable, the airfoil with a gradual stall is more desirable, because it gives warning to the pilot; however, even the sudden break can be acceptable because the wing may be designed so that stalling takes place gradually from root to tip by using a rectangular wing, using washout, etc.

Most wings have auxiliary means by which the lift coefficient may be increased for landing. These devices (slots and flaps) will be discussed at length in Chap. 10. The lift coefficient may also be increased slightly by landing with power supplied to the propellers. In any of these assisting procedures, the magnitude of the maximum lift coefficient depends upon the basic value for the wing by itself.

The change in $c_{l_{\max}}$ with Reynolds number is considerable, and the spanwise variation in Reynolds number caused by variation in chord of a tapered or elliptical wing generally tends to aggravate any tip-stalling tendencies, because of the low Reynolds number associated with the small tip chord.

9-6 Minimum Drag Coefficient, $c_{d_{\min}}$. For an average clean¹ airplane at low lift coefficient, the wing accounts for one-quarter to one-third of the total drag coefficient (at low C_L the C_{D_i} is very small). The advantages arising from reduction in c_{d_0} are therefore self-evident. The principal cause of differences among airfoils in this respect is section thickness and thickness distribution. Increasing the former causes differences in skin friction and form

¹ An airplane that is smoothly streamlined is called aerodynamically "clean."

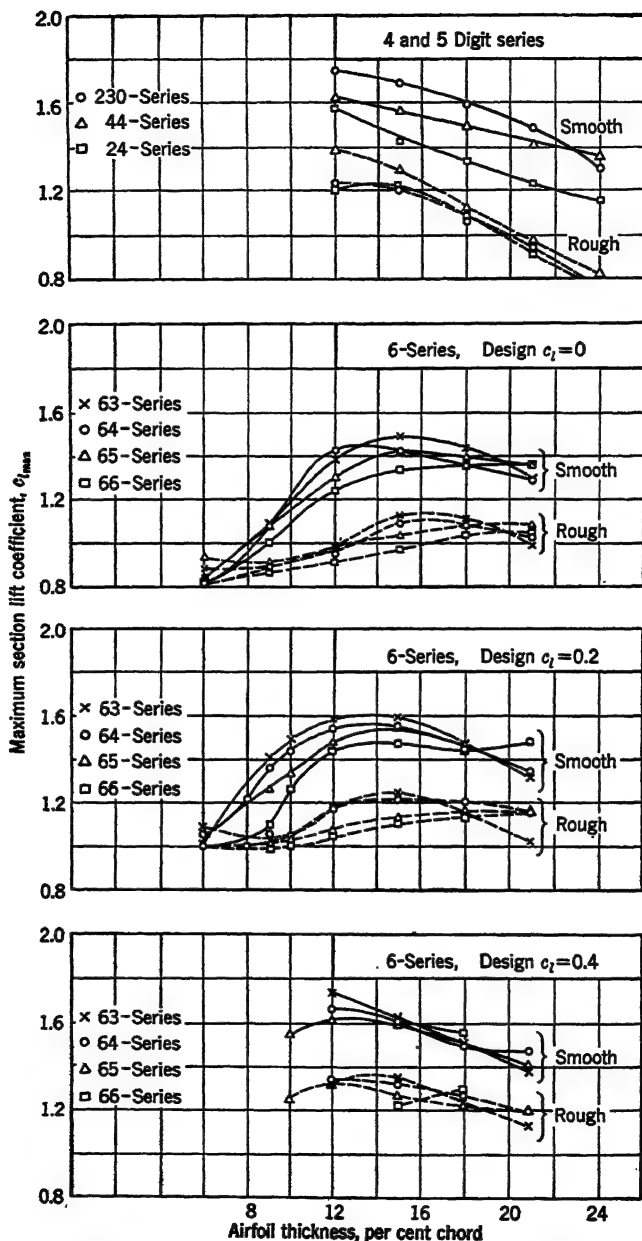


FIG. 9-11. Variation of section maximum lift coefficient with thickness for four-digit, five-digit, and 6-series airfoils. $R \approx 6 \times 10^6$. (From WR L-560.)

drag, by increasing the wetted surface and average velocity over the airfoil and by giving more cross-sectional area on which the static-pressure differential may act. Changing the latter causes differences in skin friction by modifying the pressure distribution and hence shifting the transition point (Figs. 9-8b and 9-12).

Changing thickness also causes changes in the critical Reynolds number and critical Mach number, as shown in Chaps. 7 and 8 (see also Art. 9-13).

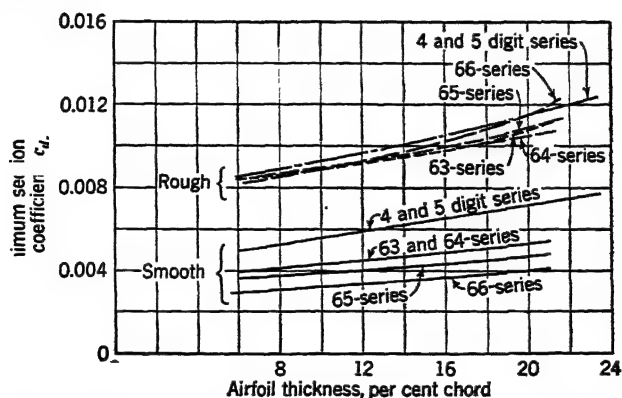


FIG. 9-12. Variation of minimum section drag coefficient with thickness for four-digit, five-digit, and six-series airfoils. $R \approx 6 \times 10^6$. (Averaged data from WR L-560.)

9-7 Section Drag-curve Shape. The shape of the drag curve for the older test data on four- and five-digit airfoils is given by dc_{d_0}/dc_t^2 , because these airfoils have drag curves that are essentially parabolic. Very thin sections that have sharp leading edges tend to give premature transition and separation, while very thick sections tend to give premature separation; hence, an average thickness (12 to 15 per cent) tends to give the minimum slope (Fig. 9-8b).

For the newer low-drag sections, the drag curve is characterized by a "bucket" of reduced drag coefficient corresponding to the region of favorable pressure gradient on both airfoil surfaces (Fig. 9-7). The slope dc_{d_0}/dc_t^2 loses most of its significance unless applied to small portions of the curve. The position and extent of the bucket is always indicated approximately by the code-number designation of the airfoil, so there is no point in making comments beyond those contained in Art. 9-2 except to state that, in general, thin airfoils have narrow buckets and thick airfoils have

wide ones. Experimental data show that the depth and width of the bucket are both dependent on Reynolds number.

9.8 Maximum Ratio of Lift to Drag, $(L/D)_{\max}$. The $(L/D)_{\max}$ for a flying wing determines its minimum glide angle, as shown in Art. 5.4. It also determines the minimum glide angle of a complete airplane, but the C_L corresponding to $(L/D)_{\max}$ is usually higher for the airplane than for the wing alone, and the $(L/D)_{\max}$ itself is always less (Fig. 9.13).

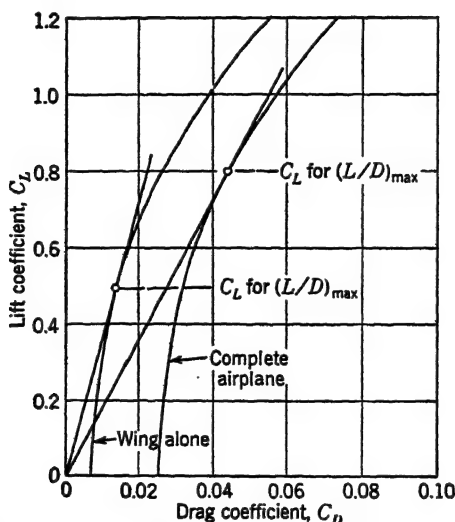


FIG. 9.13. Comparison of $(L/D)_{\max}$, and C_L for $(L/D)_{\max}$, for a wing alone and for a complete airplane.

A high $(L/D)_{\max}$ not only is desirable from a gliding standpoint but is also one of the chief factors in determining the maximum *range* (miles per gallon of fuel) of a conventional airplane and the maximum *endurance* (hours per gallon of fuel) of a jet airplane. The effect of aspect ratio on $(L/D)_{\max}$ is considerable, and this accounts for the high-aspect-ratio wings that are characteristic of gliders and long-range airplanes.

The polar curve of an airplane may be represented by the parabolic equation given in Art. 6.7:

$$C_D = C_{D_{\min}} + \frac{C_L^2}{\pi A e} \quad (9.2)$$

The drag coefficient corresponding to $(L/D)_{\max}$ may then be shown to be twice $C_{D_{p_{\min}}}$ (see Prob. 9-1); hence, at $(L/D)_{\max}$

$$C_D = 2C_{D_{p_{\min}}} \quad (9-3)$$

Combining Eqs. (9-3) and (9-2) gives the lift coefficient for $(L/D)_{\max}$:

$$C_L = \sqrt{C_{D_{p_{\min}}} \pi A e} \quad (9-4)$$

Dividing Eq. (9-4) by Eq. (9-3) gives

$$\left(\frac{L}{D}\right)_{\max} = \frac{C_L}{C_D} = \sqrt{4C_{D_{p_{\min}}}} \quad (9-5)$$

The influence of aspect ratio and minimum parasite drag coefficient on $(L/D)_{\max}$ is clearly shown by Eq. (9-5). The magnitude of both variables, in addition to the efficiency factor e , is largely controlled by the characteristics of the wing of the airplane.

9-9 Maximum Ratio of C_L^2/C_D , $(C_L^2/C_D)_{\max}$. The importance of $(C_L^2/C_D)_{\max}$ is not readily apparent but will later be shown to correspond to the minimum *sinking speed* (vertical rate of descent) and to the maximum *endurance* (time aloft per gallon of fuel) of a conventional airplane. Neither of these performance characteristics has great commercial importance.

If the airplane polar curve is again represented by Eq. (9-2), the drag coefficient corresponding to $(C_L^2/C_D)_{\max}$ may be shown to be four times as large as $C_{D_{p_{\min}}}$; hence

$$C_D = 4C_{D_{p_{\min}}} \quad (9-6)$$

Combining Eqs. (9-6) and (9-2) gives the lift coefficient for $(C_L^2/C_D)_{\max}$:

$$C_L = \sqrt{3\pi A e C_{D_{p_{\min}}}} \quad (9-7)$$

The actual ratio is seldom used and will not be developed here, but the same general requirements are favorable as for $(L/D)_{\max}$, namely, large aspect ratio and low $C_{D_{p_{\min}}}$.

9-10 Maximum Ratio of C_L^2/C_D , $(C_L^2/C_D)_{\max}$. The ratio $(C_L^2/C_D)_{\max}$ will be shown later to correspond to the condition of maximum *range* of a jet-propelled airplane. From the same assumptions as in Arts. 9-8 and 9-9, the drag coefficient corresponding to $(C_L^2/C_D)_{\max}$ may be shown to be related to $C_{D_{p_{\min}}}$ as follows:

$$C_D = \frac{4}{3}C_{D_{p_{\min}}} \quad (9-8)$$

and the corresponding lift coefficient is given by

$$C_L = \sqrt{\frac{1}{3} C_{D_{p_{\min}}} \pi A e} \quad (9-9)$$

Again, large aspect ratio and low $C_{D_{p_{\min}}}$ are advantageous for realizing a large $(C_L^{1/2}/C_D)_{\max}$.

9-11 Aerodynamic Center, ac . The aerodynamic center for most airfoils is close to the 25 per cent chord, and this is frequently used as a reference point for presenting pitching-moment data.

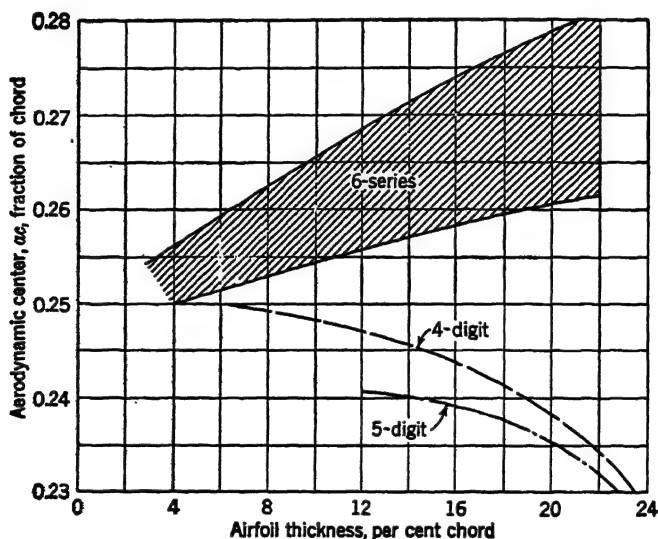


FIG. 9-14. Variation of aerodynamic center with thickness for four-digit, five-digit, and 6-series airfoils. $R \approx 6 \times 10^6$. (Experimental data averaged from *WRL-560*.)

Theoretically, the aerodynamic center for an airfoil having zero thickness occurs at exactly the 25 per cent chord, and experimental data show that this is a good average for all airfoils (Fig. 9-14).

9-12 Pitching Moment Coefficient about the Aerodynamic Center, $c_{m_{ac}}$. The pitching moment coefficient about the aerodynamic center, $c_{m_{ac}}$, is usually negative, and a small value is desirable because it implies small torsional loads on the wing at high speed. Flaps usually produce an additional diving moment that is large compared to the wing diving moment, but this consideration is important only at low speeds. The critical condition for structural design depends upon the particular wing and flap combination.

The $c_{m_{ac}}$ should generally be positive for a flying wing, which must be both stable and balanced. The influence of $c_{m_{ac}}$ on the stability equation of a complete airplane will be discussed in Chap. 15.

A symmetrical airfoil section must have zero $c_{m_{ac}}$, for it must exhibit the same aerodynamic characteristics when inverted as upright. The $c_{m_{ac}}$ becomes more negative with increase in

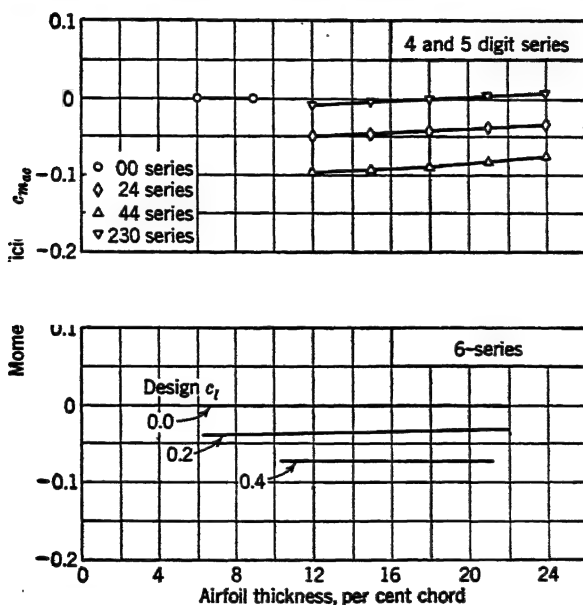


FIG. 9-15. Variation of moment coefficient about the aerodynamic center with thickness and camber for four-digit, five-digit, and 6-series airfoils. $R \approx 6 \times 10^6$. (Averaged data from WR L-560.)

amount of camber, as shown in Fig. 9-15; indeed, theoretically, $c_{m_{ac}}$ is linearly dependent upon amount of camber. It also becomes more negative with increasing rearward position of maximum camber, but experimental data showing this effect are not plentiful.

Reynolds number has a negligible effect on $c_{m_{ac}}$, and Mach number causes a change according to Eq. (8-30).

9-13 Critical Mach Number, M_{cr} . The critical Mach number is defined as the lowest remote Mach number that produces a local Mach number of 1.0 somewhere on an airfoil. It indicates a lower limit below which compressibility shock cannot occur. Since the

local Mach number depends upon the local velocity, which in turn depends upon the local static pressure, the airfoil shape and its lift coefficient both define the critical Mach number. The critical Mach number is obtained as a function of the most negative pressure coefficient on the airfoil, using the curve (due to von Kármán) presented in Fig. 9-16. The variation in critical Mach number with airfoil-thickness distribution, percent thickness (Fig. 9-17), amount of camber, and position of maximum camber (Fig. 9-18) is quite considerable.

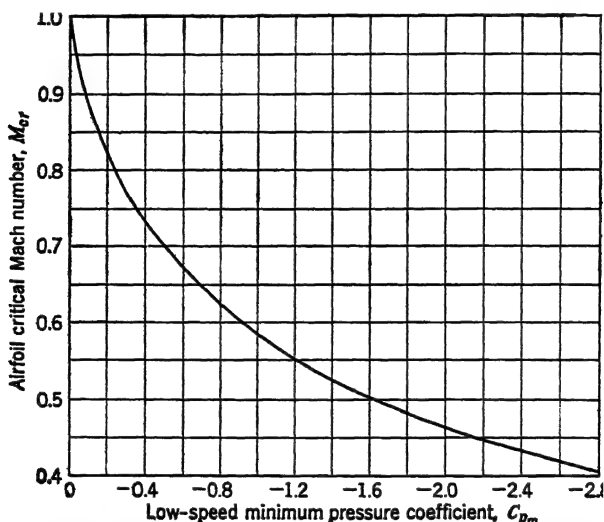


FIG. 9-16. Critical Mach number variation with minimum low-speed pressure coefficient. (From *WR L-560*.)

The proper choice of airfoil section is seen to be very important if the airplane is expected to fly either at very high speed, which corresponds to a high Mach number; or at low speed at high altitude, heavily loaded, which corresponds to a high lift coefficient. In general, the root section of a wing on an airplane experiences compressibility burble before any other spanwise station if flying at low lift coefficient (high speed, say), because the root section usually has the largest per cent thickness. This relation may not hold at lower speeds, however, as is shown in Fig. 9-17. In Figs. 9-17 and 9-18, the low-speed lift coefficient may be multiplied by $1/\sqrt{1-M^2}$, in the conventional manner, to obtain the high-speed lift coefficient.

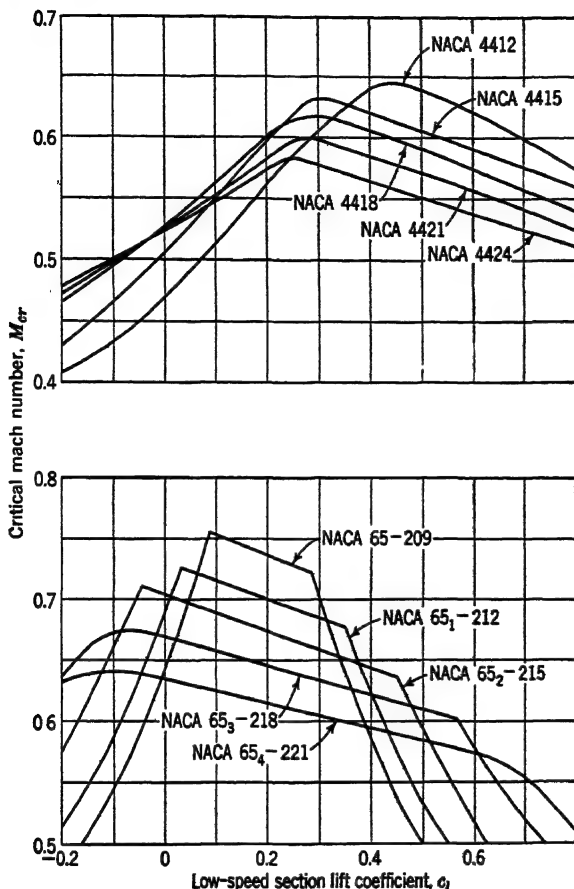


FIG. 9-17. Variation of critical Mach number with lift coefficient and thickness for four-digit and 65-series airfoils. (From *W R L-560*.)

Example. Find the critical velocity of a wing having an NACA 65₄-221 root section at $c_l = 0.5$ at 10,000 ft.

Solution. This problem may not be solved directly, because the answer must be known before the low-speed lift coefficient is found; however, successive solutions may be used, and in this particular case, the solution is rapidly convergent.

As a first approximation, the high- and low-speed c_l may be assumed equal; hence, from Fig. 9-17 at $c_l = 0.5$, $M_{cr} = 0.58$.

As a second approximation, the low-speed c_l may be solved, using the above M_{cr} .

$$c_l = (0.5) \sqrt{1 - (0.58)^2} = 0.407$$

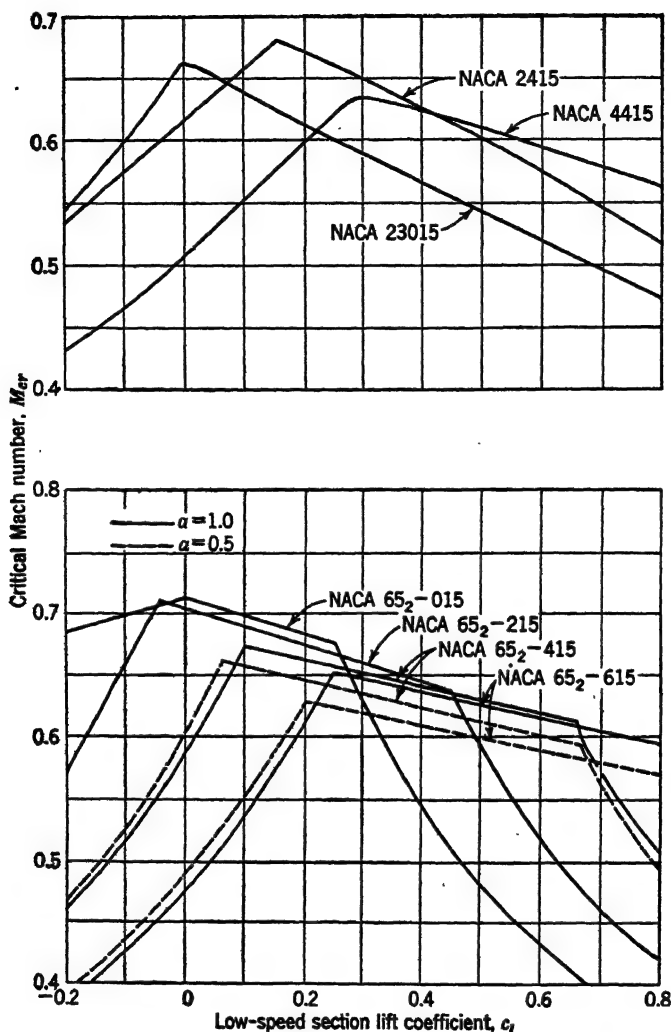


FIG. 9-18. Variation of critical Mach number with lift coefficient and camber for four-digit, five-digit, and 65-series airfoils. (From *WR L-580*.)

Now reading $M_{cr} = 0.595$ at $c_l = 0.407$, the third approximation of the low-speed c_l may be made:

$$c_l = (0.5) \sqrt{1 - (0.595)^2} = 0.402$$

Further solution is unnecessary, and the final value of M_{cr} may be

rounded out to $M_{cr} = 0.60$. The speed of sound from Table I, Appendix A, is

$$a = (0.965)(1120) = 1080 \text{ fps}$$

The critical velocity is therefore

$$V = \left(\frac{1080}{1.467} \right) (0.60) = 442 \text{ mph}$$

The breakdown of flow on an airfoil is of interest to the aerodynamicist because it is manifested as an increase in drag coefficient and decrease in lift coefficient. Although the critical Mach number is a useful criterion because it is quite simple to determine from low-speed pressure measurements, there is no assurance that the drag increase and lift decrease will correspond exactly to this Mach number. In order to compare the performance of various airfoils at high speed, it is convenient to define another Mach number that is more closely associated with the change in the aerodynamic characteristics. This *drag-divergence Mach number* is frequently defined as the Mach number for which $dc_d/dM = 0.10$. The drag-divergence Mach number is generally higher than the critical Mach number. Indeed, it would have to be higher if the drag rise could only be caused by the formation of shock waves. It is not necessarily higher, however, if the drag rise results from separation produced by subcritical compressibility effects.

PROBLEMS

9-1. *a.* Prove that C_D for $(L/D)_{\max}$ is double $C_{D_{0_{\min}}}$, if the wing polar curve may be represented by

$$C_D = C_{D_{0_{\min}}} + \frac{C_L^2}{\pi A e_w}$$

where e_w is a wing efficiency factor, corresponding to the conventional airplane efficiency factor e .

b. Show that if C_{D_0} of an airplane is constant with changing C_L , then $e_w = e$.

9-2. Verify the results of Prob. 6-3 for $A = 10$, by the relation from Prob. 9-1*a*, using $e = 0.80$ from Prob. 6-12.

9-3. Compute $(L/D)_{\max}$ and C_L at $(L/D)_{\max}$ for the airplane of Prob. 6-12, and compare these values with those obtained in Prob. 9-2, for the wing alone, with $A = 10$.

9-4. Prove that C_D for maximum $C_L^{1/2}/C_D$ is $\frac{4}{3}C_{D_{p_{\min}}}$, if the airplane polar curve may be represented by

$$C_D = C_{D_{p_{\min}}} + \frac{C_L^2}{\pi A e}$$

9-5. A 50,000-lb airplane has $(L/D)_{\max} = 17.0$, corresponding to a velocity $V = 130$ mph, at sea level. If wing area = 1300 sq ft, and aspect ratio = 11, find e .

9-6. Find the airplane efficiency factor e for an airplane having $C_{D_{p_{\min}}} = 0.0200$, $dC_{D_p}/dC_L^2 = -0.0010$, $A = 8$, and wing efficiency factor $e_w = 0.87$.

9-7. Using Fig. 9-16, verify the critical Mach numbers shown in Fig. 9-18, for the four airfoils shown in Fig. 9-5.

9-8. Explain the shape of the curves in Fig. 9-17.

CHAPTER 10

AUXILIARY LIFT DEVICES

In Art. 9-5 the stalling speed of an airplane was shown to depend upon the maximum lift coefficient, so that the highest practical value of $C_{L_{\max}}$ is therefore desirable. Several devices have been suggested and tested that allow the pilot to increase the $C_{L_{\max}}$ over that obtained from the wing itself. The *flap* is the principal device used on conventional aircraft, but the *slot* is also common, particularly in conjunction with a flap. A third device involving *boundary-layer control* has not yet (1949) been used commercially but has interesting possibilities. Each method will be described and compared.

10-1 Flaps. A *flap* consists of a plate or airfoil having a chord about one-quarter of the wing chord. In the retracted attitude it forms the trailing edge of the airfoil. It is extended by pivoting, rolling on tracks, or moving by linkages until its chord rotates through a maximum angle of about 30 to 60 deg from its retracted position. There are four principal kinds of flaps, shown in Fig. 10-1, but each may be modified to suit a particular installation.

Deflection of a *plain flap* at high angle of attack produces an increment of lift coefficient that is almost exactly the same as that produced at low angle of attack (Fig. 10-2). This might have been anticipated, since a deflected flap is somewhat similar to a large amount of camber at the trailing edge, and the effect of camber has already been demonstrated in Fig. 9-8.¹ This same principle applies, in general, to all flaps.

A *split flap* consists of a simple flat plate attached to the under surface of the airfoil. It produces approximately the same lift increment as a plain flap but naturally causes a considerably larger increment in drag because of the wake produced by its deflection. However, the moment-coefficient differential is much less.

A *slotted flap* is constructed like a simple flap, but a "slot" allows

¹ Cambering a plain flap is not quite analogous to cambering an airfoil, because of the difference in definition of wing chord and hence in angle of attack.

Plain flap

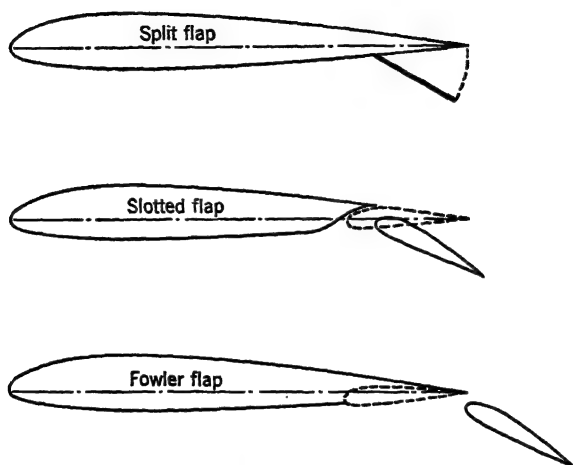


FIG. 10-1. Four principal types of flaps. The flaps shown have approximately 25 per cent chord and are mounted on an NACA 23012 airfoil. (From TR 664.)

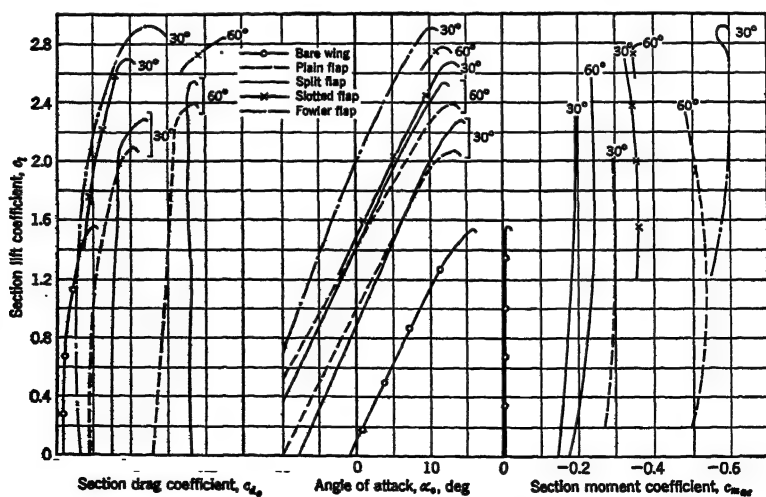


FIG. 10-2. Section characteristics of four principal types of flaps of approximately 25 per cent chord mounted on an NACA 23012 airfoil. Figures on curves refer to flap deflection. (From TR 664.)

air to pass from the lower to the upper surface of the airfoil at the flap leading edge. This high-speed air accelerates the boundary layer and delays separation. In view of the fact that it produces about the same lift increment at 30 deg as the plain and split flaps do at 60 deg, its small drag increment is quite remarkable and is explained by the lack of separation on the flap upper surface; hence, the wake, even at 30 deg deflection, is still relatively small. The moment differential is quite large because of the un-separated upper flap surface.

The *Fowler flap* is similar to a slotted flap, but it moves rearward a considerable distance, in addition to rotating, and thus effectively increases the wing area. It is seen in Fig. 10-2 to produce the greatest lift increment with the least drag increment; however, because of the rearward motion of the flap in its extended position and the fact that it is slotted, its moment coefficient is very highly negative.

Figure 10-3 shows the variation with flap angle in increment of section maximum lift coefficient, for the same four flaps shown in Fig. 10-2. The large increment at zero deflection for the Fowler flap arises because it slides rearward without rotating, for the first part of its travel.

Figure 10-4 shows the variation with flap angle in increment of section maximum lift coefficient, for four flaps of different per cent chord on two wings of different thickness. The data show that little is gained in making a flap greater than 25 to 30 per cent chord, particularly in view of the increased structural loads imposed on the wing. They also show that section thickness is very important in determining effectiveness of the flap.

The change in aerodynamic coefficients due to a flap deflection on a three-dimensional wing is not so large as those shown in Figs. 10-2, 10-3, and 10-4, because of the spanwise limitation usually imposed by the ailerons. As an approximation, the change in drag and lift coefficients at constant angle of attack and the

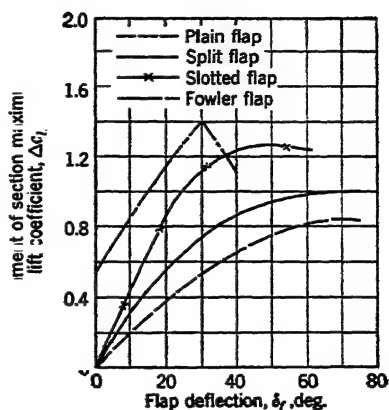


FIG. 10-3. Increment of section maximum lift coefficient due to flap deflection for four principal types of flaps of approximately 25 per cent chord mounted on an NACA 23012 airfoil. (From TR 864.)

change in maximum lift coefficient may be weighted by the ratio of flapped area S_f , included by the flap span b_f , to the wing area S (Fig. 10-5). The moment coefficient may be weighted by the ratio

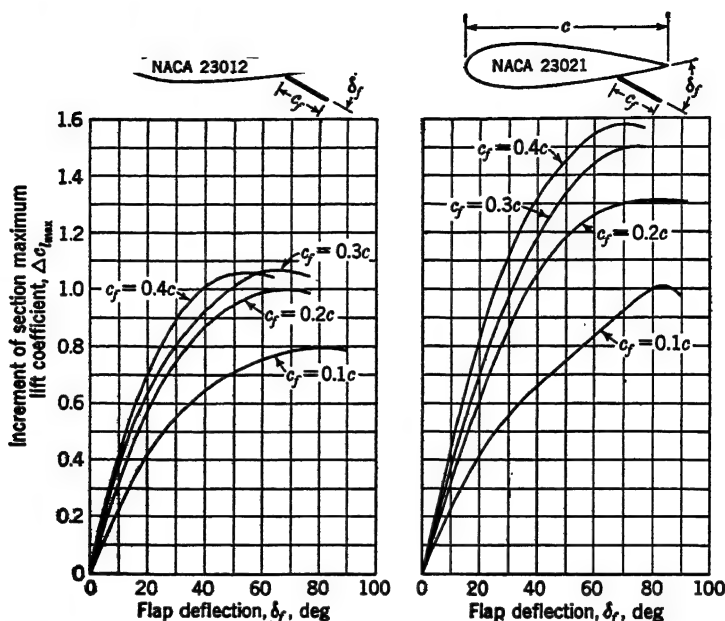


FIG. 10-4. Effect of flap chord and flap deflection on increment in section maximum lift coefficient for split flaps on a five-digit airfoil. (From TR 668.)

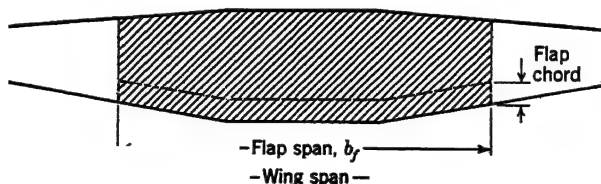


FIG. 10-5. Definition of flapped area S_f of a wing.

of flap "volume" $S_f \bar{c}_f$ to the wing "volume" $S \bar{c}$, where \bar{c}_f is the average chord of the flapped area and \bar{c} is the average chord of the wing. If the wing is tapered in thickness, it may be represented approximately by an average thickness. Figure 10-6 shows that deflection of flaps does not cause appreciable change in the type of stall (tip stall or root stall), although, of course, it generally causes stalling to occur at a lower angle of attack. Available data

indicate that the increment in $c_{l_{\max}}$ due to flap deflection is independent of Reynolds number.

Flaps are used to permit¹ low airplane velocity in making a landing, or, what amounts to the same thing, to allow a small wing area for a given landing speed. They also serve a different

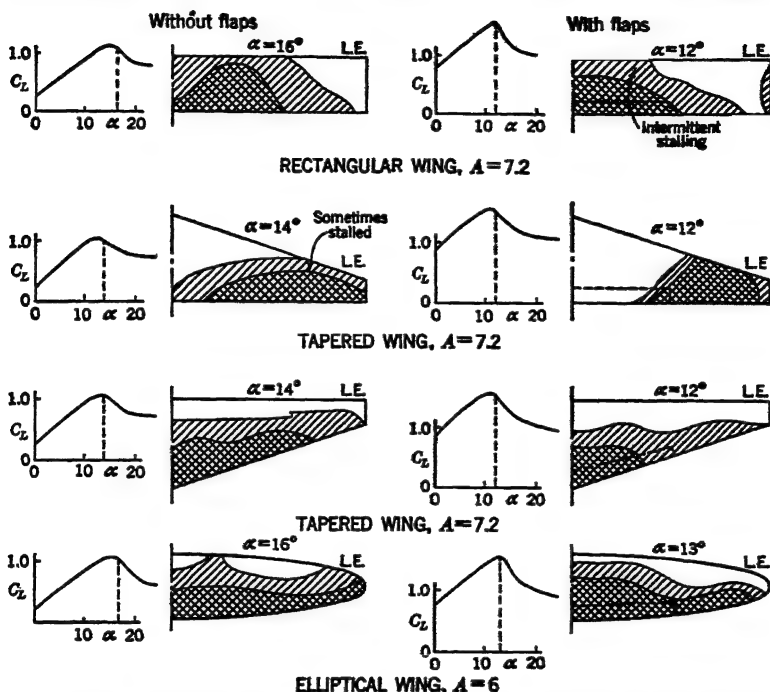


FIG. 10-6. Stall diagrams on various wings, with and without 20 per cent chord, 50 per cent span, 60-deg split flaps. Single crosshatch lines indicate disturbed region. Double crosshatch lines indicate stalled region. (From R&M 1796. Reproduced with permission of the Controller of His Britannic Majesty's Stationery Office.)

purpose, however, because a flap having a large drag increment reduces the L/D and allows a steeper glide angle without any increase in gliding speed. This steep angle allows a shorter approach to a landing field and is particularly useful in small fields surrounded by obstructions (Fig. 10-7). A combination of large drag coefficient with large lift coefficient is therefore commonly considered desirable.

¹ The word "permit" is used advisedly. The flaps are not designed to reduce the speed of the airplane; they *allow* the plane to fly at a low speed without stalling.

A second use of flaps is to *reduce* the drag coefficient. When a flap is deflected to a small angle, say 10 deg, it produces a fairly large lift increment with a small drag increment *at constant angle*

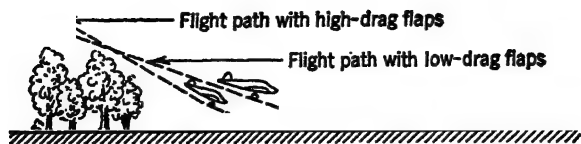


FIG. 10-7. Comparison of flight paths during landing approach for two kinds of flap.

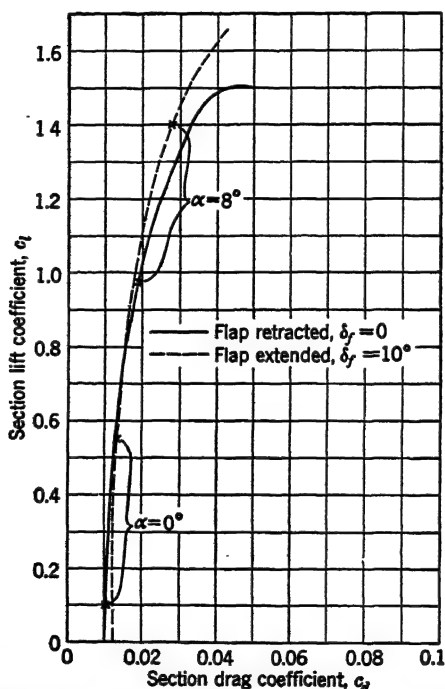


FIG. 10-8. Effect of small flap deflection on section drag coefficient for a slotted flap. (From TR 664.)

of attack. This may imply a small drag decrement *at constant lift coefficient* (Fig. 10-8). The decrement is effected only at fairly large lift coefficients, and its magnitude depends upon the particular flap and the characteristics of the airplane on which it is to be used. Small flap deflections are frequently recommended

to improve take-off and climb performance of an airplane, both of which may correspond to relatively large lift coefficients.

10-2 Slots. A second device used for increasing maximum lift coefficient is the *slot*. The slot is cut near the leading edge of an airfoil and allows passage of air from the lower surface to the upper



FIG. 10-9. Typical slot installation cut in an NACA 23015 airfoil. (From TN 702.)

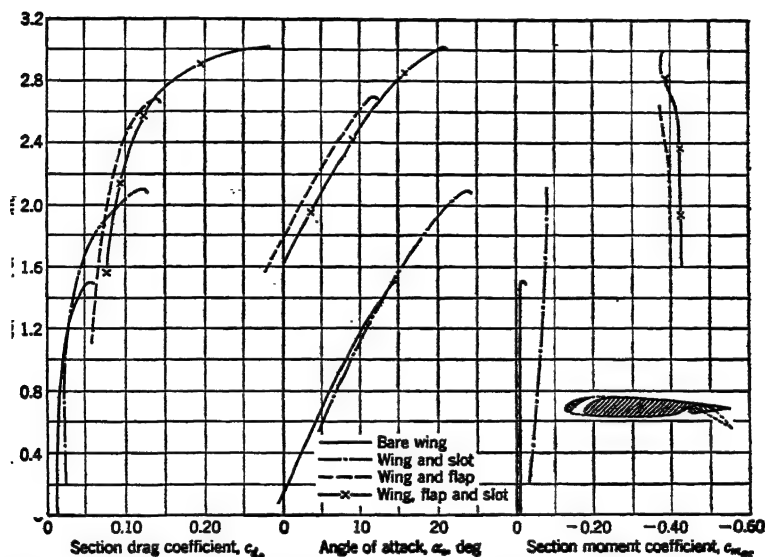


FIG. 10-10. Comparison of wing, slot, and slotted flap combinations on an NACA 23012 airfoil section. Flap deflection $\delta_f = 40$ deg. (From TN 702.)

surface (Fig. 10-9). The resulting jet of air speeds up the flow within the boundary layer and delays stalling to a larger angle of attack (Fig. 10-10). At low angles of attack the slot reduces the lift coefficient slightly and causes an increment in drag coefficient, because of the leakage of air. The effect on moment coefficient is comparatively small.

The slot just described is called a *fixed slot*. An *automatic slot* is constructed so that the *slat* in front of the slot is held against the leading edge by the local static pressure at low angles of attack,

but when the angle of attack is increased to just below the stall angle, the local static pressure becomes highly negative and lifts the slot away from the surface. The slot so formed acts like a fixed slot, and the airfoil may then continue to a much higher angle of attack before finally stalling.

10-3 Comparison of Flaps and Slots. The flap and slot differ aerodynamically as well as geometrically. The flap increases the lift coefficient at all angles of attack by about the same amount, and generally reduces the stall angle. The slot, on the other hand, causes an extension of the lift curve to a relatively large stall angle. The large stall angle is disadvantageous because it requires a correspondingly increased inclination of the fuselage in landing, which in turn, requires relatively long and therefore heavy landing gear. Slots are sometimes employed in conjunction with flaps in order to obtain a very high maximum lift coefficient. The combination has a stall angle that is slightly less than for the wing and slot (Fig. 10-10). A word of caution must be inserted here with regard to the interpretation of these curves. The stall angle shown on a curve of section characteristics is slightly misleading because the curves plotted for a wing of finite aspect ratio would have the lift increments reduced depending upon the span of the flap; also, the curves would rotate because of the addition of α_i .

A major advantage of a flap over a slot is that it may be controlled through a large range of angles and may be used to assist in take-off, climb, etc. Some flaps have large *hinge moments*,¹ however, that require heavy fittings and linkages and even mechanical or electrical boosters. Also, all flaps give large torsional loads on the wing. The Fowler flap is particularly notable for this characteristic.

Fixed slots cause a small drag increment at low lift coefficient because of their position in the critical leading-edge region of the airfoil; they are therefore not generally successful for low-drag airfoils. Fixed and automatic slots are not dependable in cold weather unless adequate precautions are taken to prevent icing.

Since ailerons are customarily situated at the outer extremities of the wing trailing edge, flaps are generally restricted to about 60 per cent of the span. No such restrictions are imposed on the employment of slots, however, except for low-wing airplanes, in

¹ A hinge moment is the torque required to deflect an auxiliary surface such as a flap.

which the slot must terminate at the fuselage, while the flap may extend across the under surface of the fuselage. Some airplanes have been constructed in which the ailerons are deflected downward to act as flaps, while still maintaining the necessary differential operation characteristic of all ailerons. Also, some ailerons rotate only upward, allowing the flaps to extend across the full span of the wing.

10-4 Boundary-layer Control. A third method for increasing the maximum lift coefficient is called *boundary-layer control*. One

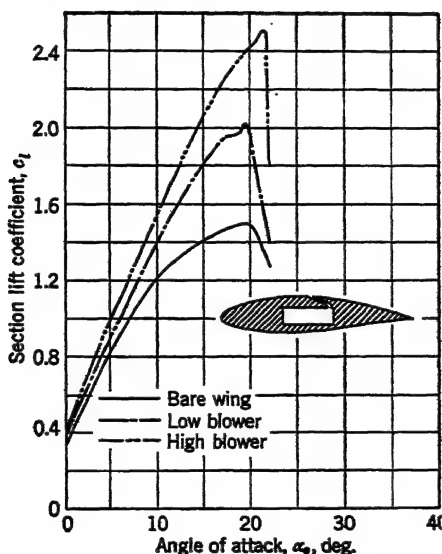


FIG. 10-11. Lift characteristics of an NACA 65g-418 airfoil with suction slot at 45 per cent chord. (From TN 1071.)

or more suction slots are located on the upper wing surface, and the low-speed air within the boundary layer is removed mechanically by suction. On low-drag airfoils, for which laminar flow is to be maintained as much as possible on the upper surface, the suction slots should be located sufficiently far back from the leading edge so that they do not cause transition at low lift coefficient when the blower is not operating. Test data using a medium-thickness low-drag airfoil are shown in Fig. 10-11 for two suction quantities. Test data on a medium-thickness (12 per cent) low-drag airfoil in which a retractable slat is incorporated are shown in Fig. 10-12. The stall angle is evidently too large to be acceptable

on conventional aircraft, but when flaps are added it is considerably reduced, in addition to giving a tremendous increase in lift coefficient.

Boundary-layer control may be used to reduce the drag coefficient of an airfoil by ensuring an assisting pressure gradient, hence

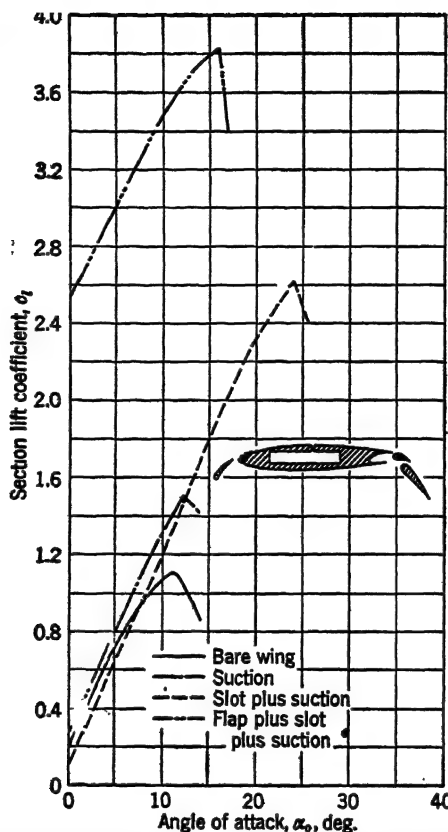


FIG. 10-12. Lift characteristics of an NACA 641-212 airfoil section with boundary-layer control, slot, and double-slotted flap. (From TN 1293.)

aiding to preserve laminar flow. It has also been suggested¹ as a means of reducing the large drag coefficient characteristic of the transonic regime, by preventing separation.

Boundary-layer control seems to hold particular promise for flying wings, because there is only slight change in pitching moment with fairly large suction. Its principal disadvantage when used

¹ TM 1168.

with a conventional reciprocating engine is that it requires a separate blower and a certain amount of ducting, which add weight to the airplane. When used with a jet-propulsion unit, there is no need for an auxiliary pump.

10-5 Dive Brakes. A dive brake is any device used to increase the drag coefficient of an airplane in order to reduce the velocity in a steep glide or dive. A common device consists of two plates that deflect in opposite directions on the wing trailing edge (Fig. 10-13). This arrangement gives a large drag coefficient with a reduction in lift coefficient and increase in wing moment coefficient.¹ The plates are frequently perforated to prevent tail buffeting arising from periodic crosscurrents on the tail that are produced by large eddies from the wing. This type of installation may have its lower element act as a conventional split flap.

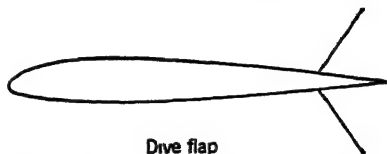


Fig. 10-13. Dive-flap installation on a wing trailing edge. (From *WR L-373*.)

Dive brakes are frequently installed on the fuselage instead of on the wing, but regardless of position they should be so arranged that no large change in pitching moment occurs during their deflection. Also, they should not interfere with aileron, rudder, or elevator control, and they should not have excessive hinge moments.

PROBLEMS

10-1. If the section lift coefficient is assumed constant across the span of a tapered wing, and if the increment in section maximum lift coefficient due to flap deflection is assumed constant across the flapped span,

a. Show that the increment in maximum lift coefficient, $\Delta C_{L_{max}}$, due to flap deflection is

$$\Delta C_L = \left(\frac{S_f}{S} \right)$$

b. Show that the increment in moment coefficient, ΔC_m , due to flap deflection is

$$\Delta C_m = \Delta c_l \left(\frac{S_f}{S} \right) \left(\frac{\bar{y}}{\bar{y}_f} \right)$$

¹ See *WR L-373*. The moment coefficient may be modified by changing the relative size of the two plates.

10-2. An airplane weighing 12,000 lb has a wing with NACA 23015 airfoil section and aspect ratio 6. Wing area is 600 sq ft. The airplane has a symmetrical fuselage, which is designed to have its axis of symmetry, or fuselage reference axis, level at a cruising speed of 220 mph at sea level. Assuming the landing speed is 10 mph greater than the stalling speed, find the landing speed at sea level, and the attitude of the fuselage reference axis at this speed. Neglect ground effect, and assume level flight for all speeds.

10-3. The wing of Prob. 10-2 has a taper ratio $\lambda = 0.3$. (The airfoil characteristics in Fig. I, Appendix B, are for a rectangular wing but may be assumed applicable for other taper ratios.) Split flaps having 60 per cent span and 20 per cent chord are deflected 40 deg for landing and stalling the airplane. Repeat Prob. 10-2. Interpolate from Fig. 10-4 for maximum-lift-coefficient increment. Assume the stall angle with flaps deflected is 1 deg less than that of the wing alone, but that the shape of the peak of the lift curve is the same with flaps up or down.

10-4. Preliminary performance calculations of a 10,000-lb airplane, with an NACA 23015 airfoil section and split flaps, indicate that the sea-level stalling speed is 80 mph, corresponding to a flaps-down $C_{L_{\max}} = 2.0$. What should the stalling speed be with Fowler flaps, assuming this installation to be 200 lb heavier, assuming the *change* in $C_{L_{\max}}$ due to flap deflection to be increased 75 per cent, and assuming the wing area to be the same as for the split flaps?

10-5. A dive bomber is in a terminal-velocity vertical dive at 5000 ft with dive flaps extended. Terminal velocity with flaps extended, $V_{T_F} = 300$ mph. If $W = 9000$ lb, $S = 500$ sq ft, and the flaps cause a change in drag coefficient, $\Delta C_{D_F} = 0.053$, what would the terminal velocity V_T be at 5000 ft with flaps retracted? Neglect effects of compressibility.

CHAPTER 11

PARASITE-DRAG AND POWER CONSIDERATIONS

For performance predictions, the power required by the airplane and the power available from the engine and propulsion unit must be known for all operating conditions. This implies that the drag and thrust must be known for all operating conditions. For a particular velocity, the drag depends mainly upon the configura-

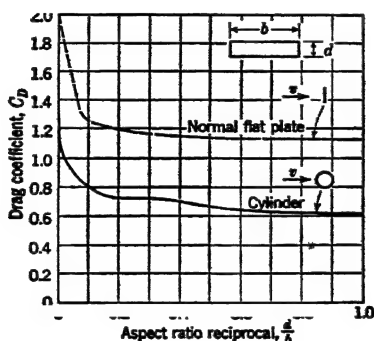


FIG. 11-1. Variation in drag coefficient with aspect ratio reciprocal for a normal flat plate and for a cylinder. Reynolds number, based on length d , is approximately 5×10^4 . (The former curve replotted by permission from "Fluid Mechanics," by R. A. Dodge and M. J. Thompson, McGraw-Hill Book Company, Inc., 1937, and the latter replotted by permission of Engineering Societies Monograph Committee from "Applied Hydro- and Aeromechanics," by L. Prandtl and O. G. Tietjens, McGraw-Hill Book Company, Inc., 1934.)

tion of the airplane, and the thrust depends upon the power of the engine and the efficiency of the propulsion unit. This chapter will be concerned primarily with drag and power required by the airplane. Subsequent chapters will be concerned with power plants and methods of propulsion.

In all performance calculations, standard altitude conditions are used in order that characteristics of various airplanes may be compared on a common basis. This, of course, applies to the power required by the airplane, engine bhp, and propulsion-unit

characteristics. It is important to realize, however, that these conditions rarely are realized, and the procedure is used only for standardization.

11-1 Parasite Drag of Some Common Bodies. Parasite drag

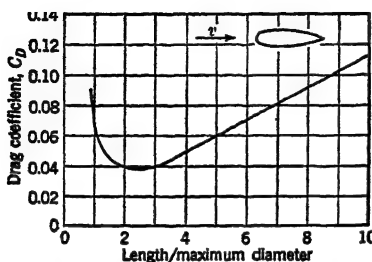


FIG. 11-2. Drag-coefficient variation with fineness ratio for a streamlined body of revolution. Drag coefficient is based on maximum frontal area. (Replotted by permission from "Air-Cooled and Liquid-Cooled Aircraft," by J. G. Lee in *JAS*, April, 1941.)

is composed of *form drag* arising from an integration of pressure-force components and *skin friction* arising from an integration of viscous shearing-force components. Bodies may be classified roughly into *bluff* or *streamlined* categories, according to whether they have predominant form drag or skin friction, respectively. Of course, a particular body may have considerable variation in the proportion of each force, dependent upon Rey-

nolds number, attitude, surface texture, etc.

An infinitely thin flat plate set parallel to the remote velocity is an example of pure skin friction. The same plate set normal to the stream is an example of pure form drag. Neither of these examples represents an extreme in drag coefficients, however: a low-drag airfoil delays transition and gives a lower drag coefficient at high Reynolds numbers than a parallel flat plate; also, a curved plate that is concave upstream produces a larger wake and hence a larger drag coefficient than a normal flat plate.

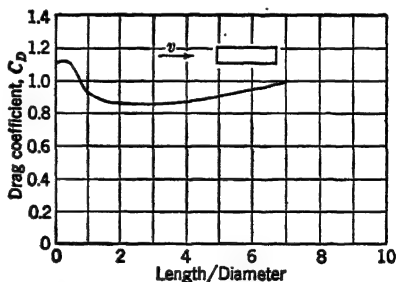


FIG. 11-3. Drag-coefficient variation with fineness ratio for a circular cylinder. Drag coefficient is based on frontal area. (Replotted by permission from "Airplane Design," by E. P. Warner, McGraw-Hill Book Company, Inc., 1936.)

The drag coefficient for bluff bodies of small aspect ratio is generally less than that for large aspect ratio, because of relief of the large pressure differential at the ends (Fig. 11-1).¹

¹ In Figs. 11-1 to 11-5, inclusive, C_D and R are based on transverse area (frontal area) and width, respectively.

The drag coefficient of a body of revolution depends upon its slenderness, or *fineness ratio* (ratio of length to maximum diameter). A streamlined body has a minimum drag coefficient corresponding to a fineness ratio of about 2 to 3 (Fig. 11-2). For

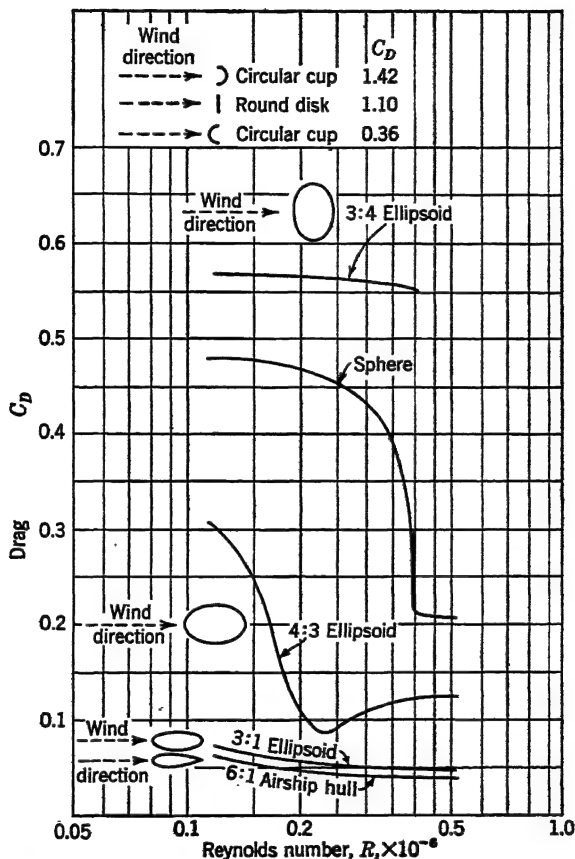


FIG. 11-4. Drag-coefficient variation with Reynolds number for several bodies of revolution. C_D is based on frontal area. R is based on diameter. (Replotted by permission, with minor modifications, from "Fluid Mechanics," by R. A. Dodge and M. J. Thompson, McGraw-Hill Book Company, Inc., 1937.)

small fineness ratio, separation takes place, giving a relatively large form drag, hence giving a relatively large drag coefficient. For large fineness ratio, the large wetted surface of the body causes relatively large skin friction, hence gives a relatively large coefficient. A bluff body like a circular cylinder has a minimum drag

coefficient corresponding to a fineness ratio of about 2 to 4. For small fineness ratio, the cylinder acts like a flat plate, giving a wake considerably larger than the area of the plate. For large

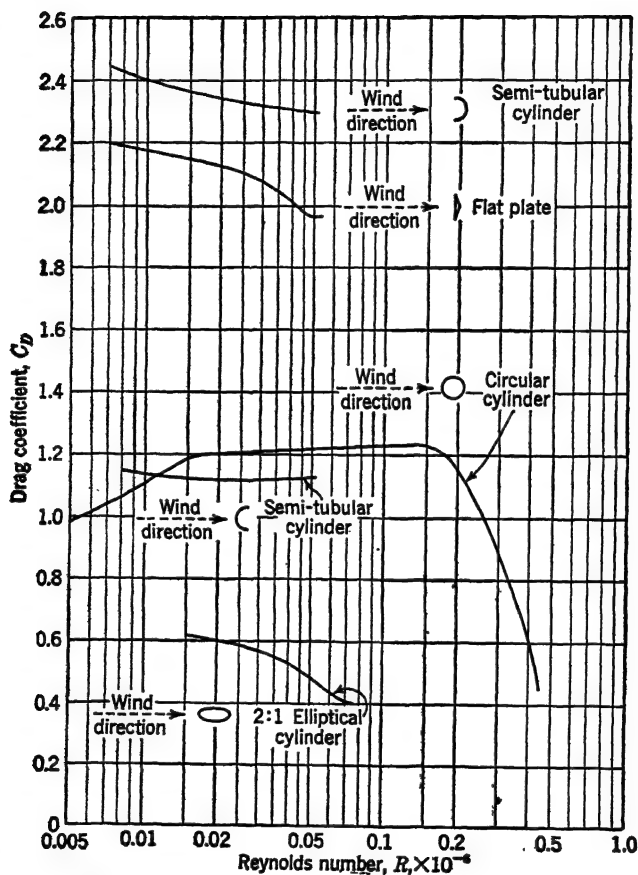


FIG. 11-5. Drag-coefficient variation with Reynolds number for several bodies having infinite aspect ratio. Drag coefficient is based on frontal area. Reynolds number is based on transverse dimension. (From TR 619.)

fineness ratio, the flow separates at the leading edge but closes in again, conforming to the shape of the cylinder at some distance from the leading edge; the relatively large skin friction is then responsible for the increase in drag coefficient (Fig. 11-3).

In Fig. 11-4 the drag coefficient for several bodies of revolution is shown as a function of Reynolds number. Presumably the 3:4

ellipsoid has a sudden drop in coefficient at a critical Reynolds number beyond the highest value shown. The peculiar shape of the curves has been discussed in Chap. 7. In Fig. 11-5 the drag coefficient for several bodies of infinite aspect ratio is shown as a function of Reynolds number.

11-2 Interference. The total drag of two bodies placed close to each other is generally different from the sum of the drags of the two bodies when tested separately. This phenomenon is called *interference*, and it arises from the change in flow pattern that accompanies the placing of two bodies in close proximity. The

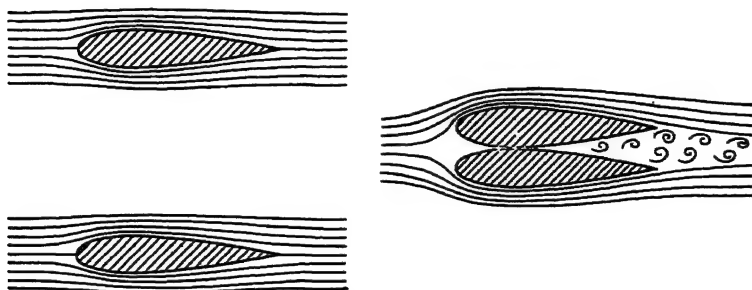


FIG. 11-6. Interference flow patterns on streamlined struts far apart and close together.

interference may be unfavorable or favorable. For instance, the drag of two wings placed close together as in Fig. 11-6 is much higher than the sum of the two individual drags, because of the large wake produced. However, the drag of a stalled wing may be reduced considerably by placing an auxiliary airfoil near the leading edge to form the familiar slot discussed in the preceding chapter. Usually the interference becomes important to the aerodynamicist when one body acts in the wake of another, as when the tail of an airplane acts in the wake of the wing, or because of the mutual distortion of flow pattern on two bodies, such as the effect of a wing on the fuselage and the converse effect of the fuselage on the wing. In the first case, the rear body may be in a velocity field that is different from the remote velocity, not only in magnitude but also in direction and periodicity. In the second case, not only is the velocity field different but also the static-pressure distribution may be drastically modified, favorably or unfavorably. These interference effects are the cause of a good

part of the approximations that are necessary in predicting airplane performance, stability, and control.

One of the most important and most illuminating of all interference phenomena is concerned with the stalling that occurs in the wing-to-fuselage juncture of some airplanes. Consider a vertical flat plate parallel to the remote velocity and allow it to intersect a stub wing at the root section (Fig. 11-7a). Owing to the growth of boundary layer on the flat plate, the velocity next to the plate along the upper wing surface is somewhat reduced, and although the static-pressure distribution is almost completely unaffected by the presence of the plate, this reduction in energy of the boundary layer may lead to local premature stalling.

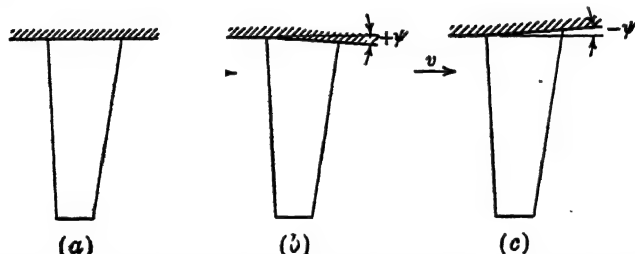


FIG. 11-7. Wing and wall combination, demonstrating various kinds of interference.

Next consider the same plate yawed so that the plate trailing edge is moved toward the wing tip (Fig. 11-7b). Here the higher velocity and lower static pressure at the wing trailing edge tend to prevent stalling.

Now consider the plate yawed in the opposite direction, so that the trailing edge is moved away from the wing tip (Fig. 11-7c). The velocity at the trailing edge is reduced, and the adverse pressure gradient is increased, both effects leading to premature stalling.

This reasoning may be applied to a wing that intersects a round fuselage. In the high-wing position (Fig. 11-8), the trailing edge is either tangent to the fuselage upper surface, in which case no interference ensues,¹ or it is buried in the fuselage, in which case the upper-surface streamlines must converge as in Fig. 11-7b, and the interference is favorable.

In the mid-wing position, inclination of the fuselage gives rise

¹ The effect on the lower surface is ignored here, because the lower surface will not generally stall for positive angles of attack.

to negative static pressures on its sides, near the front stagnation point of the wing (point x , Fig. 11-8), which becomes more positive

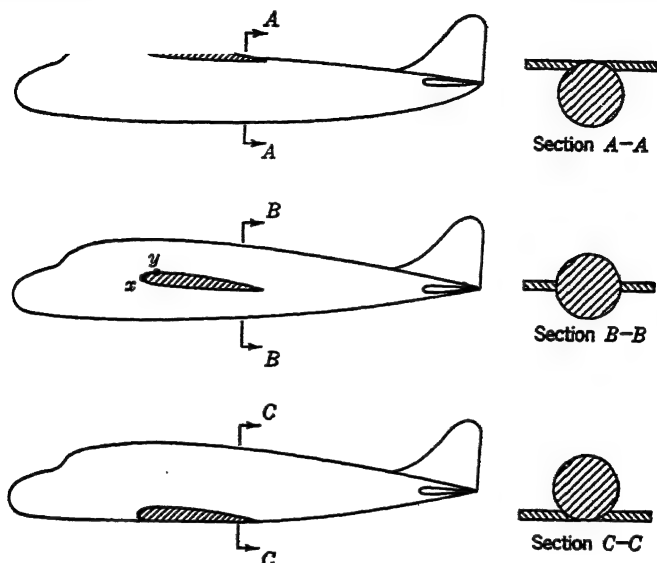


FIG. 11-8. Wing and fuselage combinations for demonstrating various kinds of interference.

in the direction of flow around the leading edge (point y). This adverse pressure gradient tends to promote leading-edge separation at a moderate lift coefficient. It may be rectified by using a thicker or more cambered airfoil section (Fig. 11-9), or by using a leading-edge fillet.

In the low-wing position, the wing leading edge is buried in the fuselage, while the trailing edge is usually about tangent with the lower surface of the fuselage. The streamlines must, therefore, diverge as in Fig. 11-7c, and interference is unfavorable. The condition may be improved by using a

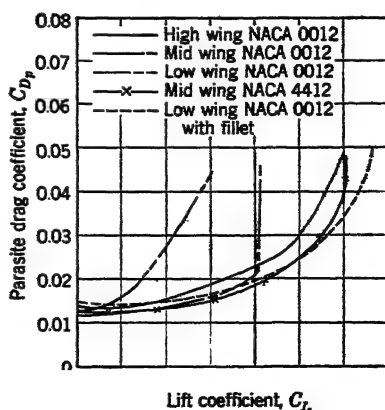


FIG. 11-9. Effect of wing position and fillets on parasite-drag characteristics. (Based on data from TR 540.)

thicker or more cambered airfoil section, and rectified by using a straight-sided fuselage or a fillet (Fig. 11-9).

11-3 Airplane Parasite Drag. Total parasite drag of an airplane is composed of the parasite drag of all its components, plus the interference drag. The customary procedure for determining parasite drag is to run tests in a wind tunnel. Usually the wing is tested alone; then nacelles are added, and the combination is tested; then the fuselage; then the empennage group. Further

0.040

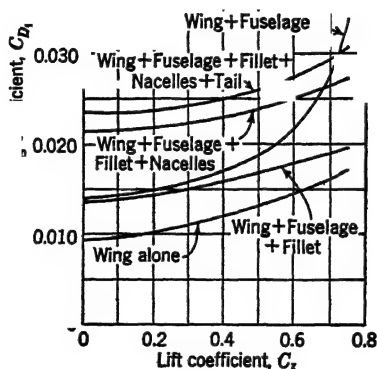


FIG. 11-10. Parasite-drag build-up for a typical four-engine airplane. (Based on UWAL data.)

tests are conducted for determining the drag coefficients of landing gear, cowl flaps, etc. A set of curves showing the drag increment resulting from the addition of each component is frequently referred to as a *parasite-drag build-up*, of which Fig. 11-10 is an example. By such a set of data, the drag increments may be compared with those anticipated from calculations, or with those of other airplanes. Improvements may be indicated as in the example shown, in which the need for filleting is clearly demonstrated.

The drag-coefficient increment resulting from addition of each component could be denoted by a subscript such as $\Delta C_{D_{4N}}$ indicating the drag-coefficient increment due to four nacelles. The drag due to nacelles would then be

$$D_{4N} = \Delta C_{D_{4N}} S q \quad (11-1)$$

The nacelles might easily have been tested individually in a wind

tunnel, without the presence of the airplane. Neglecting interference, the drag of each nacelle in this case would be one-quarter of the value given in Eq. (11-1) at the same dynamic pressure, and ΔC_{D_N} due to one nacelle would be one-quarter of $\Delta C_{D_{4N}}$. Thus the drag equation for one nacelle may be written

$$D_N = C_{D_N} S q \quad (11-2)$$

Since an aerodynamic coefficient is completely arbitrary, it may be based on any convenient area. It is based on the wing area in the above cases because all drag coefficients may be added when based on the same area, in the same manner that their corresponding drag forces may be added (at the same q). Sometimes the drag coefficient is more conveniently based on the frontal area of a body such as a nacelle or fuselage, etc. This area is called the *proper area* S_π , and the corresponding coefficient is called the *proper drag coefficient* C_{D_π} ; thus the drag equation for one nacelle may be written

$$D = C_{D_\pi} S_\pi q \quad (11-3)$$

From Eqs. (11-2) and (11-3),

$$C_{D_\pi} = \frac{\Delta C_{D_N} S}{S_\pi} \quad (11-4)$$

Thus the proper drag coefficient is merely a new nondimensional coefficient that is larger by the ratio of the two areas. The proper drag coefficient has particular significance in testing bodies that are not necessarily associated with any particular airplane. (The data presented in Figs. 11-1 to 11-5 are all really proper drag coefficients.) If, for instance, a 2:1 elliptical strut is to be installed on an airplane, its proper drag coefficient may be read from Fig. 11-5, at the correct Reynolds number, and the increment in drag coefficient based on the wing area may be computed from Eq. (11-4).

This procedure may be extended still further. Instead of indicating the aerodynamic characteristics of the nacelle, fuselage, or complete airplane by a drag coefficient, very often an *equivalent flat-plate area* is used. This means that the nacelle could be replaced mathematically by a flat plate having the same drag. In equation form,¹

$$D = C_D S q = 1.28 a q$$

¹ The flat-plate drag coefficient is arbitrarily assumed to have a constant value of 1.28.

therefore

$$a = \frac{C_D S}{1.28} \quad (11.5)$$

where a is the equivalent flat-plate area of the body that has a drag coefficient C_D based on a wing area S . The equivalent flat-plate area is a convenient and graphic way of expressing the drag of a body, for, whereas a drag coefficient of, say, 0.0025 has no significance to anyone unfamiliar with the usual size of nacelle coefficients, an equivalent flat-plate area of, say, 1.1 sq ft has a very definite physical significance.

Obviously, if the drag coefficient of a flat plate had happened to be 1.00 rather than 1.28, then Eq. (11.5) would have been very much simplified. Therefore, it is convenient to evolve a fictitious equivalent area which assumes a drag coefficient of 1.00:

$$f = \frac{C_D S}{1.00} = C_D S \quad (11.6)$$

The new area, which has no physical significance but allows simplification of calculations, is called the *equivalent parasite area*. The drag of any body may then be expressed by the following alternate equations:

$$D = C_D S q = C_{D_r} S_r q = 1.28 a q = f q$$

from which

$$C_D S = C_{D_r} S_r = 1.28 a = f$$

The significance of the last group of equations can best be appreciated by an example.

Example. A nacelle of 10 sq ft projected frontal area has a drag coefficient of 0.0020 based on a wing area of 400 sq ft. Find the proper drag coefficient, equivalent flat-plate area, and equivalent parasite area.

Solution.

$$C_{D_r} = \frac{C_D S}{S_r} = \frac{(0.0020)(400)}{10} = 0.08$$

$$a = \frac{C_D S}{1.28} = \frac{(0.0020)(400)}{1.28} = 0.625 \text{ sq ft}$$

$$f = C_D S = (0.0020)(400) = 0.8 \text{ sq ft}$$

The foregoing discussion of drag on a body emphasizes the fact that, since the general force equation merely stipulates that the force is proportional to the square of a length, then any convenient

area may be used; the only effect of changing the area is to change the value of the coefficient. Thus a coefficient is necessarily defined in conjunction with some specific area. *It should be noted that the equivalent flat-plate area, equivalent parasite area, and proper drag coefficient, when referred to a complete airplane or wing, never include induced drag. They are all measures of parasite characteristics.* The subscript p has been deleted from all drag and drag-coefficient symbols merely to make the equations less cumbersome.

11·4 Power Considerations. Power is the rate of doing work, and it may be expressed as work per second, energy per second, or the product of a force and a velocity, all three being fundamentally equivalent. The *power required* P_r to maintain steady level flight of an airplane is found from the product of its drag and velocity.

$$P_r = \frac{Dv}{550} \quad (11·7)$$

$$P_r = \frac{DV}{375} \quad (11·8)$$

where D is drag, lb

v is remote velocity, fps

V is remote velocity, mph

The power required must be supplied by an engine and propulsive device, the output of which is called *power available* P_a .

$$P_a = \frac{Tv}{550} \quad (11·9)$$

$$= \frac{TV}{375} \quad (11·10)$$

where T is thrust in pounds. For constant velocity and level flight, $P_r = P_a$, or using forces, $D = T$.

The bhp of the engine, P , is related to the power available from the propulsion unit by the propulsive efficiency η :

$$\eta = \frac{P_a}{P} \quad (11·11)$$

The power required for level, unaccelerated flight of an airplane may be obtained very simply from its aerodynamic characteristics. Solution of the power available from the propeller requires knowledge of the characteristics of the engine and the propulsive

unit. The development of power-available relations must be left until these two devices are discussed in the two following chapters.

11.5 Power Required. Drag on an airplane may be expressed as follows:

$$D = C_D S \frac{V^2 \sigma}{391} \quad (11.12)$$

Substituting Eq. (11.12) in Eq. (11.8) yields

$$P_r = \frac{C_D S V^3 \sigma}{146,600} \quad (11.13)$$

For level flight,

$$L = W = C_L S \frac{V^2 \sigma}{391} \quad (11.14)$$

For a particular airplane weight, wing area, and altitude, C_L is specified by V in Eq. (11.14). From a polar curve for the airplane

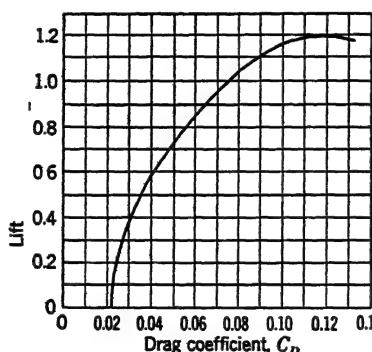


FIG. 11-11. Polar curve for an airplane having aspect ratio of 7.75. (Based on $UWAL$ data.)

(C_L vs. C_D in Fig. 11-11), the velocity indirectly specifies the drag coefficient and hence, by Eq. (11.13), specifies P_r . In this way, an airplane polar curve defines a curve of power required vs. velocity (solid line in Fig. 11-12). Curves for other altitudes and weights could be obtained by repeating the above procedure with the new conditions, but this obviously entails a good deal of labor. With a basic curve established, new ones may be found as shown in the following sections. Each method involves finding

velocity and horsepower under the new conditions of altitude or weight at the same C_L^* as the original velocity and horsepower.

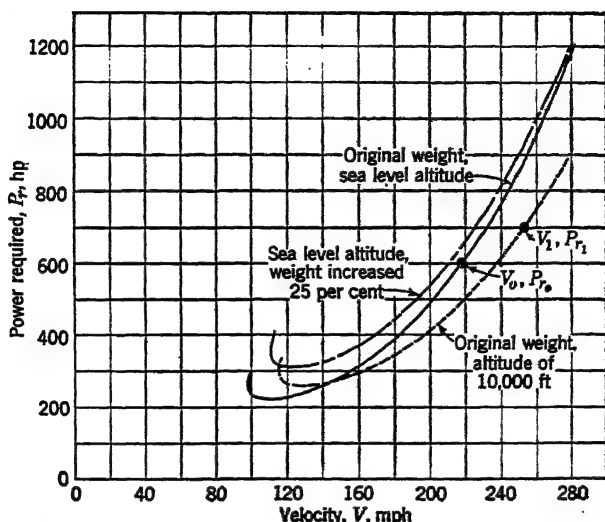


FIG. 11-12. Power required for an airplane having aspect ratio of 7.75 for two weights and altitudes (based on the polar curve of Fig. 11-11).

Effect of Change in Altitude. For the sea-level condition, with $\sigma_0 = 1.0$,

$$W_0 = C_{L_0} S_0 \frac{V_0^2}{391} \quad (11-15)$$

$$P_{r_0} = \frac{C_{D_0} S_0 V_0^3}{146,600} \quad (11-16)$$

For the altitude condition,

$$W_1 = C_{L_1} S_1 \frac{V_1^2 \sigma_1}{391} \quad (11-17)$$

$$P_r = \frac{C_{D_1} S_1 V_1^3 \sigma_1}{146,600} \quad (11-18)$$

where subscripts 0 and 1 refer to sea level and altitude, respectively.

From Eqs. (11-15) and (11-17), since $W_0 = W_1$, $S_0 = S_1$, and $C_{L_0} = C_{L_1}$,

$$V_1 = \frac{V_0}{\sqrt{\sigma}} \quad (11-19)$$

* This, of course, implies the same α and C_D also.

where σ_1 is called σ merely for simplicity. Again, from Eqs. (11.16) and (11.18), with $C_{D_0} = C_{D_1}$,

$$P_{r_1} = \left(\frac{V_1}{V_0} \right)^3 \sigma P_{r_0} \quad (11.20)$$

Substituting Eq. (11.19) in Eq. (11.20) yields

$$P_{r_1} = \frac{P_{r_0}}{\sqrt{\sigma}} \quad (11.21)$$

Equations (11.19) and (11.21), when used simultaneously, allow computation of V_1 and P_{r_1} from V_0 and P_{r_0} for any chosen σ . In Fig. 11.12 the altitude point V_1, P_{r_1} is shown corresponding to V_0, P_{r_0} . It is left to the student to prove that these two points and the origin must lie on the same straight line.

Effect of Change in Gross Weight. Equations (11.15) to (11.18), inclusive, may be used with subscripts 0 and 1 corresponding to *original* and *new* gross weight, respectively. From Eqs. (11.15) and (11.17), since $S_0 = S_1$, $C_{L_0} = C_{L_1}$, and $\sigma_0 = \sigma_1$,

$$V_1 = \sqrt{\frac{W_1}{W_0}} V_0 \quad (11.22)$$

Again from Eqs. (11.16) and (11.18), with $C_{D_0} = C_{D_1}$,

$$P_{r_1} = \left(\frac{V_1}{V_0} \right)^3 P_{r_0} \quad (11.23)$$

Substituting Eq. (11.22) in Eq. (11.23) gives

$$P_{r_1} = \left(\frac{W_1}{W_0} \right)^{3/2} P_{r_0} \quad (11.24)$$

The point V_1, P_{r_1} for the new gross-weight condition may be obtained by simultaneous use of Eqs. (11.22) and (11.24).

The effects of altitude and gross weight are shown in Fig. 11.12. The curves for various altitudes always cross each other as shown, but the curves for various gross weights never cross.

11.6 Representative Power Required. Representation of the airplane polar curve by a true parabola (Fig. 11.13) also allows representation of the power-required curve, making its computation much simpler. Thus, according to Eq. (6.37),

$$D = \left(C_{D_{p_0}} + \frac{C_L^2}{\pi A e} \right) S q$$

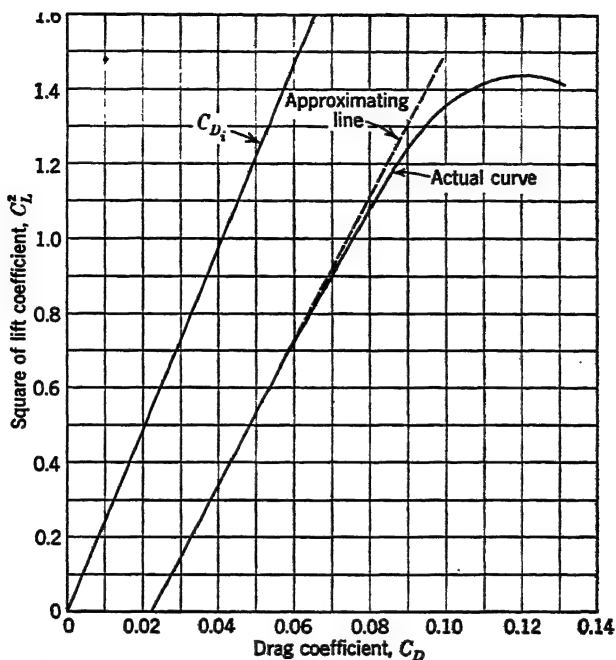


FIG. 11-13. Representative drag curve for an airplane of aspect ratio 7.75 (based on the polar curve of Fig. 11-11).

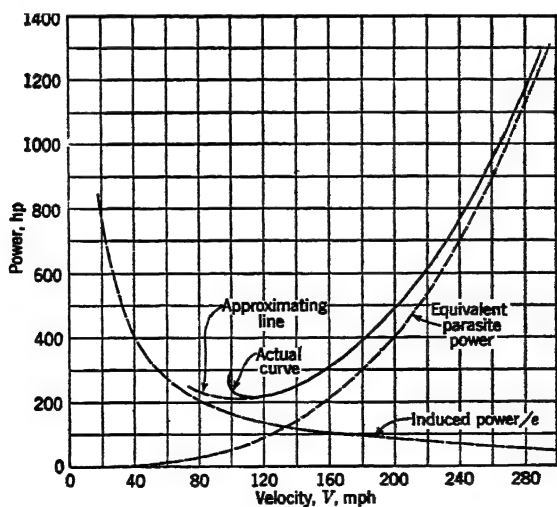


FIG. 11-14. Representative power curves for an airplane of aspect ratio 7.75 (based on the polar curve of Fig. 11-11).

For level flight, $W = L$; thus

$$D = C_{D_p} S q + \frac{W^2}{\pi q b^2 e} \quad (11-25)$$

The product $C_{D_p} S$ occurs frequently in aerodynamic calculations and is called the *airplane equivalent parasite area* (usually shortened to *equivalent parasite area*), designated by the symbol¹ f ; thus

$$D = \frac{f \sigma V^2}{391} + \frac{391 W^2}{\pi \sigma b^2 e V^2} \quad (11-26)$$

Substituting Eq. (11-26) in Eq. (11-8) yields

$$P_r = \frac{f \sigma V^3}{146,600} + \frac{W^2}{3.01 \sigma b^2 e V} \quad (11-27)$$

In Eq. (11-27) the first term may be called the *equivalent parasite power*, and the second term is evidently *induced power* divided by e .

If the equivalent parasite area, gross weight, span, efficiency factor, and altitude of an airplane are known, the horsepower-required equation has the form

$$P_r = K V^3 + \frac{K'}{V} \quad (11-28)$$

where K and K' are constants. Equation (11-28) shows that P_r is composed of two terms, the first of which is a cubic parabola, the second a hyperbola. In Fig. 11-14 the two curves are shown, along with their sum. The P_r curve is not representative at low speed, for the same reason that the parabolic drag-coefficient equation does not fit the actual polar (Fig. 11-13), namely, stalling occurs, which gives a lower limit to the velocity corresponding to $C_{L_{\max}}$ on the polar curve. Since the drag coefficient increases much more rapidly near $C_{L_{\max}}$, than is indicated by the parabolic representation, the actual P_r is much larger near V_s than is indicated by Eq. (11-28).

11-7 Scale and Compressibility Effects. The effect of Reynolds number on C_{D_p} and $C_{L_{\max}}$ of an airplane may best be obtained from wind-tunnel tests on the particular configuration. In the absence of these tests, empirical corrections based on similar airplanes may be used. At any rate, no matter how the variations

¹ There is seldom any ambiguity in the meaning of this symbol, in spite of Eq. (11-6). The above definition of f is quite standardized and is really only a specialization of the previous one.

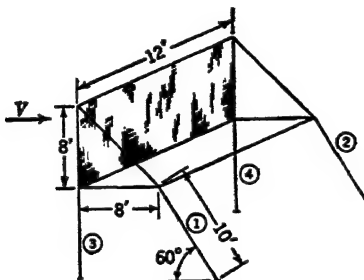
are established, C_D , and $C_{L_{\max}}$ are both fundamental determinants of the shape of the power-required curves, and in order to establish these curves accurately, the change in Reynolds number with change in velocity and altitude must technically be accounted for.

The effect of Mach number on C_D , and $C_{L_{\max}}$ must also be obtained, either measured from wind-tunnel tests or anticipated from tests on similar airplanes. Here again, the change in Mach number associated with changes in velocity and altitude must technically be accounted for.

In subsequent examples and problems in this text, these effects are ignored unless otherwise stated. It is important to realize that these simplifications might involve considerable error in an actual airplane.

PROBLEMS

11-1. A vertical billboard 12 ft long and 8 ft high is supported by members at each end, as shown in the accompanying diagram. Assuming a wind velocity of 65 mph, what compressive force acts in each of the



legs 1 and 2? Assume pin joints throughout, except that legs 3 and 4 are continuous from the ground to the top of the sign. Assume standard conditions. Use Fig. 11-1.

11-2. Find the maximum velocity of descent (mph) of a 200-lb man suspended from a 24-ft-diameter parachute, at sea level. Use Fig. 11-4. Ignore the weight of the parachute and the aerodynamic forces on the man.

11-3. An airplane nacelle has $C_D = 0.005$ based on a wing area of 500 sq ft.

- Find the equivalent flat-plate area a (sq ft).
- Find the equivalent parasite area f (sq ft).
- Find the proper drag coefficient C_{D_p} , if the projected frontal area of the nacelle is 8 sq ft.
- What horsepower is required by this nacelle if it is on an airplane cruising at 200 mph at 19,000 ft?

11-4. A 3400-lb airplane uses 480 hp from its engine at $V_{\max} = 220$ mph at sea level. Propeller efficiency $\eta = 0.85$; wing span $b = 34$ ft; wing area $S = 170$ sq ft. If $C_{D_0} = 0.0090$, find f and C_{D_r} at V_{\max} .

11-5. A two-engined airplane has an NACA 23015 airfoil, gross weight of 5000 lb, stalling speed of 50 mph, aspect ratio of 6, and cruising velocity of 100 mph at sea level. A model is tested at sea level at the airplane cruising C_L but at half the velocity, and the model-fuselage equivalent parasite area f is found to be 0.30 sq ft. The nacelle drag coefficient, based on the model-nacelle cross-sectional area (total for two engines) of 0.36 sq ft, is 0.4. The model scale is 1:5, except for the wing which has one twenty-fifth of the airplane wing area, but has an aspect ratio of 10. Neglect Reynolds number effects on C_{D_0} and C_{D_r} , neglect interference, and assume airplane $C_L = \text{wing } C_L$.

a. What is the plane f at 100 mph?

b. What bhp is required from each engine at cruising C_L if the propeller efficiency $\eta = 0.80$?

c. What is the airplane Reynolds number at 100 mph?

d. What is the model Reynolds number at 50 mph?

11-6. a. Prove that parasite power is equal to induced power divided by e at $(L/D)_{\max}$.

b. Prove that all curves of P_r vs. V for a particular airplane at various altitudes have a common tangent passing through the origin.

c. Consider two lines that pass through the origin and are tangent to curves of P_r vs. V , corresponding to two different weights of a particular airplane. Prove that the slopes of the lines are in the ratio of the respective weights.

11-7. An airplane weighs 70,000 lb and has a wing loading $l_w = 50$ psf. The wing is rectangular with aspect ratio $A = 10$, and has an NACA 23015 airfoil section. The residual drag coefficient $C_{D_r} = 0.0120$ and is independent of C_L (same airplane as in Prob. 6-12).

a. Using the airfoil data shown in Fig. I, Appendix B, plot the curve of P_r vs. V at sea level for the following velocities: $V = 110.5, 115, 125, 150, 200, 250, 300, 350$ mph. (Use 1000 hp = 2 cm or 1 in., and 40 mph = 2 cm or 1 in.)

b. Using $e = 0.80$ from Prob. 6-12, plot induced power divided by e at $V = 150, 250$, and 350 mph.

c. Plot the point for P_r at 16,000 ft at $V = 300$ mph, using the same method as in part a.

d. Plot the complete curve of P_r at 16,000 ft, using the sea-level P_r curve and Eqs. (11-19) and (11-21).

e. Plot the sea-level P_r curve for a 30 per cent increase in weight but the same wing area. Use Eqs. (11.22) and (11.24). Show that the same curve could also be determined approximately using the curve from part b.

f. Plot the sea-level P_r curve for a 30 per cent increase in weight, but with the wing area adjusted to give the same stalling speed as for the original weight. Maintain the same aspect ratio.

11-8. An airplane having a wing with NACA 23015 airfoil section and aspect ratio of 7 is glided *upside down* in a calm at 20,000 ft, at 375 mph. Total airplane $C_D = 0.0220$. The wing has a rectangular plan form and has a span of 37 ft. Glide angle = 12.4 deg. If 200 hp is supplied to the propeller, which has an efficiency $\eta = 0.60$, find

a. The weight of the airplane

b. The residual parasite area f_r at the above speed

Ignore the effect of the thrust on lift and assume cosine of small angles = 1.0.

CHAPTER 12

AIRCRAFT ENGINES

Variations of the characteristics of an engine with rotational speed, altitude, etc., are important because the engine determines, in large measure, the performance of the airplane. There are a great number of possible power-plant combinations involving the use of a reciprocating engine, turbo-jet, ram-jet, and rocket. Analysis of these various combinations for all possible kinds of airplanes, to determine optimum performance, is an unusually formidable study, particularly in view of the possibility of altering the aerodynamic characteristics of the airplane through boundary-layer control. In general, the propeller and reciprocating engine may be regarded as an effective installation for low-speed operation because of its low fuel consumption and good take-off characteristics. The ram-jet and rocket are essentially supersonic devices, because they both have comparatively low efficiencies at low speed. The turbo-jet, turbo-propeller, and ducted propeller are most effective in the intermediate range of air speeds.

Conventional aircraft usually employ either a reciprocating engine or turbo-jet, and it is with these two mechanisms that the present chapter is concerned; the discussion will deal first with reciprocating engines. Frequent reference will be made to the *rating* of the engine. An engine is customarily guaranteed by the manufacturer to operate continuously at *normal rated*¹ power and rpm; it is also guaranteed for short-period operation at greater power and rpm for take-off and military use.

12-1 Unsupercharged Engines. The average pressure differential between the engine cylinder and the atmosphere during the working stroke is called the *mean effective pressure* (mep). The product of this pressure, the area of the piston, the length of

¹ Also called *normal* and *rated*. *Maximum continuous* refers to a special rating used for climbing flight, usually equal to or slightly greater than normal rated power.

stroke, and the rotational speed defines *indicated horsepower* (ihp) of the engine.

$$\text{ihp} = K(\text{mep})LAN \quad (12-1)$$

where ihp is indicated horsepower

K is a constant that depends upon the number of cylinders and type of engine, dimensionless

mep is mean effective pressure, psi

L is length of stroke, in.

A is area of piston, sq in.

N is rotational speed, rpm

The output power of the engine is called *brake horsepower* (bhp), and it is less than ihp because of friction in the engine; thus

$$\text{bhp} = \text{ihp} - \text{fhp} \quad (12-2)$$

where bhp is brake horsepower

fhp is friction horsepower (mainly a function of rpm)

The bhp of a particular engine is thus seen to depend upon the rpm and upon the variables that affect the mean effective pressure, such as rpm, intake manifold pressure, throttle setting, and atmospheric temperature and pressure.

When the engine is operating at a chosen rpm and with full throttle, the mep is almost exactly linearly dependent upon cylinder density, and this relation is reflected in a linear dependence of bhp on atmospheric density according to the following empirical equation:¹

$$P_e = (1.132\sigma - 0.132)P_0 \quad (12-3)$$

where P_e is altitude bhp

P_0 is sea-level bhp

This linear dependence of bhp on σ is the reason why bhp is conventionally plotted against a linear density or σ scale, which implies a nonlinear altitude scale (Fig. 12-1). Equation (12-3) shows that bhp is zero at 55,400 ft; this may be regarded as only

¹ Based on an assumption that fhp is a fixed percentage of sea-level ihp. From GAGG, R. F., and E. V. FARRAR, *Altitude Performance of Aircraft Engines Equipped with Gear-driven Superchargers*, *Trans. SAE*, Vol. 34, pp. 217-223, June, 1934.

approximately true, however, since the data on which the equation was based correspond to relatively low altitudes. Generally, such extreme altitudes are only of academic interest in unsupercharged engines.

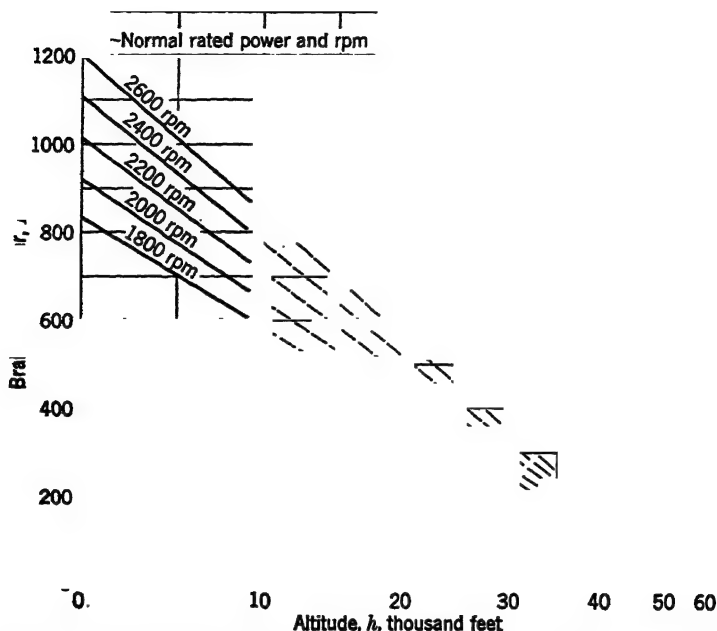


FIG. 12-1. Typical variation of bhp with altitude for an unsupercharged engine.

12-2 Gear-driven Supercharger. A supercharger is essentially an air pump of some sort, used mainly to increase air density and pressure in the intake manifold. A gear-driven supercharger is usually an integral part of the engine and obtains its power directly from the engine crankshaft (Fig. 12-2). The amount of supercharging is therefore directly dependent upon the rpm. For a highly supercharged engine, the tendency to detonate and overheat makes it necessary to operate at part throttle and to take full advantage of the supercharger only at altitude. In Fig. 12-3, point *A* corresponds to the maximum bhp of the engine at sea level, an unattainable value ordinarily, because of the limitations just discussed. Point *B* corresponds to part-throttle operation but at normal rated rpm and bhp. Point *C* corresponds to full throttle with normal rated rpm and bhp. The line *BCD* defines

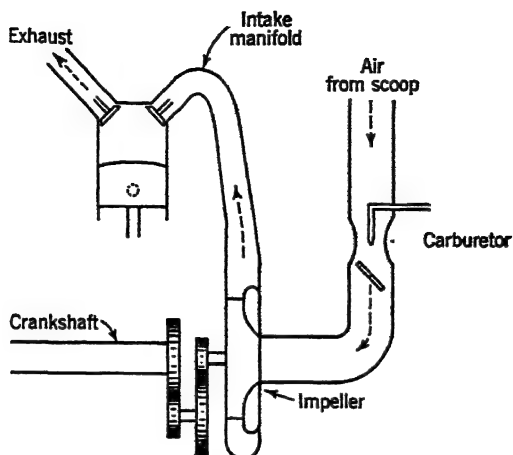


Fig. 12-2. Diagrammatic representation of a gear-driven supercharger installation.

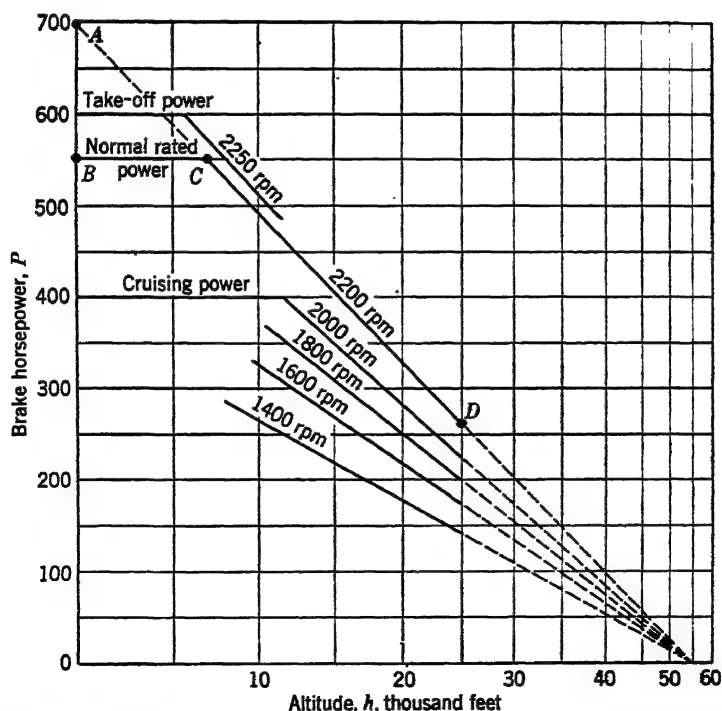


Fig. 12-3. Typical variation of bhp with altitude for an engine equipped with a single-stage, single-speed, gear-driven supercharger.

limits outside of which the engine may not be operated, at either part or full throttle, for any rpm for long periods of time. The altitude corresponding to the break in the curve at point *C* is called the *critical altitude*.

The shape of the curves for a supercharged engine is about the same as for an unsupercharged one, and the same empirical

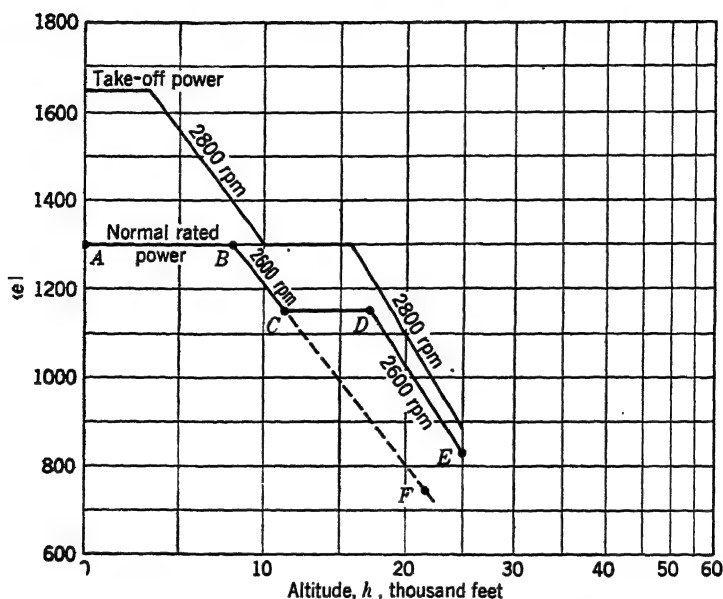


FIG. 12-4. Typical variation of bhp with altitude for an engine equipped with a single-stage, two-speed, gear-driven supercharger.

equation may be applied. It is most conveniently written in terms of the power at the critical altitude.

$$\left(\frac{\sigma - 0.117}{\sigma_c - 0.117} \right) P_c \quad (12.4)$$

where subscripts σ and c refer to conditions above the critical altitude and at the critical altitude, respectively. This equation also shows that the engine bhp is zero at 55,400 ft, as in Eq. (12.3). Equation (12.4) again must be regarded as only an approximation at altitudes approaching 50,000 ft.

Some superchargers are equipped with an alternate gear ratio on the impeller. This *single-stage, two-speed* supercharger has two

critical altitudes, as shown in Fig. 12-4. The low gear ratio is used along *ABC*. At point *C* the high gear ratio is used and allows power along *CDE* instead of along *CF*, which would have been necessary with the low gear ratio. Point *C* corresponds to full throttle and rated rpm for the lower-speed impeller, and part throttle and rated rpm for the high-speed impeller.

An engine may also have two separate gear-driven superchargers, one of which is called the *main stage* and the other the *auxiliary stage*. The latter may also be equipped with alternate impeller ratios. This installation is called a *two-stage, two-speed* supercharger. In some engines, a *variable-speed supercharger* is used to allow control over the amount of supercharging.

12-3 Turbosupercharger. The high-speed, hot, exhaust gases from the engine may be used to drive a turbine to which a con-

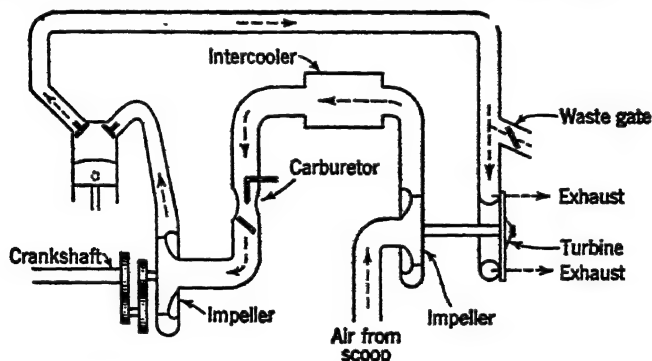


FIG. 12-5. Diagrammatic representation of a turbosupercharger added to the gear-driven supercharger installation of Fig. 12-2.

ventional supercharging impeller is attached. This *turbosupercharger* is not generally a part of the engine but is used as an accessory. It is usually used in conjunction with a gear-driven supercharger. The amount of supercharging derived from the "turbo" then depends upon the opening of the *waste gate* that controls the amount of exhaust gases passing through the turbine. Addition of a turbosupercharger to the engine of Fig. 12-2 is shown in Fig. 12-5, and typical engine characteristics with and without turbosupercharging are shown in Fig. 12-6.

An arrangement in which the turbine is connected directly to the crankshaft instead of to a supercharger is called *compounding*. This procedure is not common, however.

Injection of water into the intake manifold is very effective for increasing the amount of power that may be obtained from an engine, as may be seen in Fig. 12-6. The water reduces the internal cylinder temperature and hence reduces detonating tendencies. It is more effective than gasoline in this respect because it has a considerably higher specific heat and latent heat of vaporization.

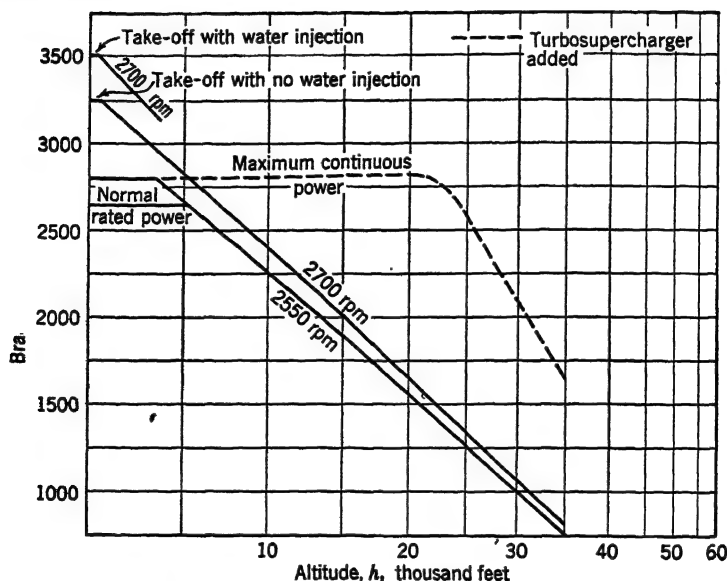


FIG. 12-6. Typical variation of bhp with altitude for an engine equipped with turbosupercharger. (Reproduced by permission from "General Specifications for the Boeing Model 377-10-19 Stratocruiser," Boeing Document 8208.)

The kinetic energy represented by the high-speed exhaust gases of a reciprocating engine, with or without supercharger, may be successfully used to augment the power output by attaching the exhaust manifold to one or more nozzles that eject burned gases rearward. For a given flow of exhaust gases, the thrust obtained in this manner is greatest for the largest exhaust velocity, but the back pressure produced by the reduction in outlet area of the nozzles reduces the bhp of the engine and places a limit on the over-all effectiveness of the arrangement. Power increments obtained in this manner may amount to as much as 15 to 20 per cent, at high speeds.¹

¹ Theory and test results are shown in *WR E-83* and *WR W-43*.

12-4 Fuel Consumption. The fuel required by an engine is usually specified by the *specific fuel consumption*¹ c in pounds per bhp-hr. The mixture of fuel and air going into the engine is called *lean* or *rich*, according to whether the ratio of fuel to air is relatively low or high. A lean fuel mixture is used for economy in low-speed operation, whereas a rich mixture is usually used in high-speed operation to prevent overheating of the engine. Specific fuel consumption is tabulated or plotted as a function of bhp and rpm on the performance charts supplied by the engine manufacturer (Fig. II, Appendix B). In general, it may be assumed independent of altitude unless otherwise specified by the manufacturer.

12-5 Jet Propulsion. A jet-propulsion device is fundamentally a tube into which fuel is injected to mix with air so as to eject hot

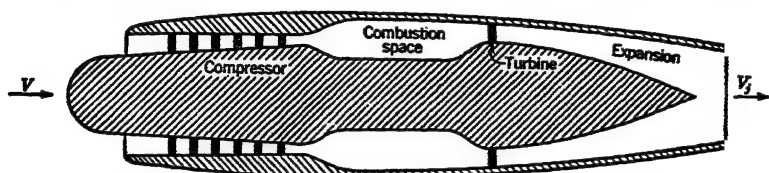


FIG. 12-7. Diagram showing the principal elements of a turbo-jet.

gases at high velocity and hence produce a thrust. The simplest device is an *athodyd* (aero-thermo-dynamic-duct), or ram-jet. It contains no moving parts and cannot be used unless the relative velocity supplies enough *ram* to compress the fuel and air within the tube, to permit their combustion. The more familiar device is the *turbo-jet*, consisting of a compressor, combustion space, and gas turbine contained within the tube as in Fig. 12-7. The compressor and turbine are connected to a common shaft; the mechanical simplicity of the device is at once apparent.

Thrust may be expressed by the conventional equation, ignoring the small influence of fuel flow:

$$T = \frac{W_a}{g} (V_j - V)(1.467) \quad (12-5)$$

where T is net thrust, lb

W_a is air flow, lb per sec

V_j is relative jet velocity, mph

V is relative intake velocity, mph

¹ More properly called *brake specific fuel consumption*.

Equation (12-5) is also written

$$T = 1.467 \frac{W_a}{\tau} V_j - 1.467 \frac{W_a}{\tau} V \quad (12-6)$$

where the first term on the right is called *gross thrust* and the second term is called *ram drag*. While the ram drag reduces the

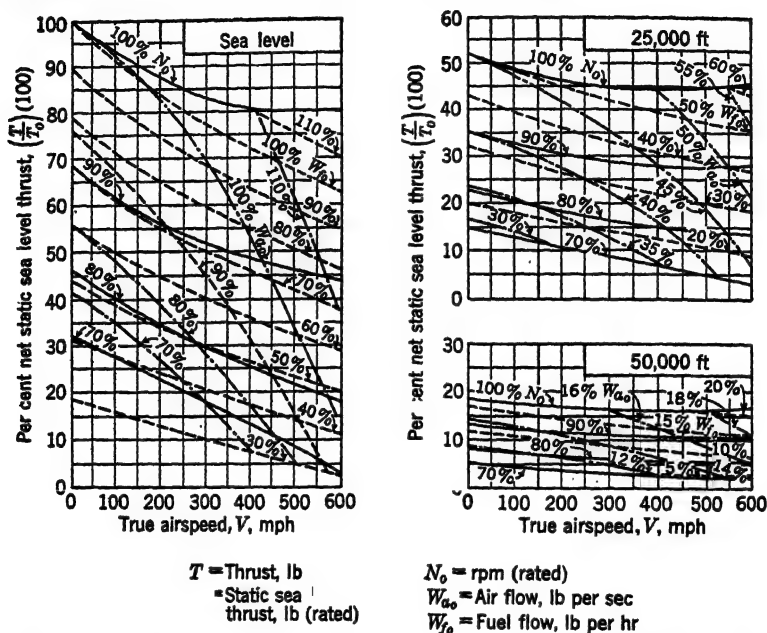


FIG. 12-8. Typical turbo-jet operating characteristics. (Reproduced by permission from *Contemporary Jet-Propulsion Gas Turbines for Aircraft*, by D. F. Warner and E. L. Auyer, in *Mechanical Engineering*, November, 1945.)

thrust of the jet unit, the ram on the intake does assist in the compression of the combustible mixture. The air flow, fuel flow, and thrust are all predictable theoretically as functions of rpm, air speed, and altitude by dimensional analysis,¹ and the agreement with experimental evidence is good within the limits of the assumptions involved. In Fig. 12-8, the thrust T , rpm N , fuel flow W_f , and air flow W_a of a turbo-jet are presented in the form of percentages of sea-level static (zero-speed) conditions for three altitudes. These curves are not to be regarded as perfectly

¹ KERN, D. J., and D. R. SHOULTS, Jet Propulsion and Its Application to High Speed Aircraft, *JAS*, August, 1946.

general, because the characteristics are a function of many variables, such as the pressure and temperature attained with the compressor, exhaust temperature and velocity, friction in the system, etc., but they are representative of a typical installation.

Example. Find the characteristics of a turbo-jet at 25,000 ft, for 9000 rpm and 400 mph true air speed. The static sea-level (rated) values are $T_0 = 5000$ lb, $N_0 = 10,000$ rpm, $W_{a_0} = 80$ lb per sec, $W_{f_0} = 5000$ lb per hr.

Solution. From Fig. 12-8, at 25,000 ft altitude and 400 mph, $(T/T_0)(100) = 28$, $W_a = (45\%)(W_{a_0})$, $W_f = (37\%)(W_{f_0})$, hence

$$\begin{aligned} T &= (0.28)(5000) = 1400 \text{ lb} \\ W_a &= (0.45)(80) = 36 \text{ lb per sec} \\ W_f &= (0.37)(5000) = 1850 \text{ lb per hr} \end{aligned}$$

The significance of the curves in Fig. 12-8 will not be fully appreciated until Art. 14-11, where airplane performance with a turbo-jet is discussed.

PROBLEMS

12-1. Prove Eq. (12-3) using the following assumptions:

1. Friction horsepower is independent of altitude.
 2. The ratio of fhp to ihp at sea level is 0.117.
 3. Indicated horsepower is directly proportional to σ .
 4. Friction horsepower and ihp are both directly proportional to rpm.
- 12-2.** Develop Eq. (12-4), using Eq. (12-3).

12-3. An engine has a single-stage, single-speed, gear-driven supercharger with critical altitude $h_c = 10,000$ ft. Assuming power varies linearly with rpm at constant altitude, find the altitude h_* for which $P_* = 0.75 P_c$ and $N_* = 0.90 N_c$, where subscripts σ and c correspond to altitudes h_* and h_c , respectively.

12-4. An airplane flying at 400 mph is equipped with a reciprocating engine and has its exhaust manifold connected to nozzles ejecting rearward to obtain propulsion from the exhaust jets. Engine power $P = 2000$ bhp. Fuel consumption $c = 0.5$ lb per bhp-hr. Fuel/air ratio = 1:15 by weight. Jet velocity relative to the airplane, $v_{j_1} = 1000$ fps. Find the thrust increment (lb) and increase in thrust horsepower expressed as per cent of engine bhp. Assume exhaust was ejected perpendicular to remote-velocity vector before installation of nozzles.

CHAPTER 13

PROPELLERS

All aerial propulsion devices operate on the same principle, namely, to change the momentum per second of air or gases in order to produce thrust, in accordance with Newton's second law of motion. Some devices continually admit air and discharge air; some continually admit air and discharge air along with products of combustion; and some admit nothing and discharge only products of combustion. The conventional propeller uses a large mass flow of air and gives it a small velocity increment; the turbo-jet and ram-jet use a small mass flow of air and give it and the products of combustion a large velocity increment. The rocket gives the products of combustion a large velocity increment. Some other devices use combinations of these methods.

Characteristics of the conventional reciprocating engine and the turbo-jet have been reviewed in Chap. 12; in this chapter the aerodynamic characteristics of propellers will be investigated. All discussions are limited to the characteristics of a propeller in combination with a reciprocating engine.

13-1 The Ideal Propeller. An actual propeller influences air in front, behind, and around the propeller disk¹ in varying degrees. It has tip vortices and variable down-wash distribution like a wing; moreover, each blade section acts at a radius that is different from an adjacent section, making it have a different relative velocity. These and other complications make the mathematical prediction of propeller characteristics very tedious and their accuracy subject to some question. As in most aerodynamic work, the results of calculations must always be checked by experimental evidence; indeed, the mathematical analyses are frequently useful only for predicting general trends.

As an introduction to propeller theory it is customary to circumvent these difficulties by considering an "ideal" propeller that consists of a tube containing the propeller disk, within which

¹ The propeller disk is the circular area swept by the propeller blades.

the air is assumed to accelerate. This procedure reduces the propeller to its simplest form, because the velocity is assumed evenly distributed across the tube and no rotational component is considered. The ideal propeller is, therefore, a device that is capable of inserting energy in the stream by increasing its total pressure, but without any of the friction or vortices, etc., that are usually associated with the losses of an actual propeller.

In Fig. 13-1, the remote velocity is v , and the corresponding static pressure is p_1 . The downstream velocity is $v(1+b)$, and the corresponding static pressure is p_4 . The thrust equation may be obtained from momentum or

inertia considerations, provided the downstream station is so far removed from the propeller that $p_4 = p_1$.

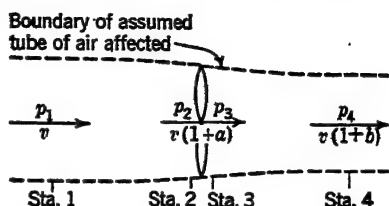


FIG. 13-1. Representative circular tube of air affected by an ideal propeller.

$$T = (M)(bv) \quad (13-1)$$

$$\begin{aligned} &= [\rho A v(1+a)]bv \\ &= \rho A v^2(b+ab) \end{aligned} \quad (13-2)$$

where M is mass per second of fluid flow. The thrust may also be obtained from the difference in static pressures before and behind the propeller disk:

$$T = (p_3 - p_2)A \quad (13-3)$$

where A is the propeller disk area. The Bernoulli equation may be written between stations 1 and 2 and between stations 3 and 4, because total pressure is constant before and also behind the propeller, although it is not constant through the propeller disk.

$$p_2 + \frac{1}{2}\rho v^2(1+a)^2 = p_1 + \frac{1}{2}\rho v^2 \quad (13-4)$$

$$p_3 + \frac{1}{2}\rho v^2(1+a)^2 = p_4 + \frac{1}{2}\rho v^2(1+b)^2 \quad (13-5)$$

Equation (13-4) is subtracted from Eq. (13-5) with due regard for the fact that $p_4 = p_1$.

$$\begin{aligned} p_3 - p_2 &= \frac{1}{2}\rho v^2[(1+b)^2 - 1] \\ &= \frac{1}{2}\rho v^2(2b + b^2) \end{aligned} \quad (13-6)$$

Equation (13·6) may be substituted in Eq. (13·3), giving

$$T = \frac{1}{2}\rho v^2 A(2b + b^2) \quad (13\cdot7)$$

Equation (13·7) may be equated to Eq. (13·2); hence,

$$a = \frac{b}{2} \quad (13\cdot8)$$

Equation (13·8) shows that half the increment in velocity occurs in front, and that half occurs behind the propeller.

The efficiency is obtained in conventional fashion from the ratio of output to input power.

$$\eta = \frac{\text{output power}}{\text{input power}}$$

The output power, or useful work per second, is the product of the thrust and the remote velocity, whereas the input power, or input work per second, is the product of the thrust and the disk velocity;¹ hence

$$\eta = \frac{Tv}{Tv(1 + a)} \quad (13\cdot9)$$

$$\frac{1}{1 + a} \quad (13\cdot10)$$

The ideal efficiency may be estimated for an airplane in level flight by equating thrust and drag; hence, from Eqs. (13·7) and (13·8),

$$T = \frac{1}{2}\rho v^2 A(4a + 4a^2) \quad (13\cdot11)$$

and, from Eq. (5·2),

$$D = C_D \frac{1}{2}\rho v^2 S \quad (13\cdot12)$$

From Eqs. (13·11) and (13·12),

$$a^2 + a = \frac{C_D S}{4A} \quad (13\cdot13)$$

Completing the square, expressing the disk area A in terms of the propeller diameter D , and solving for a yields

$$a = \sqrt{\frac{1}{4} + \frac{C_D S}{\pi D^2}} - \frac{1}{2} \quad (13\cdot14)$$

¹ Input power may be obtained by other methods (see Prob. 13·1).

Substituting Eq. (13-14) in Eq. (13-10) gives

$$\eta_i = \frac{1}{\frac{1}{2} + \sqrt{\frac{1}{4} + (C_D S, \pi D^2)}} \quad (13-15)$$

Equation (13-15) shows a good deal about the characteristics of an ideal propeller. First, consider a particular airplane flying at some arbitrary speed: since C_D and S are constant, the largest possible diameter of the propeller gives maximum ideal efficiency. Of course, clearance limitations are imposed on an actual propeller, but within these limitations, the largest propeller is best. Next consider a particular airplane of fixed wing area and propeller diameter. The equation shows that the highest efficiency is obtained at highest speed (minimum C_D); conversely the lowest efficiency is obtained at low speed. On an actual airplane, these conclusions are not entirely true, being dependent upon the design of the propeller and upon effects of viscosity and compressibility, but the equation is of interest because it does indicate a trend. The ideal efficiency is the maximum attainable and is valuable because it shows regions in which a practical propeller falls short of the ideal.

In the absence of experimental data, the factor b may be used to estimate slip-stream velocity. It is useful, for instance, in predicting the velocity increment on a tail acting in the slip stream of a propeller.

13-2 The Simple Blade-element Theory. An actual propeller consists of a number of *blades* of airfoil section. *The simple blade-element theory* considers each blade to be composed of an infinite number of elements having span dr and width b (Fig. 13-2). The combination of the rotational velocity of the propeller and the remote velocity of the airplane causes a relative velocity on each element that depends upon its radius r from the axis of the propeller. In Fig. 13-3, an element is shown in cross section, with propeller rotational velocity $2\pi n$,¹ airplane remote velocity v , and blade angle β . The relative velocity v_r forms an angle α with the chord of the section just as on an airfoil, except that the chord of a propeller section is usually defined by the tan-

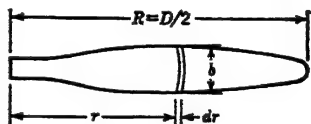


FIG. 13-2. Propeller blade showing element b by dr .

¹ The symbol n is used to designate rps. The symbol N designates rpm.

gent to the relatively flat lower surface. Differential lift and drag force vectors are shown in conventional form, perpendicular and parallel to the relative-velocity vector v_r . The angle ϕ is the difference between β and α .

The differential lift and drag are combined to form a resultant dR , then are resolved again into two vectors, dT and dF , parallel

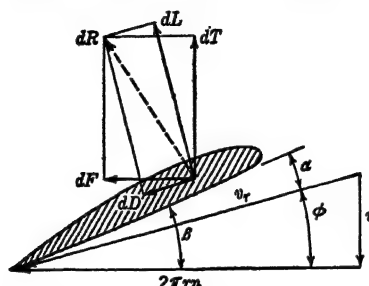


FIG. 13-3. Angle and force relations on a blade element.

and perpendicular to the axis of rotation of the propeller. The former is the differential thrust, and the latter is the differential torque force.

The total thrust T is obtained by integrating the differential thrust force:

$$T = B \int_0^R dT \quad (13-16)$$

where B is the number of blades. The torque Q is obtained by integrating the product of the torque force and the radius at which it acts:

$$Q = B \int_0^R r dF \quad (13-17)$$

Equations (13-16) and (13-17) cannot be integrated until dT and dF are found as functions of r . Determination of the functions involves a great deal of labor and is beyond the scope of this book.¹

Efficiency of the propeller may be expressed by

$$\frac{Tv}{2\pi nQ} \quad (13-18)$$

$$\frac{Tv}{550P} \quad (13-19)$$

¹ For a complete but elementary treatment, see W. C. Nelson, "Airplane Propeller Principles," Wiley, New York, 1944.

where P is input horsepower to the propeller or output bhp of the engine. Of course, the efficiency given by Eqs. (13-18) or (13-19) must always be less than the ideal efficiency given by Eqs. (13-10) or (13-15). (See Prob. 13-4b.)

13-3 Thrust Coefficients. Propeller coefficients may be developed similarly to wing coefficients, with thrust coefficients corresponding to the wing lift coefficient, and torque and power coefficients corresponding to the drag coefficient; thus,

$$T = T_c \rho v^2 D^2 \quad (13-20)$$

where T is thrust, lb

T_c is thrust coefficient, dimensionless

ρ is mass density, slug per cu ft

v is velocity, fps

D is propeller diameter, ft

The square of the diameter is used to make the thrust coefficient dimensionless; propeller blade area could have been used just as well, but the square of the diameter accomplishes the same purpose and is far more convenient. The $\frac{1}{2}$ is deleted because dynamic pressure has less significance in propeller analyses than in airfoil calculations.

The thrust coefficient could be plotted vs. angle of attack as in presenting airfoil characteristics; however, the angle of attack is variable along the blade, and hence a reference angle would be needed. The angle of attack at the tip could be used, but this would require knowing β , v , R , and n for its solution. A more convenient variable might be ϕ , because for a particular β , ϕ defines α . This angle is easily defined by knowing v , R , and n .

$$\phi = \tan^{-1} \frac{v}{\pi n D} \quad (13-21)$$

Still simpler, however, is to use v/nD . This parameter is called the *advance ratio* J .

$$J = \frac{v}{nD} \quad (13-22)$$

or

$$J = \frac{88V}{ND} \quad (13-23)$$

It usually appears in propeller charts as the variable against which

the efficiency and the propeller coefficients are plotted, just as α is used for presentation of airfoil characteristics. There is a fundamental difference, however, because the characteristics of a propeller are defined, not only by J , but also by β . The reference β for a propeller is usually chosen to correspond to the three-quarter radius.

Equation (13-20) shows thrust as a function of velocity. Another equation may be developed that is independent of velocity but dependent on rpm, by defining a new coefficient

$$C_T = T_c \left(\frac{v}{nD} \right)^2$$

Therefore,

$$\begin{aligned} T &= C_{Tp} v^2 D^2 \left(\frac{nD}{v} \right)^3 \\ &= C_{Tp} n^2 D^4 \end{aligned} \quad (13-24)$$

The thrust coefficient C_T is dimensionless, as was T_c , because v/nD is dimensionless (see again Prob. 2-15). Equation (13-24) is the customary equation used for defining propeller thrust. Curves of C_T vs. J for various β may be seen in Figs. IIIb and IVd, Appendix B. Equation (13-24) may be expressed in more convenient units

$$T = \frac{6.61}{10^7} C_{T\sigma} N^2 D^4 \quad (13-25)$$

13-4 Power Coefficients. Power coefficients may be developed in a manner similar to that used for thrust coefficients. Power input¹ to the propeller is

$$p = 2\pi nQ$$

where Q is the torque. By similarity with Eq. (13-24)

$$Q \propto \rho n^2 D^5$$

Therefore

$$\begin{aligned} p &\propto \rho n^3 D^5 \\ p &= C_{P\rho} n^3 D^5 \end{aligned} \quad (13-26)$$

where C_P is the power coefficient. In more convenient units

$$P = \frac{2}{10^{11}} C_{P\sigma} N^3 D^5 \quad (13-27)$$

¹ Throughout the text, p is used for power in foot-pounds per second, while P is used for power in horsepower.

Curves of C_P vs. J are shown in Figs. IIIb and IVc, Appendix B.

A second power coefficient that is independent of diameter is defined as follows:

$$C_s = \sqrt[5]{\frac{1}{C_P} \frac{v}{nD}}$$

$$C_s = \sqrt[5]{\frac{\rho n^3 D^5}{p} \frac{v}{nD}}$$

$$\sqrt[5]{\frac{\rho}{pn^2} v} \quad (13-28)$$

In more convenient units,

$$C_s = \frac{0.638 V \sigma^{1/2}}{P^{1/5} N^{1/5}} \quad (13-29)$$

This coefficient is called the *speed-power coefficient*, and Fig. V, Appendix B, may be used for its solution. It is shown as a function of J in Figs. IIIa and IVa, Appendix B.

13-5 Propeller Efficiency. Propeller efficiency may be expressed as

$$\eta = \frac{Tv}{p} \quad (13-30)$$

Substituting from Eqs. (13-24) and (13-26) yields

$$\eta = \frac{(C_T \rho n^2 D^4) v}{C_P \rho n^3 D^5}$$

$$= \frac{C_T}{C_P} J \quad (13-31)$$

Since C_T and C_P are both functions of J , η is also a function of J as shown in Figs. IIIa and IVb, Appendix B.

Example. The following data are given for the four-bladed propeller of Fig. IV, Appendix B: engine rpm = 2400, gear ratio = 0.475, $\beta = 40$ deg, $v = 352$ fps, $\sigma = 0.6$, bhp = 1500 hp.

a. Find C_s using Eq. (13-29).

b. Find J , η , C_P , and C_T from Fig. IV, Appendix B.

c. Check the results of b by Eq. (13-31).

Solution. a. The propeller rpm is obtained as

$$N = (2400)(0.475) = 1140 \text{ rpm}$$

and the velocity is

$$V = \frac{352}{1.467} = 240 \text{ mph}$$

From Fig. V, Appendix B,

$$P^{1/2} = 4.32$$

$$\sigma^{1/2} = 0.903$$

$$N^{1/2} = 16.7$$

Using Eq. (13-29) gives

$$C_s = \frac{(0.638)(240)(0.903)}{(4.32)(16.7)} = 1.92$$

b. From Fig. IV, Appendix B, at $C_s = 1.92$ and $\beta = 40$ deg: $J = 1.51$, $\eta = 0.83$, $C_P = 0.290$, $C_T = 0.158$.

$$c. \quad \eta = \left(\frac{0.158}{0.290} \right) (1.51) = 0.822$$

The slight discrepancy in η arises from the fact that the curves are faired from experimental data.

13-6 Comparison of Propeller and Airfoil Characteristics.

While the curves of C_L and C_D vs. α have physical significance to an engineer because of the natural association of these coefficients with their corresponding forces, the physical interpretation of propeller coefficients in relation to the forces on the propeller blades is more complex and is frequently obscure. Certainly the coefficients, when multiplied by the proper variables, give the correct thrust and power, but the significance of the shape of the curves is not immediately apparent.

As an aid to understanding and remembering the significance of the curves, three statements may be made, without proof. The statements are not accurate for large β .

1. The curve C_T vs. J for a particular β corresponds approximately to a curve of C_L vs. $\beta - \alpha$ for the basic blade section; i.e., the C_T curves are essentially C_L curves plotted "backwards." In Fig. 13-4, the thrust curves are approximately linear; also when $C_T \rightarrow 0$, $C_L \rightarrow 0$, and when $C_T \rightarrow C_{T_{\max}}$, $C_L \rightarrow C_{L_{\max}}$.
2. The curve of η vs. J for a particular β corresponds very approximately to a curve of $(L/D)(J)$ vs. $\beta - \alpha$; i.e., the efficiency curves are similar to curves of L/D that have been plotted "backwards" like the C_T curves and made to pass through the origin. In Fig. 13-5, when $\eta \rightarrow 0$ at high J , $L/D \rightarrow 0$ at low α , and when $\eta \rightarrow 0$ at low J , $L/D \rightarrow 0$ at high α ; furthermore when $\eta \rightarrow \eta_{\max}$, $L/D \rightarrow (L/D)_{\max}$.

3. The curves of C_P and C_s vs. J cannot be related simply to the conventional airfoil curves, but their shape is determined in part by the curve of C_D vs. α .

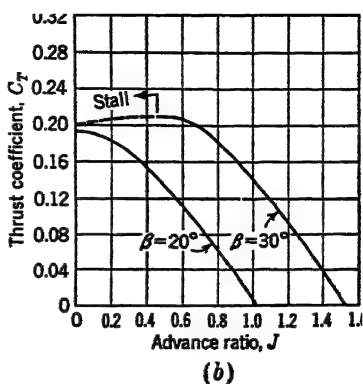
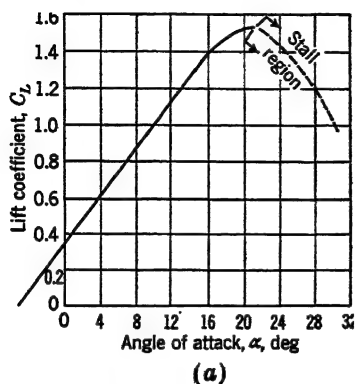


FIG. 13-4. Curves used to demonstrate the relation between airfoil and propeller variables: C_L and C_T .

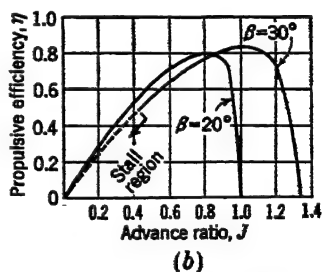
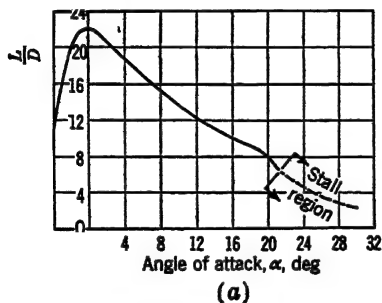


FIG. 13-5. Curves used to demonstrate the relation between airfoil and propeller variables: L/D and η .

The propeller parameters are therefore related to their airfoil counterparts according to the following table:

COMPARATIVE COEFFICIENTS AND PARAMETERS FOR AIRFOILS AND PROPELLERS

Propeller characteristic	Airfoil characteristic
J and ϕ	α
η	$\frac{L}{D}$
C_T	C_L
C_P and C_s	C_D

13.7 Propeller Geometry. The plan form of a propeller is defined by both aerodynamic and structural considerations. The low-speed propeller conventionally has a maximum width at about the 50 per cent radius that tapers toward the tip (Fig. 13.2). Propellers designed for large power absorption have relatively wide blade tips. The capability of a propeller to absorb a given amount of bhp is sometimes specified by a *solidity factor* (ratio of total blade area to propeller disk area), but this factor does not account for variations in blade width along the blade span; *i.e.*, two propellers may have the same solidity, but if one has most of its blade area at the root while the other has most of its area at the tip, their capacities for absorbing power will be widely different. This has led to the development of another parameter, called the *activity factor* (AF),¹ defined as follows:

$$AF = \frac{100,000}{16} \int_{0.2}^{1.0} \left(\frac{b}{D}\right) \left(\frac{r}{R}\right)^3 d\left(\frac{r}{R}\right) \quad (13.32)$$

where AF is activity factor, dimensionless

b is blade width at radius r , ft

R is propeller radius, ft

D is propeller diameter, ft

$\frac{100,000}{16}$ is constant inserted to give activity factor a convenient magnitude

The activity factor is derived from the fact that power absorbed by a blade element is proportional to its differential area and to the cube of the local velocity. The differential area is $b \, dr$, and the local velocity is approximately proportional to the radius; thus the differential power is proportional to the cube of the radius, the first power of the blade width, and the differential radius. The activity factor refers to a single blade and has a value ranging from about 60 to 110 for conventional propeller blades.

Compressible effects that occur on a propeller depend upon the blade section, angle of attack, and relative Mach number, in the same way as for an airfoil. The reduction in section lift coefficient and increase in section drag coefficient, which are characteristic of compressibility shock, cause a reduction in L/D and hence produce a reduction in η of the propeller. This is indicated

¹ Suggested by F. M. Thomas, F. W. Caldwell, and T. B. Rhines, Practical Airscrew Performance Calculations, *JRAS*, January, 1938.

by an efficiency correction factor F_η , by which η from the propeller charts must be multiplied.

The compressibility phenomena on a propeller are, of course, more complex than those on an airfoil. Of primary importance is the fact that the blade thickness is a function of the radius; hence while the tip section is the first to reach its critical Mach number at low forward speeds of the airplane, the root section may be first to reach its critical Mach number at high forward speeds of the airplane. This and other influences make the estimation of compressible effects on a particular propeller unusually difficult. The efficiency correction factor is usually assumed to be primarily a function of tip Mach number, but the tip Mach number is specified indirectly by an *effective helical tip speed*. This is obtained by computing the helical tip speed of the propeller that would have the same Mach number at standard sea-level conditions as the propeller does under its actual conditions. For instance, in Fig. VI, Appendix B, a propeller having $D = 12$ ft, $N = 1200$ rpm, and $V = 400$ mph at 20,000 ft has a true helical tip speed

$$\begin{aligned} v_r &= \sqrt{[(400)(1.467)]^2 + [(\pi)(12)(20)]^2} \\ &= 958 \text{ fps} \end{aligned}$$

and an effective helical tip speed

$$\begin{aligned} v_{r_{\text{eff}}} &= \frac{958}{0.929} \\ &= 1032 \text{ fps} \end{aligned}$$

The variation in F_η with effective helical tip speed depends upon all the geometric characteristics of a propeller. Many attempts have been made to reduce the great number of variables to a minimum, but at present there are insufficient test data to indicate accurate trends. The curve marked "Representative lower limit" will be used in all problems and examples in this text, because it is probably conservative for most conventional propellers operating at low airplane speeds. For the above example, F_η is therefore 0.931.

Large compressibility effects may be circumvented by choosing a lower gear ratio (if the engine has more than one available), by increasing the number of blades, by using a blade with a larger

activity factor, by using a blade section that has a higher critical Mach number, or by putting sweepback in the blade.

Compressibility shock frequently occurs on the blunt shank of the propeller. This may be delayed by using a *cuff*, which consists of an airfoil-shaped sheet that surrounds the shank and reduces its per cent thickness. The cuff is also sometimes used to increase cooling air flow through the nacelle.

13-8 Choice of Propeller Diameter. A propeller may be selected to give maximum efficiency at the high-speed condition or at the cruising condition, etc. For preliminary discussion, the design may conveniently be restricted to the condition of maximum speed. It may be assumed that the curve of P_r vs. V for the airplane is known and that the rated bhp and rpm for the engine are known. The problem consists of determining the optimum propeller diameter and blade angle. The process is one of trial and error; the following steps may be utilized:

1. Assume η . (For high-speed design choose 2 per cent less than the maximum possible value shown on the propeller chart.)
2. Calculate horsepower available, P_a .
3. Since $P_a = P_r$, get V_{\max} from curve of P_r vs. V .
4. Calculate C_s , using Fig. V, Appendix B.
5. From a plot of C_s vs. J for various β , find β and J for η_{\max} by intersection with "Line of maximum efficiency" curve.
6. From a plot of η vs. J for various β , find η . It will be on the envelope of the curves and will be the maximum η for the computed C_s .
7. From the J of step 5, compute the propeller diameter $D = (88V)/(NJ)$.
8. Correct the efficiency of step 6, using Fig. VI, Appendix B. Corrected $\eta = (F_\eta)(\eta_{\text{chart}})$.
9. If η from step 8 checks η from step 1 within 0.5 per cent, use the value from step 8; otherwise repeat steps 1 to 8 with the η from step 8 as the second assumed value.

The propeller diameter chosen in this manner gives the maximum possible speed at the particular altitude for which the analysis is made. It is frequently advisable to design for some other condition, because the high-speed design gives relatively poor take-off and climbing characteristics of the airplane. Thus

a small sacrifice in high speed often gives a very large benefit at low speed. On the other hand, the weight of a propeller and landing gear increase with increasing propeller diameter; hence a diameter slightly less than that indicated by the preceding analysis might be more desirable.

The particular analysis given is the same whether a *fixed-pitch* or *constant-speed* propeller is used. A fixed-pitch propeller consists of blades that are rigidly attached to the hub so that a

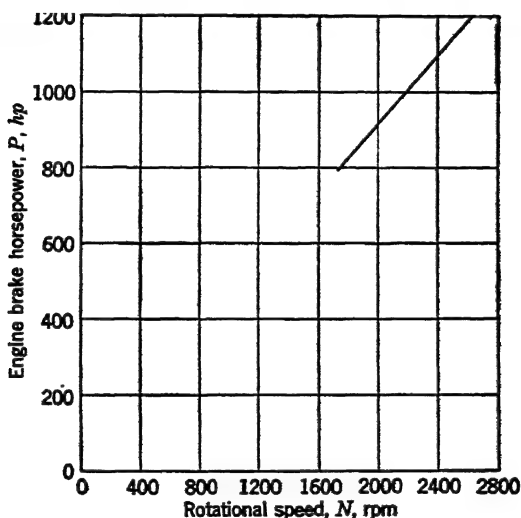


FIG. 13-6. Sea-level full-throttle power characteristics for the engine of Fig. 12-1.

constant blade angle¹ is maintained for all flight conditions. The constant-speed propeller has blades that change blade angle automatically so as to maintain the constant speed (rpm) that has been selected by the pilot.

Propeller data are usually obtained from wind-tunnel tests and must be used with caution if accurate results are expected. The propeller charts are actually applicable only to the particular configuration used in the tests. Therefore, for instance, if the propellers were run in front of a single nacelle in the absence of a wing, the effect of slip stream on the wing, fuselage, and tail should technically be accounted for by a separate calculation,

¹ The blade angle of a propeller is variable from root to tip; however, for comparison of various propellers, the blade angle at the three-quarter radius is usually used as a reference. It is in this latter sense that the word is used here.

resulting either in a change in propeller efficiency or a change in airplane drag characteristics. In this text all such effects are ignored.

13-9 Power Available. After the number of blades, activity factor,¹ and diameter of the propeller have been chosen, the power available,² P_a , from the propeller-engine combination may be obtained for any velocity and any altitude. In the following analyses, fixed-pitch and constant-speed propellers will be considered separately.

Fixed-pitch Propeller. The determination of sea-level power available for a fixed-pitch propeller is somewhat simplified if the curve of bhp vs. propeller rpm is represented by a straight line passing through the origin (Fig. 13-6). The error involved is always very small; hence

$$P = KN \quad (13-33)$$

where K is constant

N is propeller rpm

Substituting Eq. (13-33) in Eq. (13-27) yields

$$C_P = \frac{10^{11}K}{2N^2D^5\sigma} \quad (13-34)$$

C_P is thus seen to be a function only of the propeller rpm. The velocity and power available may be found in the following manner:

1. Assume a value of J .
2. Read C_P and η from the propeller charts for the design β .
3. Compute N from Eq. (13-34)

$$N = \sqrt{\frac{10^{11}K}{2D^5\sigma C_P}}$$

4. Compute V from Eq. (13-23)

$$V = \frac{JND}{88}$$

5. Correct η for tip speed.
6. Compute $P_a = \eta P = \eta KN$.

¹In this text, data are not given for various activity factors in order to simplify explanations.

²Power available usually implies the use of rated power of the engine at the particular altitude considered.

If the above steps are carried out in tabular form for several assumed values of J , several points may be established to construct a curve of P_a vs. V . This curve is conventionally superimposed on the curve of P_r , as in Fig. 13-7. The difference in power between the curves is called *excess horsepower*, and it will be shown later to be usable for climbing.

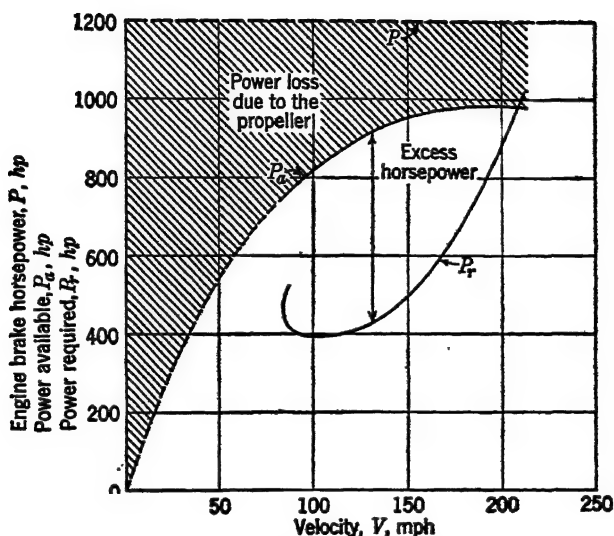


FIG. 13-7. Typical curves of power required by an airplane and power available from the propeller, with superimposed curve of engine-brake horsepower.

Altitude unsupercharged performance may be obtained in a similar manner except that K , σ , and the tip-speed correction are all changed. If no engine curves are available to show power variation with altitude, Eq. (12-3) may be used for estimation.

Use of a supercharger with a fixed-pitch propeller is not common, because the propeller cannot use all the power of the engine. This provides one of the principal arguments for using a constant-speed propeller, because it is adaptable to large changes in power through changes in blade angle.

Constant-speed Propeller. The choice of propeller diameter by the method of Art. 13.8 is the same for fixed-pitch and constant-speed propellers. Determination of power available for all velocities is very simple for a constant-speed propeller because

rpm and bhp are constant; hence, from Eqs. (13-23) and (13-29),

$$J = K_1 V$$

$$C_s = K_2 V$$

Therefore

$$\frac{J}{C_s} = K_3 \quad (13-35)$$

where K_1 , K_2 , and K_3 are constants. On a graph of C_s vs. J , a straight line from the origin defined by K_3 , allows reading of η for any chosen J , from which P_a and V may be calculated, after making the necessary tip-speed corrections.

A second, simpler method involves use of a chart showing η vs. J with C_P as a variable (Figs. IIIc and IVe, Appendix B). Since C_P is constant for a constant-speed propeller, η may be read directly from this chart for any J or V . It is interesting to note that since

$$P_a = \eta P \propto \eta$$

and

$$V = \frac{JND}{88} \propto J$$

the curve of η vs. J , for a particular C_P , may be regarded as an indication of the shape of the P_a vs. V curve.

Example. A two-engined airplane has three-bladed propellers of 10-ft diameter. Find the power available at 250 mph at 15,000 ft where the normal rated power and rpm are 800 hp and 2500 rpm, respectively, per engine. Gear ratio = 0.5.

Solution. From Eqs. (13-27) and (13-23),

$$C_P = \frac{10^{11} P}{2\sigma N^3 D^5} = \frac{(10^{11})(800)}{(2)(0.629)(1250)^3(10)^5} = 0.326$$

$$J = \frac{88V}{ND} = \frac{(88)(250)}{(1250)(10)} = 1.76$$

From Fig. IIIc, Appendix B, using $C_P = 0.326$ and $J = 1.76$: $\eta_r = 0.78$. From Fig. VI, Appendix B, $F_v = 1.0$; hence $\eta = 0.78$, and thus $P_a = 1248$ hp.

PROBLEMS

13-1. Prove input power to an ideal propeller is $P_{\text{input}} = T v (1 + a)$ by

a. Considering the kinetic energy per second entering and leaving the propulsion unit.

b. Considering input power to be the sum of the power output and power loss. The power loss can be obtained by considering the *gain* in energy per second by the atmosphere, as a result of the propeller passing through it.

13-2. Compute ideal efficiency of the propellers of a two-engined airplane operating at high speed with $C_D = 0.023$, knowing wing span/propeller diameter = 10.0, and aspect ratio = 8.0.

13-3. An ideal windmill having 20-ft diameter is operating in a 20-fps wind.

- Find the maximum axial force on the shaft (lb).
- Find the shaft horsepower corresponding to part a.
- Find the maximum shaft horsepower.
- Find the axial force on the shaft corresponding to part c (lb).
- Find the axial force if a solid circular disk of 20-ft diameter is installed on the shaft, instead of the ideal windmill (lb).

13-4. a. Develop the following expression for ideal propeller efficiency, as a function of advance ratio and power coefficient:

$$\frac{\eta_i}{1 - \eta_i} = \frac{\pi J^2}{2 C_P}$$

b. Superimpose curves of ideal efficiency η_i on Fig. IIIc, Appendix B, for $C_P = 0.1$ and 0.5, and observe the difference between actual and ideal efficiencies.

13-5. A 1000-lb light plane having a 7-ft-diameter propeller and $L/D = 5$ is flying level at 2000 ft altitude in a 10-mph head wind. If its propeller efficiency (actual) is 80 per cent, and its relative ground velocity is 90 mph, find the engine bhp P , and estimate the slip-stream velocity over the tail, V_s (mph).

13-6. Assuming power input to a propeller to be expressible by

$$p = K(\rho^n n^2 D \eta^3 \mu^4 a^3)$$

show by dimensional analysis that, in view of Eq. (13-26),

$$C_P = f(J, R, M)$$

- where
- ρ is mass density, slug per cu ft
 - n is rotational speed, rps
 - D is diameter, ft
 - v is velocity, fps
 - μ is coefficient of viscosity, slug per ft-sec
 - a is speed of sound, fps

$\alpha, \beta, \gamma, \delta, \epsilon, \lambda$ are unknown exponents

J is advance ratio, dimensionless

R is Reynolds number, dimensionless

M is Mach number, dimensionless

HINT: Obtain α , β , and γ as functions of δ , ϵ , and λ .

rpm and bhp are constant; hence, from Eqs. (13-23) and (13-29),

$$J = K_1 V$$

$$C_s = K_2 V$$

Therefore

$$\frac{J}{C_s} = K_3 \quad (13-35)$$

where K_1 , K_2 , and K_3 are constants. On a graph of C_s vs. J , a straight line from the origin defined by K_3 , allows reading of η for any chosen J , from which P_a and V may be calculated, after making the necessary tip-speed corrections.

A second, simpler method involves use of a chart showing η vs. J with C_P as a variable (Figs. IIIc and IVe, Appendix B). Since C_P is constant for a constant-speed propeller, η may be read directly from this chart for any J or V . It is interesting to note that since

$$P_a = \eta P \propto \eta$$

and

$$V = \frac{JND}{88} \propto J$$

the curve of η vs. J , for a particular C_P , may be regarded as an indication of the shape of the P_a vs. V curve.

Example. A two-engined airplane has three-bladed propellers of 10-ft diameter. Find the power available at 250 mph at 15,000 ft where the normal rated power and rpm are 800 hp and 2500 rpm, respectively, per engine. Gear ratio = 0.5.

Solution. From Eqs. (13-27) and (13-23),

$$C_P = \frac{10^{11} P}{2\sigma N^3 D^5} = \frac{(10^{11})(800)}{(2)(0.629)(1250)^3(10)^5} = 0.326$$

$$J = \frac{88V}{ND} = \frac{(88)(250)}{(1250)(10)} = 1.76$$

From Fig. IIIc, Appendix B, using $C_P = 0.326$ and $J = 1.76$: $\eta = 0.78$. From Fig. VI, Appendix B, $F_v = 1.0$; hence $\eta = 0.78$, and thus $P_a = 1248$ hp.

PROBLEMS

13-1. Prove input power to an ideal propeller is $P_{\text{input}} = T v (1 + a)$ by

a. Considering the kinetic energy per second entering and leaving the propulsion unit.

b. Considering input power to be the sum of the power output and power loss. The power loss can be obtained by considering the *gain* in energy per second by the atmosphere, as a result of the propeller passing through it.

13-2. Compute ideal efficiency of the propellers of a two-engined airplane operating at high speed with $C_D = 0.023$, knowing wing span/propeller diameter = 10.0, and aspect ratio = 8.0.

13-3. An ideal windmill having 20-ft diameter is operating in a 20-fps wind.

- Find the maximum axial force on the shaft (lb).
- Find the shaft horsepower corresponding to part a.
- Find the maximum shaft horsepower.
- Find the axial force on the shaft corresponding to part c (lb).
- Find the axial force if a solid circular disk of 20-ft diameter is installed on the shaft, instead of the ideal windmill (lb).

13-4. a. Develop the following expression for ideal propeller efficiency, as a function of advance ratio and power coefficient:

$$\frac{\eta_i}{1 - \eta_i} = \frac{\pi J^3}{2 C_P}$$

b. Superimpose curves of ideal efficiency η_i on Fig. IIIc, Appendix B, for $C_P = 0.1$ and 0.5, and observe the difference between actual and ideal efficiencies.

13-5. A 1000-lb light plane having a 7-ft-diameter propeller and $L/D = 5$ is flying level at 2000 ft altitude in a 10-mph head wind. If its propeller efficiency (actual) is 80 per cent, and its relative ground velocity is 90 mph, find the engine bhp P , and estimate the slip-stream velocity over the tail, V_s (mph).

13-6. Assuming power input to a propeller to be expressible by

$$p = K(\rho^n n^8 D \eta^3 \mu^4 v^{\lambda})$$

show by dimensional analysis that, in view of Eq. (13-26),

$$C_P = f(J, R, M)$$

- where
- ρ is mass density, slug per cu ft
 - n is rotational speed, rps
 - D is diameter, ft
 - v is velocity, fps
 - μ is coefficient of viscosity, slug per ft-sec
 - a is speed of sound, fps

$\alpha, \beta, \gamma, \delta, \epsilon, \lambda$ are unknown exponents

J is advance ratio, dimensionless

R is Reynolds number, dimensionless

M is Mach number, dimensionless

HINT: Obtain α , β , and γ as functions of δ , ϵ , and λ .

13-7. Replot the sea-level P_r curve for the airplane of Prob. 11-7a on a new sheet. The airplane has four Pratt & Whitney CA15 engines and uses a low propeller gear ratio (0.450).

a. Using the propeller data in Figs. IVa and b, Appendix B, and the engine chart in Fig. IIa, Appendix B, select four-bladed propellers to give maximum velocity at sea level, with normal rated power and rpm. Find D and β .

b. Using the propeller data in Fig. IIIa, Appendix B, and the engine chart in Fig. IIa, Appendix B, select three-bladed propellers to give maximum velocity at sea level, with normal rated power and rpm. Find D and β .

c. Using Fig. IV, Appendix B, compute and plot sea-level P_a vs. V corresponding to $J = 1.0, 1.3, 1.6$, and 1.8 , assuming the propellers of part a have fixed pitch. Assume answer to part a is $D = 12.1$ ft, $\beta = 42$ deg.

d. Using Fig. IVe, Appendix B, compute and plot sea-level P_a vs. V from 100 to 350 mph by 50-mph increments, assuming the propellers of part a are constant-speed propellers. Assume answer to part a is $D = 12.1$ ft.

e. Using the propeller data in Figs. IVa and b, Appendix B, and the engine chart in Fig. IIa, Appendix B, select four-bladed propellers to give maximum efficiency at sea level at the velocity for $(L/D)_{\max}$, using normal rated power and rpm. Find D and β . (This is a climb condition, but the velocity for $(L/D)_{\max}$ in a climb is assumed in this problem to be the same as for level flight.)

f. Using Fig. IVe, Appendix B, compute and plot sea-level P_a vs. V from 100 to 350 mph by 50-mph increments, assuming the propellers of part e are constant-speed propellers. Assume answer to part e is $D = 14.6$ ft.

13-8. Obtain the equation for rpm of a fixed-pitch propeller with an unsupercharged engine, for which $P = KN$.

$$N = f(C_s, D, J, \sigma)$$

Using this relation and the propeller charts shown in Appendix B, prove that for any fixed-pitch propeller designed to have η_{\max} at V_{\max} , the rpm must decrease with decreasing velocity, then remain essentially constant at low velocity.

13-9. A symmetrical airfoil is used as a propulsive device. It is set with chord horizontal in a horizontal stream of air having a relative velocity v . The airfoil is vibrated in the vertical direction with constant velocity v_s between stops. If $\gamma = \tan^{-1} (D/L)$ and $\alpha = \tan^{-1} (v_s/v)$, find an exact expression for propulsive efficiency $\eta = f[\tan(\alpha - \gamma), \tan \alpha]$. Assume no aerodynamic lag.

13·10. For the propulsive device of Prob. 13·9, assume the tangent of small angles equal to the angle in radians. Find η_{\max} for a rectangular wing having aspect ratio 6, for which the slope of the lift curve is $m_a = 4.25$ per radian. Other aerodynamic characteristics are tabulated below.

C_l^2	C_D
1.0	0.0500
1.2	0.0550
1.4	0.0620
1.6	0.0695
1.8	0.0783
2.0	0.0875
2.2	0.0980

CHAPTER 14

AIRPLANE PERFORMANCE

This chapter will deal with the performance characteristics of an airplane. Discussions will be concerned primarily with the conventional propeller and reciprocating-engine combination, not necessarily because this method of propulsion is considered to be more important, but because it is more complicated to analyze. Discussion of the performance estimation of an airplane equipped with a turbo-jet is confined to the end of the chapter, and it will be shown to be a relatively simple and straightforward procedure.

Most of the performance characteristics of a conventional airplane may be found after the curves of power required and power available have been established. Some characteristics, notably take-off and landing performance, require additional information. It should be made clear at the outset that performance calculations are based upon standard atmospheric conditions. In flight, these conditions are rarely encountered, and the corrections required for deviations from standard conditions result in performance that may be considerably different from that indicated by the standard performance. The reason is that the nonstandard conditions affect not only the power required by the airplane but also the engine and propeller characteristics, and therefore the horsepower available from the propeller. Curves of engine bhp vs. altitude are usually presented by manufacturers for standard conditions; however, in order to estimate engine bhp for a given airplane operating under a given set of conditions that are not standard, certain corrections must be applied, and these corrections may often be of considerable magnitude. The viscosity of the oil in the engine, the ram on the intake manifold, the back pressure on the exhaust manifold, the amount of cooling received by the engine, etc., are all dependent on atmospheric conditions, and must be accounted for in an accurate estimation of engine power output. The problem becomes increasingly complex if the particular engine has a turbosupercharger, because the bhp is then also a function

of intercooler temperature, waste-gate opening, etc. The bhp specified by the engine manufacturer provides a basis on which to estimate preliminary calculations, but precise calculations must be based upon information arising from tests on the particular installation. The justification for basing performance on standard altitude conditions is that this method allows direct comparisons among various airplanes that would be impossible on any other basis.

In all performance calculations in this text, steady (unaccelerated) conditions are assumed, and the effects of compressibility are ignored, *unless otherwise specified*.

14-1 Maximum Velocity. The maximum velocity of an airplane corresponds to the intersection of the curves of P_a and P_r .

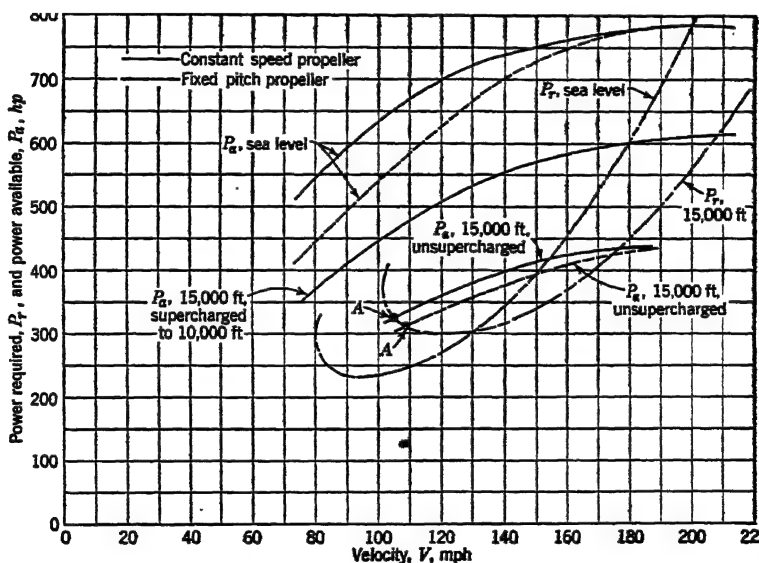


FIG. 14-1. Power required and available at sea level and 15,000 ft for a typical airplane, showing a comparison at sea level and 15,000 ft of fixed-pitch and constant-speed propellers, and a comparison at 15,000 ft of a supercharged and unsupercharged engine.

For a given airplane with a given propeller, maximum speed is primarily dependent on altitude; however even at constant altitude, maximum speed is not exactly constant for a particular flight, because during the flight fuel is used up and the weight decreases. Since P_r decreases with decreasing weight, maximum

velocity must increase. Maximum velocity is not important in commercial flying because of the increased amount of maintenance required on the engines, and because fuel consumption is excessively high for the upper range of engine bhp; it may be important in military flying, however, for obvious reasons.

For an unsupercharged engine, the maximum velocity decreases gradually with altitude, as shown in Figs. 14-1 and 14-2. For a

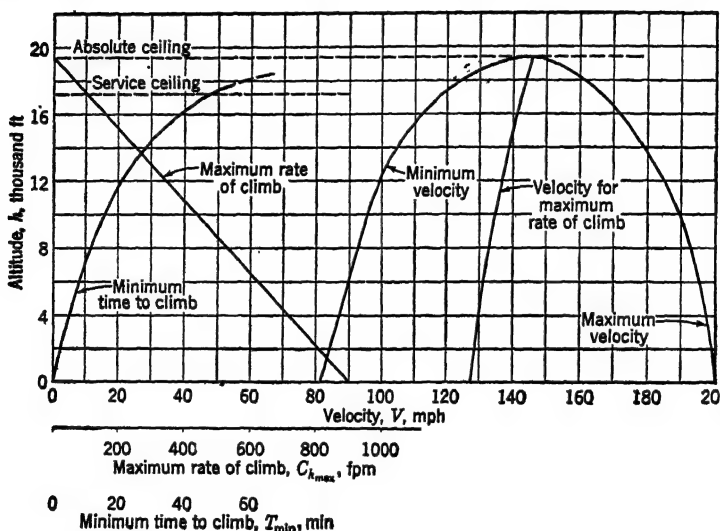


FIG. 14-2. Altitude performance characteristics of the airplane of Fig. 14-1 equipped with a fixed-pitch propeller and an unsupercharged engine. (Curves for a constant-speed propeller would be somewhat similar.)

supercharged engine, the power available is approximately constant from sea level to the critical altitude, because the bhp is generally approximately constant in this region. The power-required curve shifts up and to the right with increase in altitude (Fig. 14-1), resulting in an increase in maximum velocity that is almost exactly linear from sea level to the critical altitude (Fig. 14-3). Above the critical altitude, the maximum velocity decreases in a manner similar to that for an unsupercharged engine.

14-2 Minimum Velocity. At sea level, minimum velocity corresponds to the stalling speed, but at higher altitudes the minimum velocity may be greater than the stalling speed because of the crossing of the P_a and P_r curves (point A, Fig. 14-1). At suffi-

ciently high altitude, the P_a and P_r curves become tangent, and only one flight speed is possible. This is called the *absolute ceiling*, and it is shown in Figs. 14-2 and 14-3 as the maximum possible altitude of the airplane.

The conventional graph of P_r vs. V is for flaps retracted. Extension of the flaps may cause considerable reduction in

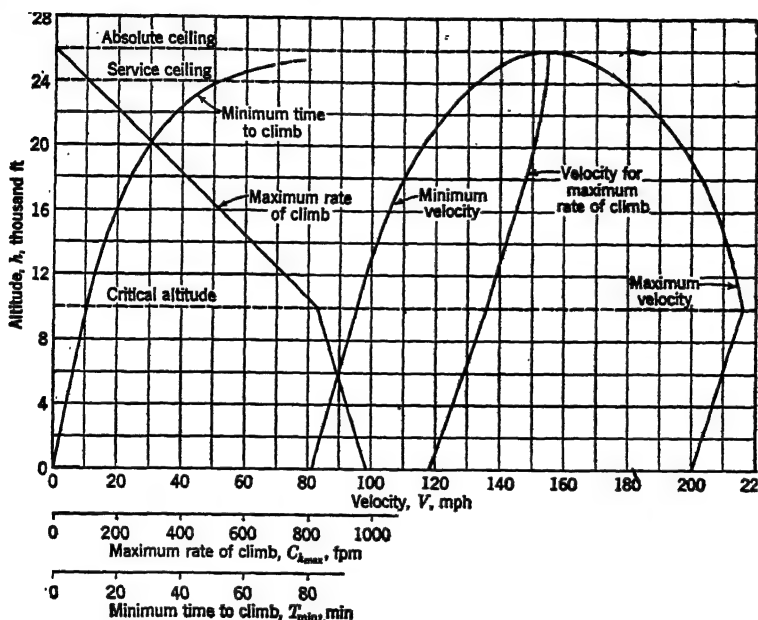


FIG. 14-3. Altitude performance characteristics of the airplane of Fig. 14-1 equipped with a constant-speed propeller and an engine that is supercharged to 10,000 ft.

minimum speed; however, in general, this is not an important altitude consideration, and the flap-extended curves are therefore not included.

14-3 Climbing Flight. When an airplane is in a climbing attitude, the thrust of the propeller must balance not only the drag of the airplane but the weight component in the plane of flight as well (see Fig. 14-4). Thus equations may be written for forces parallel and perpendicular to the remote velocity:

$$L = W \cos \theta \quad (14-1)$$

$$T = D + W \sin \theta \quad (14-2)$$

where L is lift, lb

W is weight, lb

θ is angle of climb, deg

T is thrust, lb

D is drag, lb

From the geometry of the diagram, the vertical rate of ascent, or rate of climb, is C_h .

$$C_h = \frac{W \sin \theta}{W} (88V) = \frac{TV - DV}{W} (88) \quad (14.3)$$

where C_h is rate of climb, fpm

V is velocity, mph

W is weight, lb

The product of thrust and velocity is proportional to horsepower

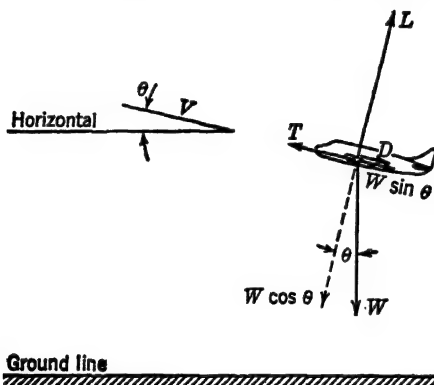


FIG. 14.4. Force relations on an airplane in climbing flight.

available, while the product of drag and velocity is proportional to horsepower required; hence

$$C_h = \frac{P_a - P_r}{W} (33,000) \quad (14.4)$$

Therefore, rate of climb is determined by the difference between the curves of P_a and P_r , and maximum rate of climb $C_{h_{\max}}$ corresponds to the greatest difference between the P_a and P_r curves.

Maximum rate of climb decreases with increasing altitude for an unsupercharged engine (Fig. 14.2) and decreases above the critical altitude for a supercharged engine (Fig. 14.3); furthermore, the curves of $C_{h_{\max}}$ vs. h may usually be represented very closely by straight lines. The altitude for which rate of climb is 100 fpm is

called the *service ceiling*. That for which maximum rate of climb is 0 fpm is the *absolute ceiling*.

For a given airplane operating at a given altitude, maximum rate of climb depends upon P_a ; thus a propeller may be designed to give improved low-speed performance by sacrificing high-speed performance. Figure 14-5 shows the airplane of Fig. 14-1 (sea

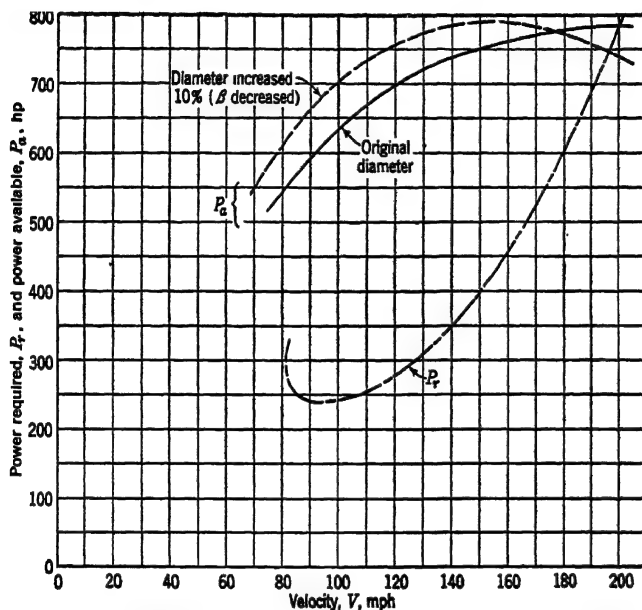


FIG. 14-5. Comparison of power available P_a with the constant-speed, sea-level propeller of Fig. 14-1 and a new propeller having 10 per cent increase in diameter.

level, constant-speed propeller) with a 10 per cent increase in propeller diameter (and consequent decrease in blade angle). The reduction in V_{\max} is only 2 per cent, but the increase in $C_{h_{\max}}$ is 13 per cent. Excessive tip speeds, clearance problems, and propeller and landing-gear weight all place limitations on the maximum permissible diameter.

The velocity for maximum rate of climb $V_{C_{h_{\max}}}$ is not an easily specified velocity because its value depends upon the accuracy with which curves of P_a and P_r have been plotted and faired. The curves in Figs. 14-2 and 14-3 must therefore be regarded as only representative of average values.

The angle of climb, θ , may be obtained from Fig. 14.4:

$$= \sin^{-1} \frac{C_h}{88V} \quad (14.5)$$

Substituting Eq. (14.4) in Eq. (14.5) gives

$$\theta = \sin^{-1} \left[\left(\frac{P_a - P_r}{WV} \right) (375) \right] \quad (14.6)$$

The maximum angle of climb is important in take-off calculations. It may be obtained by plotting $P_a - P_r$ vs. V and drawing the

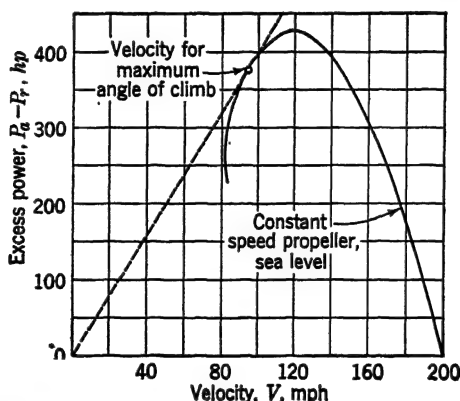


FIG. 14.6. Difference between power available P_a and power required P_r for the constant-speed, sea-level propeller of Fig. 14.1, showing the method for obtaining the velocity for maximum angle of climb θ_{\max} .

tangent from the origin to the curve as in Fig. 14.6. Substitution of the values at the point of tangency into Eq. (14.6) gives θ_{\max} ; thus, for example, if the weight of the airplane in Fig. 14.6 is 7000 lb, the maximum angle of climb is found as follows:

$$\begin{aligned} \theta_{\max} &= \sin^{-1} \left[\frac{(375)}{(7000)(95)} (375) \right] \\ &= \sin^{-1} 0.212 \\ &= 12.2 \text{ deg} \end{aligned}$$

14.4 Time to Climb. Time to climb to altitude h may be obtained from

$$T = \int_0^h \left(\frac{dt}{dh} \right) dh = \int_0^h \frac{dh}{C_h} \quad (14.7)$$

For an unsupercharged engine, rate of climb may be represented by a linear equation:¹

$$C_h = C_{h_0} \left(1 - \frac{h}{H}\right) \quad (14\cdot8)$$

where C_h is maximum rate of climb at altitude h , fpm

C_{h_0} is maximum rate of climb at sea level, fpm

H is absolute ceiling, ft

Substituting Eq. (14·8) in Eq. (14·7) and integrating gives minimum time T in minutes:

$$T = \frac{H}{C_{h_0}} \log_e \left(\frac{H}{H-h} \right)$$

or, changing to base 10,

$$T = \frac{2.3H}{C_{h_0}} \log_{10} \left(\frac{H}{H-h} \right) \quad (14\cdot9)$$

For a single-stage, single-speed, supercharged engine, an average constant rate of climb may be used to approximate the time to climb to the critical altitude; then for the remainder of the climb the following equation applies:

$$T_c = \frac{2.3(H-h_c)}{C_h} \log_{10} \left(\frac{H-h_c}{H-h} \right) \quad (14\cdot10)$$

where T_c is minimum time to climb above critical altitude, min

C_{h_c} is maximum rate of climb at critical altitude, fpm

h_c is critical altitude, ft

The total time to climb above the critical altitude is then obtained from the sum of the time below and above the critical altitude. If the engine has more than one critical altitude or uses a variable-speed supercharger, it is usually more direct to plot a curve of $1/C_h$ vs. altitude, and employ graphical integration to establish the time to climb to any altitude; i.e., according to Eq. (14·7), integration of elements measuring $1/C_h$ by dh between limits 0 and h gives time T .

14·5 Gliding Flight. Gliding flight has been mentioned previously in discussions of the significance of $(L/D)_{\max}$. They

¹ In the following analysis, the time to climb is actually the *minimum*, corresponding to the *maximum* rate of climb. Subscripts are deleted from all symbols merely for convenience.

showed that $(L/D)_{\max}$ corresponds to the minimum glide angle, with power off.

The sinking speed v_s may be shown with the aid of Fig. 14-7:

$$\begin{aligned}\frac{v}{v} &= \sin \theta = \frac{W \sin \theta}{W} = \frac{D}{W} \\ v_s &= \frac{Dv}{W} \\ &= \frac{P_r(550)}{W} \\ V_s &= \frac{P_r(375)}{W}\end{aligned}\quad (14-11)$$

where v_s is in feet per second and V_s is in miles per hour. Mini-

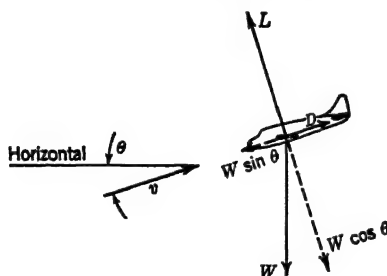


FIG. 14-7. Force relations on an airplane in gliding flight.

imum sinking speed is seen to correspond to minimum horsepower required, $P_{r_{\min}}$. It is significant only in determining the maximum time an airplane can stay aloft while gliding from a given altitude, and is not usually important except for sail planes.

Data on gliding flight are frequently presented in the form of a *glide polar*. This curve may be plotted using either Eq. (14-11) or the following equations:

$$V = \sqrt{\frac{W(\cos \theta)(391)}{\sigma C_L S}} \quad (14-12)$$

$$= \sqrt{\frac{W(\sin \theta)(391)}{\sigma C_D S}} \quad (14-13)$$

where V is gliding velocity, mph

θ is glide angle, deg

If velocity vectors are plotted so as to form an angle θ with the horizontal, a curve may be drawn that joins the extremities of the vectors to form the glide polar (Fig. 14-8). Glide angles corresponding to all glide velocities may be found on this curve. The maximum gliding velocity is called the *terminal velocity*. (It need not correspond to exactly vertical flight.) If no compressibility corrections are applied for the high-velocity region and if no account is taken of the additional drag of the propellers, the glide polar is likely to be seriously in error.

14-6 Cruising Conditions.

The velocity at which an airplane cruises is dependent upon fuel-consumption and engine-maintenance considerations. As a result of both these considerations, it is customary to cruise at between 50 and 70 per cent normal rated bhp. The factor that may decide whether a low or high cruising speed is desirable is the purpose of the flight. For commercial operation, competition may dictate speeds higher than are most economical, and head and tail winds may require variations in cruising velocity in order to meet schedules. For military operation, the length of flight is usually of primary importance in determining the cruising speed; i.e., for long bombing flights, where fuel is precious, the cruising speed may be determined entirely from the standpoint of minimum gallons consumption per mile of flight, which corresponds to a fairly low speed. For photographic missions, on the other hand, where the objective is near at hand, the cruising condition may correspond to *military power*, with a velocity that is higher than the *design* maximum speed. The cruising condition may be divided into high-speed cruise (using more than about 65 to 70 per cent normal rated bhp) and low-speed cruise (less than 65 to 70 per cent normal rated

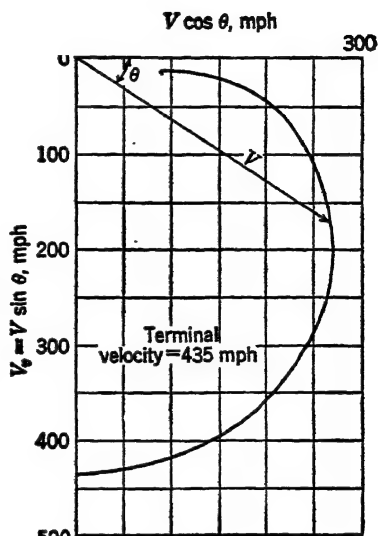


FIG. 14-8. Glide polar at sea level for the airplane of Fig. 14-1 (no compressibility corrections applied).

bhp.) A rich mixture is generally used for the former condition and a lean mixture for the latter.

Fixed-pitch Propeller. Cruising flight automatically implies level flight, for which $C_h = 0$. By Eq. (14.4), P_a must therefore equal P_r . For reasonably high speeds, since P_r varies approximately as the cube of the velocity, P_a must vary in the same manner; hence

$$P_a = K\sigma V^3 \quad (14.14)$$

where K is a constant. Power available may also be written

$$P_a = P\eta = (C_P \rho_0 n^3 D^5 \sigma) \eta \quad (14.15)$$

Since at high speed, efficiency is roughly constant, Eqs. (14.14) and (14.15) may be combined to give

$$C_P = K_2 J^3 \quad (14.16)$$

where K_2 is a constant for a particular propeller diameter. From a curve of C_P vs. J on a propeller chart, the C_P decreases with increasing J for constant β ; however, Eq. (14.16) shows that C_P increases with increasing J . Equation (14.16) and the propeller chart are therefore incompatible unless C_P and J are both constant with changing velocity. For constant J ,

$$N \propto V \quad (14.17)$$

In other words, the rpm of the fixed-pitch propeller decreases almost linearly with decreasing velocity in the high-speed cruising region.¹ The exact rpm may be found by trial and error, but it will invariably be close to that shown by Eq. (14.17).

Low-speed cruising is usually concerned with an attempt to obtain the maximum number of miles per gallon of fuel, which is the range condition analyzed in Art. 14.7.

Constant-speed Propeller. A constant-speed propeller allows any combination of rpm and bhp within the limits of the engine. The high-speed-cruise condition may be assumed to occur at approximately constant C_P , so that Eq. (14.17) is roughly true for a constant-speed propeller also.

Again low-speed cruise is usually associated with the range problem.

¹ Notice that the discussion is concerned with level cruising flight. The rpm variation with velocity for climbing flight is entirely different.

14-7 Range. Range is the distance an airplane can fly without landing. Maximum range has considerable importance in both commercial and military flying, because the airplane that is capable of flying the farthest with a given pay load is often the most desirable for certain kinds of flying. Range may be obtained from the fundamental equation

$$R = \int_0^T V dt \quad (14-18)$$

where R is range, miles

V is velocity, mph

t is time when velocity is V , hr

T is total time of flight, hr

In order to integrate, an equation for dt may be obtained in the following manner: The change in weight of the airplane during flight is related to the specific fuel consumption by

$$\frac{dW}{dt} = -Pc \quad (14-19)$$

where W is weight of airplane, lb

P is total power of all engines, bhp

c is specific fuel consumption, lb per bhp-hr

The negative sign is inserted because the weight reduces as fuel is used. For level flight,

$$P = \frac{DV}{\eta 375} \quad (14-20)$$

Substituting Eq. (14-20) in Eq. (14-19) and solving for dt gives

$$dt = -375 \frac{\eta}{c} \frac{dW}{DV} \quad (14-21)$$

Substituting Eq. (14-21) in Eq. (14-18) yields

$$R = -375 \int_{W_0}^{W_1} \frac{\eta}{c} \frac{dW}{D} \quad (14-22)$$

where subscripts 0 and 1 refer to original and final, respectively. In order to integrate Eq. (14-22), the propeller efficiency, specific fuel consumption, and angle of attack are all assumed constant. The latter assumption implies that L/D is also constant; hence

$$R = -375 \frac{L}{D} \frac{\eta}{c} \int_{W_0}^{W_1} \frac{dW}{W} \quad (14-23)$$

After integration

$$R = 375 \frac{\eta}{c} \frac{L}{D} \log_e \frac{W_0}{W_1}$$

or, by changing to base 10,

$$R = 863.5 \frac{\eta}{c} \frac{L}{D} \log_{10} \frac{W_0}{W_1} \quad (14.24)$$

Equation 14.24 is one form of the *Breguet range equation*. For a given initial and final weight of the airplane, maximum range is seen to correspond to $[(\eta/c)(L/D)]_{\max}$. The maximum range of an airplane may be determined approximately by making certain operating assumptions, the degree of accuracy desired being dependent upon the number of assumptions. A precise determination at constant lift coefficient is very tedious, first because the weight varies during flight, which causes variation in velocity and power required. Second, η is a function of P , N , and V , while c is a function of P and N ; hence these two variables change continuously during flight. Thus, the product $[(\eta/c)(L/D)]$ can be made a maximum for every stage of the flight only by very elaborate analysis. Fortunately, such extreme accuracy is entirely without justification; first, because long-range flight is usually broken up into several short legs, with constant indicated air speed maintained during each leg; second, because minor head and tail winds upset the exact calculations; and, third, because the Breguet equation takes no account of fuel consumed during climb to and glide from the operating altitude.

The calculations may be greatly simplified by assuming that for maximum range, η/c and L/D are maximum *individually*, and that η/c and L/D are constant during the flight. An "average" condition may be analyzed, corresponding to the weight when half the fuel is used. For this condition, V , P , η , etc., may be assumed representative of the complete flight.

Maximum L/D may be obtained by drawing a tangent from the origin to *any* P_r curve on a plot of P_r vs. V , since

$$\begin{aligned} \left(\frac{L}{D}\right)_{\max} &= \left(\frac{W}{D} \frac{V}{375}\right)_{\alpha} \\ &= \left(\frac{W}{375}\right) \left(\frac{V}{P_r}\right)_{\max} \end{aligned} \quad (14.25)$$

The velocity and power required corresponding to half the fuel

used may be obtained from Eqs. (11-22) and (11-24), respectively. The following steps may be taken to obtain $(\eta/c)_{\max}$:

1. Assume a value of N . Choose the minimum operating rpm as a first estimate.
2. Compute J using "average" velocity corresponding to half fuel used up.
3. Compute

$$C_P = \frac{10^{11}}{2N^3 D^5 \sigma} \frac{P_r}{\eta}$$

$$= \frac{K}{\eta}$$

4. From a plot of η vs. J with C_P as variable, only one η is possible at the J from step 2 that will satisfy the equation in step 3.
5. Compute $P = P_r/\eta$, where η is from step 4.
6. From the engine chart, find the fuel consumption corresponding to the P from step 5 and the assumed N .
7. Compute η/c .
8. Repeat steps 1 to 7 for other assumed values of N .
9. Plot η/c vs. N to obtain a maximum η/c .
10. Substitute $(\eta/c)_{\max}$ from step 9 and $(L/D)_{\max}$ from Eq. (14-25) in the Breguet equation and compute maximum range.

The procedure outlined may not be sufficiently accurate for extreme range, in which case several short legs may be considered.

14-8 Endurance. Endurance is the time an airplane is able to remain aloft, at a fixed altitude, without landing. Maximum endurance is of little interest in commercial flying except in very peculiar circumstances; however, in military flying it may be important in convoy work or submarine hunting. Endurance for a condition of constant angle of attack may be found in the following manner.

Differential time of flight may be written as in Eq. (14-21):

$$dt = -375 \frac{dW}{DV} \frac{\eta}{c} \quad (14-26)$$

Velocity at any point in the flight may be written in terms of the weight at that point, the starting velocity, and starting weight:

$$V = V_0 \sqrt{\frac{W}{W_0}} \quad (14-27)$$

Substituting Eq. (14-27) in Eq. (14-26) gives

$$dt = -375 \frac{dW}{DV_0} \sqrt{\frac{W_0}{W}} \frac{\eta}{c} \quad (14-28)$$

This equation may be integrated using the same specifications as in the range equation, namely, constant efficiency, specific fuel consumption, and angle of attack.

$$E = \int_0^E dt = -375 \frac{\sqrt{W_0}}{V_0} \frac{L}{D} \frac{\eta}{c} \int_{W_0}^{W_1} \frac{dW}{W^{3/2}} \quad (14-29)$$

where E is endurance in hours. After integration

$$E = \frac{750}{V_0} \frac{L}{D} \frac{\eta}{c} \left(\sqrt{\frac{W_0}{W_1}} - 1 \right) \quad (14-30)$$

Maximum endurance may be assumed to occur for $(\eta/c)_{\max}$ and $(L/DV_0)_{\max}$ separately. However

$$\frac{L}{DV_0} = \frac{L_0}{D_0 V_0} = \frac{W_0}{375 P_{r_0}} \quad (14-31)$$

Equation (14-31) shows that for maximum endurance the starting horsepower should be a minimum, but since angle of attack is constant for the complete flight, $P_{r_{\min}}$ should be maintained for the complete flight. A procedure similar to that outlined for maximum range may be used to obtain maximum endurance. It is left to the student to prove that $C_L^{3/2}/C_D$ is a maximum when P_r is a minimum.

14-9 Take-off. The accuracy with which take-off performance can be predicted depends upon the success with which pilot technique, runway condition, wind velocity, *ground effect*,¹ and propeller thrust can be predicted. Take-off is generally considered to consist of three phases: the *ground run*, the *transition* or *flare*, and the *climb over a 50-ft obstacle*. The ground run is concerned with the distance and time during which the wheels are in contact with the ground. The transition accounts for the distance and time re-

¹ *Ground effect* is the influence of the presence of the ground in modifying the flow pattern on the wing and tail. The ground restricts the tip vortices, giving an effective increase in wing and tail aspect ratios; furthermore, it changes the direction of down-wash over the tail (see Art. 6-3).

quired to change from horizontal flight on the ground to steady climb. The climb over a 50-ft obstacle is arbitrarily specified, but is a reasonable and practical criterion; it is, of course, concerned with the distance and time from the end of the transition to a 50-ft altitude.

Take-off calculations may be made as simple or as refined as desired. The ground run usually constitutes the major portion of the total take-off distance, and it is here that most of the care must be exercised in careful prediction of characteristics. Specifically, accurate estimation of the thrust is of major importance.

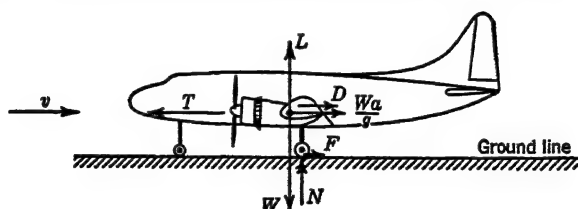


FIG. 14-9. Force relations on an airplane during the ground run.

A 2 per cent error in thrust estimation may easily be as important as a 50 per cent error in estimation of either the airplane drag coefficient or the coefficient of friction. Estimation of thrust, therefore, sets the pace for the whole take-off analysis, and it is futile to be too much concerned about precise determination of any of the variables that define take-off unless thrust is accurately known. Unfortunately, thrust is difficult to ascertain at very low speed (low J), because the propeller blades are usually at least partially stalled, particularly near the central part of the propeller disk. With these general statements, the calculation of take-off distance may be introduced.

Ground-run time for take-off in a calm is given by

$$t = \int_0^{v_i} \frac{dv}{a} \quad (14-32)$$

where v is airplane velocity during ground run, fps

v_i is take-off velocity, fps

The corresponding ground-run distance is

$$s = \int_0^{v_i} v \frac{dv}{a} \quad (14-33)$$

These two equations require an expression for $a = f(v)$ before integration can be carried out. This may be obtained from consideration of the forces acting on the airplane during the ground run (Fig. 14-9).

$$N = W - L \quad (14-34)$$

$$F = \mu N \quad (14-35)$$

$$T = D + \frac{Wa}{g} + F \quad (14-36)$$

where N is normal ground reaction, lb

W is weight, lb

L is lift, lb

F is friction force, lb

μ is coefficient of friction, dimensionless

T is thrust, lb

D is drag, lb

a is acceleration, fps per sec

Substituting from Eqs. (14-34) and (14-35) in Eq. (14-36) and solving for a gives

$$a = \frac{g}{W} [T - D - \mu(W - L)] \quad (14-37)$$

Equation (14-37) is the required function of velocity. It may be used for integration in the distance and time equations, provided the lift coefficient during the ground run is assumed constant. Usually the integration is accomplished graphically by plotting T , D , and F vs. v , as in Fig. 14-10.

Thrust. Thrust may be obtained in the following manner for fixed-pitch and constant-speed propellers:

FIXED-PITCH PROPELLER. Thrust is obtained on the same assumption as in Art. 13-9, namely, that bhp varies linearly with rpm.

1. Assume a value of J .
2. Read C_P and C_T from the propeller charts for the design β .
3. Compute N from Eq. (13-34).

$$N = \sqrt{\frac{10^{11} K}{2D^5 \sigma C_P}}$$

4. Compute V from Eq. (13-23).

$$V = \frac{JND}{88}$$

- Correct C_T for tip speed, using the product of C_T from step 2 and F_v from Fig. VI, Appendix B.
- Compute T from Eq. (13-25).

$$T = \frac{6.61}{10^7} C_{T\sigma} N^2 D^4$$

The above steps may be carried out in tabular form for several assumed values of J .

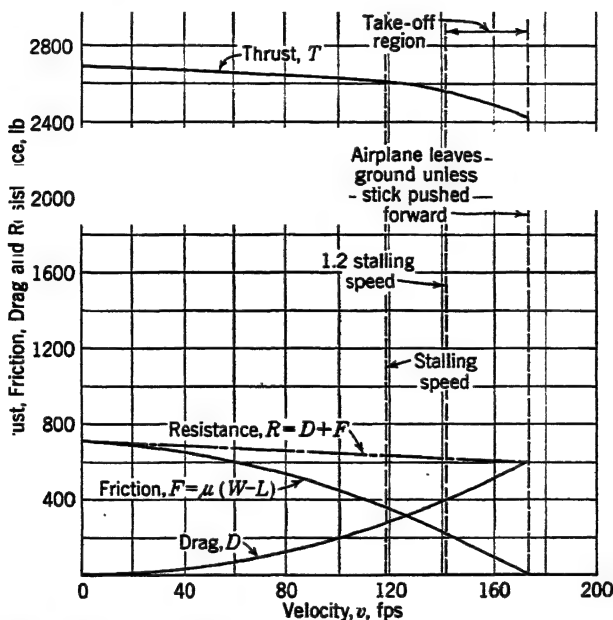


FIG. 14-10. Thrust and resistance variation with air speed during the ground run for the airplane of Fig. 14-1.

CONSTANT-SPEED PROPELLER. Thrust is obtained from the following steps:

- Assume a value of J .
- Compute C_P corresponding to take-off P and N .
- Read β from the propeller charts corresponding to J and C_P from steps 1 and 2.
- Read C_T at J and β from steps 1 and 3.
- Compute V from Eq. (13-23).

$$V = \frac{JND}{88}$$

6. Correct C_T for tip speed, using the product of C_T from step 4 and F_v from Fig. VI, Appendix B.
7. Compute T from Eq. (13·25).

$$T = \frac{6.61}{10^7} C_T \sigma N^2 D^4$$

The above steps may be carried out in tabular form for several assumed values of J .

Drag. Drag may be obtained from a polar curve of the airplane using an arbitrarily assumed constant lift coefficient for the complete ground run. Since cowl flaps and landing gear are extended, and flaps may be deflected through a small angle, account should be taken of their effects on the polar curve. Also, as was pointed out earlier, the effect of ground and slip stream should be considered. All these effects are ignored in this text in order to maintain simplicity of analysis. The lift coefficient required to produce a minimum ground run is¹

$$C_L = \frac{\pi}{2} A e \mu$$

where A is aspect ratio, dimensionless

e is airplane efficiency factor, dimensionless

μ is coefficient of friction between wheels and ground, dimensionless

This lift coefficient corresponds to a nonconservative drag coefficient but does allow solution of a lower limit for take-off distance. To provide a degree of conservatism, the lift coefficient corresponding to maximum angle of climb is used exclusively for the ground run in this text, for all problems and examples.

Friction Force. Friction force may be obtained, with the assumed constant lift coefficient, from Eq. (14·35). Friction coefficients may be obtained from the following table:²

¹ Obtained by writing the equation for total resistance, which consists of ground friction and drag, then differentiating with respect to lift and equating to zero.

² From TR 450 and Wood, K. D., "Technical Aerodynamics," McGraw-Hill, New York, 1947.

Surface	μ
Concrete.....	0.02-0.05
Hard turf.....	0.04-0.05
Short grass.....	0.05
Long grass.....	0.10
Soft ground.....	0.10-0.30
Wet concrete.....	0.05
Snow- or ice-covered.....	0.02

In Fig. 14-10, the drag and friction force may be added to obtain total resistance R ; then

$$a = \frac{y}{W} (T - R) \quad (14-38)$$

From Eq. (14-38), curves of $1/a$ and v/a may be plotted vs. v for use in the distance and time equations (Fig. 14-11). The take-off

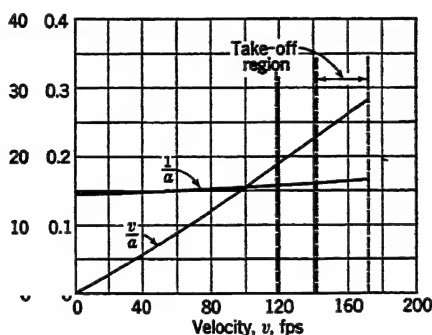


FIG. 14-11. Ground-run parameters $1/a$ and v/a as a function of velocity for the airplane of Fig. 14-1.

velocity must occur between two limits; the lower limit is the stalling speed of the airplane, and the upper limit corresponds to the constant lift coefficient used during the ground run. The airplane cannot be air-borne at a speed less than the stall, and it will automatically leave the ground as soon as $L = W$. In the latter case, the pilot allows the plane to fly itself off the ground. For any lesser speed, he pulls back the stick in order to increase C_L for take-off. Of course, take-off at exactly the stalling speed is likely to be dangerous, because during transition the lift must equal not only the weight component perpendicular to the flight path but also the centrifugal force due to the flight curvature; hence, an attempt to take off at exactly the stalling speed is

almost certain to lead to difficulties. A safe criterion for the take-off speed is the following:

$$v_t > 1.2v_s$$

where v_s is the stalling speed. It should be noted that this specification may prove too conservative if the increase in $C_{L_{\max}}$ due to running propellers is great.

The preceding method allows solution of the ground run for an assumed take-off speed. For instance, if take-off is to occur at

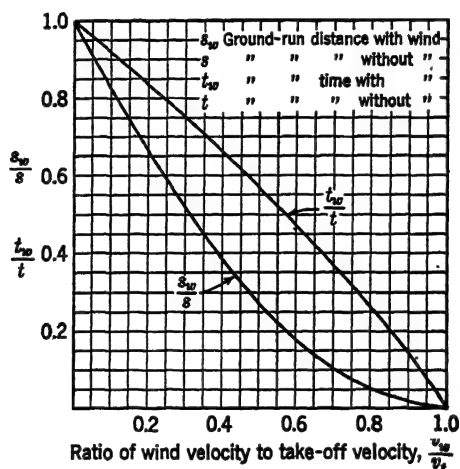


FIG. 14-12. Chart showing approximate effect on wind on ground-run time and distance during take-off or landing. (Based on an unpublished analysis by V. J. Martin.)

20 per cent greater than the stalling speed, the areas under the curves in Fig. 14-11 would be integrated from $v = 0$ to $v = 142$ fps. To compute total time and distance required to climb to 50-ft altitude, accounting for transition and climb, is not generally simple, because the airplane has an angular acceleration during transition. The difficulties may be circumvented by the following simplified procedure.

1. Compute the time and distance *including transition* by integrating the area under curves such as those depicted in Fig. 14-11 from zero velocity to the velocity corresponding to maximum angle of climb.

2. Compute the time and distance to climb from the ground to 50-ft altitude, assuming a constant velocity equal to the velocity for maximum angle of climb.
3. Add the times and distances from steps 1 and 2 to get total time and distance, respectively.

The above procedure represents the actual path of the airplane by a horizontal line to the velocity for maximum angle of climb, then by an inclined line forming an angle with the horizontal equal to the maximum angle of climb.¹

An airplane usually takes off into the wind, and the effect of wind on the ground run may be accounted for in the original time and distance equations [Eqs. (14-32) and (14-33)], remembering that s is a *ground* distance and v is an *air* speed. The effect of wind is more conveniently shown graphically, as in Fig. 14-12. Effect of wind on the climb to 50-ft altitude may be accounted for by separate analysis.

14-10 Landing. The landing run may be assumed to occur

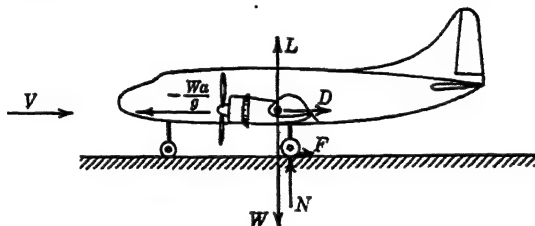


FIG. 14-13. Force relations on an airplane during the landing run.

without power, and with flaps and landing gear extended. For simplicity, ground effect and gear drag are ignored in this text.

The time consumed in landing is seldom computed, for practical reasons. The ground-run-distance equation is the same as that used for take-off, except that the limits of integration are reversed:

$$s = \int_{v_1}^0 \frac{v \, dv}{a} \quad (14-39)$$

where v_1 is landing speed in feet per second. Fortunately, the

¹ The suggested method for computing take-off time and distance is open to criticism; however, it must be pointed out that nearly all techniques are subject to considerable error because of the number of approximations involved. It is only the principles that are of interest in this text.

expression for acceleration as a function of velocity is very simple, so that Eq. (14.39) may be integrated directly. From Fig. 14.13,

$$-\frac{Wa}{g} = D + F \quad (14.40)$$

$$F = \mu(W - L) \quad (14.41)$$

Substituting Eq. (14.41) in Eq. (14.40) and solving for a yields

$$\begin{aligned} a &= -g \left[\frac{D}{W} + \mu \left(1 - \frac{L}{W} \right) \right] \\ &= -g \left[\frac{L}{W} \left(\frac{D}{L} - \mu \right) + \mu \right] \end{aligned} \quad (14.42)$$

Assuming C_L is constant from the moment of contact when $v = v_i$, until the end of the ground run when $v = 0$,

$$\frac{L}{W} = \left(\frac{v}{v_i} \right)^2 \quad (14.43)$$

Substituting Eq. (14.43) in Eq. (14.42) gives

$$a = -g\mu - \frac{g}{v_i^2} \left(\frac{D}{L} - \mu \right) v^2 \quad (14.44)$$

When Eq. (14.44) is substituted in Eq. (14.39) the integral has the form

$$s = \int_{v_i}^0 \frac{v \, dv}{M + Nv^2} \quad (14.45)$$

where

$$M = -g\mu \quad (14.46)$$

$$N = -\frac{g}{v_i^2} \left(\frac{D}{L} - \mu \right) \quad (14.47)$$

Integrating Eq. (14.45) and substituting limits gives

$$s = -\frac{1}{2N} \log_e \left(\frac{N}{M} v_i^2 + 1 \right) \quad (14.48)$$

Substituting Eqs. (14.46) and (14.47) in Eq. (14.48) yields

$$s = \frac{v_i^2}{2g[\mu - (D/L)]} \log_e \left(\frac{L\mu}{D} \right) \quad (14.49)$$

or in terms of landing speed in miles per hour and logarithm to the base 10,

$$s = \frac{V_i^2}{13[\mu - (D/L)]} \log_{10} \left(\frac{L\mu}{D} \right) \quad (14.50)$$

Equation (14-50) gives landing distance in feet, for no head wind. The landing speed V_l may arbitrarily be assumed to correspond to

$$V_l = 1.2V_{s_f}$$

where V_{s_f} is stalling speed with flaps. The L/D may be obtained from a polar for the flapped configuration at the above velocity, and μ may be obtained from the previously listed values used in take-off if no brakes are used. If brakes are used, the following values are appropriate:¹

Surface	μ
Concrete.....	0.4-0.6
Hard turf.....	0.4
Wet concrete.....	0.3
Snow- or ice-covered.....	0.07-0.10

The effect of wind may be accounted for mathematically, but is computed more simply by using Fig. 14-12.

The total landing distance, accounting for descent from 50-ft altitude through transition to the moment of contact with the ground, may be treated in a manner similar to the take-off analysis, but here the velocity during descent can be approximated by $V = 1.2V_{s_f}$.

14-11 Performance with a Turbo-jet. The performance computations for an airplane equipped with a turbo-jet are considerably simpler than for a conventional propeller and reciprocating engine, because the characteristics of the engine are plotted in convenient form as a function of true air speed of the airplane. In Fig. 14-14 the data of Fig. 12-8 have been reproduced with the following assumed sea-level values:

Rated static thrust = 4000 lb

Rated rpm = 8000 rpm

Fuel flow at rated rpm and static thrust = 4000 lb per hr

The air-flow curves have been deleted because they have little aerodynamic importance, but a group of curves have been superimposed that are obtained by dividing the velocity by its corresponding fuel flow. For example, at 25,000 ft, $V = 300$ mph, and $W_f = 1200$ lb per hr; $V/W_f = 300/1200 = 0.25$ mile per lb of

¹ From Wood, *ibid.*

fuel. These curves will later be shown to be valuable for defining the maximum range of the airplane.

In computing the performance of a conventional airplane in the preceding articles, the effects of compressibility were completely ignored except in so far as they affected propeller characteristics. This was done to keep a rather complex study as simple as possible. The performance computations involving the use of a turbo-jet are

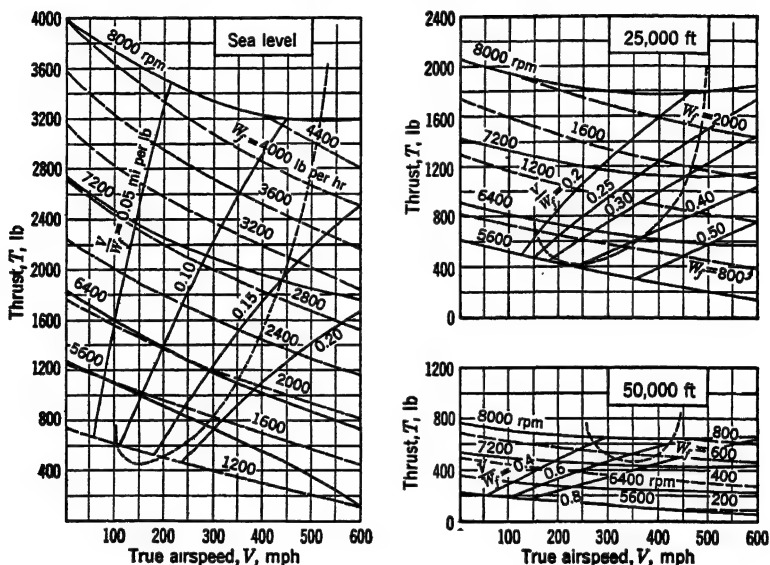


FIG. 14-14. Airplane drag and turbo-jet thrust characteristics for a typical installation (based on Figs. 8-19 and 12-8).

unusually simple, so that compressibility phenomena may be included here with little danger that the discussions will be unduly complicated. Of course, a more fundamental reason for including compressibility effects here is that the turbo-jet engine is inherently a high-speed device, and an assumption that compressibility effects are negligible would lead to very serious errors.

In Fig. 14-14, curves of airplane drag vs. velocity for a typical high-speed single-engined airplane have been superimposed on the engine characteristics. These curves were obtained using the dotted curves of Fig. 8-19, assuming a wing loading of 40 psf and gross weight of 9000 lb. *If there were no effect of compressibility*, the drag curve at altitude could be obtained from that at sea level in

the same fashion as the altitude P_r curve was obtained from the sea-level curve; *i.e.*, at constant lift coefficient the velocity at altitude is obtained from

$$W_0 = C_L S \frac{V_0^2}{391} \quad (14.51)$$

$$W_\sigma = C_L S \frac{V_\sigma^2}{391} \quad (14.52)$$

where subscripts 0 and σ refer to sea level and altitude, respectively: hence

$$V_\sigma = \frac{V_0}{\sqrt{\sigma}} \quad (14.53)$$

The drag at altitude is obtained by

$$D_0 = C_D S \frac{V_0^2}{391} \quad (14.54)$$

$$D_\sigma = C_D S \frac{V_\sigma^2}{391} \quad (14.55)$$

Hence

$$D_\sigma = D_0 \quad (14.56)$$

Equation (14.56) shows that the drag at a particular sea-level velocity occurs at a higher velocity at altitude, because of Eq. (14.53). For low speed (high lift coefficient), the Mach number is low, and the effects of compressibility are negligible; hence this relationship holds with good accuracy, but at higher speed (low lift coefficient), the Mach number is high, and this relationship is entirely too optimistic. For example, in Fig. 14-14, at sea level the drag is 600 lb at 107 mph and at 235 mph. At 50,000 ft, $1/\sqrt{\sigma} = 2.57$; hence the velocities corresponding to 600-lb drag should be 275 mph and 604 mph, respectively. The actual values read from Fig. 14-14 are 275 mph and 425 mph, respectively; thus the important role played by compressibility is demonstrated.

With these general remarks, the performance of the airplane may now be discussed.

Maximum Velocity. The maximum velocity corresponds to the intersection of the drag curve and the thrust curve for rated rpm.

Minimum Velocity. The minimum velocity is equal to the stalling speed for the lower altitudes, but at altitudes near the absolute ceiling, the drag curve crosses the curve of rated rpm in

such a manner as to make the minimum velocity higher than the stalling speed [see 50,000-ft curve (Fig. 14-14), where this effect is just beginning to show at $V = 260$ mph].

Climbing Flight. Rate of climb is obtained as follows:

$$C_h = \frac{(T - D)V}{W} \quad (88) \quad (14-57)$$

Maximum rate of climb is thus obtained, not from the maximum difference between the thrust and drag curves, but from the maximum product of this difference and the velocity. Maximum rate of climb usually decreases approximately linearly with increasing altitude, and is zero at the absolute ceiling.

Time to Climb. The minimum time to climb to altitude may be obtained in the same manner as in Art. 14-4 from the curve of maximum rate of climb vs. altitude.

Maximum Range. Maximum range corresponds to minimum gallons of fuel consumed per mile and is obtained from the tangent to the drag curve formed by the V/W_f curve. Range is then given by the product of the weight of fuel and the miles per pound of fuel.

Example. Compute the maximum range of the airplane shown in Fig. 14-14 at 25,000 ft, using 500 lb of fuel. Find the corresponding V and N .

Solution. The tangent to the drag curve occurs for $V/W_f = 0.41$; hence the range is $R = (0.41)(500) = 205$ miles. $V = 325$ mph. $N = 6100$ rpm.

If the weight change during flight is appreciable, an average value of fuel consumption may be used, corresponding to the airplane weight for half the fuel used; i.e., a drag curve corresponding to half the fuel used may be constructed, and the tangent to this curve may be used to define the consumption.

Range may also be obtained from a modified Breguet equation, derived in a manner similar to that used to develop Eq. (14-24). Again assuming the flight takes place at constant C_L , and assuming the specific fuel consumption is constant during the flight,

$$R = \frac{39.55}{w} \frac{1}{\sqrt{\sigma}} \frac{\sqrt{C_L}}{C_D} \left(\sqrt{\frac{W_0}{S}} - \sqrt{\frac{W_1}{S}} \right) \quad (14-58)$$

where R is range, miles

S is wing area, sq ft

w is specific fuel consumption, lb per hr of fuel per pound of thrust

W_0 is original gross weight, lb

W_1 is final gross weight, lb

Maximum range at a particular altitude is then seen to occur for a maximum value of $C_L^{3/2}/(wC_D)$, or since w is assumed constant, maximum range occurs at maximum $C_L^{3/2}/C_D$. The corresponding velocity may be shown to correspond to the tangent from the origin to the drag curve.

For low altitudes, where compressibility effects are not important at the speed for maximum range, and where the assumption that

$$C_D = C_{D_{pmin}} + \frac{C_L^2}{\pi A e}$$

is justified, maximum range may be shown to occur when

$$C_D = \frac{4}{3}C_{D_{pmin}}$$

which corresponds to a higher speed than that for $(L/D)_{max}$. Thus an airplane using a turbo-jet obtains maximum range at a higher speed than one using a propeller and reciprocating engine. This may also be shown in Fig. 14-14: maximum L/D occurs at minimum drag, which is at a lower velocity than that corresponding to the tangent to the drag curve from the origin. Notice that by this method, maximum range does not correspond exactly to the velocity for which the V/W_f curve is tangent to the drag curve.

Endurance. Maximum endurance corresponds to minimum pounds of fuel consumed per hour and therefore corresponds to the tangent to the drag curve formed by the W_f curve. Endurance is then given by the product of the weight of fuel and the reciprocal of the pounds of fuel per hour, read from Fig. 14-14 at the point of tangency. Changes in weight may again be accounted for as in the range calculations.

Take-off. Take-off calculations are considerably simplified because the basic data are already presented in the form of thrust vs. velocity.

All other performance calculations are carried out in a manner similar to that used for the conventional propeller and reciprocating engine.

14.12 Rapid Performance Methods. The performance methods described in this chapter for airplanes equipped with reciprocating engines are tedious, particularly if a great number of weights and altitudes of a particular airplane are to be investigated. For this reason, several methods have been suggested to allow rapid estimation of performance. In this article, these methods will be treated quite generally, so as to show the basic procedure that is characteristic of most methods.

In the first method to be described, the work of computing is reduced by using a modified set of variables for plotting. The power-required curves for all weights and altitudes may be condensed to a common curve (neglecting compressibility effects) when plotted on coordinates of P_{t_w} and V_{t_w} , where

$$P_{t_w} = \sqrt{\sigma} \left(\frac{\text{reference gross weight}}{\text{new gross weight}} \right)^{3/4} P \quad (14.59)$$

$$V_{t_w} = \sqrt{\sigma} \left(\frac{\text{reference gross weight}}{\text{new gross weight}} \right)^{1/4} V \quad (14.60)$$

The power-available curves, of course, take on a different appearance when plotted in this fashion. The true power and velocity at a point are obtained by use of Eq. (14.59) and (14.60), respectively. For example, in Fig. 14.15 the data from Fig. 14.1 for a constant-speed propeller at sea level and 15,000 ft (supercharged to 10,000 ft) have been plotted on coordinates of P_{t_w} and V_{t_w} . In addition, a 15,000-ft curve is shown for 10 per cent increase in gross weight. The intersection of the "15,000-ft, reference gross weight = W " curve and the power-required curve comes where $P_{t_w} = 487$ hp and $V_{t_w} = 164.5$ mph. The corresponding true power and velocity, by Eqs. (14.59) and (14.60), are as follows:

$$P = \frac{P_{t_w}}{\sqrt{\sigma}} = 1.261 P_{t_w} = 615 \text{ hp}$$

$$V = \frac{V_{t_w}}{\sqrt{\sigma}} = 1.261 V_{t_w} = 207.5 \text{ mph}$$

These values check the corresponding intersection on Fig. 14.1.

The method described above involves no approximations that are not already contained in the conventional curves of P_r and P_a vs. V . It is merely a convenient way of presenting the data, so that only one P_r vs. V curve is needed.

In most other methods, the power-required equation is represented by the approximate equation developed in Art. 11-6

$$P_r = \frac{f\sigma V^3}{146,600} + \frac{W^2}{3.01\sigma b^2 e V} \quad (14-61)$$

because it lends itself to mathematical manipulation. In one method in particular, this equation is made dimensionless by

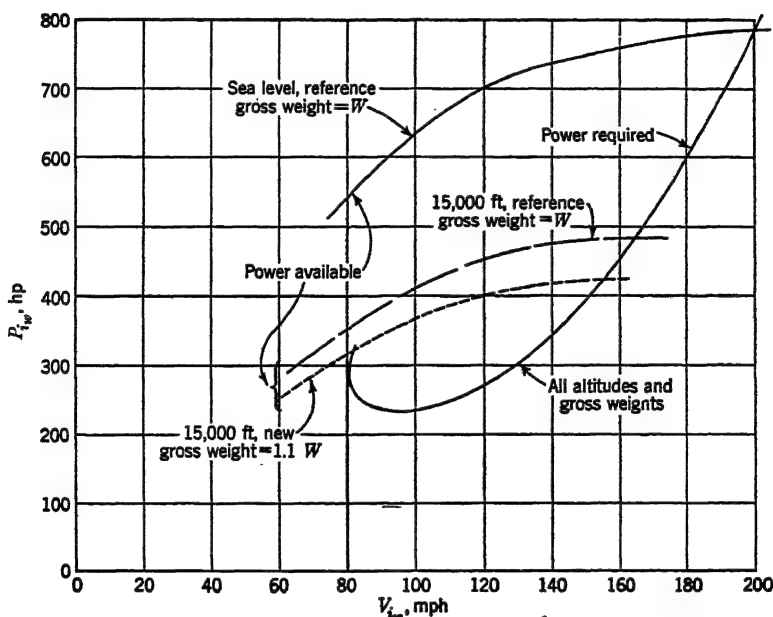


FIG. 14-15. Power relationships for the airplane of Fig. 14-1, using a simplified method of plotting.

dividing both sides by the power required at $(L/D)_{\max}$; *i.e.*, power required at $(L/D)_{\max}$ may be represented by either of the following equations:

$$P'_r = 2P'_{r_p} = \frac{2f\sigma(V')^3}{146,600} \quad (14-62)$$

$$P'_r = \frac{2P'_{r_i}}{e} = \frac{2W^2}{3.01\sigma b^2 e V'} \quad (14-63)$$

where P'_r is power required at $(L/D)_{\max}$, hp

P'_{r_p} is equivalent parasite power required at $(L/D)_{\max}$, hp

P'_{r_i} is induced power required at $(L/D)_{\max}$, hp

V' is velocity at $(L/D)_{\max}$, mph

Dividing the left side of Eq. (14-61) by P'_r , the first term on the right by Eq. (14-62), and the second term on the right by Eq. (14-63),

$$\frac{P_r}{P'_r} = \frac{1}{2} \left[\left(\frac{V}{V'} \right)^3 + \frac{V'}{V} \right] \quad (14-64)$$

A unique nondimensional relationship is thus obtained for representing the power-required equation for all weights, altitudes, wing areas, and aspect ratios. The power-available curve may not generally be represented mathematically, except by examination of existing curves¹ of η vs. J for constant C_P (the discussion is limited here to constant-speed propellers). The success with which the power available is represented then depends upon the success with which the propeller characteristics are represented. There is no particular point in pursuing this train of thought further, except to state that it is possible to find a fair degree of correlation of aerodynamic characteristics between propellers having the same activity factor, advance ratio, and power coefficient, so that curves may be plotted, based upon experimental evidence, that allow graphical solution of the efficiency and hence P_a , if the three variables are known.²

The problem of devising a system for rapid performance estimation is tempered by the end result desired. The rapidity with which the computations can be made depends largely upon the number of approximations involved. The principal utility of a rapid performance method is not so much that it allows the computer to make *one* rapid computation, but that it allows him to go through a great number of computations with small changes in the particular variables involved, which allows him to arrive at an optimum configuration of the airplane. Even though the actual performance figures he computes might not be precise, the *variations* in performance produced by variations in the physical properties of the airplane are usually estimated quite accurately; *e.g.*, the effect of a 10 per cent change in wing aspect ratio on performance may be shown very quickly, even though the absolute values of the performance may not be precise.

These same general statements may also be applied to turbo-jet performance, except that there is no propeller-efficiency variation

¹ Recall that such a curve has the same shape as a curve of P_a vs. V .

² Boeing Document No. 4842, A General Propeller Chart Suitable for a Wide Range of Propellers, Boeing Aircraft Co., 1943.

to complicate the estimation. Effects of compressibility may be more serious, however.

PROBLEMS

14-1. A high-speed airplane is constructed so that the outboard wing panel slides into the inboard panel, producing a 20 per cent reduction in wing area. For the original configuration, the residual parasite area f_r is 60 per cent of the total parasite area f . If $dP_a/dV = 0$ at V_{\max} , find the per cent increase in V_{\max} corresponding to the reduced area. Ignore effects of compressibility, and make any reasonable assumptions that are necessary.

14-2. In Prob. 14-1 find the per cent reduction in P_r corresponding to flight at the same V_{\max} , with the reduced wing area.

14-3. Prove that the velocity for maximum rate of climb occurs when $dP_a/dV = dP_r/dV$, and verify the truth of this relation on Fig. 14-1.

14-4. Rated power of an engine = 1500 bhp at sea level; $\eta = 0.70$ at the velocity for $C_{k_{\max}}$; $f = 12$ sq ft at $C_L = 0$; $S = 400$ sq ft; $W = 16,000$ lb; $dC_D/dC_L^2 = 0.03$.

a. Find the sea-level velocity corresponding to $(L/D)_{\max}$.

b. Find sea-level $C_{k_{\max}}$, assuming it to occur at the velocity of part a. (Assume cosine of climb angle is 1.0.)

14-5. The vertical component of the velocity of an airplane in a power-off glide is called *sinking speed*. Find an equation for sinking speed v_s in feet per second. Do not assume glide angle is a small angle. Find v_s as a function of *only* the variables shown:

$$v_s = f(l_w, \sigma, C_L, C_D)$$

14-6. Using the results of Prob. 14-5, find an equation for minimum sinking speed. Assume the glide angle is small, so that cosine of small angles may be considered 1.0. Find $v_{s_{\min}}$ as a function of *only* the variables shown:

$$v_{s_{\min}} = f(f, W, b, e, \sigma)$$

Check the equation dimensionally, with due regard for the dimensions of any constants.

14-7. Replot the curves of P_a and P_r vs. V from Probs. 11-7a and d and 13-7d on a new sheet of graph paper.

a. Superimpose P_a and P_r curves for altitudes of 6000, 9000, 16,000, and 24,000 ft from 100 to 350 mph for the same airplane, engines, and propellers as in Probs. 11-7a and d and 13-7d.

b. Using the data in part a, plot V_{\max} , V_{\min} , $V_{C_{k_{\max}}}$, $C_{k_{\max}}$, and T_{\min} vs. altitude from sea level to the absolute ceiling.

c. Find $C_{k_{\max}}$ at sea level for two engines inoperative.

d. Compute $C_{h_{\max}}$ and V_{\max} at sea level for 30 per cent increase in gross weight, using the results of Prob. 11-7e.

e. Assuming the airplane carried 15,000 lb of gasoline (included in the 70,000 lb weight), find the maximum range at sea level, and the time corresponding. Assume the minimum operating N of the engine is 1400 rpm.

f. For standard sea-level conditions, compute take-off time and distance to clear a 50-ft obstacle, using take-off power (without water). Assume the complete take-off to occur at $C_L = 1.25$, which is the lift coefficient corresponding to maximum angle of climb. Assume no wind, $\mu = 0.02$, and neglect the change in aerodynamic characteristics due to landing-gear extension, proximity of the ground, etc. Assume cosine of climb angle is 1.0. Use Figs. IVc and d, Appendix B.

g. Compute landing distance, for standard sea-level conditions, to clear a 50-ft obstacle with power off, flaps extended. Assume the complete landing to occur at $C_L = 2.0$, for which the complete airplane drag coefficient, including that due to flap extension, is $C_D = 0.20$. Assume no wind, $\mu = 0.4$, and neglect the change in aerodynamic characteristics due to landing-gear extension, proximity to the ground, etc. Assume cosine of glide angle = 1.0. $W = 70,000$ lb.

14-8. Develop equations similar to Eqs. (14-32) and (14-33) for ground-run time and distance to take-off with head wind.

14-9. Plot V_{\max} , V_{\min} , $C_{h_{\max}}$, and T_{\min} vs. altitude for the 9000-lb airplane depicted in Fig. 14-14.

CHAPTER 15

STABILITY AND CONTROL

Stability may be defined as the tendency for a body to return to a position of equilibrium after an infinitesimal displacement. Controllability may be defined as the ease of operation and the effectiveness of the mechanism used to cause the displacement.

Stability may be illustrated by a simple example. Let a ball be placed in a concave surface (Fig. 15-1). If displaced, it tends



Fig. 15-1. Physical illustrations of stability.

to return to its original position of equilibrium; it is, therefore, *stable*. Let the ball be placed on a flat surface. If displaced it exhibits no tendency to move in any direction; it is, therefore, *neutrally stable*. Now let the ball be placed on a convex surface. If displaced it tends to move away from the original position of equilibrium; it is, therefore, *unstable*. These three conditions are concerned with *static* stability.

Dynamic stability has to do with the continued motion of the body and may be illustrated by considering the ball in the concave surface. The friction forces on the ball are always in a direction opposite from its motion. They provide a positive *damping force* that tends to make the ball oscillate with decreasing amplitude and finally come to rest; the ball is *dynamically stable*. If friction and aerodynamic forces are zero (an impossible condition, but convenient for these discussions), there is no damping force, and the ball oscillates indefinitely with constant amplitude; it is *neutrally dynamically stable*. If the friction force is overcome by some external force, achieved, for instance, by blowing on the ball in the direction of its motion, the ball oscillates with increasing amplitude or does not return at all to its position of

equilibrium, according to the magnitude of the external force. In either case, it does not return to equilibrium after an indefinite time interval; it is, therefore, *dynamically unstable*. In Fig. 15·2, curves of displacement vs. time are plotted for several conditions, showing examples of static and dynamic stability and instability.

The fact that a body is stable is often not a sufficient specification. For instance, an automobile with no shock absorbers, although statically and dynamically stable, is uncomfortable because the oscillations do not damp out quickly enough. Installation of shock absorbers increases positive damping and causes a more rapid decrease in amplitude with time. Again, an airplane

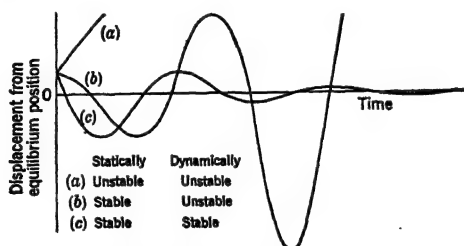


FIG. 15·2. Graphical illustrations of stability.

may have too much static stability, making it difficult to control, or too little dynamic stability, making it uncomfortable for riding or exasperating for a bombardier or gunner.

Stability of an airplane is referred to the airplane axes passing through its center of gravity; consequently only angular displacements are accounted for. Loss in altitude, or sideways displacement is never charged against the stability of the airplane, even though it may accompany a stable or unstable condition. Dynamic-stability studies of an airplane are very complicated, but fortunately most rigid¹ conventional airplanes are dynamically stable if they are statically stable. Furthermore, the static stability is an *indication* of the amount of dynamic stability; consequently airplanes may frequently be designed according to static-stability criteria. Throughout the rest of the discussion, "stability" will imply "static stability" unless stated otherwise.

All stability considerations are concerned with control surfaces, *fixed* or *free* (floating), giving rise to *fixed stability* and *free stability*.

¹ Structural elasticity of an airplane results in deformations that may produce static or dynamic instability. These considerations are beyond the scope of this text.

In general, an airplane should be at least neutrally stable, with control surfaces free.

15-1 Definitions. An airplane must be stable in all possible flight attitudes. The most convenient method of analysis is to consider three mutually perpendicular axes that intersect at the center of gravity of the airplane; then if the airplane is stable about these three axes, it must be stable about any axes. Two separate systems of axes are frequently used: one is referred to

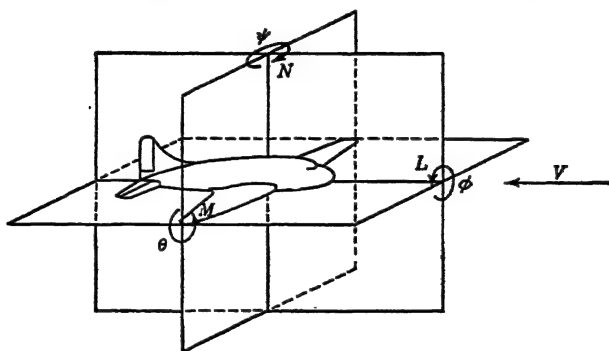


FIG. 15-3. Positive moment and angle conventions.

the remote velocity, called the *wind axes*, and the other is referred to the longitudinal axis of the fuselage, called the *body axes* or *stability axes*. Wind axes will be chosen in the present discussions, not only because most wind-tunnel data are presented in this form but also because they lead to simpler explanations. In Fig. 15-3, positive forces, moments, and angles are shown for reference. In the following table the moments and angles are further clarified:

Motion		Moment	Coefficient
Roll.....	ϕ	L^*	$C_l = \frac{L}{qSb}$
Pitch.....	θ^\dagger	M	$C_m = \frac{M}{qSc}$
Yaw.....	ψ	N	$C_n = \frac{N}{qSb}$

* The use of the symbol L for both rolling moment and lift is somewhat confusing but is standard NACA nomenclature.

† The symbol θ is perfectly general for angle of pitch, whereas α refers specifically to the wing chord.

15.2 Longitudinal Stability. Longitudinal stability is concerned with the motion of an airplane in pitch. Stability requires that a restoring moment accompany an angular displacement from equilibrium, and this is indicated by a negative $dC_{m_{cg}}/dC_L$; i.e., stability results if a diving moment accompanies an increment

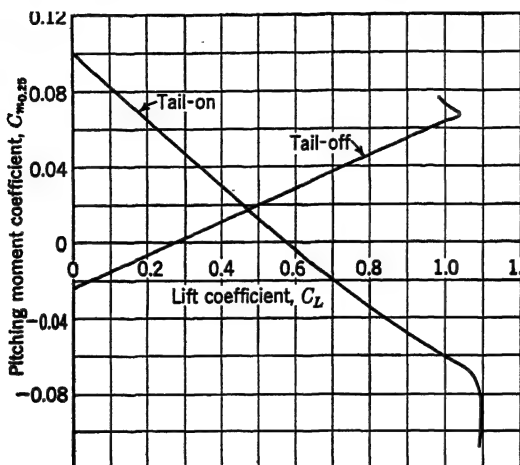


FIG. 15.4. Typical pitching moment curves. (Based on UWAL data.)

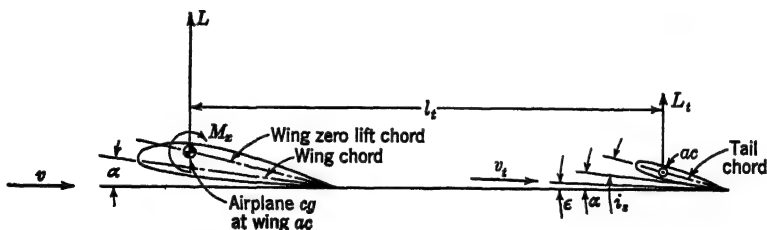


FIG. 15.5. Positive force, moment, and angle definitions on the wing and tail of an airplane.

in C_L . An airplane without tail may be stable or unstable depending upon the location of the cg with respect to the wing ac, but in general it is not both stable and balanced. The function of the tail surface is to control, balance, and stabilize the airplane (Fig. 15.4).

The equations for $C_{m_{cg}}$ for tail-on may be obtained from the geometry of the airplane. In the following equations all moments will be assumed to refer to the airplane cg, and the cg will be

assumed to be at the wing ac. Furthermore, the ac will be assumed to be on the zero-lift chord. From Fig. 15-5.

$$M = M_x + M_t \quad (15.1)$$

where M is the total pitching moment (in pound-inches) about the airplane cg. Subscripts x and t refer to "tail-off" and "tail," respectively. The tail-off pitching moment arises from the wing, nacelles, fuselage, etc., and depends upon the horizontal position of the lift vector and the vertical position of the drag vector of each component with respect to the wing ac. Generally speaking, C_{m_x} is negative when $C_L = 0$, while dC_{m_x}/dC_L is positive. The tail pitching moment arises mainly from the product of its lift and the tail length (distance from cg to tail ac). The moment about the tail ac, and the product of the tail drag and its lever arm, are usually negligible by comparison. Furthermore, the cosine of small angles may be assumed equal to 1.0; hence, from Fig. 15-5,

$$M = M_x - L_t l_t \quad (15.2)$$

where L_t is tail lift, lb

l_t is the tail length, from airplane cg to tail ac, in.

The tail lift is

$$L_t = C_{L_t} S_t q_t \quad (15.3)$$

where subscript t refers to the tail. Substituting Eq. (15.3) in Eq. (15.2) and dividing by qSc allows solution for C_m .

$$C_m = C_{m_x} - \frac{q_t}{q} \frac{l_t}{c} \frac{S_t}{S} C_{L_t} \quad (15.4)$$

The ratio q_t/q is called the *tail efficiency factor* (see section headed Interference, page 335) and is denoted by η_t . The tail lift coefficient may be expressed in terms of its angle of attack, assuming a symmetrical tail section.

$$C_m = C_{m_x} - \eta_t \frac{l_t}{c} \frac{S_t}{S} a_t \alpha_t \quad (15.5)$$

where a_t is slope of tail lift curve, per deg

α_t is tail angle of attack, referred to local velocity v_t at tail, deg

The tail angle of attack is related to the wing angle of attack by

$$\alpha_t = \alpha + i_s - \epsilon \quad (15.6)$$

where α is wing angle of attack, deg

i_s is stabilizer setting referred to wing chord, deg

ϵ is down-wash at tail from wing, deg

Substituting Eq. (15.6) in Eq. (15.5) yields

$$C_m = C_{m_x} - \eta_t \frac{S_t l_t}{S c} a_t (\alpha + i_s - \epsilon) \quad (15.7)$$

The wing angle of attack may be expressed in terms of the wing lift coefficient:

$$\alpha = \frac{C_L}{a} + \alpha_{L_0} \quad (15.8)$$

where a is slope of wing lift curve, per deg

α_{L_0} is angle of zero lift of wing, deg

Also the down-wash angle may be expressed in terms of the wing lift coefficient. Theoretically, the down-wash angle is double the wing induced angle at a great distance from the wing trailing edge, but it may be more or less than this value depending upon the wing plan form, the horizontal and vertical positions of the tail with respect to the wing, etc. For present analyses, however, it will be represented by the conventional equation

$$\begin{aligned} \epsilon &= 2\alpha_t \\ &= 2 \frac{C_L}{\pi A} \quad (57.3) \end{aligned} \quad (15.9)$$

where A is wing aspect ratio.

Substituting Eqs. (15.8) and (15.9) in Eq. (15.7) gives

$$C_m = C_{m_x} - \eta_t \frac{S_t l_t}{S c} a_t \left[\left(\frac{1}{a} - \frac{36.5}{A} \right) C_L + \alpha_{L_0} + i_s \right] \quad (15.10)$$

Equation (15.10) may be differentiated with respect to C_L :

$$\frac{dC_m}{dC_L} = \frac{dC_{m_x}}{dC_L} - \eta_t \frac{S_t l_t}{S c} a_t \left(\frac{1}{a} - \frac{36.5}{A} \right) \quad (15.11)$$

Equation (15.11) shows that the addition of the tail causes a rotation in a clockwise direction of the C_m vs. C_L curve, as in Fig. 15.4. The amount of rotation is represented by the second

group of terms on the right and is seen to depend directly upon tail area and tail length. The tail efficiency factor η_t varies among airplanes from about 0.70 to about 0.90 (power off), being dependent upon tail position and model configuration. For light planes, the ratio of tail area to wing area, S_t/S , is about 0.15; the tail-length ratio l_t/c is usually about 2.7; and the tail aspect ratio is about 4. For heavy multiengined airplanes, the ratio of

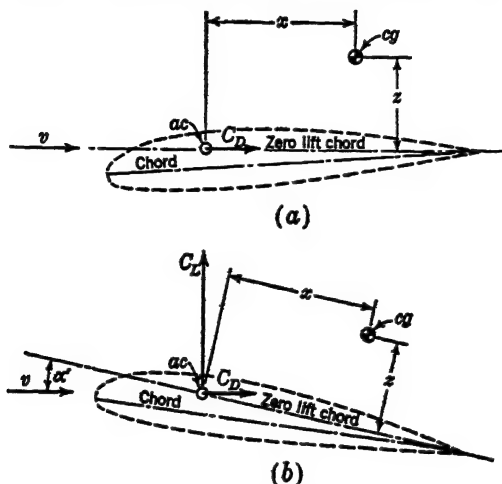


FIG. 15-6. Diagram of airplane cg location with respect to wing ac: (a) zero lift, (b) angle of attack = α' referred to zero-lift chord.

tail area to wing area is about 0.20; the tail-length ratio is usually about 4.0; and the tail aspect ratio is usually about 5.

Equation (15-11) is one form of the stability equation. It is not completely general, however, because a number of variables have been ignored in its development. Before continuing, these variables will be discussed, and the equation itself will be the subject of closer scrutiny.

It should be noted that the experimental data shown in Figs. 15-4 and 15-7 to 15-13 are presented in conventional form as obtained from wind-tunnel tests, but during such tests the model configuration and power (if any) are held constant. An airplane in flight has control surfaces deflected in such a manner that the sum of all the moments arising from aerodynamic forces and thrust (if any) about the cg is zero. For instance, the elevator deflection at any lift coefficient must be sufficient to balance the

airplane ($C_{m_{cg}} = 0$) and therefore is evidently a function of lift coefficient. Since longitudinal stability of an airplane is dependent upon $dC_{m_{cg}}/dC_L$ at constant control-surface deflection, the curves as presented are indicative of *stability* but must be shifted vertically in order to produce *balance*, this vertical shift being accomplished by elevator deflection.

Center-of-gravity Position. The assumption that the cg is coincident with the wing ac is by no means justified in most aircraft. It may be displaced horizontally or vertically, or both. In Fig. 15-6a, a condition is chosen for which the cg is aft and above the ac by distances¹ x and z , respectively, at $C_L = 0$. For an arbitrary *positive* lift coefficient, the cg then assumes a new attitude shown in Fig. 15-6b. The change in pitching moment coefficient at the corresponding angle of attack, α' , measured from the angle of zero lift, is

$$\Delta C_m = x(C_L \cos \alpha' + C_D \sin \alpha') + z(C_L \sin \alpha' - C_D \cos \alpha') \quad (15-12)$$

Since α' is a small angle, no large error is introduced by assuming $\cos \alpha' = 1.0$, $C_D \sin \alpha' = 0$, and $\sin \alpha' = \alpha' = C_L/m$; thus

$$\Delta C_m = xC_L + z\left(\frac{C_L^2}{m} - C_D\right) \quad (15-13)$$

The drag coefficient C_D may be expressed in terms of C_L .

$$C_D = C_{D_{p_{\min}}} + \frac{C_L^2}{\pi A e} \quad (15-14)$$

Substituting Eq. (15-14) in Eq. (15-13) gives

$$\Delta C_m = xC_L + zC_L^2\left(\frac{1}{m} - \frac{1}{\pi A e}\right) - zC_{D_{p_{\min}}} \quad (15-15)$$

Compared to all the other terms in the above equation, the last one will generally be very small and may usually be ignored. The reciprocal slope of the lift curve may be expressed in terms of the reciprocal slope of the lift curve for infinite aspect ratio by differentiating Eq. (6-4) with respect to C_L .

$$\frac{1}{m} = \frac{1}{m_0} + \frac{1}{\pi A} \quad (15-16)$$

¹ x and z are in fraction of chord.

Thus

$$\Delta C_m = x C_L + z C_L^2 \left[\frac{1}{m_0} + \frac{1}{\pi A} \left(1 - \frac{1}{e} \right) \right] \quad (15-17)$$

The last group of terms is always small compared to $1/m_0$ and may be neglected; thus the final equation is

$$\Delta C_m = x C_L + z \frac{C_L^2}{m_0} \quad (15-18)$$

Inspection of Eq. (15-18) reveals that the effect of rearward dis-

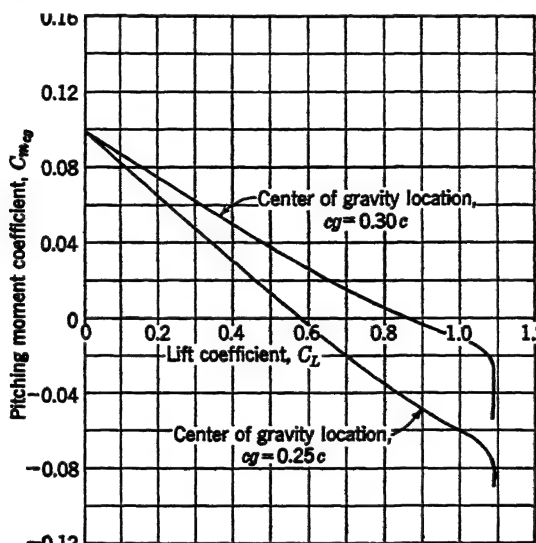


FIG. 15-7. Effect on pitching moment of the horizontal position of the center of gravity.

placement of the cg is to produce a climbing moment that is linearly dependent upon C_L and that an upward displacement produces a climbing moment that is dependent upon the square of the lift coefficient. In Fig. 15-7, the effect of horizontal displacement of the cg is illustrated, while in Fig. 15-8, the effect of vertical displacement is shown. It is evident that the most critical position of the cg, from the standpoint of stability, is when the cg is aft and above the ac. Notice that Eq. (15-18) and its derivative may be added directly to Eqs. (15-10) and (15-11), respectively, in order to make these equations more general.

A word of caution should be inserted here because of a simplifying assumption made in the development of the equations. At high lift coefficient the drag coefficient usually increases rather rapidly, and on some airplanes this produces a considerable destabilizing moment. This condition may be important, because it occurs at a low speed where control is most critical.

Stabilizer Effect. The effect of changing stabilizer setting is to produce a parallel shift in the pitching-moment curve, as in

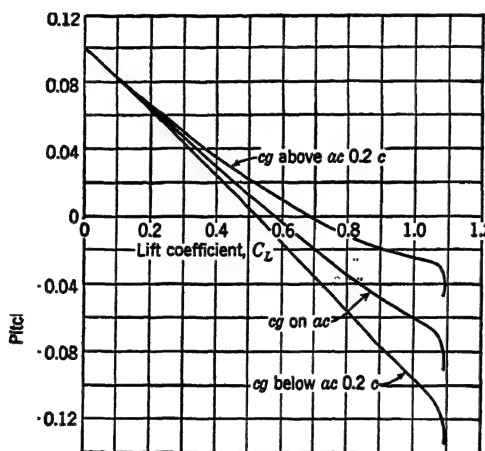


FIG. 15-8. Effect on pitching moment of the vertical position of the center of gravity.

Fig. 15-9, because the lift increment produced by a change in setting is independent of the airplane angle of attack. The moment change arises from the product of the lift increment and the constant tail length. This is verified by Eq. (15-10), which shows that an increment in stabilizer setting causes a negative pitching-moment change that is independent of lift coefficient. These statements, of course, imply that a change in stabilizer setting has no influence on stability.

Elevator Effect. Positive deflection of the elevator (trailing edge down) produces an increment in tail lift coefficient that is independent of the angle of attack of the tail, in a manner similar to the effect of a plain flap on C_L (see Art. 10-1). The tail length may be assumed independent of angle of attack of the airplane; hence deflection of the elevator produces a constant moment

change as in Fig. 15-10. The effectiveness of an elevator in producing a moment change is greatest for small deflections and usually becomes nonlinear after about 15 or 20 deg. Furthermore, the hinge moment frequently increases rapidly for these larger

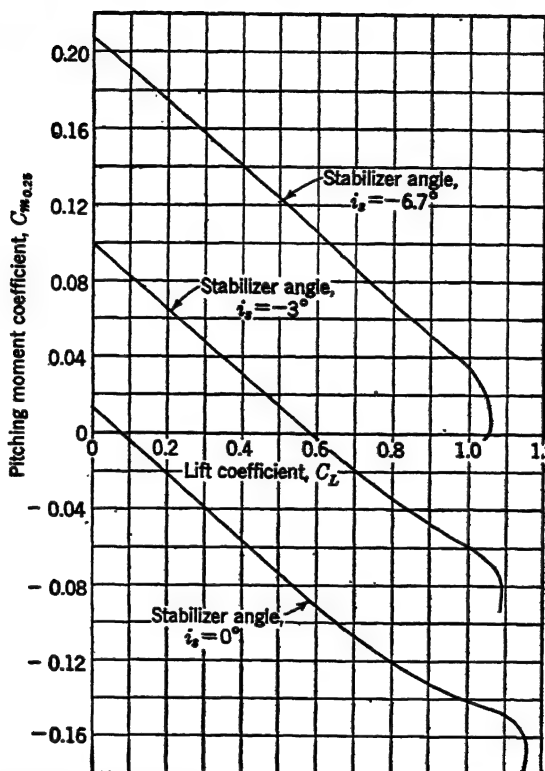


FIG. 15-9. Effect of stabilizer setting on pitching moment. Elevator setting, $\delta_e = 0^\circ$. (Based on UWAL data.)

angles; consequently, there is little advantage in designing an elevator for more than about 30-deg deflection.

If the elevator is allowed to float (hands off the stick), the effectiveness of the horizontal tail is considerably impaired, and the slope reduces as shown by the elevator-free curve in Fig. 15-10.

Tail Position. If the tail is in the wake of the wing, it will be subjected to the down-wash from the wing and will be in a region of retarded flow. If the tail is high, it will be less influenced by both of these effects.

The flow over the tail is also dependent upon engine power setting and upon the particular configuration of the wing such as plan form, flap setting, etc.

Slope of the Tail Lift Curve. Several equations have been suggested for predicting the lifting properties of an airfoil of low

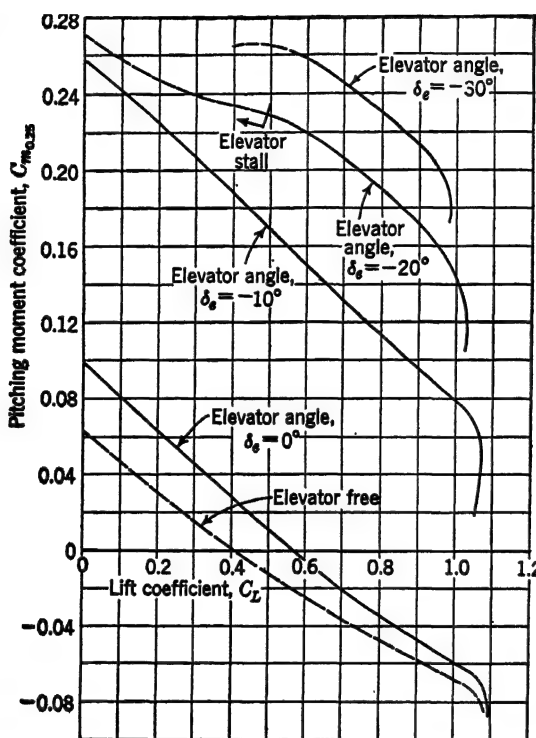


FIG. 15-10. Effect of elevator setting on pitching moment. Stabilizer setting, $i_s = -3^\circ$. (Based on UWAL data.)

aspect ratio, such as that used on a tail surface. None has received universal acceptance. The equation

$$m = 2\pi \left(\frac{A}{A+3} \right)$$

or

$$a = 0.1095 \left(\frac{A}{A+3} \right) \quad (15-19)$$

has been suggested by K. D. Wood¹ and is used in this text for all aspect ratios less than 6, *e.g.*, for tail surfaces.

Twin vertical surfaces are frequently mounted at the extremities of the horizontal surface, and this increases the effective aspect ratio of the horizontal surface. The following equation² may be used for estimating the effective aspect ratio of the horizontal surface:

$$A_E = A \left[1 + \left(\frac{5}{3} \right) \left(\frac{h}{b} \right) \right] \quad (15-20)$$

where A_E is effective aspect ratio of horizontal surface, dimensionless

A is geometric aspect ratio of horizontal surface, dimensionless

h is over-all height of one vertical surface, ft

b is span between vertical surfaces, ft

This equation assumes that the chord lengths of the horizontal and vertical surfaces are equal at the juncture.

Interference. The horizontal tail does not act as an independent airfoil, because the inboard region is immersed in the boundary layer of the fuselage or the vertical tail; consequently, its lifting properties are generally less than would be predicted for an airfoil of the same aspect ratio when acting alone. This is generally accounted for in the tail efficiency factor, which merely means that η_t is not strictly just a ratio of dynamic pressures.

Flaps. Flaps on a wing alone produce a large diving moment at constant lift coefficient, because of the large lift increment concentrated near the wing trailing edge. On the complete airplane, this moment is counteracted by another arising from the increased down-wash over the tail; *i.e.*, for a particular lift coefficient the flaps cause a redistribution of wing down-wash that gives a greater down-wash in the inboard region of the wing. This increased down-wash tends to reduce the tail lift and produce a climbing moment. The final effect of deflecting the flaps depends upon their geometry and upon the tail position. Flap deflection may cause a shift in the curve of $C_{m_{cg}}$ vs. C_L but ordinarily does not have a large effect on the slope (Fig. 15-11).

¹ Wood, K. D., "Technical Aerodynamics," McGraw-Hill, New York, 1947.

² From *TR* 267.

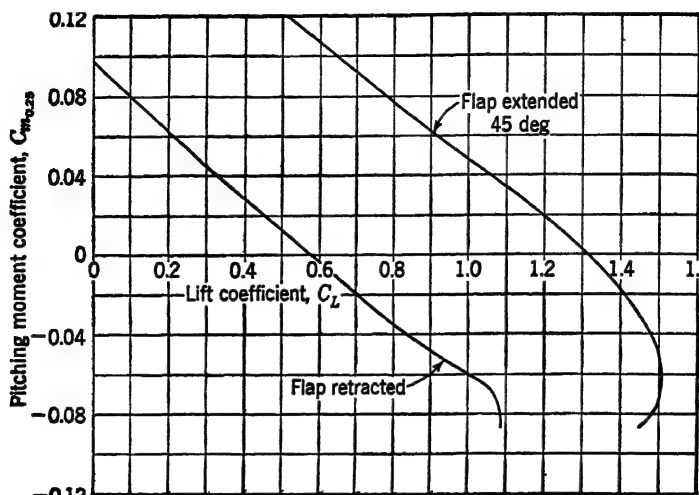


FIG. 15-11. Effect of flap deflection on pitching moment of an airplane. (Based on UWAL data.)

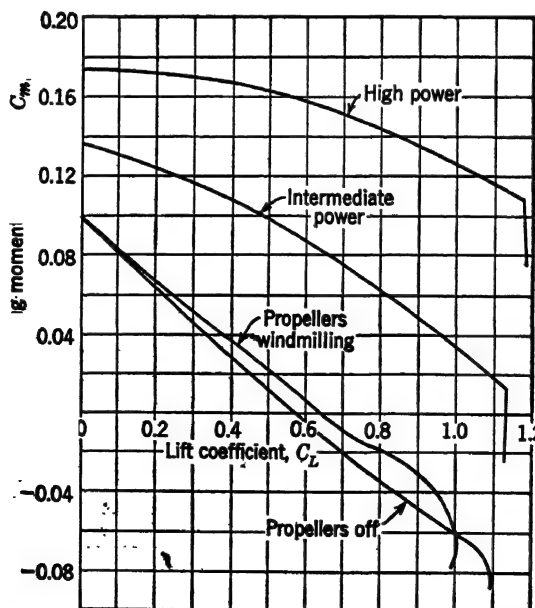


FIG. 15-12. Effect of power on pitching moment of an airplane. (Based on UWAL data.)

Power. The effect of power depends upon several variables. First, if the thrust axis is below the cg, a climbing moment is produced. Second, if the tail is immersed in the slip stream of the propeller, the velocity and down-wash angle are considerably modified, the usual combined effect being destabilizing, as shown in Fig. 15-12. Third, as the wing angle of attack is increased, the propeller is pitched positively, and this produces a lifting force that arises from the modified blade torque forces:¹ if the propeller is well forward of the cg, as in a single-engined airplane, the resulting destabilizing moment may be appreciable.

Ground Effect. Proximity to the ground causes an effective increase in aspect ratio of the wing, which reduces its drag coefficient at a particular lift coefficient, but *has no appreciable effect on its pitching moment.* The tail aspect ratio is also effectively increased, which effectively increases its lift-curve slope. Superimposed on this is the influence of the ground in changing the flow pattern on the tail: it provides a constraint that forces the air to follow the contour of the level ground. The cumulative effect is to produce a considerable increase in stability near the ground as shown in Fig. 15-13. Similar results occur with flap deflected and with power.

With all the above variables to consider in stability prediction, there is small wonder that wind tunnels are necessary for accurately determining the characteristics of a particular configuration. Of course, a great number of tests have been run on many airplanes, and empirical factors have been evolved that apply to particular classes of airplanes. These factors allow power-off (gliding) stability to be predicted quite accurately.

There are two limits to the amount of stability an airplane should have, or, put another way, there are two limits to the size of stabilizer and elevator. First, the airplane should be stable for all possible flight attitudes and configurations, including elevator-free, and second, it must not be so stable that the elevator is unable to provide balance at the landing C_L near the ground, with flaps and landing gear down. These two specifications are directly related to the *cg travel* of the airplane. The cg cannot be allowed to move so far rearward that the airplane is not suffi-

¹ For a complete discussion of this effect, see *WR L-219* and *WR L-336*.

ciently stable according to the first requirement above, nor may it be allowed to move so far forward that the elevator cannot balance the plane under landing conditions according to the second requirement.

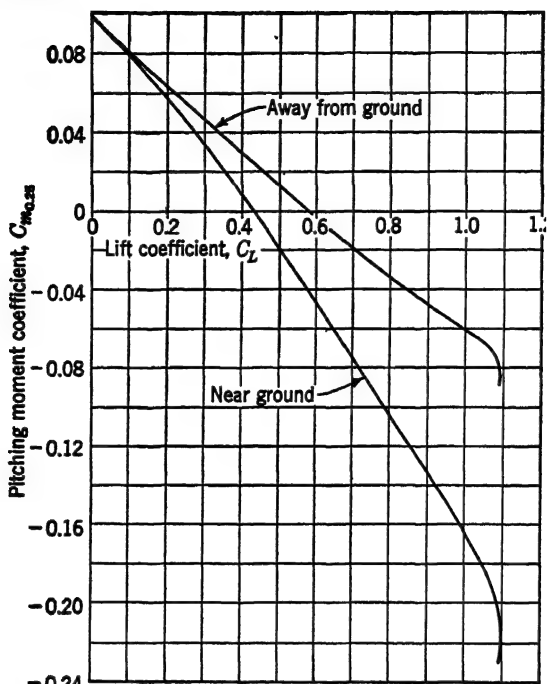


FIG. 15-13. Effect of proximity to the ground on pitching moment of an airplane, flaps retracted, power off. (Based on UWAL data.)

15-3 Directional Stability. Directional stability is concerned with the motion of the airplane in yaw. Stability requires that a restoring moment accompany an angular displacement from equilibrium, and this is indicated by a negative $dC_{n_{cg}}/d\psi$; i.e., the airplane is stable if a negative yawing moment accompanies an increment in yaw angle. The wing, fuselage, nacelles, etc., of an airplane are usually unstable, and the vertical tail supplies the required moment to provide stability. Directional stability is considerably easier to analyze than longitudinal stability because of the symmetry in the problem. The yawing moment for the complete airplane about the cg may be written

$$N = N_x + N_t \quad (15-21)$$

where N is total yawing moment (in pound-inches) about the airplane cg. Subscripts x and t refer to tail-off and tail, respectively. The tail yawing moment may be written in terms of the lateral force on the vertical tail and its lever arm to the airplane cg, ignoring tail drag, assuming a symmetrical tail section, and assuming $\cos \psi = 1.0$.

$$N_t = -Y_t l_t \quad (15\cdot22)$$

The lateral force may be expressed

$$\begin{aligned} Y_t &= C_{Y_t} q_t S_t \\ &= \left(\frac{dC_Y}{d\psi} \right)_t \psi q_t S_t \end{aligned} \quad (15\cdot23)$$

where C_{Y_t} is tail lateral force coefficient. Equation (15·23) may be substituted in Eq. (15·22), and the result substituted in Eq. (15·21). After division by qSb ,

$$C_n = C_{n_x} - \eta_t \frac{S_t l_t}{S b} \left(\frac{dC_{Y_t}}{d\psi} \right) \psi \quad (15\cdot24)$$

Equation (15·24) may be differentiated with respect to ψ :

$$\frac{dC_n}{d\psi} = \frac{dC_{n_x}}{d\psi} - \eta_t \frac{S_t l_t}{S b} \frac{dC_{Y_t}}{d\psi} \quad (15\cdot25)$$

Equation (15·25) is somewhat similar to its counterpart for longitudinal stability [Eq. (15·11)] and may be treated in much the same manner.

Change in fore-and-aft position of the center of gravity has negligible effect upon stability. Rudder deflection produces a shift in the yawing-moment curves similar to that for the elevator, and a free rudder causes a reduction in stability (Fig. 15·14).

The presence of the horizontal tail increases the effective aspect ratio of a conventional vertical tail about 30 per cent if the horizontal tail is placed at the base of the vertical tail. It has no effect, however, if placed at the mid-span.¹

The vertical position of the wing is very important in determining the flow pattern over the vertical tail and hence the directional stability. A high-wing position is destabilizing, and a low-wing position is stabilizing. The slope of the yawing moment curve,

¹ See *TN 1050* for a complete discussion.

$dC_n/d\psi$, increases about 0.0001 for each per cent of wing span that the wing is moved vertically upward.¹

Ground effect is not very important in affecting directional stability, but flap deflection may or may not be important, depending on wing position, flap configuration, etc.

The effect of power depends upon whether single or dual rotation is used and on whether the airplane is single-engined or multiple-engined; in other words, it depends upon the direction of the

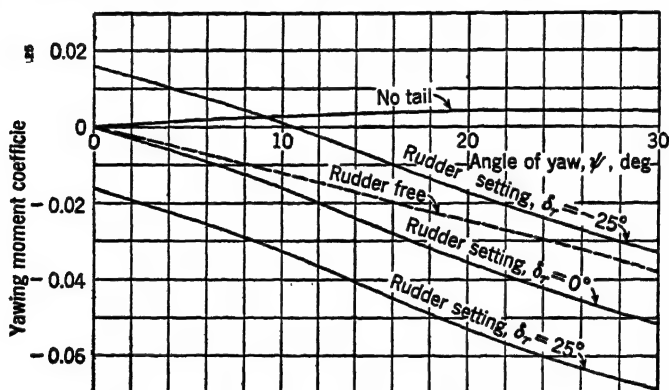


FIG. 15-14. Effect of rudder setting on yawing moment of an airplane. (Based on UWAL data.)

flow over the tail and upon how much of the tail is immersed in the slip stream. The directional stability may be increased when the tail is within the slip stream, but may be decreased when the airplane is yawed sufficiently to cause the slip stream to miss the tail. Superimposed on the effects of slip stream is the destabilizing effect of a yawed propeller. This is the counterpart of the effect of a pitched propeller discussed under Longitudinal Stability on page 337.

An airplane should be at least stable for all possible flight attitudes and configurations, including rudder-free, but must not be so stable that the airplane cannot be balanced by the rudder for all possible flight maneuvers. The latter specification is, of course, directly associated with the design of the rudder. For any airplane, the sideslip in landing may be a critical maneuver. For a multiengined airplane, an unsymmetrical power condition

¹ See NACA-University Conference on Aerodynamics, A Compilation of Papers Presented, June 21-23, 1948.

(engines on one side inoperative) may be critical. For an engine with conventional landing gear, "ground looping" may be critical. Ground looping is caused by main-wheel friction F in the yawed attitude of an airplane equipped with conventional landing gear, during landing, and is critical for the rearmost cg position (Fig. 15-15).

15-4 Lateral Stability. Lateral stability is concerned with the motion of an airplane after an initial roll. Unfortunately for purposes of analysis, an airplane is unable to execute a pure roll without an accompanying yaw, because, as is shown in Fig. 15-16, the lift vector is tilted sideways, giving a resultant side force. The

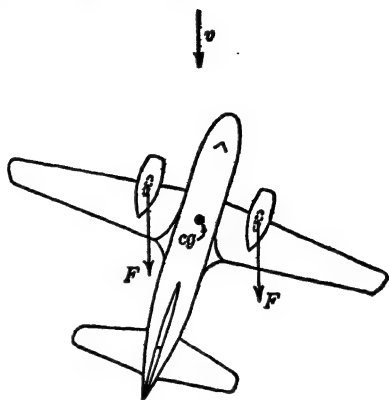


FIG. 15-15. Forces on an airplane equipped with conventional landing gear when yawed in the landing attitude.

roll, therefore, produces a sideslip. If the vertical tail is very large and the dihedral is small, the airplane goes into a spiral dive, producing *spiral instability*. If the vertical tail is small and the dihedral is large, the sideslip produces a greater lift on the down wing than on the up wing, which causes a rolling moment in the opposite direction. The airplane, therefore, sideslips in the opposite direction. The resulting pendulumlike motion gives an instability called *Dutch roll* because of its resemblance to a Dutchman on skates (Fig. 15-17). In general, a tendency toward spiral instability is not undesirable, because it gives the pilot plenty of warning and causes no physical discomfort as does Dutch roll. The requirement for satisfactory lateral stability is a rather nebulous specification based upon a fairly complicated theory. Practically, it is usually attained by empirical criteria based on experience gained from similar airplanes.

If the airplane is just at the stall angle and is then rolled, the increased angle of attack on the down wing causes stalling and consequent further roll. Ultimately, with both wings stalled at a mean angle of perhaps 45 deg, the down wing has the lesser lift coefficient and higher drag coefficient, with the result that the airplane *autorotates*, producing a *spin*. Usually ailerons and

elevator are almost completely ineffective because of their stalled condition; hence the rudder must be used to reduce angular

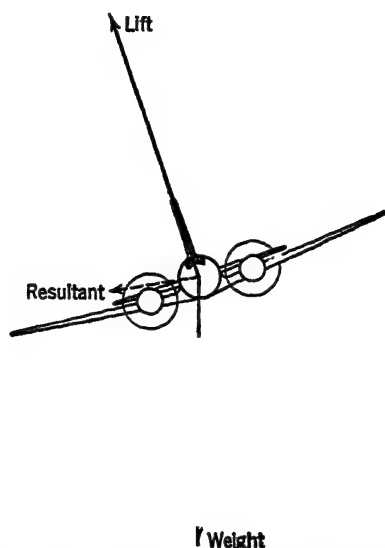


FIG. 15-16. Forces on an airplane in sideslip.

velocity. Then, although the airplane loses altitude, it gains forward speed and becomes unstalled.

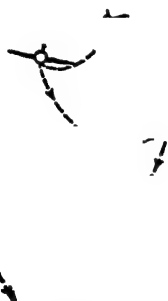


FIG. 15-17. Path of an airplane having Dutch-roll instability.

Prevention of inadvertent spinning hinges mostly on proper design of the wing. The tips should be the last region to stall, so that good aileron control is maintained even though the wing is partially stalled. This provides warning to the pilot before he is in serious difficulty.

15-5 Theoretical Hinged-surface Characteristics. Prediction of the aerodynamic characteristics of an elevator, rudder, or aileron is a difficult problem that usually is solved by relying

heavily upon experimental data. The theoretical aspects of the problem must be understood before an evaluation of the experimental data is attempted, and for this reason the present article is concerned with an explanation of the characteristics of

a simple hinged surface operating in a perfect fluid. Article 15-6 will deal with some of the important variables that affect an actual hinged surface in a real fluid.

This simple hinged surface consists of a main surface and flap. Both are flat plates, and the hinge is located at the leading edge of the flap. The problem is to predict the normal force coefficient C_N on the hinged surface and the hinge moment coefficient C_H

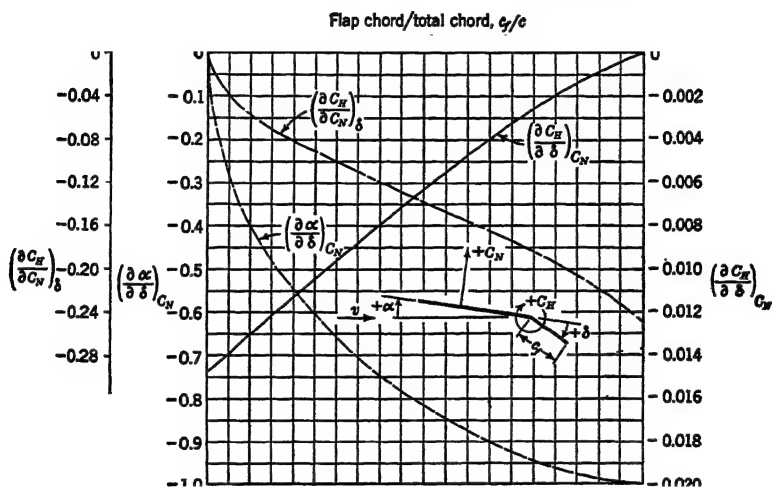


FIG. 15-18. Theoretical characteristics of a hinged flat plate without aerodynamic balance or gap. All angles are in degrees. (From TR 721.)

on the flap, resulting from either a change in angle of attack or from a flap deflection. The normal force, when multiplied by the appropriate lever arm (depending upon whether the hinged surface is associated with the elevator, rudder, or aileron), gives a moment about the airplane center of gravity that is used to control the airplane.¹ The hinge moment, when divided by the appropriate lever arm (which is a function of the linkage system used), gives the control force that must be exerted by the pilot on the stick, wheel, or pedal in order to deflect the flap. The normal force coefficient and hinge moment coefficient are defined as follows:

$$C_N = \frac{N}{qS} \quad (15-26)$$

¹ In these discussions the moment coefficient of the main surface itself and the chordwise force coefficient are both neglected.

$$C_H = \frac{H}{qS_f\bar{c}_f} \quad (15\cdot27)$$

where N is normal force, lb

q is dynamic pressure, psf

S is combined area of main surface and flap, sq ft

H is hinge moment, lb-in.

S_f is area aft of hinge line of flap, sq ft

\bar{c}_f is average chord of flap aft of hinge line, in.

Positive-sign conventions are shown in Fig. 15·18.

Both the normal force coefficient and hinge moment coefficient are functions of the angle of attack of the main-surface chord and of the flap deflection. Discussion of the relation among these variables requires that some of the elementary properties of partial derivatives be recalled. From the calculus, the differential of a function of two variables is shown to be expressible in terms of the partial derivatives of the function with respect to the two variables separately:

$$df = \left(\frac{\partial f}{\partial x}\right)_y dx + \left(\frac{\partial f}{\partial y}\right)_x dy \quad (15\cdot28)$$

where df is differential of function f

$\left(\frac{\partial f}{\partial x}\right)_y$ is derivative of function f with respect to x , with y held constant

$\left(\frac{\partial f}{\partial y}\right)_x$ is derivative of function f with respect to y , with x held constant

dx is differential of x

dy is differential of y

Furthermore, if the differential of the function is set equal to zero,

$$\left(\frac{\partial f}{\partial x}\right)_y = -\left(\frac{\partial f}{\partial y}\right)_x \left(\frac{\partial y}{\partial x}\right)_f \quad (15\cdot29)$$

These two equations will now be used to analyze the characteristics of hinged surfaces.

The normal force coefficient is a function of the angle of attack,¹ α , and the flap setting δ ; thus

$$dC_N = \left(\frac{\partial C_N}{\partial \alpha}\right)_\delta d\alpha + \left(\frac{\partial C_N}{\partial \delta}\right)_\alpha d\delta \quad (15\cdot30)$$

¹ The angle of attack must be measured from the zero-lift chord of the main surface, but this causes no complications in the present analysis.

The hinge moment coefficient is expressed conveniently as a function of C_N and δ :

$$dC_H = \left(\frac{\partial C_H}{\partial C_N} \right)_\delta dC_N + \left(\frac{\partial C_H}{\partial \delta} \right)_{C_N} d\delta \quad (15-31)$$

If a linear relationship is assumed to exist among the variables in the above equations, the differentials may be replaced by their corresponding variables:

$$C_N = \left(\frac{\partial C_N}{\partial \alpha} \right)_\delta \alpha + \left(\frac{\partial C_N}{\partial \delta} \right)_\alpha \delta \quad (15-32)$$

$$C_H = \left(\frac{\partial C_H}{\partial C_N} \right)_\delta C_N + \left(\frac{\partial C_H}{\partial \delta} \right)_{C_N} \delta \quad (15-33)$$

Physically, Eq. (15-32) means that the normal force coefficient of a hinged surface at angle of attack, α , and with control surface deflection δ , is obtained by adding the increment due to α to that due to δ . Similar statements may be made regarding C_H . The four derivatives are all predictable from perfect-fluid theory for the simple system considered. All but $(\partial C_N / \partial \alpha)_\delta$ depend upon the ratio of flap chord to total-surface chord. Each of the derivatives will be discussed separately in the following paragraphs.

The derivative $(\partial C_N / \partial \alpha)_\delta$ is merely the slope of the lift curve a , since $C_N \approx C_L$. It is obtained in the conventional fashion from Eq. (15-19).

According to Eq. (15-29), the derivative $(\partial C_N / \partial \delta)_\alpha$ may be written in the form

$$\left(\frac{\partial C_N}{\partial \delta} \right)_\alpha = - \left(\frac{\partial C_N}{\partial \alpha} \right)_\delta \left(\frac{\partial \alpha}{\partial \delta} \right)_{C_N} \quad (15-34)$$

where the derivative appearing first on the right is again the lift-curve slope and the second one is frequently called the *effectiveness factor*, designated by the symbol K . Its significance may be clarified by a physical interpretation. If a 10-deg flap deflection (with constant angle of attack) produces the same increment in normal force coefficient as a 5-deg change in angle of attack (with constant flap deflection), then the flap is half as "effective" as the total surface, and $K = -0.5$. A theoretical curve of the effectiveness factor as a function of flap chord is given in Fig. 15-18.

Theoretical values of the derivative $(\partial C_H / \partial C_N)_\delta$ are also given in Fig. 15-18. The hinge moment coefficient varies when C_N varies because the pressures on the flat plate are a linear function of its normal force coefficient. In Fig. 15-19 the theoretical pressure distribution on a flat plate is shown for a normal force coefficient of 1.0. Clearly, the moment coefficient about the hinge line is due to the pressures on the flap alone.

Theoretical values of the derivative $(\partial C_H / \partial \delta)_{C_N}$ are given in Fig. 15-18. Variation in the hinge moment due to flap deflection

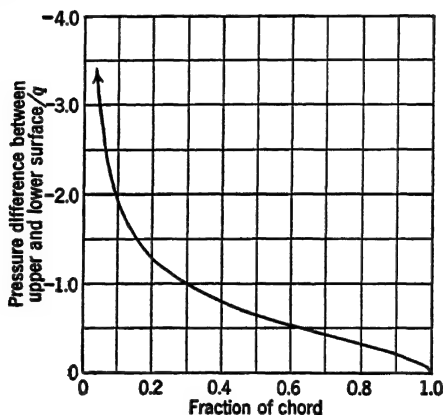


FIG. 15-19. Theoretical pressure distribution on a flat plate for which $C_N = 1.0$.

may be appreciated by referring to Fig. 15-20a, where pressure distribution on a hinged plate is plotted for $\delta = 10$ deg and $C_N = 0$. Again the moment coefficient about the hinge line is due to the pressures on the flap alone.

Figure 15-20b shows the pressure distribution from Fig. 15-20a added¹ to that of Fig. 15-19 to give the pressure distribution with $\delta = 10$ deg at $C_N = 1.0$. The hinge moment arising from the combined pressures is then the total hinge moment expressed by Eq. (15-33).

The three derivatives shown in Fig. 15-18 have fundamental significance, because they are all independent of aspect ratio. They will be used in the next article for comparing the characteristics of actual hinged surfaces.

¹ According to Art. 9-2, the velocities, not the pressures, should be added; however, direct addition of pressures is permissible as an approximation.

15-6 Actual Hinged-surface Characteristics. The characteristics of an actual control surface may be considerably different from those shown in Art. 15-5 because of several variables to be discussed in this article. First, the conclusions drawn in the

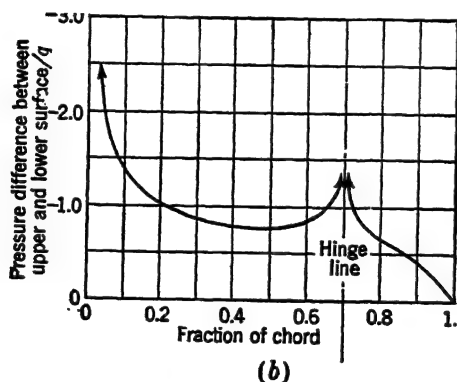
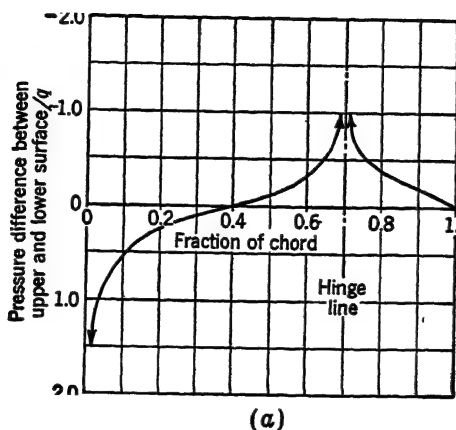


FIG. 15-20. Theoretical pressure distribution on a flat plate hinged at 0.7c: (a) $C_N = 0$ and $\delta = 10^\circ$, (b) $C_N = 1.0$ and $\delta = 10^\circ$.

preceding article were based upon an assumption that the fluid was perfect. In a real fluid, the simple hinged surface discussed would not be likely to operate at very large angles of attack or flap deflection without separation occurring somewhere on its surface. Even with a well-streamlined airfoil section and flap, the effect of the boundary layer on flap hinge-moment char-

acteristics is likely to be considerable, particularly since it is a function of the stream turbulence and of the roughness or waviness of the surface. Experimental tests are generally run on control surfaces constructed of solid and smooth-surfaced material. Some difference in characteristics on an actual airplane must usually be anticipated because of structural imperfections and surface deflections under load.

Second, the hinged surface considered previously consisted of two flat plates. A conventional hinged surface consists of a well-streamlined combination of the main surface and flap. Thickness and camber both alter the hinge-moment characteristics, because they partly determine the pressure distribution over the flap; *i.e.*, the theoretical pressure distribution due to airfoil thickness and camber may be added (see footnote, page 346) to the values given in Fig. 15-20*b* to approximate the over-all pressure difference on an airfoil at a particular angle of attack and with a particular flap deflection. The contour near the flap trailing edge is particularly important in defining the flap pressure distribution and hence the hinge moment.

Third, conventional flaps are never hinged at the flap leading edge, because this results in unnecessarily large hinge moments. There is usually about 30 per cent *aerodynamic balance* or *overhang* (measured in per cent of flap chord), the optimum amount being a function of the configuration of the fixed surface and of the flap. A flap having a circular leading edge, whose center is at the hinge line, has no effect in balancing the flap, because all pressures on its leading edge must act through the hinge line (Fig. 15-21*a*). Except on this one configuration, the area ahead of the hinge line may be regarded as balance area (Fig. 15-21*b*). A blunt flap leading edge *unports* at a smaller flap deflection than a relatively sharp one, if the aerodynamic balance is the same on the two flaps. Decreasing the amount of aerodynamic balance increases the flap angle at which unporting occurs. The gap between the main surface and the flap leading edge is sometimes sealed with fabric, or with some similar material (Fig. 15-21*c*). There is considerable difference in some of the characteristics with sealed and unsealed gap. An *internally sealed flap* has cover plates extending over a considerable area forward of the hinge line (Fig. 15-21*d*). The position of the vent dictates the pressure differential within the chamber so formed, and hence specifies the hinge-moment characteristics of the flap.

Lastly, the effects of compressibility vary between configurations. In the subsonic and supersonic regions, the effects of compressibility may be estimated, because the pressure distribution may be anticipated theoretically. In the transonic region, the pressure coefficient depends upon the position and extent of the shock wave (see again Fig. 8-12), which in turn depends upon the shape of the basic airfoil, its angle of attack, and the flap deflection.

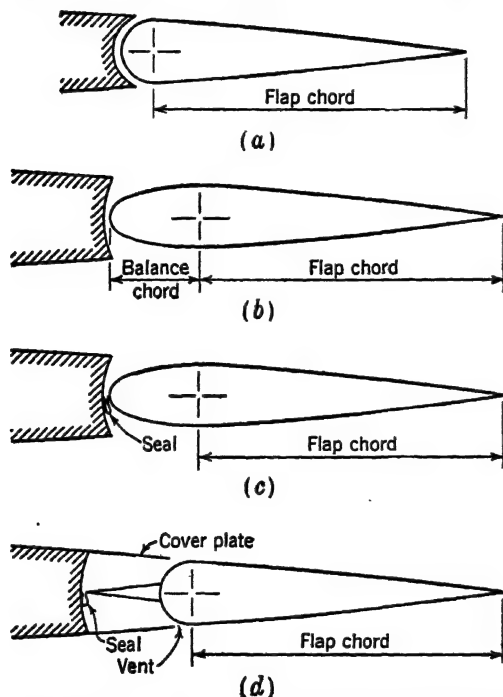


FIG. 15-21. Representative flap configurations: (a) without balance, (b) with balance, (c) with seal, (d) with internal seal.

With all these variables to be accounted for, the reason that wind-tunnel tests are used extensively is at once apparent. Available test results are not very well coordinated and do not cover thoroughly all the possible variables; therefore it is difficult to make positive statements about the effects of each variable on the four derivatives. At the same time, it is interesting to compare the results of some test data with the variations predicted for the flat-plate system given in Art. 15-5. Figures 15-22, to 15-24 show that the amount of overhang, nose shape, and gap have an

appreciable effect on the three derivatives shown. Similar effects could be shown for airfoil section, trailing-edge angle, and Mach number.¹

A hinged surface should have a large increment in C_N for a particular increment in either α or δ ; hence, by Eqs. (15-30) and (15-34), the absolute values of $(\partial C_N/\partial \alpha)_\delta$ and $(\partial \alpha/\partial \delta)_{C_N}$ should be as large as possible. Desirable values for $(\partial C_H/\partial C_N)_\delta$ and

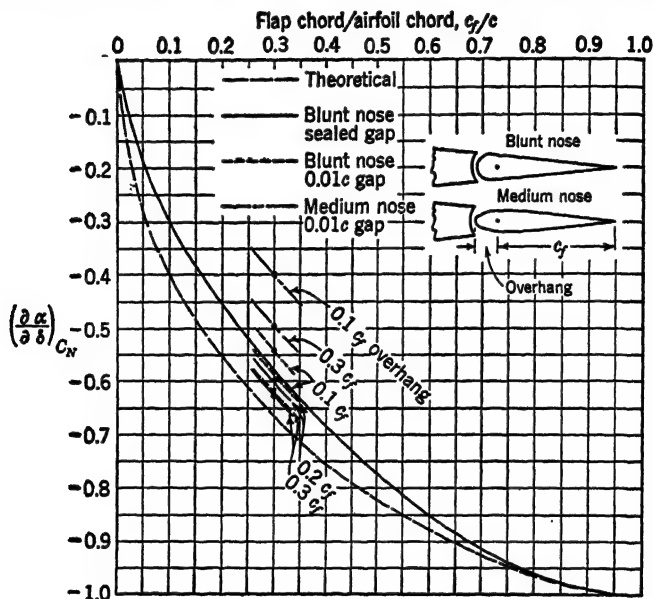


FIG. 15-22. Comparison of theoretical characteristics of a hinged flat plate (from Fig. 15-18) with actual characteristics of a hinged NACA 0009 airfoil (from *WR L-663*).

$(\partial C_H/\partial \delta)_{C_N}$ are not so simply stated. The control forces on the stick, wheel, or pedal that are required for maneuvering the airplane must not exceed the physical limitations of an average pilot; however, they must be large enough to provide "feel" at small deflections, and they must be able to overcome friction so as to return the flap to zero. Moreover, the control forces must increase continuously with increase in flap deflection. The magnitude of the control force depends upon the type and size of the airplane and upon the geometry of the control surface and its linkages.

¹ See *WR L-663* and *TN 1245*.

Increasing the speed, maneuverability, or size of an airplane increases the magnitude of the hinge moments, but of course the

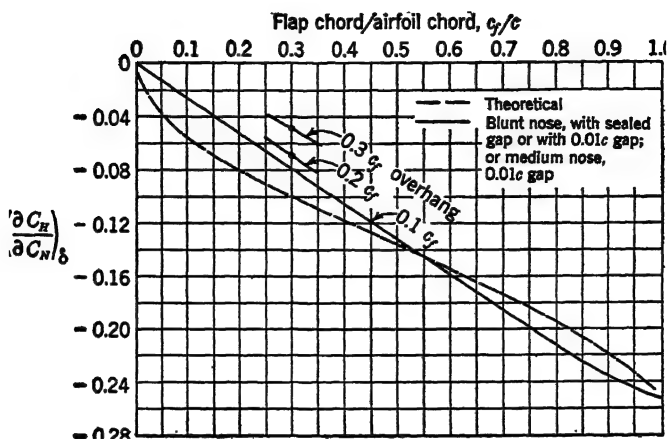


FIG. 15-23. Comparison of theoretical characteristics of a hinged flat plate (from Fig. 15-18) with actual characteristics of a hinged NACA 0009 airfoil (from *WR L-663*).

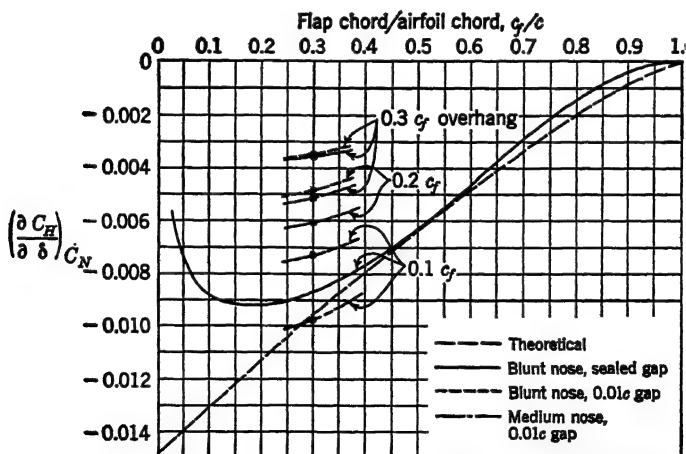


FIG. 15-24. Comparison of theoretical characteristics of a hinged flat plate (from Fig. 15-18) with actual characteristics of a hinged NACA 0009 airfoil (from *WR L-663*). All angles are in degrees.

ability of the pilot to deflect the control surface remains constant. The use of aerodynamic balance to reduce hinge moments may prove unsatisfactory, because the balancing problem becomes

increasingly acute. An aerodynamic, hydraulic, or electrical booster system may then be used. The aerodynamic system is in the form of a *tab* at the flap trailing edge. The simplest ar-

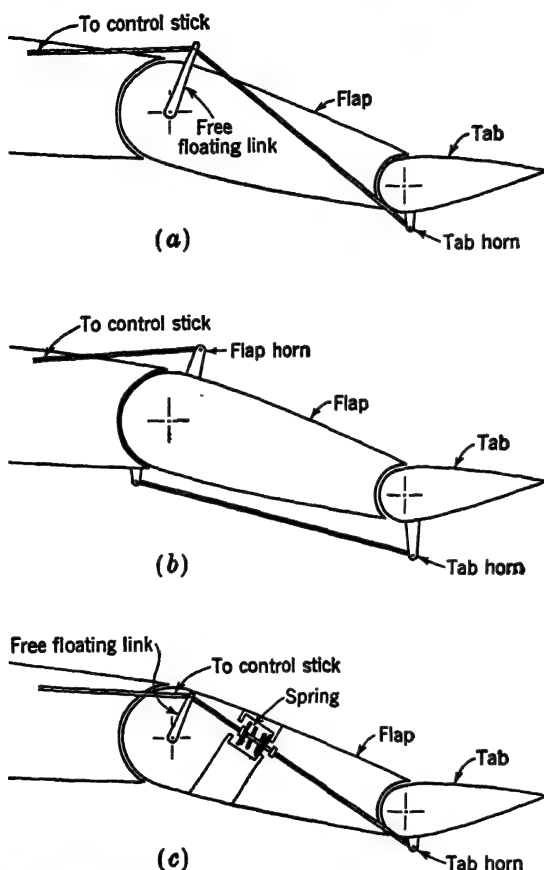


FIG. 15-25. Representative aerodynamic booster systems: (a) servo tab, (b) geared tab, (c) spring tab.

angement is called a *servo tab* (Fig. 15-25a). Deflection of the flap is accomplished indirectly by deflecting the tab in the opposite direction. Obviously, less force is required by the pilot to deflect the tab than the flap itself. A *geared tab* (Fig. 15-25b) has a linkage that provides a fixed relation between the deflections of the tab and flap. A *spring tab* (Fig. 15-25c) has a spring whose compression determines the amount of tab deflection with respect

to the flap. The relative tab deflection increases with increase in force exerted by the pilot. If the spring is preloaded, the tab is ineffective until the spring force is equal to its preload value. Above this value, the tab acts as a conventional spring tab. Most aerodynamic booster systems are based on one of these three types. The hydraulic and electrical systems are used to augment the force of the pilot through direct attachment to the flap. The requirement of high power for a short period of time requires that the electrical system be unusually heavy. The hydraulic system has an advantage from this standpoint because energy may be stored in a hydraulic accumulator.

An entirely different use is made of tabs that are used to *trim* an airplane to reduce pilot fatigue. For instance, an elevator may be designed to produce zero hinge moment at some design speed, gross weight, and cg position, but if any of these variables are changed, an elevator deflection is required to balance the airplane. The stick force or hinge moment required to deflect the elevator may be reduced to zero by deflecting a *trim tab* in a direction opposite to the desired elevator deflection.

There are many kinds of control-surface sections used in aircraft. Most of the peculiar shapes arise from a consideration of the control force or hinge moment that must be used for their deflection, rather than of their effectiveness. On ailerons there are other additional considerations because of the inherent lack of symmetry: not only are the wing and aileron usually cambered, but the ailerons on each side of the wing operate in opposite directions. A negatively deflected aileron produces less drag than a positively deflected one, and as a consequence, it produces an adverse yawing moment in sideslip. In order to nullify this effect, ailerons are frequently either linked differentially so that there is a greater negative than positive deflection, or a sharp leading edge is used on a projecting lip so that a negative deflection produces approximately the same drag as a positive one. The Frise aileron is a good example of this latter type (Fig. 15-26).

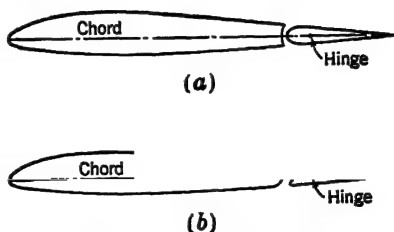


FIG. 15-26. Representative aileron configurations: (a) plain aileron, (b) Frise aileron.

15·7 Practical Aspects of High-speed Flight. Compressibility effects on stability and control may be very great. The problem is unusually complicated because of interference between the wing and tail, and because compressibility phenomena do not occur simultaneously on all surfaces. Compressibility shock on the wing, at a particular angle of attack, not only produces a change in wing characteristics but also causes a change in tail pitching moment that arises from the reduced down-wash. Because of its thinner section, the tail generally has a critical Mach number that is higher than that of the wing; however, ultimate breakdown of flow on the tail involves not only a change in the stability and balance of the airplane, but also a change in the pressure distribution on the elevator and rudder. This causes a change in the hinge-moment characteristics, which is manifested as a change in the anticipated stick forces. Of more consequence is the possibility that deflection of a control surface may produce a local velocity that defines the critical Mach number of the complete airplane. For instance, an upward-deflected Frise aileron could produce a local velocity on the projecting lip that is the highest velocity on the airplane. Therefore, compressibility shock could occur here first. By the same token, deflection of the rudder or elevator could produce high local velocities and hence give undesirable hinge-moment characteristics, because of compressibility shock occurring first on these surfaces.

Superimposed on the problems of compressibility are those associated with structural elasticity. In order to obtain an airplane configuration that is reasonable from an aerodynamic standpoint, the airfoil section used in the wing and tail must be very thin. However, this implies a structure that is characterized by relatively large deflections. An interesting example is the problem arising from wing torsional deflection. A downward deflection of the aileron produces a twisting of the wing that reduces its angle of attack. At low speed the torsional deflection is very small, but at high speed the deflection may be sufficient to produce a decrement, rather than an increment, in lift. This phenomenon is called *aileron reversal*. The problem is a very serious one, not because an airplane would necessarily attain such a critical speed, but because aileron effectiveness decreases with increase in speed.

While no attempt is made here to treat these effects in any detail, their importance cannot be overemphasized.

PROBLEMS

15-1. Equations (15-10) and (15-11) were developed assuming a symmetrical horizontal tail section. How would these equations be modified if the horizontal tail section were not assumed symmetrical?

15-2 Figure 15-4 corresponds to an airplane having $W = 70,000$ lb, $l_w = 50$ psf, wing aspect ratio $A = 7.5$, horizontal tail aspect ratio $A_t = 5.5$, tail length ratio $l_t/c = 2.5$, $S_t/S = 0.23$. Assume that for the wing the slope of the lift curve for infinite aspect ratio is $a_0 = 0.096$ per deg. Estimate η_t using Eq. (15-11).

15-3. For an airplane, $dC_{m_{0.25}}/dC_L = -0.10$, and when $C_L = 0$, $C_{m_{0.24}} = 0.04$.

a. What is the cg position for which $dC_{m_{cg}}/dC_L = 0$?

b. At what lift coefficient is the airplane balanced with the cg at the 26 per cent chord?

15-4. Positive deflection of the elevator of an airplane produces a negative change in pitching moment coefficient about the airplane center of gravity, $-\Delta C_{m_{cg}}$, at constant angle of attack. Find an expression for change in airplane lift coefficient, ΔC_L (based on the wing area), at constant angle of attack due to positive elevator deflection, as a function of the geometric characteristics of the airplane and $-\Delta C_{m_{cg}}$.

15-5. An airplane has the following specifications: gross weight = 10,000 lb; wing area = 500 sq ft; cruising speed is 250 mph at 10,000 ft; cg location at cruising speed is $0.25c$, for which the elevator angle $\delta_e = 0$ and $dC_{m_{0.25}}/dC_L = -0.10$. With all cargo and passengers removed, the weight is reduced to 8000 lb, and the cg moves to $0.30c$. Find the elevator angle required to balance the ship at this reduced weight at 250 mph at 10,000 ft, knowing that $dC_m/d\delta_e = -0.022$ per deg at constant lift coefficient.

15-6. Figure 15-14 corresponds to a four-engined airplane having $W = 70,000$ lb, $l_w = 50$ psf, and wing aspect ratio $A = 7.5$. The distance from the fuselage center line to the thrust axis of the inboard and outboard propellers is 12 and 24 ft, respectively. Take-off speed is $V_t = 90$ mph. Take-off power $P = 1600$ bhp per engine; propeller efficiency $\eta = 0.70$; maximum rudder angle $\delta_r = \pm 25$ deg. At the moment of take-off, two engines on one side become inoperative. Determine whether or not the rudder is able to counteract the resulting yawing moment by solving for the velocity at which the maximum rudder deflection is able to balance the airplane at $\psi = 0$. Ignore the drag of the stopped propellers. Assume standard conditions.

15.7. Show that the elevator effectiveness factor K_e may be obtained from

$$K_e = - \frac{(\partial C_m / \partial \delta_e)_{i_s}}{(\partial C_m / \partial i_s)_{i_s}}$$

at constant airplane C_L .

15.8. Using the relation from Prob. 15.7, estimate the elevator effectiveness factor K_e for the airplane of Prob. 15.2. Use Figs. 15.9 and 15.10 at $C_L = 0.5$, and assume K_e is constant for $0 \lesssim \delta_e \lesssim -10$.

15.9. *a.* Obtain an equation for C_H of a simple hinged surface,

$$C_H = f\left(\frac{\Delta p}{q}, \frac{x}{c_f}\right)$$

where Δp is pressure difference between upper and lower flap surface at point x , psf

x is distance aft from flap leading edge, in.

c_f is flap chord, in.

b. Using the data contained in Fig. 15.19, verify the value of $(\partial C_H / \partial C_N)_s$ in Fig. 15.18 for $c_f/c = 0.5$. (Notice that Fig. 15.19 corresponds to $C_N = 1.0$.)

BIBLIOGRAPHY

The following is a list of publications of the National Advisory Committee for Aeronautics (NACA) and the Aeronautical Research Council (ARC) that have been referred to in the text. Numbers in parentheses refer to the chapters in this book in which the publication appears as a reference.

Technical Reports

- TR* 116 Applications of Modern Hydrodynamics to Aeronautics, by L. Prandtl, 1921 (Chaps. 5, 6).
- TR* 147 Standard Atmosphere, by Willis Ray Gregg, 1922 (Chap. 1).
- TR* 218 Standard Atmosphere—Tables and Data, by Walter S. Diehl, 1925 (Table I, Appendix A).
- TR* 267 Drag of Wings with End Plates, by Paul E. Hemke, 1927 (Chap. 15).
- TR* 416 The N.A.C.A. Variable-Density Wind Tunnel, by Eastman N. Jacobs and Ira H. Abbott, 1932 (Chap. 4).
- TR* 431 Characteristics of Clark Y Airfoils of Small Aspect Ratios, by C. H. Zimmerman, 1932 (Chap. 6).
- TR* 450 The Calculation of Take-off Run, by Walter S. Diehl, 1933 (Chap. 14).
- TR* 460 The Characteristics of 78 Related Airfoil Sections from Tests in the Variable-Density Wind Tunnel, by Eastman N. Jacobs, Kenneth E. Ward, and Robert M. Pinkerton, 1933 (Chap. 3).
- TR* 474 Nomenclature for Aeronautics, by National Advisory Committee for Aeronautics, 1933 (Chap. 3).
- TR* 492 Tests of 16 Related Airfoils at High Speeds, by John Stack and Albert E. von Doenhoff, 1934 (Chap. 3).
- TR* 497 Computation of the Two-Dimensional Flow in a Laminar Boundary Layer, by Hugh L. Dryden, 1934 (Chap. 7).
- TR* 537 Tests in the Variable-Density Wind Tunnel of Related Airfoils Having the Maximum Camber Unusually Far Forward, by Eastman N. Jacobs and Robert M. Pinkerton, 1935 (Chap. 3).
- TR* 540 Interference of Wing and Fuselage from Tests of 209 Combinations in the N.A.C.A. Variable-Density Tunnel, by Eastman N. Jacobs and Kenneth E. Ward, 1935 (Chap. 11).
- TR* 563 Calculated and Measured Pressure Distributions over the Mid-span Section of the N.A.C.A. 4412 Airfoil, by Robert M. Pinkerton, 1936 (Chap. 9).

- TR* 572 Determination of the Characteristics of Tapered Wings, by Raymond F. Anderson, 1936 (Chap. 6).
- TR* 586 Airfoil Section Characteristics As Affected by Variations of the Reynolds Number, by Eastman N. Jacobs and Albert Sherman, 1937 (Chap. 7).
- TR* 610 Tests of Related Forward-Camber Airfoils in the Variable-Density Wind Tunnel, by Eastman N. Jacobs, Robert M. Pinkerton, and Harry Greenberg, 1937 (Chap. 3).
- TR* 619 Drag of Cylinders of Simple Shapes, by W. F. Lindsey, 1938 (Chap. 11).
- TR* 646 The Compressibility Burble and the Effect of Compressibility on Pressures and Forces Acting on an Airfoil, by John Stack, W. F. Lindsey, and Robert E. Littell, 1939 (Chap. 8).
- TR* 658 Test of Two Full-Scale Propellers with Different Pitch Distributions, at Blade Angles up to 60° , by David Biermann and Edwin P. Hartman, 1939 (Fig. III, Appendix B).
- TR* 664 Wind-Tunnel Investigation of an N.A.C.A. 23012 Airfoil with Various Arrangements of Slotted Flaps, by Carl J. Wenzinger and Thomas A. Harris, 1939 (Chap. 10).
- TR* 668 Wind-Tunnel Investigation of N.A.C.A. 23012, 23021 and 23030 Airfoils with Various Sizes of Split Flap, by Carl J. Wenzinger and Thomas A. Harris, 1939 (Chap. 10).
- TR* 669 Airfoil Section Data Obtained in the N.A.C.A. Variable-Density Tunnel As Affected by Support Interference and Other Corrections, by Eastman N. Jacobs and Ira H. Abbott, 1939 (Chaps. 3, 5, 6, 9; Table III, Appendix A; Fig. I, Appendix B).
- TR* 721 Determination of Control-surface Characteristics from NACA Plain-flap and Tab Data, by Milton B. Ames, Jr., and Richard I. Sears, 1941 (Chap. 15).
- TR* 747 Wind-Tunnel Tests of Four- and Six-Blade Single- and Dual-Rotating Tractor Propellers, by David Biermann and Edwin P. Hartman, 1942 (Fig. IV, Appendix B).

Technical Notes

- TN* 606 Empirical Corrections to the Span Load Distribution at the Tip, by H. A. Pearson, 1937 (Chap. 6).
- TN* 702 Wind-Tunnel Tests of Several Forms of Fixed Wing Slot in Combination with a Slotted Flap on an N.A.C.A. 23012 Airfoil, by M. J. Bamber, 1939 (Chap. 10).
- TN* 976 Tests of Airfoils Designed to Delay the Compressibility Burble, by John Stack, 1944 (Chap. 3).
- TN* 1050 Wind-Tunnel Investigation of End-Plate Effects of Horizontal Tails on a Vertical Tail Compared with Available Theory, by Harry E. Murray, 1946 (Chap. 15).
- TN* 1071 Wind-Tunnel Investigation of Boundary-Layer Control by Suction on the NACA 653-418, $\alpha = 1.0$ Airfoil Section with a 0.29 Airfoil-Chord Double Slotted Flap, by John H. Quinn, Jr., 1946 (Chap. 10).

- TN* 1143 Charts for Determining the Characteristics of Sharp-Nose Airfoils in Two-Dimensional Flow at Supersonic Speeds, by H. Reese Ivey, George W. Stickle, and Alberta Schuettler, 1947 (Chap. 8).
- TN* 1179 Notes on the Theoretical Characteristics of Two-Dimensional Supersonic Airfoils, by H. Reese Ivey, 1947 (Chap. 8).
- TN* 1200 Tentative Tables for the Properties of the Upper Atmosphere, by Calvin N. Warfield, 1947 (Chap. 1; Table I, Appendix A).
- TN* 1211 The Flow and Force Characteristics of Supersonic Airfoils at High Subsonic Speeds, by W. F. Lindsey, Bernard N. Daley, and Milton D. Humphreys, 1947 (Chap. 3).
- TN* 1245 Summary of Lateral-Control Research, by Research Department, compiled by Thomas A. Toll, 1947 (Chap. 15).
- TN* 1293 Tests of the NACA 64 $\frac{1}{2}$ A212 Airfoil Section with a Slat, a Double Slotted Flap, and Boundary-Layer Control by Suction, by John H. Quinn, Jr., 1947 (Chap. 10).
- TN* 1349 Performance and Ranges of Application of Various Types of Aircraft-Propulsion Systems, by Cleveland Laboratory Staff, 1947 (Chap. 3).
- TN* 1449 Theoretical Supersonic Wave Drag of Untapered Sweptback and Rectangular Wings at Zero Lift, by Sidney M. Harmon, 1947 (Chap. 8).
- TN* 1792 Study by the Prandtl-Glauert Method, of Compressibility Effects and Critical Mach Number for Ellipsoids of Various Aspect Ratios and Thickness Ratios, by Robert V. Hess and Clifford S. Gardner, 1949 (Chap. 8).

Technical Memoranda

- TM* 897 Airfoil Theory at Supersonic Speed, by H. Schlichting (Translated from the German), 1939 (Chap. 8).
- TM* 1105 Plane and Three-dimensional Flow at High Subsonic Speeds, by B. Göthert (Translated from the German), 1946 (Chap. 8).
- TM* 1113 Investigations of Compression Shocks and Boundary Layers in Gases Moving at High Speed, by J. Ackert, F. Feldmann, and N. Rott (Translated from the German), 1947 (Chap. 8).
- TM* 1168 Drag Reduction by Suction of the Boundary Layer Separated behind Shock Wave Formation at High Mach Numbers, by B. Regenscheit (Translated from the German), 1947 (Chap. 10).

Wartime Reports

- WR* A-90 The Effects of a Highly Cambered Low-Drag Wing and of Auxiliary Flaps on the High-Speed Aerodynamic Characteristics of a Twin-Engine Pursuit Airplane Model, by Victor M. Ganzer, 1948 (Chap. 8).
- WR* E-83 Design of Nozzles for the Individual Cylinder Exhaust Jet Propulsion System, by Benjamin Pinkel, L. Richard Turner, and Fred Voss, 1946 (Chap. 12).

- WR L-143* Completed Tabulation in the United States of Tests of 24 Airfoils at High Mach Numbers (Derived from Interrupted Work at Guidonia, Italy, in the 1.31- by 1.74-Foot High-Speed Tunnel), by Antonio Ferri, 1946 (Chap. 3).
- WR L-219* Propellers in Yaw, by Herbert S. Ribner, 1946 (Chap. 15).
- WR L-336* Proposal for a Propeller Side-Force Factor, by Herbert S. Ribner, 1946 (Chap. 15).
- WR L-373* Wind Tunnel Investigation of Perforated-Split Flaps for Use as Dive Brakes on a Tapered NACA 23012 Airfoil, by Paul E. Purser and Thomas R. Turner, 1947 (Chap. 10).
- WR L-382* Determination of General Relations for the Behavior of Turbulent Boundary Layers, by Albert E. von Doenhoff and Neal Tetervin, 1947 (Chap. 7).
- WR L-560* Summary of Airfoil Data, by Ira H. Abbott, Albert E. von Doenhoff, and Louis S. Stivers, Jr., 1947 (Chaps. 2, 3, 7, 9).
- WR L-663* Wind-Tunnel Data on the Aerodynamic Characteristics of Airplane Control Surfaces, by Richard I. Sears, 1943 (Chap. 15).
- WR W-43* Tests of Exhaust Propulsion Nozzles, by Paul J. Campbell, 1946 (Chap. 12).

Reports and Memoranda

- R&M 1226* The Characteristics of a Tapered and Twisted Wing with Sweep-Back, by H. Glauert and S. B. Gates, 1928 (Chap. 6).
- R&M 1796* Some Aerodynamic Characteristics of Tapered Wings Fitted with Flaps of Various Spans, by H. B. Irving, A. S. Batson, J. H. Warsap, and H. J. Gummer, 1937 (Chaps. 6, 10).
- R&M 1838* The Calculation of the Profile Drag of Aerofoils, by H. B. Squire and A. D. Young, 1937 (Chap. 7).
- R&M 2001* The Supersonic Theory of Wings of Finite Span, by M. J. Light-hall, 1944 (Chap. 8).

■

Appendix A

TABLES

■

TABLE I. STANDARD AIR PROPERTIES AT ALTITUDE*

Altitude, ft/1000	Absolute pressure, psf	Temperature, °F	Density ratio, $\sigma = \frac{\rho}{\rho_0}$	Mass density, ρ , slug/cu ft	$\frac{1}{\sqrt{\sigma}}$	Viscosity,† $\mu \times 10^5$, slug/it-sec	Kinematic viscosity reciprocal, $\frac{1}{\nu}$, sec/sq ft	Speed-of- sound; ratio a/a_0 ($a_0 =$ 1120 fps)
0	2116.4	59.0	1.0000	0.002 378	1.0000	373	6380	1.000
1	2041.3	55.4	0.9710	0.002 309	1.0148	371	6220	0.997
2	1967.8	51.9	0.9428	0.002 242	1.0299	369	6080	0.993
3	1896.3	48.3	0.9151	0.002 176	1.0454	367	5930	0.990
4	1827.7	44.7	0.8881	0.002 112	1.0611	365	5790	0.986
5	1760.5	41.2	0.8616	0.002 049	1.0773	363	5640	0.983
6	1696.2	37.6	0.8358	0.001 988	1.0938	361	5510	0.979
7	1633.2	34.0	0.8106	0.001 928	1.1107	359	5370	0.976
8	1571.7	30.5	0.7859	0.001 869	1.1280	357	5240	0.972
9	1512.3	26.9	0.7619	0.001 812	1.1456	355	5100	0.968
10	1455.7	23.3	0.7384	0.001 756	1.1637	352	4990	0.965
11	1399.8	19.8	0.7154	0.001 702	1.1822	350	4880	0.962
12	1346.0	16.2	0.6931	0.001 648	1.2012	348	4740	0.958
13	1293.7	12.6	0.6712	0.001 596	1.2206	346	4610	0.954
14	1242.8	9.1	0.6499	0.001 545	1.2404	344	4490	0.950
15	1194.0	5.5	0.6291	0.001 496	1.2608	342	4370	0.947
16	1146.6	1.9	0.6088	0.001 448	1.2816	340	4260	0.943
17	1100.6	-1.6	0.5891	0.001 401	1.3029	338	4150	0.940
18	1056.7	-5.2	0.5698	0.001 355	1.3247	335	4040	0.936
19	1013.6	-8.8	0.5509	0.001 311	1.3473	333	3940	0.932
20	972.6	-12.3	0.5327	0.001 267	1.3701	331	3830	0.929
21	932.2	-15.9	0.5148	0.001 225	1.3937	329	3720	0.925
22	893.3	-19.5	0.4974	0.001 183	1.4179	327	3620	0.921
23	855.9	-23.0	0.4805	0.001 143	1.4426	325	3520	0.917
24	819.8	-26.6	0.4640	0.001 103	1.4681	323	3410	0.914
25	785.1	-30.2	0.4480	0.001 065	1.4940	321	3320	0.910
26	751.2	-33.7	0.4323	0.001 028	1.5209	318	3230	0.906
27	718.6	-37.3	0.4171	0.000 992	1.5484	316	3140	0.903
28	687.5	-40.9	0.4023	0.000 957	1.5766	314	3050	0.899
29	657.1	-44.4	0.3879	0.000 922	1.6056	312	2960	0.895
30	628.1	-48.0	0.3740	0.000 889	1.6352	310	2870	0.891
31	599.8	-51.6	0.3603	0.000 857	1.6659	308	2780	0.887
32	572.9	-55.1	0.3472	0.000 826	1.6971	306	2700	0.883
33	546.8	-58.7	0.3343	0.000 795	1.7295	303	2620	0.879
34	522.0	-62.2	0.3218	0.000 765	1.7628	301	2540	0.875
35	498.0	-65.8	0.3098	0.000 736	1.7966	299	2460	0.871
36	474.6	-69.0	0.2982	0.000 704	1.8374	298	2380	0.870
37	452.0	-72.0	0.2824	0.000 671	1.8818	298	2250	0.870
38	431.5	-75.0	0.2692	0.000 640	1.9273	298	2150	0.870
39	411.0	-77.0	0.2566	0.000 610	1.9738	298	2050	0.870
40	391.9	-79.0	0.2447	0.000 582	2.0215	298	1950	0.870
41	373.5	-81.0	0.2332	0.000 554	2.0707	298	1860	0.870
42	356.5	-83.0	0.2224	0.000 529	2.1207	298	1780	0.870
43	339.5	-85.0	0.2120	0.000 504	2.1719	298	1690	0.870
44	324.0	-87.0	0.2021	0.000 481	2.2244	298	1610	0.870
45	308.4	-89.0	0.1926	0.000 459	2.2785	298	1540	0.870
46	294.2	-91.0	0.1837	0.000 437	2.3332	298	1470	0.870
47	280.8	-93.0	0.1751	0.000 417	2.3893	298	1400	0.870
48	267.4	-95.0	0.1669	0.000 397	2.4478	298	1330	0.870
49	255.3	-97.0	0.1591	0.000 379	2.5071	298	1270	0.870
50	243.3	-99.0	0.1517	0.000 361	2.5675	298	1210	0.870

TABLE I. STANDARD AIR PROPERTIES AT ALTITUDE* (Continued)

Altitude, ft/1000	Absolute pressure, psf	Temperature, °F	Density ratio, $\sigma = \frac{\rho}{\rho_0}$	Mass density, ρ , slug/cu ft	$\frac{1}{\sqrt{\sigma}}$	Viscosity, $\mu \times 10^6$, slug/ft-sec	Kinematic viscosity reciprocal, $\frac{1}{\nu}$, sec/sq ft	Speed-of-sound† ratio $\frac{a}{a_0}$ ($a_0 = 1120$ fps)
55	191.5	-67.0	0.1195	0.000 284	2.8928	298	950	0.870
60	180.8	-67.0	0.0941	0.000 224	3.2599	298	750	0.870
70	93.5	-67.0	0.0584	0.000 139	4.138	298	470	0.870
80	58.0	-67.0	0.0362	0.000 086	5.256	298	290	0.870
90	36.0	-67.0	0.0225	0.000 053	6.666	298	180	0.870
100	22.3	-67.0	0.0139	0.000 033	8.482	298	110	0.870

* Based on data contained in *TE 218* and *TN 1200*.

† Based on Eq. (1-34).

‡ Based on Eq. (1-25).

TABLE II. CHARACTERISTICS OF COMMON MANOMETER FLUIDS*

Liquid	Approximate specific gravity at 59 F	Combustible at 30-100 F	Attacks natural rubber	Attacks Neo-prene	Attacks nonrigid Vinylite	Attacks rigid Vinylite	Attacks Saran (rigid)
Silicone liquids†.....	Available 0.76-0.96	No‡	No	No	No	No	No
Methyl alcohol.....	0.79	Yes	No	No	Yes	No	No
Kerosene.....	0.80	Yes	Yes	No	Yes	No	No
Benzol.....	0.88	Yes	Yes	No	Yes	No	Slight
Water‡.....	1.00	No	No	No	No	No	No
Carbon tetrachloride.....	1.59	No	Yes	Yes	Yes	No	No
Acetylene tetrabromide‡..	2.97	No	Yes	Yes	Yes	Slight	Slight
Mercury‡.....	13.6	No	No	No	No	No	No

* Information on tubing supplied through the courtesy of United States Rubber Company, E. I. Dupont de Nemours & Company, Bakelite Corporation, and The Dow Chemical Corporation.

† Costly.

‡ The high surface tension of water may be reduced by using a "wetting agent," such as Aerosol solution.

§ The lighter liquids are combustible.

|| May extract compounding ingredients of rubber and change liquid specific gravity.

TABLE III. AIRFOIL CHARACTERISTICS*
From Tests Run in the Variable-Density Tunnel

Airfoil section	Section characteristics†								A = 6 characteristics, round tips‡	
	$C_{L_{max}}$	α_0 , deg	α_0 , per deg	$C_{D_{0min}}$	C_{mac}	sg, per cent chord	$\frac{C_{L_{max}}}{C_{D_{0min}}}$	cp at $\frac{C_{L_{max}}}{C_{D_{0min}}}$, per cent chord	m_e , per radian	$C_{D_{0min}}$
NACA 0006	0.91	0	0.098	0.0051	0	24.3	178	35	4.28	0.0051
NACA 0009	1.39	0	0.098	0.0058	0	24.0	240	26	4.28	0.0058
NACA 0012	1.66	0	0.099	0.0060	0	24.4	277	26	4.32	0.0060
NACA 0015	1.66	0	0.097	0.0064	0	23.8	259	25	4.24	0.0064
NACA 0018	1.53	0	0.096	0.0070	0	23.3	219	25	4.20	0.0070
NACA 0021	1.48	0	0.093	0.0080	0	22.0	185	24	4.11	0.0080
NACA 0025	1.26	0	0.085	0.0094	0	22.3	134	25	3.82	0.0094
NACA 0030	1.06	0	0.074	0.0117	-0.005	18.1	91	19	3.48	0.0117
NACA 2212	1.72	-1.8	0.099	0.0062	-0.029	24.1	277	27	4.31	0.0063
NACA 2409	1.62	-1.7	0.099	0.0060	-0.044	24.3	270	28	4.31	0.0061
NACA 2412	1.72	-2.0	0.098	0.0061	-0.043	24.5	282	28	4.28	0.0062
NACA 2415	1.66	-1.7	0.097	0.0068	-0.040	23.6	244	28	4.24	0.0069
NACA 2418	1.53	-1.9	0.094	0.0076	-0.038	23.9	201	27	4.14	0.0076
NACA 4406	1.32	-3.9	0.100	0.0062	-0.087	24.6	213	32	4.34	0.0071
NACA 4409	1.77	-3.9	0.096	0.0066	-0.088	24.4	268	31	4.20	0.0072
NACA 4412	1.74	-4.0	0.098	0.0071	-0.088	24.2	245	31	4.28	0.0073
NACA 4415	1.72	-4.0	0.097	0.0076	-0.085	24.0	226	31	4.24	0.0079
NACA 4418	1.57	-3.7	0.092	0.0079	-0.078	23.6	199	31	4.07	0.0081
NACA 4421	1.41	-3.4	0.089	0.0088	-0.071	23.1	160	32	3.96	0.0089
NACA 23006	1.17	-1.2	0.100	0.0057	-0.012	24.0	205	26	4.34	0.0058
NACA 23009	1.66	-1.1	0.099	0.0059	-0.009	24.1	281	25	4.32	0.0060
NACA 23012	1.74	-1.2	0.100	0.0060	-0.008	23.8	290	25	4.34	0.0061
NACA 23015	1.73	-1.1	0.098	0.0067	-0.008	23.9	258	24	4.28	0.0068
NACA 23018	1.58	-1.2	0.097	0.0074	-0.006	23.3	214	24	4.24	0.0074
NACA 23021	1.50	-1.2	0.092	0.0080	-0.005	22.7	188	24	4.07	0.0080
NACA 43012	1.84	-2.3	0.100	0.0068	-0.019	24.0	271	27	4.34	0.0071
NACA 43015	1.76	-2.3	0.101	0.0070	-0.015	23.8	251	26	4.37	0.0071
NACA 43018	1.63	-2.4	0.096	0.0078	-0.013	23.2	209	26	4.20	0.0079
NACA 63012	1.84	-3.5	0.100	0.0075	-0.033	22.3	245	26	4.34	0.0087
NACA 63018	1.63	-3.4	0.097	0.0080	-0.020	22.9	204	26	4.24	0.0081
Clark Y	1.68	-5.0	0.092	0.0071	-0.069	23.9	237	29	4.07	0.0072
Göttingen 398	1.68	-6.0	0.094	0.0076	-0.081	24.6	221	31	4.14	0.0079
NACA M6	1.51	-0.8	0.095	0.0066	+0.002	25.4	229	26	4.18	0.0066

* From TR 669. Test $R \approx 3,000,000$, $R_e \approx 8,300,000$.

† Round as viewed from top, not front.

‡ To convert these data to infinite-aspect-ratio characteristics, use the following relations. The term on the left of each equation refers to infinite aspect ratio.

$$C_{D_0} = c_{D_0} - 0.0016 c_t^2 + \left(\frac{2t}{3} - 4\right) (0.0001)$$

where $t \geq 6$ and is per cent thickness.

$$\alpha'_0 = \alpha_0 - 0.39 c_t \quad \text{deg}$$

$$C_{L_{max}} = 0.935 c_{L_{max}}$$

NOTE: In the first two equations, corrections are applied at constant lift coefficient; hence $c_t = C_L$.

■

■

▼

■

●

●

●

Appendix B

CHARTS

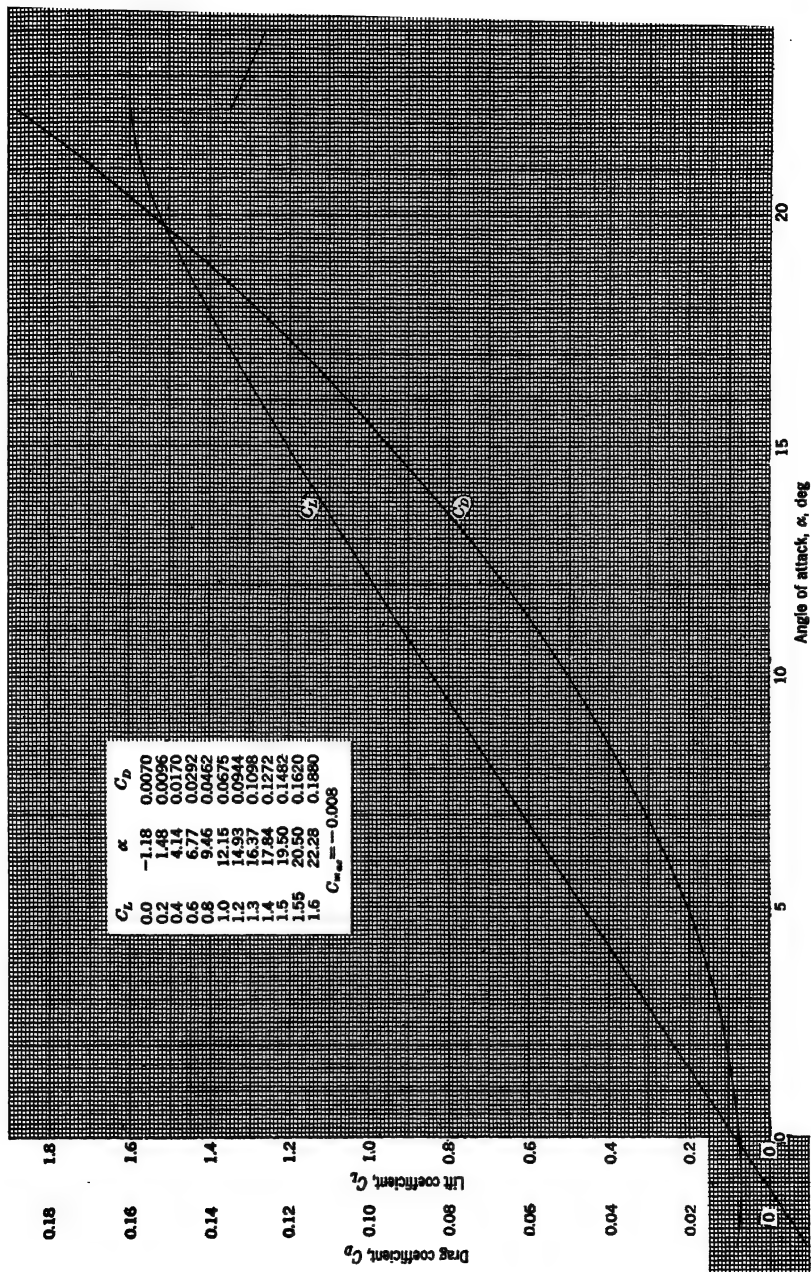


FIG. 1. Aerodynamic characteristics of an NACA 23015 airfoil having aspect ratio of 6. The data were obtained from tests on a rectangular wing at a Reynolds number of 8,370,000. (From TR 669.)

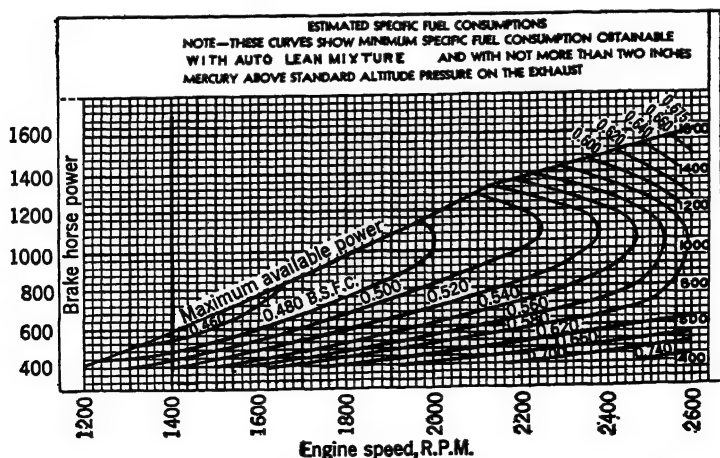
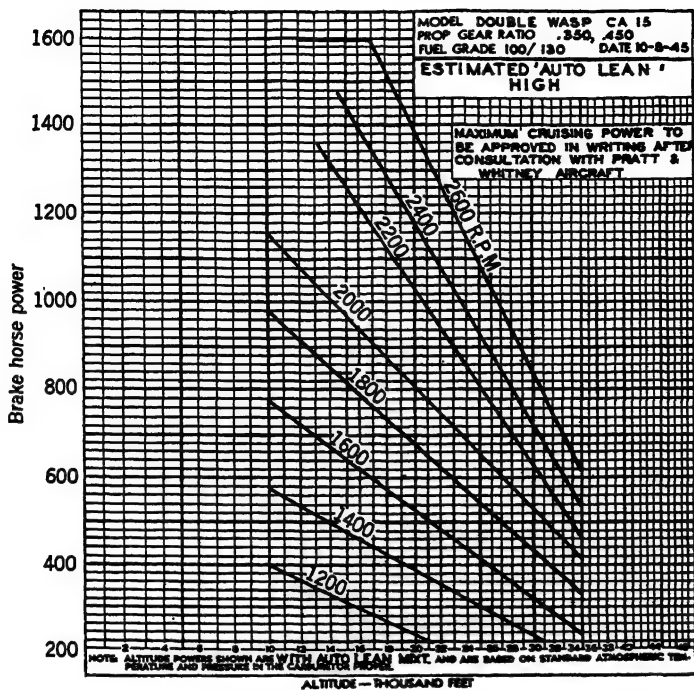


FIG. IIb. Cruising-power variation with low impeller ratio for a Pratt & Whitney Double Wasp engine, showing "Auto-lean" fuel consumption. The fuel consumption may be assumed independent of altitude. (Reproduced by permission of Pratt & Whitney Aircraft.)

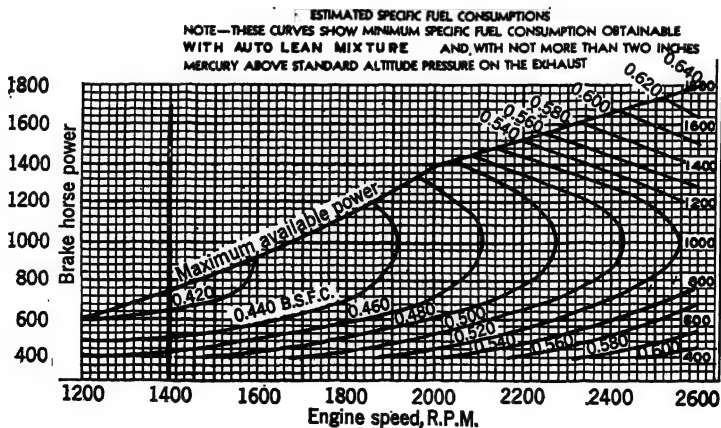
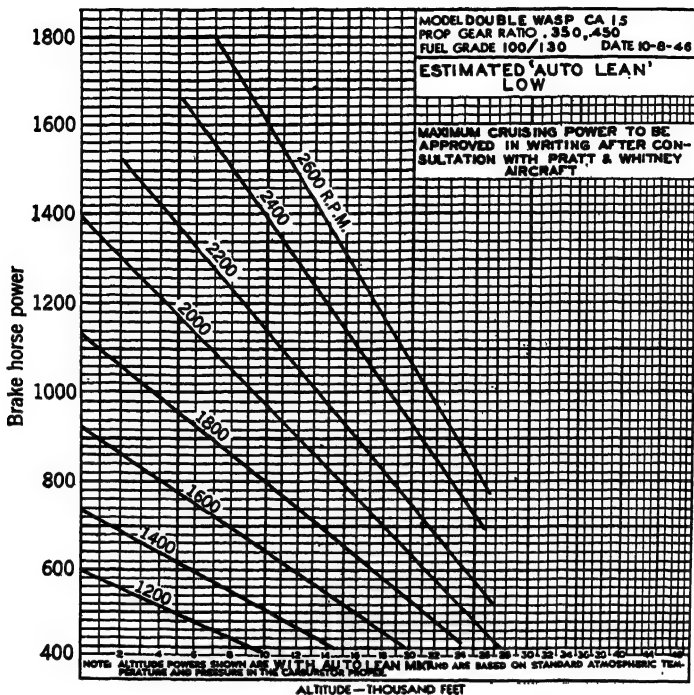


FIG. 11c. Cruising-power variation with high impeller ratio for a Pratt & Whitney Double Wasp engine, showing "Auto-lean" fuel consumption. The fuel consumption may be assumed independent of altitude. (Reproduced by permission of Pratt & Whitney Aircraft.)

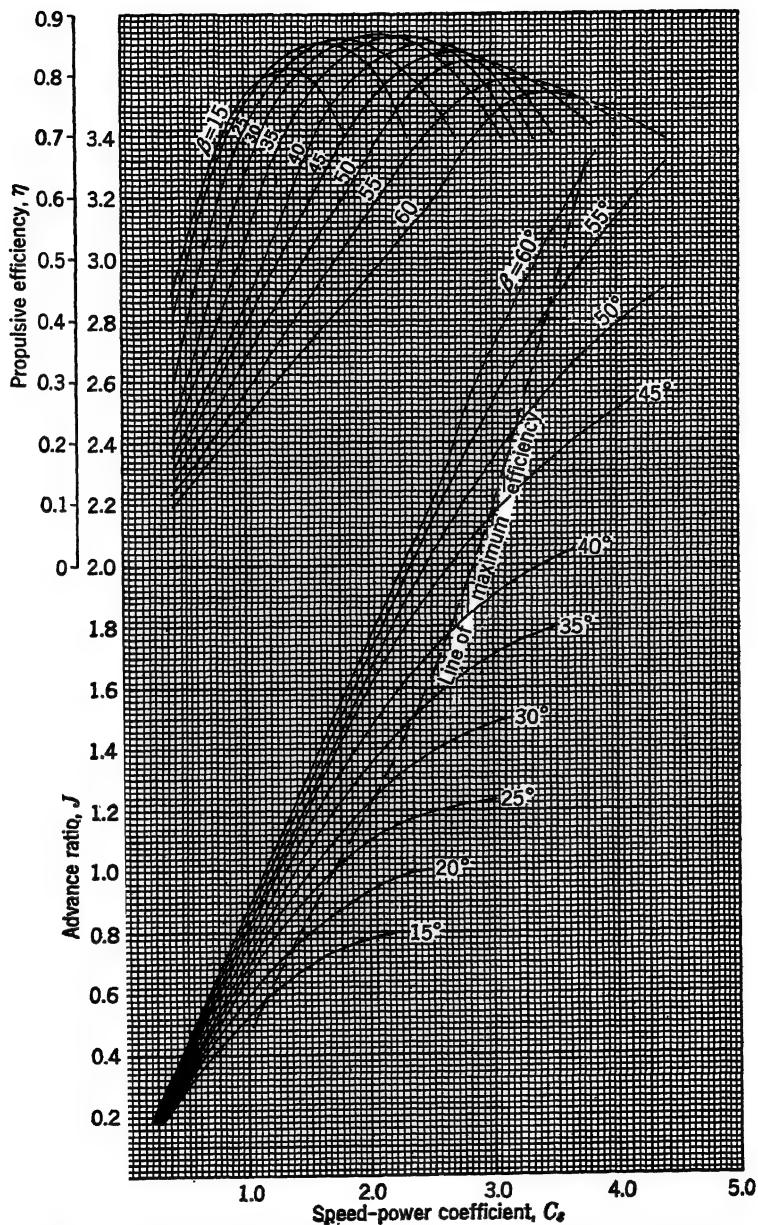


FIG. IIIa. Aerodynamic characteristics of a three-bladed propeller. The data were obtained from tests on a propeller in front of a radial-engine nacelle without wing. (From TR 658.)

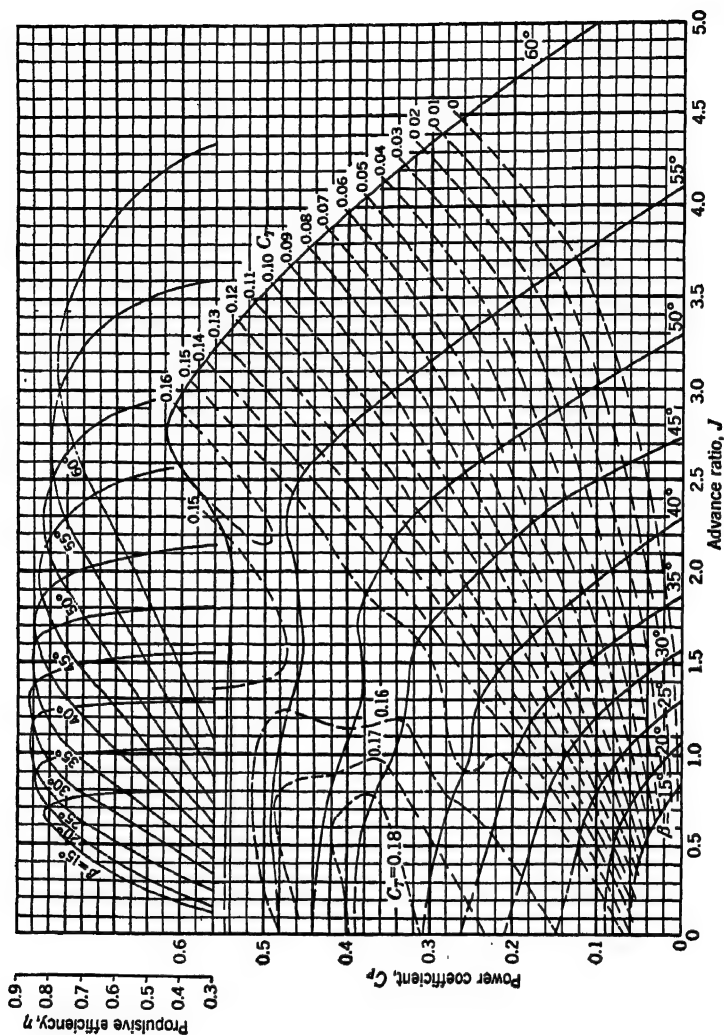


FIG. IIIb. Aerodynamic characteristics of a three-bladed propeller. The data were obtained from tests on a propeller in front of a radial-engine nacelle without wing. (From TR 658.)

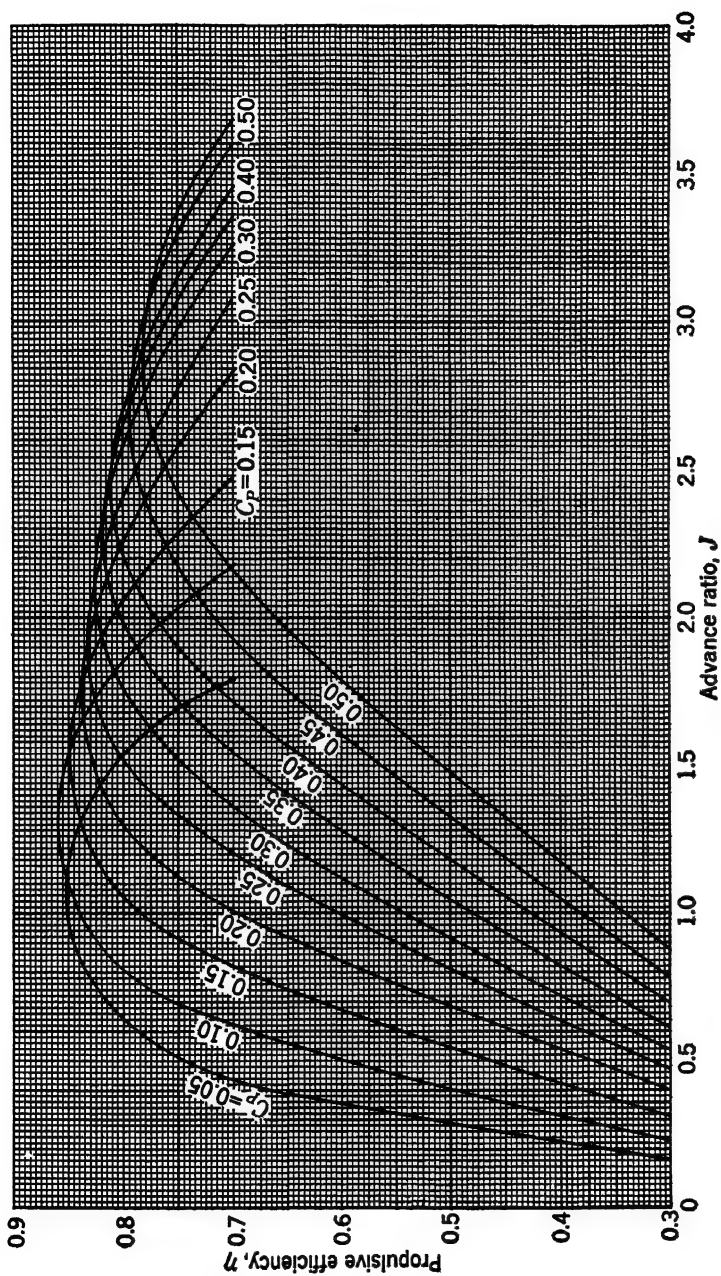


Fig. IIIc. Aerodynamic characteristics of a three-bladed propeller. The data were obtained from tests on a propeller in front of a radial-engine nacelle without wing. (From Fig. IIIb.)

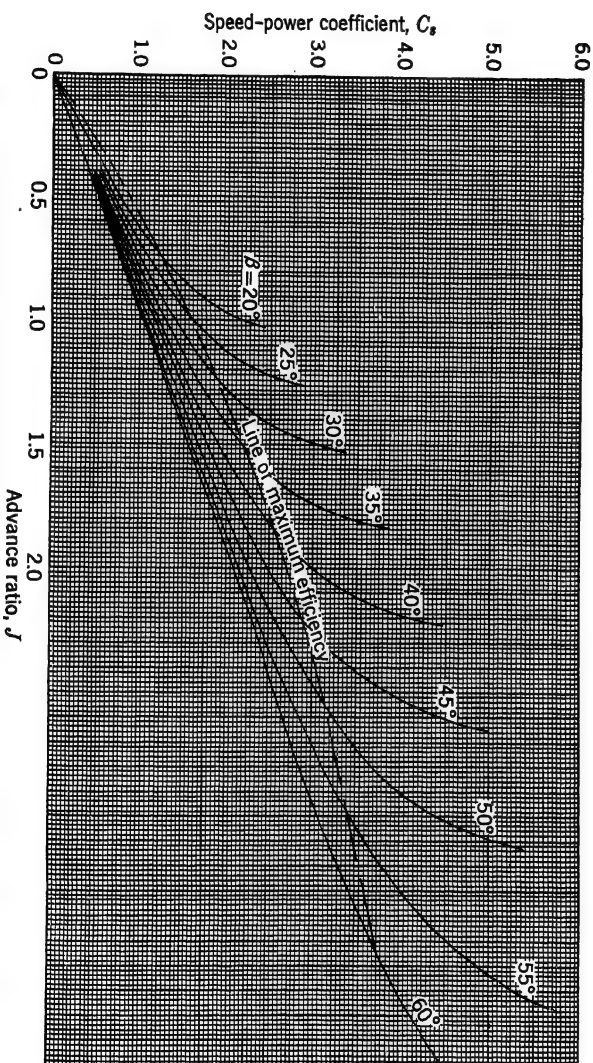


FIG. 1V α . Aerodynamic characteristics of a four-bladed propeller. The propeller in front of an in-line engine nacelle with wing. (From T.R. 747.)

ined from tests
single-rotor

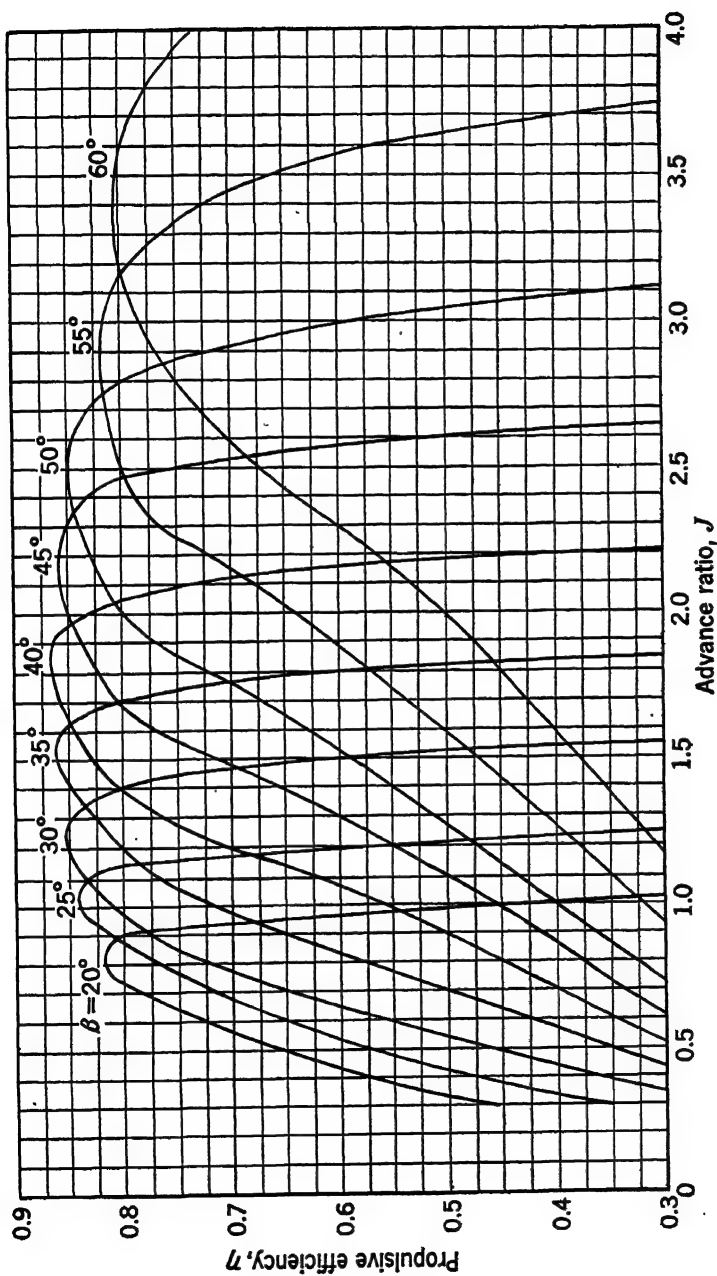


FIG. IVb. Aerodynamic characteristics of a four-bladed propeller. The data were obtained from tests on a single-rotating propeller in front of an in-line engine nacelle with wing. (From TR 747.)

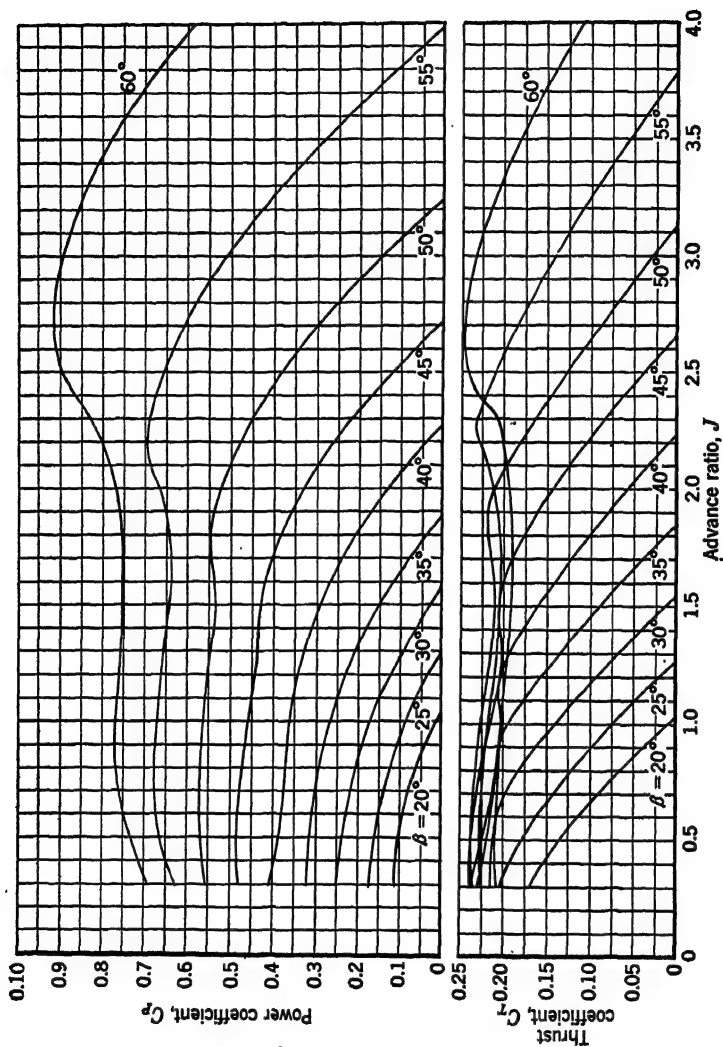


Fig. IVc and d. Aerodynamic characteristics of a four-bladed propeller. The data were obtained from tests on a single-rotating propeller in front of an in-line engine nacelle with wing. (From TR 747.)

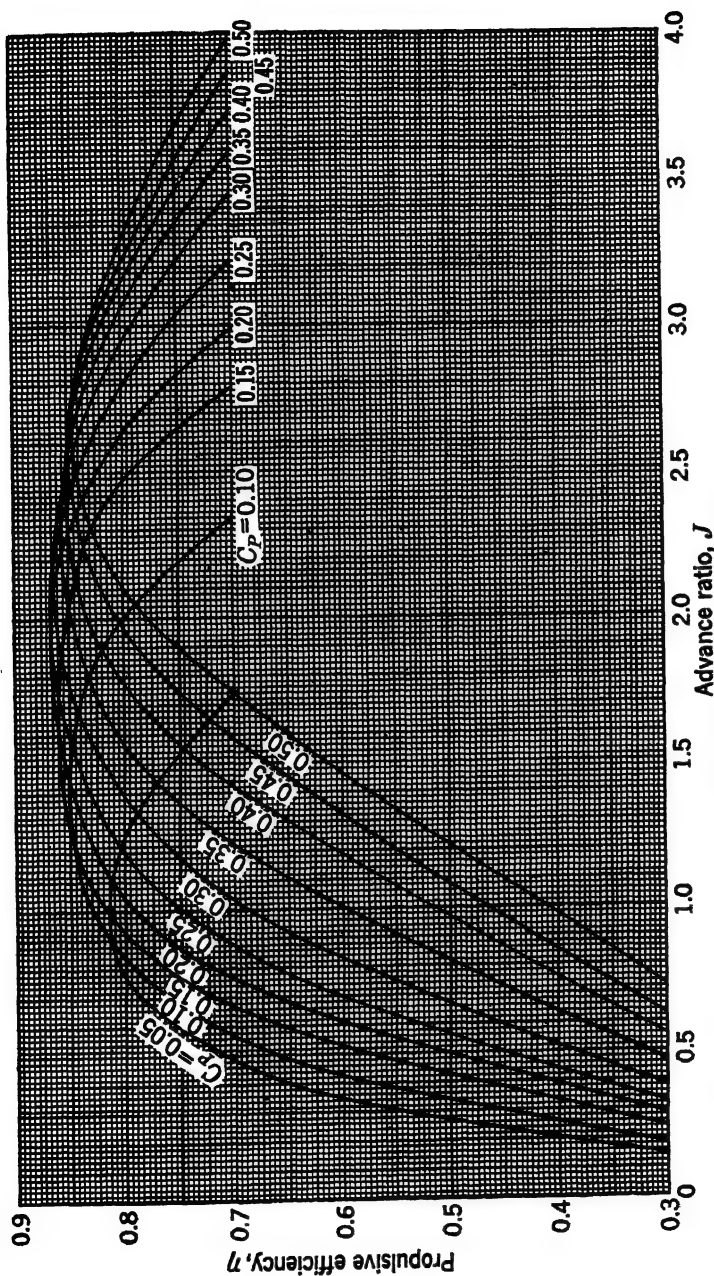


FIG. IVe. Aerodynamic characteristics of a four-bladed propeller. The data were obtained from tests on a single-rotating propeller in front of an in-line engine nacelle with wing (from Fig. IVb and c).

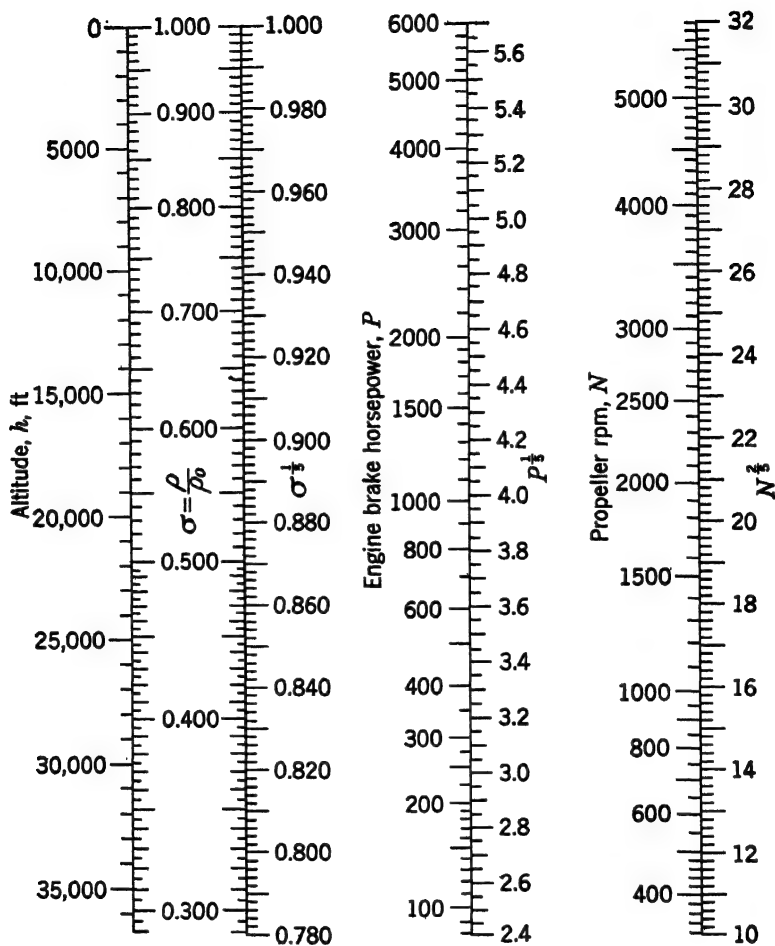


Fig. V Chart for solution of speed-power coefficient $C = \frac{0.638 V \sigma^{1/2}}{P}$

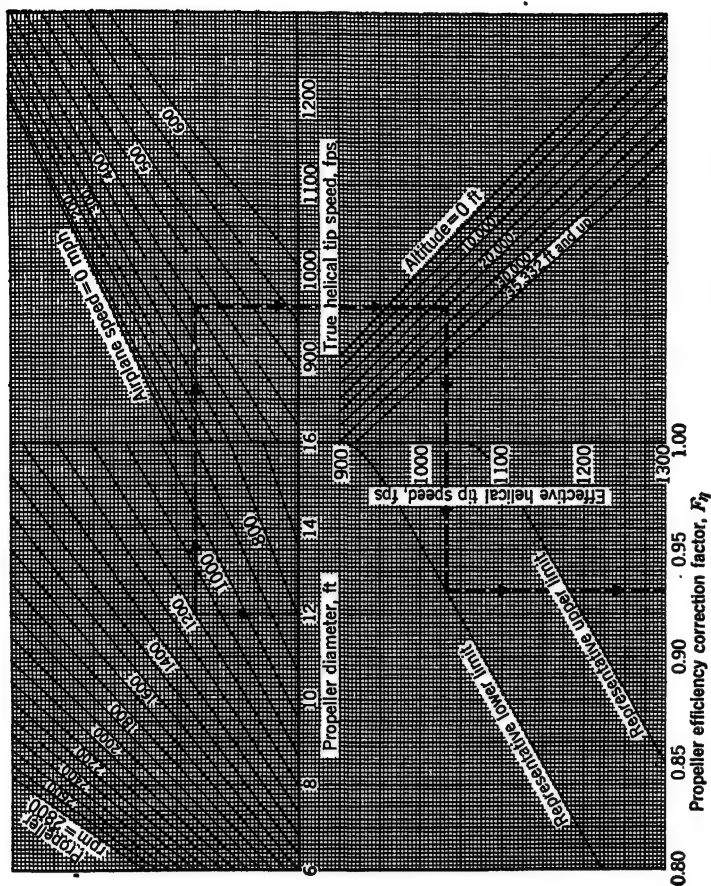


FIG. VI. Chart for solution of propeller efficiency factor F_p . (Example: propeller $D = 12$ ft., propeller $N = 1200$ rpm, airplane $V = 400$ mph, altitude = 20,000 ft. Therefore, $F_p = 0.831$.)

INDEX

- Absolute ceiling, 293, 295
- Adiabatic condition, 5
- Advance ratio, 275
- Aerodynamic center, 114, 222, 365
- Afterburning, 70
- Aileron, 71
 - characteristics of, 341-355
- Aileron reversal, 354
- Air, altitude characteristics of, 12-15, 363, 364
 - effect of humidity on, 11
 - equation of state for, 4
 - mass density of, 4
 - standard, 11, 12, 363, 364
- Air exchanger for wind tunnel, 85, 86
- Aircraft, components of, 58, 59
 - types of, 57, 58
- Airfoil, aerodynamic center of, 114, 222, 365
 - angle for maximum lift of, 108
 - angle of attack of, 53, 61
 - angle of zero lift of, 108, 213
 - area of, 59
 - aspect ratio of, 59
 - correction for, 124-131, 143-146, 334, 335
 - balance of, 118-120
 - boundary-layer control for, 237, 238
 - boundary-layer growth on, 166-171
 - camber of, 61
 - effect of, on aerodynamic characteristics, 113, 208-211, 213, 217, 223, 224, 247, 248
 - center of pressure on, 98, 114-116, 365
 - chord of, 59, 61
 - circulation theory of, two-dimensional, 100-107
 - three-dimensional, 124, 133-138
 - critical Mach number of, 190, 197, 198, 223-227
 - dive brakes on, 239
 - down-wash of, 125-127, 132, 137-141, 335
 - drag of (*see* Drag, of an airfoil)
 - efficiency factor of, 214-216
 - with flaps, 229-237
 - flow visualization on, 94-97
 - geometry of, 59-67, 208-212
 - ground effect on, 135, 136
 - high-speed (*see* High-speed airfoils)
 - induced angle of attack of, 127, 128
 - induced drag of, 99, 130, 131, 143-145
 - interference of, with fuselage, 246, 247
 - lift of (*see* Lift, of an airfoil)
 - momentum theory for, 124-131
 - NACA, 62-67, 206-213
 - (*See also* NACA standard airfoil sections)
 - pitching moments on, 52, 112-120, 184, 189, 197, 222, 223, 365
 - pressure distribution on, 41-45, 63-66, 113, 179-182, 187, 191, 208-212
 - roughness, effect of, on, 171, 207, 208
 - scale effects on, 166-170
 - section characteristics of, 138, 365
 - slots on, 71, 143, 235-237
 - spanwise lift distribution on, 139-143
 - stability of, 118-120
- Airfoil, compressibility effects on,
 - subsonic, 44, 179-184, 196, 197, 202-204, 354
 - supersonic, 184-190, 198-202
 - transonic, 44, 45, 190-195, 197, 198, 223-227

- Airfoil, stall of, 108, 141-143, 166, 216, 217
 stream turbulence, effect of, on, 163, 171, 207
 supersonic, characteristics of, 66, 184-190, 198-202
 taper ratio of, 60
 effect of, 139-141
 thickness of, effect of, 213-227
 velocity distribution on, 41-45, 208-212
 washout of, 60, 143
- Airplane, axes of, 325
 components of, 58, 59
 compressibility effects on, 202-204, 354
 control of, 323, 342-353
 efficiency factor of, 148
 engines of, 260-269
 (See also Engine)
 interference on, 245-247
 parasite drag of, 99, 146, 248-251, 254-257
 performance of, 290-321
 (See also Performance)
 power required by, 251-257
 propellers for, 270-286
 (See also Propeller)
 stability of, 323-342, 354
 (See also Stability)
 types of, 57, 58
- Airspeed indicator, 28, 29, 72-74
 compressibility correction for, 179n.
- Altitude, air-property variation with, 363, 364
 critical, 264
 density variation with, 13, 14, 363, 364
 effect of, on power required, 253, 254
 pressure variation with, 13, 14, 363, 364
 speed of sound variation with, 14, 363, 364
 standard, 11-15
 temperature variation with, 12, 363, 364
 viscosity variation with, 15, 363, 364
- Angle, of attack, 53, 61
 of climb, 296
 induced, 127, 128
 for maximum lift, 108
 of zero lift, 108, 213
- Area, equivalent flat-plate, 249, 250
 equivalent parasite, 250
 proper, 249
 wing, 59
- Aspect ratio, 59
 effect of, on drag of a cylinder, 242
 on drag of a normal flat plate, 242
 on induced angle of attack, 127, 128, 143-145
 on induced drag, 130, 131, 143-145
 on lift-curve slope, 129, 145
 on maximum lift, 146
 effective, caused by end plate, 335, 339
 caused by ground, 135, 136
- Athodyd, 69, 267
- Atmosphere, standard, 11, 12, 363, 364
- Attack, angle of, 53, 61
- Autogiro, 57
- Autorotation, 341
- B
- Balance, of an airfoil, 118-120
 of an airplane, 326, 338
- Bellows, for measuring pressure, 15
- Bernoulli equation, for compressible fluid, 175
 for perfect fluid, 24-26
- Biot-Savart law, 134
- Blade angle of propeller, 273
- Booster, for control surfaces, 352, 353
- Boundary layer, 42, 153-171
- Boundary-layer control, 89, 237-239
- Bourdon tube, for measuring pressure, 15
- Boyle's law, 5
- Brake horsepower, 261
- Breguet range equation, 302
 modified for turbo-jet airplane, 316
- Bucket, in drag curve, 170

- Bulk modulus of elasticity, 7
 - relation of, to speed of sound, 7
- Burbles, angle, 108
 - (See also Airfoil, stall of)
 - compressibility, 45, 191
- Camber, 61
 - (See also Airfoil, camber of)
- Ceiling, absolute, 293, 295
 - service, 295
- Center of gravity, effect of location
 - on, 330-332, 339
- Center of pressure, 98
- Characteristics of airfoils, aerodynamic, 213-227, 365
 - geometric, 53, 59-67
- Chord, of airfoil, 59, 61
 - zero-lift, 61
- Circulation, 101
- Circulation theory, three-dimensional, 133-138
 - two-dimensional, 100-107
- Climbing flight, 293-296
- Compound engine, 265
- Compressibility, 6-8, 23, 173-204
 - effects of, on an airfoil, 44, 45, 179-203
 - on an airplane, 202-204, 314, 315, 354
 - in a Laval nozzle, 177, 179
 - on a pitot tube, 179*n*.
 - of a fluid, 6-8
- Compressibility burble, 45, 191
- Consumption of fuel, 267, 268
- Continuity equation, 24, 174, 175
- Control, 323
- Control surface characteristics, 342-355
- Control surfaces, 71, 72
- Cooling, of engines, 69
- Cowl, 69
- Cowl flap, 69
- Cuff for propeller, 69, 232
- Cylinder, drag of, 244, 245
 - rotation of, 100, 103-105
 - scale effect on, 164, 244, 245
- Cylinder, surface velocity and pressure on, 39, 40, 43, 44
- D
- Damping, 323
- Density, of air, 4-6
 - at altitude, 14, 363, 364
 - effect of, on power, 261, 264
 - of manometer liquids, 364
- Diameter of propeller, choice of, 282, 283
- Diaphragm, for measuring pressure, 15
- Dihedral angle, 60, 341
- Dimensional analysis, 45-51
- Directional stability, 338-341
- Dive, terminal velocity in, 299
- Dive brakes, 239
- Dorsal fin, 71
- Down-wash behind an airfoil, 125-127, 132, 137-141, 335
- Drag, 35, 52
 - of an airfoil, 98, 111
 - compressibility effect on, subsonic, 44, 45, 183, 197, 202, 203
 - supersonic, 188, 189, 199-202
 - transonic, 191-195, 197, 198
 - effect of aspect ratio on, 130, 131, 143-145
 - with flap, 229-237
 - increase with dive brakes, 239
 - induced, 99, 130, 131, 143-146
 - minimum section, 217, 219, 365
 - profile, 99, 130, 146, 147
 - reduction of, with boundary-layer control, 238
 - representative, 111, 147
 - scale effect on, 166-171
 - section, 138, 365
 - with slot, 235-237
- of an airplane, 146-149, 202-204, 254-257
 - parasite, 99, 146-149, 248-257
 - representative, 147
 - residual, 99, 146
- of bodies of infinite aspect ratio, 245

Drag, of bodies of revolution, 244, 245
 of a cylinder, fineness ratio effect
 on, 243, 244
 scale effect on, 164, 244
 form, 43, 99, 154, 242
 interference, 245-248
 of a normal flat plate, 165, 166, 242
 of a parallel flat plate, 156, 158, 159
 pressure, 99
 proper, 249
 ram, 267
 skin-friction, 43, 99, 156, 158, 159,
 242
 of a sphere, 160-164
 wave, 188
 Ducted propeller, 70
 Dutch-roll instability, 341
 Dynamic stability, 323

E

Effective helical tip speed, 281
 Effectiveness factor for control sur-
 face, 345
 Efficiency, of actual propeller, 274,
 275, 277-279
 of ideal propeller, 272, 273
 relation of, to lift-drag ratio, 278,
 279
 Efficiency factor for propeller, 280,
 281
 Elevator, 71
 characteristics of, 342-354
 effect of, on airplane pitching mo-
 ment, 332, 333
 Empennage, 71
 End-plate effect on aspect ratio, 335,
 339
 Endurance, calculation of, 220, 221,
 303, 304, 317
 Engine, 68-70
 chart for, 370-372
 fuel consumption for, 267, 268
 jet-propulsion, 267-269
 method of rating, 260
 supercharged, 262-266
 unsupercharged, 260-262
 Equation of state, 4

Equivalent flat-plate area, 249, 250
 Equivalent parasite area, 250
 of an airplane, 256
 Equivalent parasite power, 256
 Exchange coefficient, 157
 Exchanger, air, for wind tunnel, 85,
 86

F

Fillet, 67, 247, 248
 Fin, 71
 dorsal, 71
 Fineness ratio, 164
 effect of, on a body of revolution,
 243, 244
 Five-digit airfoil, geometry of, 62, 63
 Flap, 71, 229-237, 335
 comparison of, with slot, 236, 237
 effect of, on airplane pitching mo-
 ment, 335
 on directional stability, 340
 hinge moment of, 236n., 342-353
 Flat plate, drag on, normal-to-flow,
 165, 166, 249, 250
 parallel-to-flow, 156, 158, 159
 Flow, circulatory, 100, 101
 rectilinear, 103
 Flow visualization, 94-97
 Fluid, perfect, 23, 24
 Form drag, 43, 99, 154, 242
 Four-digit airfoil, geometry of, 62
 Fowler flap, 231, 236
 Friction, ground, with brakes, 313
 without brakes, 309
 skin, 43, 99, 156, 158, 159, 242
 Froude number, 50, 51
 Fuel consumption, 267, 268
 Fuselage, compressibility effects on,
 203
 geometry of, 66, 67
 interference effects on, 245-248

G

General force equation, 45-51
 General moment equation, 51, 52
 Glauert correction for aspect ratio,
 144

Glide angle, minimum, condition for, 112

Glider, 57

Gliding flight, 112, 297-299

Ground effect, on airfoil, 135, 136
on complete airplane, 337

Ground friction, with brakes, 313
without brakes, 309

Ground run, during landing, 311-313
during take-off, 304-310

H

Helicopter, 57

High-lift devices, 229-239

High-speed airfoils, geometry of, 63
(*See also* Airfoil, compressibility effects on)

Hinge moment, 236*n.*, 343

Hinged surface, characteristics of, 342-353
effectiveness factor of, 345

Homogeneity, of fluid, 23

Honeycomb, 89

Hull, 68

Humidity, 11

I

Ideal propeller, 270-273

Indicated airspeed, 72-74

Induced angle of attack, 127, 128

Induced drag, 99, 130, 131, 143-146

Induced power, 256

Instruments, 15-19, 72-74, 94-97

Integrating manometer, 19

Interference, 245-247

effect of, on stability, 335

Interferometer method of flow visualization, 94, 96, 97

Isentropic process, 5

Isobaric process, 5

Isochoric process, 5

Isothermal process, 5

J

Jet propulsion, 38, 39, 69, 70, 267-269
from exhaust, 266
performance with, 313-317

Jets, accelerated, 36-39
decelerated, 31-36

K

Kármán-Tsien equation, 180

Kármán vortex trail, 164

Kutta-Joukowski lift equation, 104

L

Laminar boundary-layer phenomena, 154-156

Laminar flow, 8

Landing gear, 71

Landing performance, 311-313

Lateral control, 341-353

Lateral stability, 143, 341, 342

Laval nozzle, characteristics of, 177-179

Lift, 52, 98

of an airfoil, circulation theory of, 133-138

compressibility effect

on, subsonic, 182, 196, 197

supersonic, 187, 188, 199, 200

transonic, 190-195, 197, 198

with flap, 229-237

horseshoe-vortex concept of, 135, 136

Kutta-Joukowski equation for, 104

maximum, 108, 141-143, 166, 216, 217, 365

momentum theory of, 124-131

relation of, to pressure distribution, 181, 182

scale effect of, on maximum, 166

section, 138

slope of curve of, (*see* Slope of lift curve)

with slot, 235-237

spanwise distribution of, 139-143

of a rotating cylinder, 100, 104, 105

of a rotating sphere, 105

Lift/drag ratio, 111, 112, 220, 221

Lifting line, 138

Low-drag airfoils, geometry of, 64-67

M

- Mach number, 48, 50, 51
 critical, 190, 223-227
 (See also Compressibility)
 Magnus effect, 100
 Manometers, 17, 19
 characteristics of fluids for, 20, 364
 Mass, 1-3
 Mass density, 4
 Mean line, of an airfoil, 61
 Median line, 61
 Micromanometer, 18
 Moment, 51, 52
 hinge, 342-353
 pitching, of an airfoil, 52, 112-117
 about the aerodynamic center,
 114, 222, 223, 365
 effect of compressibility on,
 subsonic, 184, 187
 supersonic, 189
 of an airplane, 71, 222, 325-338
 effect of flaps on, 222, 229-233,
 335
 effect of slots on, 235
 rolling, 71, 325, 341, 342
 yawing, 71, 325, 338-341
 Momentum theory, for an airfoil,
 124-131
 for a propeller, 38, 270-273
 Multiple manometer, 18, 19

N

- NACA standard airfoil sections, aero-
 dynamic characteristics of, 206-
 227, 365, 369
 geometry of, 62-67
 Nacelle, 68
 Newton, laws of motion of, 1
 shearing-stress equation of, 9
 Newtonian fluids, 9*n*.
 Nomenclature, aircraft, 57-72

O

- Oswald efficiency factor, 148*n*.

P

- Parasite drag, 99, 146

- Parasite drag, of an airplane, 99, 146-
 149, 248-251, 254-257
 of bodies of infinite aspect ratio, 245
 of bodies of revolution, 244, 245
 of a cylinder, fineness ratio effect
 on, 243, 244
 scale effect on, 164, 244
 effect of interference on, 245-248
 of a normal flat plate, 165, 166, 242
 of a parallel flat plate, 156, 158, 159
 of a sphere, 160-164
 Perfect fluid, 23, 24
 Performance, 290-321
 with reciprocating engine, calcula-
 tion of, 290-313, 318-321
 climbing flight, 293-296
 cruising flight, 299, 300
 endurance, 221, 303, 304
 gliding flight, 112, 297-299
 landing, 311-313
 maximum angle of climb, 296
 maximum velocity, 291, 292
 minimum sinking speed, 221, 298
 minimum velocity, 292, 293
 range, 220, 221, 301-303
 rapid estimation of, 318-321
 take-off, 304-311
 time to climb, 296, 297
 with turbo-jet, 313-317
 Pitching moment (see Moment,
 pitching)
 Pitot tube, 28, 29, 72-74
 effect of compressibility on, 179*n*.
 Polar curve, 111
 glide, 298, 299
 Power, 251
 available from propeller, 251, 284-
 286
 brake, 261
 of engines, 260-266
 effect of, on stability, 337
 friction, 261
 indicated, 261
 rating of, of engines, 260
 required by an airplane, 251-257
 representative, 254-256, 318-320
 Power characteristics of engines, 260-
 266

- Power coefficients, 276-279
- Prandtl-Gebbers transition, 159
- Prandtl-Glauert equation, 180
- Prandtl-Meyer expansion, 186
- Pressure, absolute, 15
- chordwise distribution of, on an airfoil, 41-45, 63-66, 113, 179-182, 187, 191, 208-212
 - effect of compressibility on, subsonic, 179-182
 - supersonic, 45, 187
 - transonic, 44, 191
- distribution of, on a cylinder, 39-41, 43, 44
- on a sphere, 41
 - on a streamlined body, 41
- dynamic, 25
- gage, 15
- stagnation, 30
- correction of, for compressibility, 179, 180
- static, 25
- measurement of, 15-19
 - variation of, with altitude, 13, 14, 363, 364
- total, 25
- Pressure coefficient, 40, 208, 224
- Profile drag, 99, 130, 146, 147
- Propeller, 38, 68
- activity factor of, 280
 - advance ratio for, 275
 - charts for, 373-379
 - choice of diameter of, 282-284
 - constant-speed, 283
 - ducted, 70
 - effects of compressibility on, 280, 281
 - efficiency of, 272-275, 277-279
 - comparison of, with airfoil characteristics, 278, 279
 - fixed-pitch, 283
 - geometry of, 280-282
 - ideal, 270-273
 - inclined, 337, 340
 - momentum theory of, 38, 270, 273
 - power coefficient for, 276
 - simple blade-element theory of, 273-275
- Propeller, solidity factor of, 280
- speed-power coefficient for, 277, 380
 - thrust coefficient for, 276
 - comparison with airfoil characteristics, 278, 279
 - tip-speed correction for, 280-281, 381
 - yawed, (*see* Propeller, inclined)
- Proper drag, 249
- R
- Ram, 69*n.*, 267
- Ram-drag, 268
- Ram-jet, 69, 267
- Range, calculation of, 220, 221, 301-303, 316, 317
- Rapid performance estimation, 318-321
- Rate of climb, calculation of, 293-296
- Residual drag, 99, 146
- Reynolds number, 48, 49, 51
- critical, 159, 163
 - effect of, on an airfoil, 166-171
 - on a body of infinite aspect ratio, 245
 - on a body of revolution, 244, 245
 - on a cylinder, 164, 244
 - on a normal flat plate, 165, 166
 - on a parallel flat plate, 153-160
 - on a sphere, 160-164
- Rocket, 36, 37
- Roll, angle of, 325
- Rolling moment, 71, 325, 341, 342
- Rotating cylinder, 100, 103-105
- Rotating sphere, 105
- Roughness, effect of, on aerodynamic characteristics, 171, 207, 208
- Rudder, 71
- characteristics of, 342-355
 - effect of, on airplane yawing moment, 339
- Sailplane, 57
- Scale effect, (*see* Reynolds number, effect of)
- Schlieren method of flow visualization, 94-96

- Section characteristics of airfoils, 138, 365
 Separation, 23, 160
 (See also Reynolds number, effect of)
 Service ceiling, 295
 Shadow method of flow visualization, 94, 95
 Shearing stress, in laminar flow, 9, 153, 156
 in turbulent flow, 157, 158
 Shock wave, 45, 178, 179, 186
 Simple blade-element theory, of propellers, 273-275
 Skin friction, 43, 99, 156, 158, 159, 242
 Slat, 235
 Slipstream velocity, 38, 271, 287, 340
 Slope of lift curve, 108, 110, 214, 216, 365
 effect of aspect ratio on, 129, 145
 effect of compressibility on, subsonic, 182, 196, 197
 supersonic, 187, 188
 transonic, 200
 for tail surfaces, 145, 334, 335
 Slots, 71, 143, 235-237
 comparison of, with flaps, 236, 237
 Smoke, for flow visualization, 94
 Sound, speed of, 7, 8
 variation of, with altitude, 14, 363, 364
 Speed, climbing, 295
 cruising, 299
 gliding, 298, 299
 indicated, 72-74
 landing, 313
 local, 30
 maximum, 291, 292, 315, 316
 minimum, 292, 293, 315
 relative, 30
 remote, 30
 sinking, 221, 298
 of sound, 7, 8
 stalling, 110
 take-off, 309, 310
 terminal, 299
 Speed-power coefficient, 277, 380
 Sphere, rotating, 105
 Sphere, scale effect on, 160-164
 Spin, 341, 342
 Spiral instability, 341
 Stability, 323, 324
 of an airfoil, 118-120
 of an airplane, 323-342, 354
 directional, 338-341
 lateral, 143, 341, 342
 longitudinal, 326-338
 effect of center-of-gravity position on, 330-332
 effect of elevator deflection on, 332, 333
 effect of flap deflection on, 335
 effect of ground on, 337
 effect of interference on, 335
 effect of power on, 337
 effect of stabilizer setting on, 332
 effect of tail lift curve on, 334, 335
 effect of tail position on, 333, 334
 Stabilizer, 71
 effect of, on pitching moment, 332
 Stagnation point, 30
 Stalling, 108
 Standard air, 11-15
 properties of, 363, 364
 Static pressure (see Pressure, static)
 Stokes' law, 160
 Stratosphere, 12
 Stream tube, 24
 Striae method of flow visualization, 94-96
 Sublayer, laminar, 157
 Subsonic, 45*n.*, 173, 174
 Supercharger, gear-driven, 262-265
 turbo-driven, 265, 266
 Supersonic, 45*n.*, 173, 174, 196
 Supersonic airfoils, aerodynamic characteristics of, 184-190, 198-202
 geometry of, 66
 Supersonic flow in Laval nozzle, 177-179
 Sweepback, 63
 aerodynamic characteristics of, 141, 197, 198, 201, 202

T

- Tab, 71
- Take-off calculations, 304-311, 317
- Taper ratio, 60
- Temperature variation with altitude, 12
- Testing, wind-tunnel, 76-97
- Thrust, from exhaust, 266
- Thrust coefficient, 276
 - comparison of, with airfoil characteristics, 278, 279
- Transition, of a boundary layer, 158-160, 207
 - (*See also* Reynolds number, effect of)
- Transonic, 45*n.*, 173, 174, 196
- Tropopause, 12
- Troposphere, 12
- Turbo-jet, 69, 267-269
 - performance with, 313-317
- Turbo-propeller, 70
- Turbo-ram-jet, 70
- Turbulence, stream, 171, 207, 208
- Turbulence factor, 163
- Turbulent flow, 8

U

- U-tube manometers, 17, 18

V

- Velocity (*see* Speed)
- Vena contracta, 37, 88
- Venturi tube, 27, 177-179
- Viscosity, absolute, 8-11
 - variation of, with altitude, 15, 363, 364
 - with temperature, 15
- kinematic, 11
 - variation of, with altitude, 363, 364
- Vortex, bound, 134
 - filament, 133*n.*
 - free, 135
 - horseshoe, 135
 - image, 135
 - trailing, 132, 135
- Vortex trail, 164

W

- Wake, 30, 35, 36
- Washout, 60, 143
- Wave drag, 188
- Whirling-arm method for testing, 76
- Wind, effect of, on gliding distance, 112
 - on landing, 313
 - on take-off, 311
- Wind tunnel, 76
 - air exchanger for, 85, 86
 - annular-return, 81
 - atmospheric slot for, 85
 - bellmouth for, 88
 - boundary-layer control for, 89
 - classification of, 77
 - closed-circuit, 80
 - closed-throat, 86
 - double-return, 81
 - flow improvement in, 88-91
 - flow visualization in, 94-97
 - force measurement in, 92-94, 206
 - free-flight, 78
 - free-spinning, 77
 - gust, 77
 - honeycomb for, 89
 - low-turbulence, 89-91, 206-208
 - model support in, 91, 92
 - open-circuit, 80
 - open-throat, 86
 - pressurized, 81, 85
 - screens for, 91
 - single-return, 80
 - two-dimensional, 87
 - vanes for, 89
 - variable-density, 81
- Wing (*see* Airfoil)
- Wing efficiency factor, 149
- Wing-fuselage combinations, 57, 58

Z

- Yaw, angle of, 325
- Yawing moment, 71, 325, 338-341
- Zero lift, angle of, 108, 213

